

UPoN 2015

*7th International Conference on
Unsolved Problem on Noise*

July 13-17, 2015

*Casa Convalescència
Barcelona, Spain*

UAB

Universitat Autònoma
de Barcelona



BARCELONA 2015

Proceedings of the
**7th International Conference on Unsolved
Problems on Noise**

July 13-17, 2015

Casa Convalescència, Barcelona, Spain

<http://europe.uab.es/upon2015/index.html>

Organizing Committee:

Xavier Oriols (Chair), Jordi Suñé, Rosana Rodríguez, David Jiménez, Xavier Cartoixà,
Guillem Albareda, Javier Martín-Martínez, Zhen Zhan, Enrique Colomé, Damiano Marian

ISBN: 978-84-942706-9-7



Acknowledgements

The 7th *International Conference on Unsolved Problems on Noise* (UPoN 2015) would like to acknowledge the generous support by the following:



Foreword

On behalf of the organizing committee, I would like to welcome all participants to the 7th International Conference on Unsolved Problems on Noise (UPoN). The study of random fluctuations has always been an interdisciplinary subject that has attracted some of the best scientists. The aim of the UPoN conferences is to provide a forum for researchers working at the frontiers of noise in different (but related) disciplines.

One of the most fascinating stories about the importance of exchanging scientific knowledge comes from the Ancient Library of Alexandria, in Egypt. During centuries, it attracted many of the most famous thinkers of the ancient world. At some times, it housed 900.000 books (papyrus scrolls). However, the library suffered several fires and was finally destroyed. It is unknown how much scientific knowledge was lost there.

Today, international conferences are the modern forums for exchanging scientific knowledge. Your help is needed for a fruitful conference. The UPoN conference deals with unsolved problems on noise that are starting to become understandable. At such frontiers of research, our knowledge is still unstable, somehow immature and, certainly, not free from controversies. I encourage all participants to promote discussions on noise, asking and answering questions, in a friendly atmosphere. We are all in the same team trying to understand, at the end of the day, how Nature works.

I would also like to encourage all participants (especially those who are in Barcelona for the first time) to discover our city. Barcelona is worldwide famous for its modernist architecture, the Sagrada Família being one of its maximum exponents. Indeed, the conference site (casa Convalescència) is another example of the modernist style. This is one of the reasons for choosing this place to hold the conference.

Finally, I would like to thank our sponsors *Panstanford Publishing*, *Universitat Autònoma de Barcelona*, *Agència de Gestió d'Ajuts Universitaris i de Recerca* from *Generalitat de Catalunya* and *Secretaría de Estado de Investigación, desarrollo e innovación* from *Gobierno de España*. Special thanks to the scientific committee of the UPoN conference for its help and effort in the elaboration of the excellent and *noisy* program that you will find in this book of abstracts.

I really wish all of you a very pleasant and scientifically very fruitful stay in Barcelona during this week.

Yours faithfully,



Xavier Oriols

Chair UPoN 2015

Casa Convalescència, Barcelona, July 13, 2015





BARCELONA 2015

List of Invited Speakers

Yaroslav M. Blanter Delft University of Technology (THE NETHERLANDS)

Classical and quantum non-linear dynamics in optomechanical systems

Topic: 2. - Quantum noise and coherence

Gianpietro Cagnoli Laboratoire des Matériaux Avancés (FRANCE)

Thermal and mechanical noise in gravitational wave detectors

Topic: 8. - Experimental frontiers of noise and fluctuations

Sergio Ciliberto Laboratoire de Physique de l'ENS (FRANCE)

Fluctuation theorems: applications to energy fluctuations in electric circuits and micro devices

Topic: 1. - Theoretical trends in noise and fluctuations

Irene Donato Centre of Theoretical Physics (FRANCE)

Is it possible to detect long-range interactions among biomolecules through noise and diffusion?

Topic: 4. - Fluctuations in biological systems

Mark Dykman Michigan State University (USA)

Rates of rare events: scaling, fragility, and delay effects

Topic: 5. - Noise in complex and non-linear systems/circuits

Zoltan Gingl University of Szeged (HUNGARY)

How can the fluctuations in the motion of kayak-paddlers be used to estimate performance?

Topic: 9. - Other topics of noise and fluctuations

Peter Hänggi University of Augsburg (GERMANY)

The role of temperature in different thermodynamic ensembles

Topic: 2. - Quantum noise and coherence

Laszlo Kish Texas A&M University (USA)

All that glitters is not gold: Zero-point energy in the Johnson noise of resistors

Topic: 1. - Theoretical trends in noise and fluctuations

Sigmund Kohler Instituto de Ciencias de Materiales de Madrid (SPAIN)

Adiabatic Passage and Noise in Quantum Dots

Topic: 2. - Quantum noise and coherence



BARCELONA 2015

List of Invited Speakers

Pietro Massignan ICFO - Institute of Photonic Sciences Barcelona (SPAIN)

From cell membranes to ultracold gases: classical and quantum diffusion in inhomogeneous media

Topic: 4. - Fluctuations in biological systems

Vyacheslav R. Misko Universiteit Antwerpen (BELGIUM)

Active Brownian motion in confined geometries

Topic: 7. - Applications of noise

Bernard Plaçais Département de Physique de l'ENS Paris (FRANCE)

Noise in graphene and carbon nanotube devices

Topic: 3. - Fluctuations in materials and devices

H. Eugene Stanley Boston University (USA)

Novel Statistical Physics Approaches to Understanding Economic Fluctuations

Topic: 6. - Fluctuations in econophysics and financial markets

Aneta Stefanovska Lancaster University (UK)

Chronotaxic dynamics: when the characteristic frequencies fluctuate and the system is stable

Topic: 4. - Fluctuations in biological systems



BARCELONA 2015

UPoN International Scientific Committee

- Derek Abbott** (*Adelaide University, Australia*)
Dean Astumian (*University of Maine, USA*)
Kamal K. Bardhan (*Saha Institute of Nuclear Physics, India*)
Ludovic Bellon (*École Normale Supérieure de Lyon, France*)
Sergey Bezrukov (*National Institutes of Health, USA*)
Paolo Bordone (*Università di Modena e Reggio Emilia, Italy*)
Gijs Bosman (*University of Florida, USA*)
Anna Carbone (*Torino Polytechnique, Italy*)
Sergio Ciliberto (*École Normale Supérieure de Lyon, France*)
Jamal Dean (*McMaster University, Canada*)
Charlie Doering (*University of Michigan, USA*)
Gianfranco Durin (*Istituto Electronico Nazionale, Italy*)
Peter Hänggi (*University of Augsburg, Germany*)
Kumiko Hayashi (*Tohoku University, Japan*)
Laszlo Kish (*Texas A&M University, USA*)
Andre Longtin (*Center for Neural Dynamics, Canada*)
Lukasz Machura (*University of Silesia, Poland*)
Massimo Macucci (*University of Pisa, Italy*)
Peter McClintock (*Lancaster University, England*)
Xavier Oriols (*Universitat Autònoma de Barcelona, Spain*)
Cecilia Pennetta (*University of Salento, Italy*)
Lino Reggiani (*University of Salento, Italy*)
Sergey Rumyantsev (*Ioffe Physico-Technical Institute, Russia*)
Michael Shlesinger (*Office of Naval Research, USA*)
H. Eugene Stanley (*Boston University, USA*)
Luca Varani (*University of Montpellier, France*)
Stefano Zapperi (*CNR-IENI, Italy*)

Monday, July 13 2015

8:00-9:00 Registration

9:00-9:30 **Welcome and opening remarks UPoN 2015**

Ferran Sancho Piffaré – Rector de la *Universitat Autònoma de Barcelona* (UAB)

Emilio Lora-Tamayo D'Ocón - President of the *Consejo Superior de Investigaciones Científicas* (CSIC)

Xavier Oriols – Chairman *UPoN 2015*

Fluctuations in econophysics

9:30-10:00 **Novel Statistical Physics Approaches to Understanding Economic Fluctuations.**
(INVITED) (pp. 1-2)
*H. Eugene Stanley*¹
¹*Boston University, USA*

Applications of noise (I)

CHAIRMAN: Michael F. Shlesinger (Office of Naval Research ONR, USA)

10:00-10:30 **Active Brownian motion in confined geometries. (INVITED)** (pp. 3-4)
Vyacheslav R. Misko^{1,2}
¹*Universiteit Antwerpen, Belgium,* ²*CEMS, Japan*

10:30-10:50 **Brownian motion and weak ergodicity breaking. (ORAL)** (pp. 5-6)
*P. Massignan*¹, *C. Manzo*¹, *J. A. Torreno-Pina*¹, *M. F. García-Parajo*¹, *M. Lewenstein*¹, *G. J. Lapeyre Jr*¹
¹*ICFO, Institute of Photonic Sciences, Spain*

10:50-11:10 **Brownian motors in the micro-scale domain: Enhancement of efficiency by noise.**
(ORAL) (pp. 7)
*Jakub Spiechowicz*¹, *Peter Hänggi*², *Jerzy Łuczka*³
¹*University of Silesia, Poland,* ²*Universität Augsburg, Germany,* ³*Silesian Center for Education and Interdisciplinary Research, University of Silesia, Poland*

11:10-11:30 Unconditional security in practical Kirchhoff-law-Johnson-noise key exchangers. (ORAL) (pp. 8-9)
Berry Chen¹, Laszlo B. Kish¹, Claes G. Granqvist², Robert Mingesz³, Zoltan Gingl³
¹Texas A&M University, USA, ²Uppsala University, Sweden, ³University of Szeged, Hungary

11:30-12:00 Coffee Break

Noise in complex and non-linear systems (I)

CHAIRMAN: Lukasz Machura (University of Silesia, Poland)

12:00-12:30 Rates of rare events: scaling, fragility, and delay effects. (INVITED) (pp. 10-11)
Mark Dykman¹
¹Michigan State University, USA

12:30-12:50 Stochastic resonance and diversity-induced resonance in complex systems. (ORAL) (pp. 12-13)
Marco Patriarca¹, Els Heinsalu¹, Emilio Hernández-García², Raúl Toral²
¹NICPB-National Institute of Chemical Physics and Biophysics, Estonia, ²CSIC-UIB, Spain

12:50-13:10 Non-hermitian diffusion. (ORAL) (pp. 14-15)
Maciej A. Nowak¹
¹Jagiellonian University, Poland

13:10-14:40 Lunch (at the Dining Room of Casa Convalescència)

Fluctuations in biological systems (I)

CHAIRMAN: Aneta Stefanovska (Lancaster University, UK)

14:40-15:10 From cell membranes to ultracold gases: classical and quantum diffusion in inhomogeneous media. (INVITED) (pp. 16-17)
Pietro Massignan¹, G. J. Lapeyre^{1,2}, J. A. Torreno-Pina¹, Aniello Lampo¹, Jan Wehr³, M. F. García-Parajo¹, M. Lewenstein¹
¹ICFO-Institut de Ciències Fotòniques, Spain, ²IDAEE-CSIC, Spain, ³University of Arizona, USA

15:10-15:30 A motor that detects the length of DNA by using chain fluctuation. (ORAL) (pp. 18-19)
Ana Maria Florescu¹, Kuni H Iwasa^{1,2}
¹Max Planck Institute for Physics of Complex Systems, Germany, ²National Institutes of Health (NIH), USA

15:30-15:50 Model and parameter determination for molecular motors from single molecule experiment. (ORAL) (pp. 20-21)
Francisco Javier Cao¹
¹Universidad Complutense de Madrid, Spain

15:50-16:10 Free energy measurement of ligands binding nucleic acids using fluctuation theorems. (ORAL) (pp. 22)
Joan Camunas-Soler¹, Anna Alemany¹, Felix Ritort^{1,2}
¹Universitat de Barcelona, Spain, ²Instituto de Salud Carlos III, Madrid, Spain

16:10-16:40 Coffee Break

Fluctuations in biological systems (II)

CHAIRMAN: Bernardo Spagnolo (Università di Palermo, Italy)

16:40-17:10 Is it possible to detect long-range interactions among biomolecules through noise and diffusion? (INVITED) (pp. 23)
I. Donato¹, M. Gori¹, I. Nardecchia¹, M. Pettini¹, J. Torres², L. Varani²
¹Aix-Marseille University, France, ²Montpellier University, France

17:10-17:30 Electrochemical noise analysis to probe ion transport mechanisms in a membrane channel. (ORAL) (pp. 24-25)
Maria Queralt-Martin¹, M. Lidón López¹, Antonio Alcaraz¹
¹Universitat Jaume I, Spain

17:30-17:50 Coulomb Blockade of Stochastic Permeation in Biological Ion Channels. (ORAL) (pp. 26-27)
W.A.T. Gibby¹, I. Kh. Kaufman¹, D. G. Luchinsky¹, P.V.E. McClintock¹, R.S. Eisenberg²
¹Lancaster University, UK, ²Rush University, Chicago, USA

17:50-18:10 Antipersistent Random Walk in a Two State Flashing Magnetic Potential. (ORAL) (pp. 28)
Pietro Tierno¹, Francesc Sagués¹, Tom H. Johansen^{2,3}, Igor M. Sokolov⁴
¹Universitat de Barcelona, Spain, ²University of Oslo, Norway, ³Center for Advanced Study at The Norwegian Academy of Science and Letter, Norway, ⁴Humboldt-Universität zu Berlin, German

18:10-18:30 Giant acceleration of diffusion observed in a single-molecule experiment on F1-ATPase. (ORAL) (pp. 29-30)
Kumiko Hayashi¹
¹Tohoku University, Japan

Tuesday, July 14 2015

Quantum noise and coherence (I)

CHAIRMAN: Wolfgang Belzig (University of Konstanz, Germany)

- 9:00-9:30** **The role of temperature in different thermodynamic ensembles. (INVITED)** (pp. 31-32)
*Peter Hänggi*¹
¹Universität Augsburg, Germany
- 9:30-10:00** **Adiabatic passage and noise in quantum dots. (INVITED)** (pp. 33-34)
*Sigmund Kohler*¹
¹CSIC, Madrid, Spain
- 10:00-10:20** **Non-zero probability of detecting identical electrons at the same position: How does it affect the Landauer-Büttiker noise expression at high temperatures? (ORAL)** (pp. 35-36)
*Enrique Colomé*¹, *Damiano Marian*¹, *Xavier Oriols*¹
¹Universitat Autònoma de Barcelona, Spain
- 10:20-10:40** **Dissipative dynamics of a quantum particle strongly interacting with a super-Ohmic heat bath. (ORAL)** (pp. 37-38)
Luca Magazzù^{1,2}, *Davide Valenti*¹, *Bernardo Spagnolo*^{1,2,3}
¹Università di Palermo, Italy, ²Lobachevsky State University, Russia, ³INFN Catania, Italy
- 10:40-11:00** **Fractional quantum Hall spectroscopy investigated by a resonant detector. (ORAL)** (pp. 39-40)
*Alessandro Braggio*¹, *Matteo Carrega*¹, *Dario Ferraro*^{2,3}, *Maura Sassetti*^{4,1}
¹SPIN-CNR, Italy, ²Université de Toulon, France, ³Université de Genève, Switzerland, ⁴Università di Genova, Italy

11:00-11:30 **Coffee Break**

Experimental frontiers of noise

CHAIRMAN: Luca Varani (University of Montpellier, France)

- 11:30-12:00** **Thermal and mechanical noise in gravitational wave detectors. (INVITED)** (pp. 41-42)
*Gianpietro Cagnoli*¹
¹Université de Lyon, France

12:00-12:20 The quest for the missing noise in a micro-mechanical system out of equilibrium. (ORAL) (pp. 43-44)
Mickael Geitner¹, Felipe Aguilar Sandoval^{1,2}, Éric Bertin³, Ludovic Bellon¹
¹Université de Lyon & CNRS, France, ²Universidad de Santiago del Chile, Chile, ³Université Joseph Fourier & CNRS, France

12:20-12:40 Noise Thermal Impedance: a way to access electron dynamics. (ORAL) (pp. 45-46)
E. Pinsolle¹, B. Reulet¹
¹Université de Sherbrooke, Canada

12:40-15:30 Poster session & Lunch (at the Dining Room of Casa Convalescència)

Applications of noise (II)

CHAIRMAN: Laszlo Kish (Texas A&M University, USA)

15:30-15:50 Towards an information-theoretic model of the Allison mixture. (ORAL) (pp. 47-48)
L. Gunn¹, F. Chapeau-Blondeau², A. Allison¹, D. Abbott¹
¹The University of Adelaide, Australia, ²University of Angers, France

15:50-16:10 How a player with finite memory can win by switching in a sequence of Parrondo Games? (ORAL) (pp. 49-50)
Ka Wai CHEUNG¹, Ho Fai MA¹, Degang Wu¹, Ga Ching LUI¹, Kwok Yip Szeto¹
¹The Hong Kong University of Science and Technology, China

16:10-16:30 Asymmetry in Genetic Code and the Role of Parrondo's Paradox in Nature. (ORAL) (pp. 51-52)
Lee Kee Jin¹, Shu Jian Jun¹
¹Nanyang Technological University, Singapore

16:30-17:00 Coffee Break

Fluctuations in materials and devices (I)

CHAIRMAN: Javier Mateos (University of Salamanca, Spain)

17:00-17:20 Percolation noise at the metal-insulator transition of nanostructured VO₂ films. (ORAL) (pp. 53-54)
Zareh Topalian¹, Shu-Yi Li¹, Gunnar A. Niklasson¹, Claes G. Granqvist¹, Laszlo B. Kish^{1,2}
¹Uppsala University, Sweden, ²Texas A&M University, USA

17:20-17:40 Frequency-dependent shot noise in single-electron devices interpreted by means of waiting time distributions. (ORAL) (pp. 55-56)

Vincent Talbo¹, Javier Mateos¹, Sylvie Retailleau², Philippe Dollfus², Tomás González¹

¹Universidad de Salamanca, Spain, ²Université Paris-Sud, France

17:40:18:00 Conductance fluctuation in Si nanowires studied from first-principles. (ORAL) (pp. 57-58)

Riccardo Rurali¹, F. Iori², S. Ossicini²

¹ICMAB-CSIC, Spain, ²Università di Modena e Reggio Emilia, Italy

Wednesday, July 15 2015

Fluctuations in biological systems (III)

CHAIRMAN: Peter McClintock (Lancaster University, UK)

9:00-9:30 Chronotaxic dynamics: when the characteristic frequencies fluctuate and the system is stable. (INVITED) (pp. 59-60)

Aneta Stefanovska¹, Philip Clemson¹, Y. F. Suprunenko²

¹Lancaster University, UK, ²University of Liverpool, UK

9:30-9:50 Fluctuations and effective temperature in an active dumbbell system. (ORAL) (pp. 61-62)

Giuseppe Gonnella¹, Antonio Suma², Leticia F. Cugliandolo³

¹Università di Bari and INFN, Italy, ²SISSA, Trieste, Italy, ³Sorbonne Universités, Paris, France

9:50-10:10 Fluctuation Relations applied to characterize heterogeneous molecular ensembles. (ORAL) (pp. 63-64)

Alvaro Martínez-Monge¹, Anna Alemany¹, Felix Ritort¹

¹Universitat de Barcelona, Spain

10:10-10:30 Stochastic facilitation in the brain? (ORAL) (pp. 65-66)

Lawrence M. Ward¹, Priscilla E. Greenwood¹

¹University of British Columbia, Canada

10:30-10:50 Seeking for a fingerprint: analysis of point processes in actigraphy recording. (ORAL) (pp. 67-68)

Ewa Gudowska-Nowak¹

¹Jagiellonian University in Kraków, Poland

10:50-11:20 Coffee Break

Fluctuations in materials and devices (II)

CHAIRMAN: Gijs Bosman (University of Florida, USA)

- 11:20-11:50 Noise in graphene and carbon nanotube devices. (INVITED)** (pp. 69-70)
Bernard Plaçais¹, C. Voisin¹, G. Fève¹, J. M. Berroir¹
¹Département de Physique de l'ENS Paris, France
- 11:50-12:10 Is the peculiar behavior of 1/f noise in graphene the result of the interplay between band-structure and inhomogeneities? (ORAL)** (pp. 71-72)
B. Pellegrini¹, P. Marconcini¹, M. Macucci¹, G. Fiori¹, G. Basso¹
¹Università di Pisa, Italy
- 12:10-12:30 Monte Carlo study of velocity fluctuations during transient regimes in graphene. (ORAL)** (pp. 73-74)
José M. Iglesias¹, R. Rengel¹, E. Pascual¹, María J. Martín¹
¹Universidad de Salamanca, Spain

12:30 Photo of the UPoN 2015 conference

12:45-14:30 Lunch (at the Dining Room of Casa Convalescència)

Fluctuations in materials and devices (III)

CHAIRMAN: Massimo Macucci (Università di Pisa, Italy)

- 14:30-14:50 Measurements of RF noise in InGaAs/InAlAs recessed diodes: Signatures of shot-noise suppression. (ORAL)** (pp. 75-76)
Ó. García-Pérez¹, T. González¹, S. Pérez¹, A. Westlund², J. Grahn², J. Mateos¹
¹Universidad de Salamanca, Spain, ²Chalmers University of Technology, Gothenburg, Sweden
- 14:50-15:10 1/f noise arising from time-subordinated Langevin equations. (ORAL)** (pp. 77-78)
Julius Ruseckas¹, Bronislovas Kaulakys¹
¹Vilnius University, Lithuania
- 15:10-15:30 Plasmonic Noise of Field-Effect Transistors Operating at Terahertz Frequencies. (ORAL)** (pp. 79-80)
C. Palermo¹, A. Mahi¹, H. Marinchio¹, L. Varani¹, P. Shiktorov², E. Starikov², V. Gruzinskis²
¹University of Montpellier, France, ²Center for Sciences and Technology, Vilnius, Lithuania

17:00 Visit to Sagrada Familia / Catedral del mar

Committee dinner

Thursday, July 16 2015

Theoretical trends in noise and fluctuations (I)

CHAIRMAN: Peter Hänggi (Universität Augsburg, Germany)

- 9:00-9:30** **Fluctuation theorems and stochastic thermodynamics: applications to energy fluctuations in electric circuits and micro devices. (INVITED)** (pp. 81)
*Sergio Ciliberto*¹
¹Laboratoire de Physique de l'ENS de Lyon, France
- 9:30-9:50** **Experimental realization of a microscopic Carnot engine. (ORAL)** (pp. 82-83)
*L. Dinis*¹, *I. A. Martínez*², *E. Roldán*³, *J. M. R. Parrondo*¹, *R. A. Rica*⁴
¹Universidad Complutense de Madrid, Spain, ²Ecole Normale Supérieure, Lyon, France, ³Max Plank Institute, Dresden, Germany, ⁴ICFO, Spain
- 9:50-10:10** **Equilibrium and non-equilibrium fluctuations at the single molecule level: from free-energy measurements to inference. (ORAL)** (pp. 84)
*M. Ribezzi-Crivellari*¹, *F. Ritort*¹
¹Universitat de Barcelona, Spain
- 10:10-10:30** **Fluctuations of intensive variables and non-equivalence of thermodynamic ensembles. (ORAL)** (pp. 85)
*A. Ya. Shul'man*¹
¹V. A. Kotel'nikov Institute of Radio Engineering and Electronics of the RAS, Russia
- 10:30-11:00** **Coffee Break**

Other topics of noise

CHAIRMAN: Felix Ritort (Universitat de Barcelona, Spain)

- 11:00-11:30** **How can the fluctuations in the motion of kayak-paddlers be used to estimate performance? (INVITED)** (pp. 86-87)
*Gergely Vadaí*¹, *Zoltan Gingl*¹
¹University of Szeged, Hungary
- 11:30-11:50** **Is There an Optimal Search Strategy? (ORAL)** (pp. 88-89)
*Michael F. Shlesinger*¹
¹Office of Naval Research ONR, USA

11:50-12:10 A stochastic model for phytoplankton dynamics in the Tyrrhenian Sea. (ORAL) (pp. 90-91)

Davide Valenti¹, Giovanni Denaro¹, Bernardo Spagnolo^{1,2,3}, Fabio Conversano⁴, Christophe Brunet⁴

¹Università di Palermo, Italy, ²Lobachevsky State University, Russia, ³INFN Catania, Italy, ⁴Stazione Zoologica Anton Dohrn, Italy

12:10-14:50 Poster session & Lunch (at the Dining Room of Casa Convalescència)

Theoretical trends in noise and fluctuations (II)

CHAIRMAN: Ludovic Bellon (Université de Lyon, France)

14:50-15:20 All that glitters is not gold: Zero-point energy in the Johnson noise of resistors. (INVITED) (pp. 92-93)

Laszlo B. Kish¹

¹Texas A&M University, USA

15:20-15:40 The spectral characteristics of steady-state Lévy flights in an infinitely deep rectangular potential well. (ORAL) (pp. 94-95)

A. A. Kharcheva¹, A. A. Dubkov¹, B. Spagnolo^{2,3}, D. Valenti²

¹Lobachevsky State University, Russia, ²Università di Palermo, Italy, ³INFN Catania, Italy

15:40-16:00 Stationary states in 2D systems driven by Lévy noises. (ORAL) (pp. 96-97)

B. Dybiec¹, K. Szczepaniec¹

¹Jagiellonian University, Poland

16:00-16:20 Typical pure states and rare events for quantum many-body systems. (ORAL) (pp. 98-99)

Takaaki Monnai¹

¹Seikei University, Japan

16:20-16:50 Coffee Break

Noise in complex and non-linear systems (II)

CHAIRMAN: Derek Abbott (The University of Adelaide, Australia)

16:50-17:10 Degradation Stochastic Resonance Concept: Benefits of Controlled Noise Injection in Adaptive Averaging cell-based Architecture. (ORAL) (pp. 100-101)

Nivard Aymerich¹, Sorin Cotofana², Antonio Rubio³

¹Broadcom Networks Spain, ²Delft University, Netherlands, ³UPC, Spain

17:10-17:30 Noise on resistive switching: a Fokker-Planck approach. (ORAL) (pp. 102-103)

G. A. Patterson¹, D. F. Grosz^{2,3}, P. I. Fierens^{1,2}

¹Instituto Tecnológico de Buenos Aires, Argentina, ²Consejo Nacional de Investigaciones Científicas y Técnicas, Argentina, ³Instituto Balseiro, Argentina

17:30-17:50 Stochastic enhancement of absolute negative mobility. (ORAL) (pp. 104)

Lukasz Machura¹, Jakub Spiechowicz¹, Jerzy Łuczka¹

¹University of Silesia, Poland

17:50-18:10 Cascade Amplification of Fluctuations. (ORAL) (pp. 105-106)

Michael Wilkinson¹, Marc Pradas¹, Robin Guichardaz², Alain Pumir²

¹The Open University, UK, ²Ecole Normale Supérieure de Lyon, France

18:10-18:30 Conversion of mechanical noise into useful electrical energy using piezoelectric 2D Materials. (ORAL) (pp. 107-108)

Gabriel Abadal¹, M. López-Suárez², W. Venstra³, F. Torres¹, L. Gammaitoni², R. Rurali⁴

¹Universitat Autònoma de Barcelona, Spain, ²University of Perugia, Italy, ³Delft University, Netherlands, ⁴ICMAB-CSIC, Spain

20:30 Gala dinner (Museu d'art de Catalunya)

Friday, July 17 2015

Quantum noise and coherence (II)

CHAIRMAN: Paolo Bordone (Università di Modena e Reggio Emilia, Italy)

9:00-9:30 Classical and quantum non-linear dynamics in optomechanical systems. (INVITED)

(pp. 109-110)

Yaroslav M. Blanter¹

¹Delft University of Technology, Netherlands

9:30-9:50 Pauli-Heisenberg Oscillations in Electron Quantum Transport. (ORAL)

(pp. 111-112)

Karl Thibault¹, Julien Gabelli², Christian Lupien¹, Bertrand Reulet¹

¹Université de Sherbrooke, Canada, ²Université Paris-Sud, France

9:50-10:10 **Effects of non-Gaussian α -stable noise sources on the transient dynamics of long Josephson junctions. (ORAL)** (pp. 113-114)

Claudio Guarcello^{1,2}, Davide Valenti¹, Bernardo Spagnolo^{1,2,3}

¹Università di Palermo, Italy, ²Lobachevsky State University, Russia, ³INFN Catania, Italy

10:10-10:30 **On the weak measurement of the electrical THz current: a new source of noise? (ORAL)** (pp. 115-116)

Damiano Marian¹, Nino Zanghì², Xavier Oriols¹

¹Universitat Autònoma de Barcelona, Spain, ²Università di Genova and INFN Genova, Italy

10:30-11:00 **Coffee Break**

Quantum noise and coherence (III)

CHAIRMAN: Yaroslav M. Blanter (Delft University of Technology, Netherlands)

11:00-11:30 **Elementary events and probabilities in time-dependent quantum transport. (ORAL)** (pp. 117-118)

Wolfgang Belzig¹, Mihajlo Vanevic²

¹University of Konstanz, Germany, ²University of Belgrade, Serbia

11:30-11:50 **Electron interferometry in quantum Hall edge channels. (ORAL)** (pp. 119-120)

Jerôme Rech¹, Claire Wahl¹, Thibaut Jonckheere¹, Thierry Martin¹

¹Aix Marseille Université, France

11:50-12:10 **Functional approach to heat-exchange, application to the spin boson model: from Markov to quantum noise regime. (ORAL)** (pp. 121-122)

Matteo Carrega¹, Paolo Solinas¹, Alessandro Braggio¹, Maura Sassetti², Ulrich Weiss³

¹SPIN-CNR, Italy, ²Università di Genova, Italy, ³Universität Stuttgart, Germany

12:10-12:30 **Heat and charge current fluctuations in a thermoelectric quantum dot. (ORAL)** (pp. 123-124)

Adeline Crépieux¹, Fabienne Michélini¹

¹Aix Marseille Université, France

12:30-12:45 **Concluding remarks**

Lino Reggiani¹

¹University of Salento, Italy

POSTER SESSION

- P.01 Non-Gaussian Stochastic Diffusion: Accounting Fourth Cumulant** (pp. 125)
*Boris Grafov*¹
¹A.N. Frumkin Institute of Physical Chemistry and Electrochemistry of Russian Academy of Sciences, Russia
- P.02 Quasi-stable PDF of velocities of accelerated metal clusters on graphite before joining an island** (pp. 126-127)
Ekaterina I. Anashkina^{1,2}, *Aleksey V. Kargovsky*¹, *Olga A. Chichigina*¹, *Alexandra K. Krasnova*¹
¹Lomonosov Moscow State University, Russia, ²Università di Palermo, Italy
- P.03 Random walks in random stochastic environments** (pp. 128-129)
*M. A. García-March*¹, *Gerald J. Lapeyre Jr.*², *Pietro Massignan*¹, and *Maciej Lewenstein*^{1,3}
¹ICFO-Institut de Ciències Fotòniques, Spain, ²IDAEE – Institute of Environmental Assessment and Water Research, Spain, ³ICREA – Institució Catalana de Recerca i Estudis Avançats, Spain
- P.04 Independence of superdiffusion in random low-density Lorentz gas on geometrical properties of moving scatterers** (pp. 130-131)
Alexandra K. Krasnova^{1,2}, *Olga A. Chichigina*¹, *Ekaterina I. Anashkina*¹
¹Moscow State University, Russia, ²Schmidt Institute of Physics of the Earth of the Russian Academy of Sciences, Russia
- P.05 Single molecule measurement of the effective temperature in nonequilibrium steady states** (pp. 132)
*E. Dieterich*¹, *J. Camunas-Soler*^{2,3}, *M. Ribezzi-Crivellari*^{2,3}, *U. Seifert*¹, *F. Ritort*^{2,3}
¹Universität Stuttgart, Germany, ²Universitat de Barcelona, Spain, ³Instituto de Salud Carlos III, Madrid, Spain
- P.06 Finite-frequency noise in a non-interacting quantum dot** (pp. 133-134)
*Redouane Zamoum*¹, *Mirelle Lavagna*², *Adeline Crépieux*³
¹Université de Bouira, Algeria, ²Commissariat à l'Energie Atomique de Grenoble INAC/SPSMS, France, ³Aix Marseille Université, France
- P.07 Features of Noise in Ultrathin Gold Nanowire Structures** (pp. 135-136)
*Volodymyr Handziuk*¹, *Sergii Pud*¹, *Alexandre Kisner*², *Svetlana Vitusevich*¹
¹Forschungszentrum Jülich, Peter Grünberg Institute (PGI 8), Germany, ²Rutgers University, USA
- P.08 High Frequency Cutoff in 1/f Spectra of Hole Doped LaxCa1-xMnO3 Manganite Single Crystals** (pp. 137-138)
*Jacek Przybytek*¹, *Jan Fink-Finowicki*², *Roman Puźniak*², *Grzegorz Jung*^{2,3}
¹University of Warsaw, Poland, ²Institute of Physics PAS, Poland, ³Ben Gurion University of the Negev, Israel

- P.09** **Noise-induced resonance-like phenomena in InP crystals embedded in fluctuating electric fields** (pp. 139-140)
D. Persano Adorno¹, N. Pizzolato¹, P. Alaïmo¹, B. Spagnolo^{1,2}
¹Università di Palermo, Italy, ²INFN Catania, Italy
- P.10** **Study on the origin of 1/f noise in bulk acoustic wave resonators** (pp. 141-142)
F. Sthajl¹, M. Devel¹, J. Imbaud¹, R. Bourquin¹, S. Ghosh¹, G. Cibiel²
¹FEMTO-ST Institute, France, ²CNES, France
- P.11** **The electron transit time is not the ultimate responsible for the high-frequency noise: The frontier between electronics and electromagnetism** (pp. 143-144)
Zhen Zhan¹, E. Colomés¹, A. Benali¹, X. Oriols¹
¹Universitat Autònoma de Barcelona, Spain
- P.12** **Random Telegraph Noise (RTN) analyzed by using Weighted Time Lag Method in Resistive Switching devices** (pp. 145-146)
M. Maestro¹, J. Diaz¹, A. Crespo-Yepes¹, J. Martin-Martinez¹, R. Rodriguez¹, M.B. Gonzalez², F. Campabadal², M. Nafria¹, X. Aymerich¹
¹Universitat Autònoma de Barcelona, Spain, ²Institut de Microelectronica, IMB-CNM (CSIC), Spain
- P.13** **On the Role of Current-Voltage Correlations on the Electric Power Consumption of Electronic Devices** (pp. 147-148)
Guillermo Albareda¹, Fabio Lorenzo Traversa², Xavier Oriols³
¹Universitat de Barcelona, Spain, ²University of California, USA, ³Universitat Autònoma de Barcelona, Spain
- P.14** **1/f^B fluctuations from sequences of rectangular pulses** (pp. 149-150)
Vaidas Juknevičius¹, Bronislovas Kaulakys¹, Julius Ruseckas¹
¹Vilnius University, Lithuania
- P.15** **D'yakonov-Perel' spin decay in the weak scattering regime and the case of graphene** (pp. 151-152)
Xavier Cartoixa¹
¹Universitat Autònoma de Barcelona, Spain
- P.16** **Current Fluctuations Originating from Non-Metallic (Physical) Leads** (pp. 153-154)
Guillermo Albareda¹, Liping Chen², Xavier Oriols³, Ignacio Franco²
¹Universitat de Barcelona, Spain, ²University of Rochester, USA, ³Universitat Autònoma de Barcelona, Spain
- P.17** **Elastic response and secondary structure of single-stranded DNA** (pp. 155)
Xavier Viader-Godoy¹, Joan Camunas-Soler¹, Maria Marti-Prieto¹, Felix Ritort^{1,2}
¹Universitat de Barcelona, Spain, ²Instituto de Salud Carlos III, Madrid, Spain

- P.18** **Thermodynamic and kinetic analysis of a DNA hairpin using optical tweezers and a temperature controller** (pp. 156-157)
Marc Rico Pastó¹, Marco Ribezzi-Crivellari¹, Felix Ritort^{1,2}
¹Universitat de Barcelona, Spain, ²Instituto de Salud Carlos III, Madrid, Spain
- P.19** **Causality analysis of ANS activities by multidimensional directed coherence on body temperatures variations** (pp. 158-159)
Akio Nozawa¹, Shizuka Bando¹
¹Aoyama Gakuin University, Japan
- P.20** **Fluctuations on cancer growth dynamics in Chronic Myeloid Leukemia** (pp. 160-161)
N. Pizzolato¹, D. Persano Adorno¹, D. Valenti¹, B. Spagnolo^{1,2}
¹Università di Palermo, Italy, ²INFN Catania, Italy
- P.21** **Analysis of Fluctuation in Repeated Handwriting Based on Psychophysiological Factors** (pp. 162-163)
Amir Maleki¹, Yuki Oshima¹, Akio Nozawa², Tota Mizuno¹, Masafumi Uchida¹
¹The University of Electro-Communications, Japan, ²Aoyama Gakuin University, Japan
- P.22** **Probabilistic characteristics of noisy Van der Pol type oscillator with polynomial damping** (pp. 164-165)
A. A. Dubkov¹, I. A. Litovsky¹
¹Lobachevsky State University, Russia
- P.23** **Noise activated switching of a levitated nanoparticle in a bistable potential** (pp. 166)
F. Ricci¹, R. A. Rica¹, M. Spasenovic², R. Quidant¹
¹ICFO-Institut de Ciències Fotoniques, Spain, ²University of Belgrade, Serbia
- P.24** **Modeling long-range dependent inverse cubic distributions by nonlinear stochastic differential equations** (pp. 167-168)
Bronislovas Kaulakys¹, Miglius Alaburda¹, Julius Ruseckas¹
¹Vilnius University, Lithuania
- P.25** **Passive and active vibrations allow self-organization in large-scale electromechanical systems** (pp. 169-170)
Arturo Buscarino¹, Carlo Famoso¹, Luigi Fortuna¹, Mattia Frasca¹
¹University of Catania, Italy
- P.26** **Randomness and Earth's climate variability** (pp. 171-172)
Levinshtein M.E.¹, Dergachev V. A.¹, Dmitriev A. P.¹, Smakov P. M.¹
¹Ioffe Institute, Russia

Novel Statistical Physics Approaches to Understanding Economic Fluctuations

H. Eugene Stanley¹

¹*Departments of Physics, Chemistry and Biomedical Engineering, Boston University, Boston, MA 02215
e-mail address: hes@bu.edu*

I. INTRODUCTION

Recent analysis of truly huge quantities of empirical data suggests that classic economic theories not only fail for a few outliers, but that there occur similar outliers of every possible size. Specifically, if one analyzes only a small data set (say 10^4 data points), then outliers appear to occur as “rare events.” However, when we analyze orders of magnitude more data (10^8 data points), we find orders of magnitude more outliers—so ignoring them is not a responsible option, and studying their properties becomes a realistic goal. We find that the statistical properties of these “outliers” are identical to the statistical properties of everyday fluctuations. For example, a histogram giving the number of fluctuations of a given magnitude x for fluctuations ranging in magnitude from everyday fluctuations to extremely rare fluctuations that occur with a probability of only 10^{-8} is a straight line in a double-log plot, so one can quantify the probability of an event of any given size.

II. TWO UNIFYING PRINCIPLES

Two unifying principles that underlie much of the finance analysis we will present are scale invariance and universality.¹ Scale invariance is a property not about algebraic equations but rather about functional equations, which have as their solutions not numbers but rather functional forms power laws, e.g., the solution of the functional equation $f(\lambda x) = \lambda^p f(x)$ is $f(x) = x^p$. The key idea of universality is that the identical set of “scaling laws” hold across diverse markets, and over diverse time periods, e.g., the inverse cubic law for price changes seems to hold for a huge range of indices.

We demonstrate the principles of scaling and universality by describing very recent work.²⁻⁴ Financial market fluctuations are characterized by many abrupt switchings on very short time scales from increasing “microtrends” to decreasing “microtrends”—and vice versa. We ask whether these ubiquitous switching processes have quantifiable features analogous to those present in phase transitions, and find striking scale-free behavior of the time intervals between transactions both before and after the switching occurs. We interpret our findings as being consistent with time-dependent collective behavior of financial market participants.

We demonstrate the principles of scaling and universality by describing very recent advances.³ Financial market fluctuations are characterized by many abrupt switchings on very short time scales from increasing “microtrends”

to decreasing “microtrends”—and vice versa. We ask whether these ubiquitous switching processes have quantifiable features analogous to those present in phase transitions, and find striking scale-free behavior of the time intervals between transactions both before and after the switching occurs. We interpret our findings as being consistent with time-dependent collective behavior of financial market participants.

III. THE FRAGILITY OF INTERDEPENDENCY: INTERDEPENDENT NETWORKS & SWITCHING PHENOMENA IN ECONOMIC SYSTEMS

Recent disasters ranging from financial “shocks” to large-scale power and terrorists attacks dramatically exemplify the fact that the most dangerous vulnerability is hiding in the many interdependencies among different networks. We quantify failures in interconnected networks, and demonstrate the need to consider mutually dependent network properties in designing resilient systems. Specifically, we have uncovered new laws governing the nature of switching phenomena in coupled networks, and found that phenomena that are continuous “second order” phase transitions in isolated networks become discontinuous abrupt “first order” transitions in interdependent networks.^{2,5} For example, we find that the same laws governing the formation and bursting of the largest financial bubbles also govern the tiniest finance bubbles, over a factor of 1,000,000,000 in time scale.^{3,4}

IV. PREDICTING THE FUTURE

Finally, we demonstrate that by analyzing changes in Google query volumes for search terms related to finance, we find patterns that may be early warning signs of stock market moves.⁶ We conclude by discussing the network basis for understanding sudden death in the elderly, and the possibility that financial “flash crashes” are not unlike the catastrophic first-order failure incidents occurring in interdependent networks.⁷

ACKNOWLEDGMENTS

This work was supported by IARPA and ONR, and was carried out in collaboration with a number of colleagues, including S. Havlin (Bar-Ilan), S. V. Buldyrev (Yeshiva), B. Podobnik (Zagreb), T. Preis and H. S. Moat (Warwick), & D. Y. Kenett (BU).

- ¹ R. N. Mantegna and H. E. Stanley, Introduction to Econophysics: Correlations & Complexity in Finance, 2nd Edition (Cambridge University Press, in preparation).
- ² J. Gao, S. V. Buldyrev, H. E. Stanley, and S. Havlin, “Novel Behavior of Networks Formed from Interdependent Networks,” *Nature Physics* **8**, 40 (2012).
- ³ T. Preis, J. Schneider, and H. E. Stanley, “Switching Processes in Financial Markets,” *Proc. Natl. Acad. Sci. USA* **108**, 7674 (2011).
- ⁴ T. Preis and H. E. Stanley, “Bubble Trouble: Can a Law Describe Bubbles and Crashes in Financial Markets?” *Physics World* **24**[5], 29 (May 2011).
- ⁵ S. V. Buldyrev, R. Parshani, G. Paul, H. E. Stanley, and S. Havlin, “Catastrophic Cascade of Failures in Interdependent Networks,” *Nature* **464**, 1025 (2010).
- ⁶ T. Preis, H. S. Moat, and H. E. Stanley, “Quantifying Trading Behavior in Financial Markets Using Google Trends,” *Nature Scientific Reports* **3**, 1684 (2013).
- ⁷ A. Majdandzic, B. Podobnik, S. V. Buldyrev, D. Y. Kenett, S. Havlin, and H. E. Stanley, “Spontaneous Recovery in Dynamical Networks,” *Nature Physics* **10**, 34 (2014).

Active Brownian motion in confined geometries

Vyacheslav R. Misko^{1,2}

¹*Departement Fysica, Universiteit Antwerpen, B-2020 Antwerpen, Belgium*
e-mail address: Vyacheslav.Misko@uantwerpen.be

²*CEMS, RIKEN, Saitama, 351-0198, Japan*

I. INTRODUCTION

Rectification of Brownian motion has been the focus of a concerted effort, both conceptual¹ and technological², aimed at establishing net particle transport on a periodic substrate in the absence of external biases. According to the Pierre Curie's conjecture, two basic ingredients are required for this purpose: a spatial asymmetry of the substrate and a time correlation of the (non-equilibrium) fluctuations.

Brownian diffusion in a narrow, corrugated channel can also be rectified according to Curie's conjecture. Subjected to an a.c. drive, repelling particles drift in the easy-flow direction of such a collective geometric ratchet, where the average compartment corrugation is the less steep³, although with much lower efficiency than in ordinary ratchet potentials. Such collective ratchets have been experimentally demonstrated for a.c. drives and relatively high particle densities⁴, whereas the net current vanishes at low densities³. Rectification of repelling particles in an asymmetric channel can also be induced by time-correlated thermal fluctuations (thermal ratchets). However, being thermal ratchets weak in general and collective geometric ratchets less performing than potential ratchets, demonstration of such an effect seems beyond reach. On the other hand, rectification of Brownian diffusion by an internal energy source, like the nonequilibrium fluctuations invoked to power thermal ratchets, is very appealing: The diffusing particles would harvest kinetic energy directly from their environment, without requiring any externally applied field (though unbiased), and transport would ensue as an *autonomous* symmetry-directed particle flow.

To enhance rectification of time correlated-diffusion in a modulated channel with zero drives, we propose⁶ to use active, or self-propelled, Brownian particles. Recently, a new type of microswimmers has been synthesized, where self-propulsion takes advantage of the local gradients that asymmetric particles can generate in the presence of an external energy source (self-phoretic effect). Such particles, called Janus particles⁵, consist of two distinct "faces", only one of which is chemically or physically active. Such two-faced objects can induce either concentration gradients, by catalyzing some chemical reaction on their active surface, or thermal gradients, by inhomogeneous light absorption (self-thermophoresis) or magnetic excitation (magnetically induced self-thermophoresis). We also demonstrated the ability of Janus microswimmers to and separate colloidal mixtures, due to their selective interaction with the constituents of the mixture⁷.

II. ACTIVE SWIMMER IN A CHANNEL

An active microswimmer acquires a continuous push from the environment, which in the overdamped regime corresponds to a self-propulsion velocity \vec{v}_0 with constant modulus v_0 and direction randomly varying in time with rate τ_θ^{-1} . In a two-dimensional (2D) boundless suspension, the position $\vec{r}(t) = (x(t), y(t))$ of the microswimmer diffuses according to F urth's law $\langle \Delta \vec{r}(t)^2 \rangle = 4(D_0 + v_0^2 \tau_\theta / 4)t + (v_0^2 \tau_\theta^2 / 2)(e^{-2t/\tau_\theta} - 1)$, where $\Delta \vec{r}(t) = \vec{r}(t) - \vec{r}(0)$ and D_0 is the translational diffusion constant of a passive particle of the same geometry at a fixed temperature. The mechanisms responsible for translational and rotational diffusion are not necessarily the same and therefore D_0 , v_0 and τ_θ can be treated as independent model parameters. The F urth's diffusion law is due to the combined action of two statistically independent 2D Gaussian noise sources⁸, a delta-correlated thermal noise, $\vec{\xi}_0(t)$ and a colored effective propulsion noise, $\vec{\xi}_c(t)$, with correlation functions $\langle \xi_{0,i}(t) \rangle = 0$, $\langle \xi_{c,i}(t) \rangle = 0$, $\langle \xi_{0,i}(t) \xi_{0,j}(0) \rangle = 2D_0 \delta_{ij} \delta(t)$, and $\langle \xi_{c,i}(t) \xi_{c,j}(0) \rangle = 2(D_c / \tau_\theta) \delta_{ij} e^{-2|t|/\tau_\theta}$, with $i, j = x, y$ and $D_c = v_0^2 \tau_\theta / 4$. Correspondingly, the microswimmer mean self-propulsion path is $l_\theta = v_0 \tau_\theta$.

In a channel, with compartment size smaller than l_θ , the microswimmer undergoes multiple collisions with the walls and the confining geometry comes into play (Knudsen diffusion). Contrary to standard thermal ratchets in asymmetric potentials⁹, where the strength of the colored noise is kept constant, here D_c grows linearly with τ_θ (i.e., the variance of $\vec{\xi}_c(t)$ is set to v_0^2). As a consequence, increasing τ_θ not only makes geometric rectification effective even in the case of a single particle, but also enhances the power dissipated to fuel its self-propulsion. As a result, rectification in active Brownian ratchets can be so much stronger than in ordinary thermal ratchets that *direct observation* becomes possible.

III. AUTONOMOUS JANUS RATCHET

The rectification of a Janus particle in a 2D asymmetric channel was simulated⁶ by numerically integrating the Langevin equations⁸, $\dot{x} = v_0 \cos \theta + \xi_{0,x}(t)$, $\dot{y} = v_0 \sin \theta + \xi_{0,y}(t)$, $\dot{\theta} = \xi_\theta(t)$, where $\xi_{0,x}(t)$ and $\xi_{0,y}(t)$ have been defined above and $\xi_\theta(t)$ is an additional 1D Gaussian noise with $\langle \xi_\theta(t) \rangle = 0$ and $\langle \xi_\theta(t) \xi_\theta(0) \rangle = 2D_\theta \delta(t)$, modeling the fluctuations of the self-propulsion angle θ , measured, say, with respect to the *positive* channel easy-flow direction.

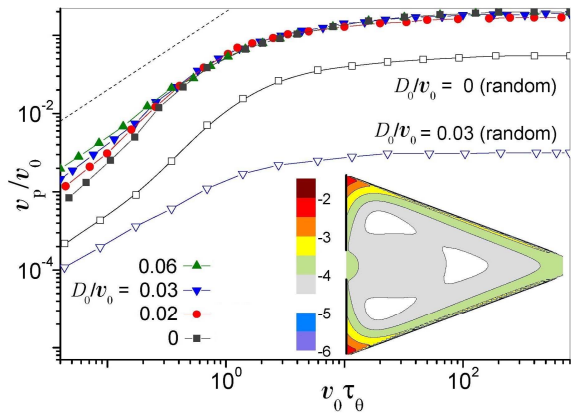


FIG. 1. Rectification of a single pointlike Janus particle with self-propulsion speed v_0 in a triangular channel with compartment size $x_L = y_L = 1$: the average velocity \bar{v} vs. τ_θ for channel pore size $\Delta = 0.1$, different D_0 and sliding (filled symbols) or randomized b.c. (empty symbols). probability density $P(x, y)$ in a channel compartment. [After Ref. 6].

Fig. 1 shows the results⁶ for the rectification current, $v_p \equiv \langle \dot{x} \rangle$ (in units of v_0), of a pointlike Janus particle in a triangular channel with fixed compartment dimensions and varying τ_θ . At large τ_θ , microswimmer diffusion is of the Knudsen type and rectification is dominated by self-propulsion; all curves $\bar{v}(\tau_\theta)$ increase monotonously with τ_θ until they level off. The curves $v_p(\tau_\theta)$ at low τ_θ shift upwards on raising the thermal noise level D_0 , therefore, thermal noise *assists* the rectification process. At large τ_θ the rectification power is *suppressed* by the thermal fluctuations⁶: $\xi_0(t)$ assists the Janus particle to bypass the compartment corners. Therefore, the diode-funneling effect exerted by the triangular compartments can be either enhanced or weakened by delta-correlated fluctuations.

IV. BINARY MIXTURES SEPARATION

We proposed⁷ a new mechanism of binary mixtures separation, using self-propelled Janus microswimmers. The average velocity (along the channel) $\langle V_x \rangle$ of particles A and B versus the effective self-propulsion force

\vec{F}_{drx} is shown in Fig. 2. In general case, particles A (small) move *faster* than their counterpart. We distinguish four regimes. (1): *Rigid body motion*. (2): *Inverse velocity motion*. This unusual behavior is explained by the stronger interaction of the MS with particles B than with particles A. As a consequence, particles B are carried along by the MS while the dynamical friction due to the particle motion is very small in this case and can be neglected. (3): *Strong flow separation*. With increasing velocity, the dynamical friction becomes increasingly important, and type A particles (characterized by a larger self-diffusion coefficient) move faster. (4): *Fast MS motion*. At large F_{drx} , the system undergoes a transition to a “quasi-rigid body” regime when the MS moves too fast to produce any response of the binary system.

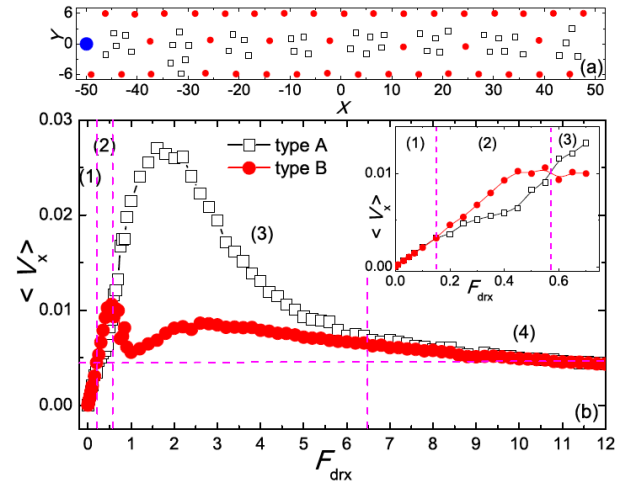


FIG. 2. (a) Equilibrium configuration of a system with equal number of particles of the two species $N_A = N_B = 40$. (b) The average velocity of particles of type A, $\langle V_x^A \rangle$ (open squares) and B, $\langle V_x^B \rangle$ (red dots), as a function of F_{drx} . The MS is shown by a blue filled circle. [After Ref. 7].

ACKNOWLEDGMENTS

We thank RICC for computational resources. We acknowledge support from the Odysseus Program of the Flemish Government and FWO-VI.

¹ P. Reimann, Phys. Rep. **361**, 57 (2002).
² P. Hänggi and F. Marchesoni, Rev. Mod. Phys. **81**, 387 (2009); P. Hanggi, F. Marchesoni, F. Nori, Brownian motors, Annalen der Physik **14**, 51 (2005).
³ J.F. Wambaugh, C. Reichhardt, C.J. Olson, F. Marchesoni, and F. Nori, Phys. Rev. Lett. **83**, 5106 (1999).
⁴ J.E. Villegas *et al.*, Science **302**, 1188 (2003); Y. Togawa *et al.*, Phys. Rev. Lett. **95**, 087002 (2005); C.C. de Souza Silva *et al.*, Nature **440**, 651 (2006); N.S. Lin, T.W. Heitmann, K. Yu, B.L.T. Plourde, and V.R. Misko, Phys. Rev. B **84**, 144511 (2011).

⁵ S. Jiang and S. Granick (Eds.), *Janus Particle Synthesis, Self-Assembly and Applications* (RSC Publishing, Cambridge, 2012).
⁶ P.K. Ghosh, V.R. Misko, F. Marchesoni, and F. Nori, Phys. Rev. Lett. **110**, 268301 (2013).
⁷ W. Yang, V.R. Misko, K. Nelissen, M. Kong, and F.M. Peeters, Soft Matter **8**, 5175 (2012).
⁸ Y. Fily and M.C. Marchetti, Phys. Rev. Lett. **108**, 235702 (2012).
⁹ R. Bartussek, P. Reimann, and P. Hänggi, Phys. Rev. Lett. **76**, 1166 (1996).

Brownian motion and weak ergodicity breaking

P. Massignan,¹ C. Manzo,¹ J. A. Torreno-Pina,¹ M. F. García-Parajo,¹ M. Lewenstein,¹ and G.J. Lapeyre, Jr.¹

¹*ICFO, The Institute of Photonic Sciences, Castelldefels Spain*
e-mail address: john.lapeyre@icfo.es

I. INTRODUCTION

Non-ergodicity observed in single-particle tracking experiments is usually modeled by transient trapping rather than spatial disorder. I will talk about our models¹ of a particle undergoing Brownian motion in a medium with inhomogeneous random diffusivities, but no traps. For some values of model parameters, we find that the mean squared displacement displays subdiffusion due to non-ergodicity for both annealed and quenched disorder. This is significant because Brownian motion itself is the prototypical example of ergodic, normal, diffusion. I will also discuss recent results on extensions of these models to quenched 2-d disorder.

The significance of this work is best understood in the context of unanswered questions in the study of naturally occurring stochastic transport. Consider, for example, receptors (molecules) diffusing laterally in the cell membrane. In this setting, these questions include, “To what extent do tracking data point to ergodic or non-ergodic processes”, and, “What are the physical/structural mechanisms behind these processes?”. In the case that non-ergodic processes are observed, basic characteristics of traps, such as their size or physical origin are not known. Furthermore, the present work shows that it is not even necessary to assume the presence of traps. We have, in fact, found that there are systems for which inhomogeneity provides a quantitatively more accurate description than than traps².

In the talk, I will focus mainly on the theoretical story, touching only briefly on the application to real systems.

II. MODEL

In our models of diffusion in inhomogeneous media, one may assume annealed or quenched disorder. For concreteness, we introduce here a particular annealed model. We consider a particle that undergoes Brownian motion with a random diffusivity for a random time. Then, new, independent random diffusivities and times are chosen and the particle again undergoes Brownian motion. This process is repeated. The asymptotic behavior, in particular the mean squared displacement, shows either ordinary or anomalous behavior with weak-ergodicity breaking depending on the model parameters.

More precisely, consider sequences of random variables, the diffusivities $\{D_j\}$ and the transit times $\{\tau_j\}$. The elements of $\{D_j\}$ are identically distributed as are the elements of $\{\tau_j\}$. All pairs are independently distributed with the exception of pairs (D_j, τ_j) , for all j . We assume the (common) probability density function (PDF) for D_j

has the form

$$P_D(D) \sim D^{\sigma-1} \quad \text{with } \sigma > 0, \quad (1)$$

for small D . Furthermore, we require that the PDF for transit times τ conditioned on D , $P_\tau(\tau|D)$, has mean

$$E[\tau|D] = D^{-\gamma} \quad \text{with } -\infty < \gamma < \infty, \quad (2)$$

with all moments $P_\tau(\tau|D)$ being finite. In this simple case, the two parameters σ and γ characterize the model completely.

We analyzed this model in a generalized continuous time random walk framework using Fourier-Laplace transforms. In particular, the asymptotic ensemble averaged mean-squared displacement (MSD) is

$$\langle x^2(t) \rangle \sim t^\beta \quad \text{with } 0 \leq \beta \leq 1, \quad (3)$$

and β taking values depending on the model parameters as shown in Tab. (1). Exponents for the model in one-dimension when the diffusivities are quenched (fixed in space for the duration of the walk) are also shown.

	(0)	(I)	(II)
	$\gamma < \sigma$	$\sigma < \gamma < \sigma + 1$	$\sigma + 1 < \gamma$
Annealed	1	σ/γ	$1 - 1/\gamma$
Quenched 1d	1	$2\sigma/(\sigma + \gamma)$	Unknown

TAB. 1. Ensemble averaged MSD exponent β in (3) for the annealed model, and the one-dimensional quenched model, as a function of σ and γ defined in (1) and (2). The exponent β for the 1D quenched case in region II is unknown at present.

By itself, the anomalous exponent in (3) is not enough to demonstrate weak ergodicity breaking. However with some additional assumptions, which are supported by Monte Carlo studies, one finds that the result of performing both the ensemble averaged and the time averaged MSD has the asymptotic form

$$\overline{\langle x^2(t) \rangle}_T \sim T^{\beta-1} t \quad \text{for } t \ll T \quad (4)$$

where T is the observation time over which time averages of functions of the lag time t are performed. The most significant feature of (4) is that it is not equal to the ensemble averaged quantity in (3). That is, the motion is not ergodic. Furthermore, as is the case with the standard continuous time random walk, for short lag times t , the particle shows ordinary diffusion.

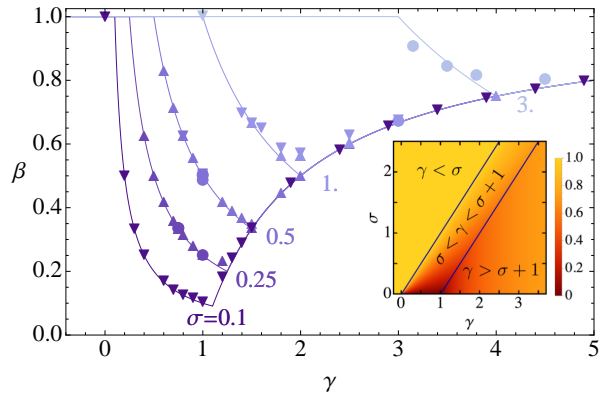


FIG. 1: Exponent β in (3) for annealed models. Lines are analytic results as in Tab. (1), for various values of σ indicated in the figure. Symbols are numerical simulations. Numerical estimates of β are extracted by fitting Monte Carlo simulations of the ensemble average of annealed models (\blacktriangledown and \blacktriangle) to (3), and simulations of the combined time-ensemble average (circles) to (4). The inset shows a density plot of β vs. both γ and σ .

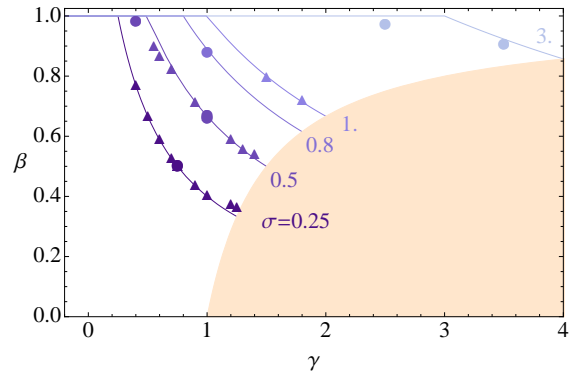


FIG. 2: Exponent β in (3) for the 1d quenched model. Lines as in Fig. 1. Symbols are exponents extracted from numerical simulations of the ensemble MSD (\blacktriangle) and time-ensemble MSD (circles). Lines and symbols vary from dark to light with increasing σ . Shading indicates region (II), where the exponent is at present unknown.

The analytically determined exponents and Monte Carlo estimates for the annealed model are plotted in Fig. (1). The lines in the figure were drawn by fixing σ at a sequence of values and varying γ along the coordinate axis, computing the analytic expression for β . The points correspond to Monte Carlo estimates of β computed for various values of σ and γ . An analogous plot for the 1-d annealed case is shown in Fig. (2) We are currently studying higher-dimensional quenched models. For many situations (specifically, when spatial correlations are not important), we expect to recover the annealed exponents.

To reiterate, the significance of this work in the context of this conference is that it provides a clear example of the fact the the characterization of the possible subdiffusive processes arising from disorder is far from closed. In particular, if the distribution of diffusivities is anomalous, even ordinary Brownian motion can exhibit anomalous statistics.

¹ Non-ergodic subdiffusion from Brownian motion in an inhomogeneous medium, P. Massignan, C. Manzo, J. A. Torreno-Pina, M. F. Garca-Parajo, M. Lewenstein, and G. J. Lapeyre Jr Phys. Rev. Lett. **112**, 150603 (2014).

² Weak ergodicity breaking of receptor motion in living cells stemming from random diffusivity, C Manzo, J.A. Torreno-Pina, P. Massignan, G.J. Lapeyre Jr, M. Lewenstein, and M.F. Garcia-Parajo Accepted for publication in Phys. Rev. X., arxiv:1407.2552

Brownian motors in the micro-scale domain: Enhancement of efficiency by noise

Jakub Spiechowicz,¹ Peter Hänggi,² and Jerzy Luczka^{1,3}¹University of Silesia, Institute of Physics, 40-007 Katowice, Poland*²University of Augsburg, Institute of Physics, 86135 Augsburg, Germany³Silesian Center for Education and Interdisciplinary Research, University of Silesia, 41-500 Chorzów, Poland

Transport occurring in the micro-scale domain is strongly influenced by fluctuations and random perturbations. The impact has seemed to be usually destructive, i.e. transport is weakened with respect to such quantifiers like averaged velocity or current. However, a constructive role of both equilibrium and non-equilibrium fluctuations has since been demonstrated for many situations with the occurrence of several intriguing, noise-assisted phenomena such as Brownian ratchets¹, stochastic resonance², molecular motors and machines³, genetic and biochemical regulatory systems^{4,5}, intracellular transport⁶, to mention only a few. Fluctuations and noise may enhance the average velocity, reverse the natural transport direction, or induce anomalous transport processes.

We study a noisy drive mechanism for efficiency enhancement of Brownian motors operating on the microscale domain. It was proven⁷ that biased noise $\eta(t)$ can induce normal and anomalous transport processes⁸ similar to those generated by a static force F acting on inertial Brownian particles in a *reflection-symmetric* periodic structure in the presence of *symmetric* unbiased time-periodic driving. Here, we show that within selected parameter regimes, noise $\eta(t)$ of the mean value $\eta(t) = F$ can be significantly more effective than the deterministic force F : the motor can move much faster, its velocity fluctuations are much smaller, and the motor efficiency increases several times⁹. These features hold true in both normal and absolute negative mobility regimes. We demonstrate this with detailed simulations by resource to generalized white Poissonian noise.

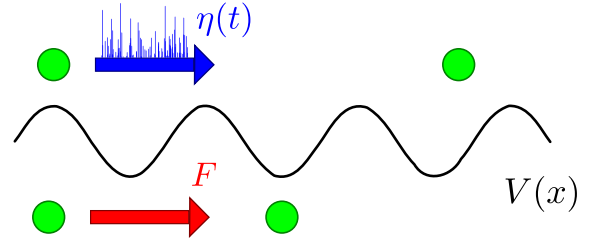


FIG. 1. Brownian motors moving in symmetric periodic structures in the presence of an unbiased harmonic force and driven by a static, biasing force F can be transported much faster and in a more effective way when F is replaced by noise $\eta(t)$ of equal average bias $\eta(t) = F$.

Our theoretical results can be tested and corroborated experimentally by use of a setup that consists of a resistively and capacitively shunted Josephson junction. The suggested strategy to replace F by $\eta(t)$ may provide a new operating principle in which micro- and nanomotors could be powered by biased noise.

Yet, a number of open questions of the studied system still remain to be answered. Prominent examples of such problems may include the following: Does the main conclusion of this work hold true also for other models of non-equilibrium perturbation? Is the inherent non-linearity of the system necessary for the observation of this effect? Can this phenomenon be detected also in the limiting case of over-damped dynamics? Is our proposed strategy of the efficiency enhancement *universal* and may be realized both in classical and quantum systems?..

* j.spiechowicz@gmail.com

¹ P. Hänggi and F. Marchesoni, Rev. Mod. Phys. **81**, 387 (2009).² L. Gammaitoni, P. Hänggi, P. Jung and F. Marchesoni, Rev. Mod. Phys. **70**, 223 (1998).³ M. Schliwa (ed.), *Molecular Motors* (Viley-VCH, Weinheim, 2003).⁴ E. R. Kay, Angew. Chem. Int. Ed. **46**, 72 (2007).⁵ R. Steuer, C. Zhou, J. Kürths, Biosystems **72**, 241 (2003).⁶ P. C. Bressloff and J. M. Newby, Rev. Mod. Phys. **85**, 135 (2013).⁷ J. Spiechowicz, J. Luczka and P. Hänggi, J. Stat. Mech. **P02044**, (2013).⁸ L. Machura, M. Kostur, P. Talkner, J. Luczka and P. Hänggi, Phys. Rev. Lett. **98**, 40601 (2007).⁹ J. Spiechowicz, P. Hänggi and J. Luczka, Phys. Rev. E **90**, 032104 (2014).

Unconditional security in practical Kirchhoff-law–Johnson-noise key exchangers

Barry Chen¹, Laszlo B. Kish¹, Claes G. Granqvist², Robert Mingesz³, and Zoltan Gingl³

¹ Department of Electrical and Computer Engineering, Texas A&M University, College Station, TX 77843-3128, USA

e-mail address: barrychen@tamu.edu ; Laszlokish@tamu.edu

² Department of Engineering Sciences, The Ångström Laboratory, Uppsala University, P. O. Box 534, SE-75121 Uppsala, Sweden

e-mail address: Claes-Goran.Granqvist@angstrom.uu.se

³ Department of Technical Informatics, University of Szeged, Szeged-6720, Hungary

e-mail address: mingesz@inf.u-szeged.hu ; gingl@inf.u-szeged.hu

In physical secure key exchangers, the mathematical definition of the unconditional security¹ of the distributed keys is that the probability p of successfully guessing the bit by Eve can arbitrarily approach the value 0.5 when enough resources are available to Alice and Bob. One should note that this definition supposes a technically unlimited Eve, which means that the speed and accuracy of Eve’s measurements are curtailed only by the laws of physics and by rules of the protocol. For example, while Eve’s technical skills are unlimited she still cannot violate the *Second Law of Thermodynamics* or the *Quantum No-Cloning Theorem*, and she cannot record a *longer* sample of the signal than its *actual cut-off length* set by the protocol of Alice and Bob, who are in control of gating the signal. Similarly, Eve cannot utilize higher bandwidth with non-zero frequency components than the actual bandwidth set by Alice and Bob. Alternative definitions of unconditional security are based on statistical distance measures^{2,3} between the shared keys and ideal, perfectly secure keys, but these definitions are equivalent with the above one when the key bits are *identical, independently distributed* random variables¹.

Whereas the unconditional security of practical quantum key distribution (QKD) systems is still debated²⁻⁴, the classical physical Kirchhoff-law–Johnson-noise (KLJN) key exchange scheme^{1,5-24} (Figure 1) has a general security proof¹ that is valid even for practical, weakly non-ideal situations.

The unconditional security¹ against *passive* attacks in the *ideal* KLJN scheme is founded on the Second Law of Thermodynamics^{1,5-8}, Kirchhoff’s Loop Law and the statistical properties of Gaussian noise^{1,4,6,10,11}. For *active* (invasive) attacks^{1,5,6,9}, however, an additional law is required: the information limit posed by *Nyquist’s Sampling Theorem* for signals with finite length and bandwidth^{1,5,6,9}. For the practical cases with weak non-ideality, an additional, fundamental rule applies to offer unconditional security, namely, the continuity of classical physical functions in linear systems and in stable non-linear systems¹. As an example, will also show a new (capacitance) attack type with the so far highest success rate and the defense against it.

Important practical applications of KLJN¹²⁻¹⁵, impose the less fundamental but still essential question:

How much would it take in terms of resources to reach a prescribed (outstanding) security level?

Various ways have been proposed to reduce *practical* information leaks based on non-ideal components^{7,8}, and the extraordinarily small^{16,17} bit-error probabilities (after error removal) in the KLJN scheme allow plenty of privacy amplification¹⁸ to further diminish the information leak under laboratory conditions²⁰ to imperceptible levels. Still, important attack types have not been analyzed for practical conditions, such as:

- (i) information leak due to propagation delays in steady-state conditions, and
- (ii) information leak due to propagation delays at transients.

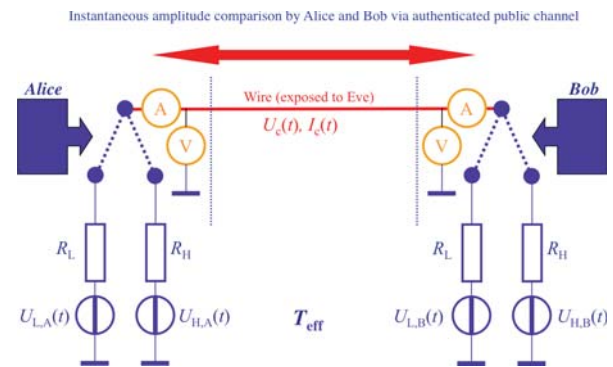


Figure 1. Schematic of the Kirchhoff-law–Johnson-noise (KLJN) secure key exchange system. At the beginning of the key exchange, Alice and Bob make a random choice from the resistors representing the two bit-values and connect the selected one to the wire. Then they execute passive and public current/voltage noise measurements on the cable and, based on these data, they determine the total loop resistance from the Johnson formula. The unknown resistance at the other end of the cable is then the difference between their own resistor and the total loop resistance. Eve does not know any of the connected resistor values; thus for her the loop resistance tells only if a secure bit exchange was performed (High/Low or Low/High situation). The High/High and Low/Low situations are not secure, and those bits are discarded. To defend against active and hacking attacks, the cable parameters and cable integrity are randomly monitored; the instantaneous voltage $U_c(t)$ and current $I_c(t)$ amplitudes in the cable are measured and compared via public authenticated data exchange, and full spectral and statistical analysis/checking is carried out by Alice and Bob. R , t and T_{eff} denote resistance, time and effective temperature, respectively. Line filters, *etc.*, are not shown. The effective noise temperature of the generators is public knowledge and is very much higher than room temperature (800 million to 800 billion Kelvin during an experimental demonstration²⁰).

Concerning item (i), Pao-Lo Liu, with a model-KLJN scheme²⁵, proved that, in the steady-state, even if propagating signal components were known in the two directions (by a directional coupler), the KLJN system would have remained perfectly secure. Gunn–Allison–Abbott (GAA)²¹ recently tried to build a directional coupler for a new attack scheme by utilizing propagation effects during steady-state conditions, and their experiments seemed to demonstrate a huge information leak even under quasi-ideal conditions. However, subsequent careful studies clarified that the GAA scheme²¹ was flawed at all levels²²⁻²⁴; fundamentally, conceptually and experimentally. Moreover,

provided that the KLJN system is implemented with care, GAA's scheme²¹ actually yields less information leak than in an old cable-resistance attack²³. Furthermore, and analogously to the old situation, even this small leak can completely be nullified by the protocol⁸ eliminating wire resistance based attacks, which also indicates that the scheme is a wire loss based attack. Nevertheless the GAA attack and its analysis were beneficial by highlighting that security is a very serious matter and that a KLJN system, which is able to approach the security of idealized situations, requires very careful and thorough design even though its principle circuit looks relatively simple.

In conclusion, currently there is no successful attack against the KLJN scheme that is able to extract information from propagation effects under *steady-state* conditions.

Concerning item (ii), which considers *transient* effects, the situation is similar. Such effects should provide some information leak at the beginning and/or end of the key-exchange period. While a generic analysis shows⁵ that unconditional security cannot be challenged by this kind of attack, it is essential to consider such attacks schemes in order to estimate the required

resources in a practical KLJN design.

However, we have not yet seen any serious attack against even the most primitive transient protocol, such as ramping up/down the noise at the beginning/end of the measurement²⁰. Such transient protection, when done in the simplest way²⁰, protects only against high-frequency reflections and its excessive information leak however it still leaks out about a single-point noise measurement information²⁵, (which can easily be eliminated).

So far, the most elaborate transient defense protocol has embodied a simple random walk of resistance values and noise envelopes until they reach the desired values⁷.

But there must be transient-based attacks on the KLJN scheme—at least intuition suggests that would extract information even in such a case. What are those schemes and what ways can they be eliminated?

These represent important unanswered questions which are open for future research.

- ¹ L.B. Kish, C.G. Granqvist, "On the security of the Kirchhoff-law–Johnson-noise (KLJN) Communicator", *Quantum Inf. Process.* **13**, 2213–2219 (2014).
- ² H.P. Yuen, "Essential lack of security proof in quantum key distribution", arXiv:1310.0842 (2013).
- ³ O. Hirota, "Incompleteness and limit of quantum key distribution theory", arXiv:1208.2106 (2012).
- ⁴ N. Jain, E. Anisimova, I. Khan, V. Makarov, C. Marquardt, G. Leuchs, "Trojan-horse attacks threaten the security of practical quantum cryptography", *New J. Phys.* **16**, 123030 (2014).
- ⁵ L.B. Kish, D. Abbott, C.G. Granqvist, "Critical analysis of the Bennett–Riedel attack on secure cryptographic key distributions via the Kirchhoff-law–Johnson-noise scheme", *PLoS ONE* **8** (2013) e81810.
- ⁶ L.B. Kish, "Totally secure classical communication utilizing Johnson (-like) noise and Kirchoff's law", *Phys. Lett. A* **352**, 178–182 (2006).
- ⁷ L.B. Kish, "Enhanced secure key exchange systems based on the Johnson-noise scheme", *Metrol. Meas. Syst.* **20**, 191–204 (2013).
- ⁸ L.B. Kish, C.G. Granqvist, "Elimination of a Second-Law-attack, and all cable-resistance-based attacks, in the Kirchhoff-law–Johnson-noise (KLJN) secure key exchange system", *Entropy* **16**, 5223–5231 (2014).
- ⁹ L.B. Kish, "Protection against the man-in-the-middle-attack for the Kirchhoff-loop–Johnson(-like)-noise cipher and expansion by voltage-based security", *Fluct. Noise Lett.* **6**, L57–L63 (2006).
- ¹⁰ Z. Gingl, R. Mingesz, "Noise properties in the ideal Kirchhoff-law–Johnson-noise secure communication system", *PLoS ONE* **9**, e96109 (2014).
- ¹¹ R. Mingesz, G. Vadai, Z. Gingl, "What kind of noise guarantees security for the Kirchhoff-loop–Johnson-noise key exchange?" *Fluct. Noise Lett.* **13**, 1450021 (2014).
- ¹² L.B. Kish, Ch. Kwan, "Physical uncloneable function hardware keys utilizing Kirchhoff-law–Johnson-noise secure key exchange and noise-based logic", *Fluct. Noise Lett.* **12** (2013) 1350018.
- ¹³ L.B. Kish, O. Saidi, "Unconditionally secure computers, algorithms and hardware, such as memories, *Fluct. Noise Lett.* **8** (2008) L95–L98.

- ¹⁴ E. Gonzalez, L.B. Kish, R. Balog, P. Enjeti, *PLoS ONE* **8** (2013) e70206.
- ¹⁵ Y. Saez, X. Cao, L. B. Kish, G. Pesti, "Securing vehicle communication systems by the KLJN key exchange protocol", *Fluct. Noise Lett.* **13** (2014) 1450020.
- ¹⁶ Y. Saez, L.B. Kish, R. Mingesz, Z. Gingl, C.G. Granqvist, "Current and voltage based bit errors and their combined mitigation for the Kirchhoff-law–Johnson-noise secure key exchange", *J. Comput. Elect.* **13**, 271–277 (2014).
- ¹⁷ Y. Saez, L.B. Kish, "Errors and their mitigation at the Kirchhoff-law–Johnson-noise secure key exchange", *PLoS ONE* **8**, e81103 (2013).
- ¹⁸ T. Horvath, L.B. Kish, J. Scheuer, "Effective privacy amplification for secure classical communications", *EPL* **94**, 28002 (2011).
- ¹⁹ J. Smulko, "Performance analysis of the 'intelligent' Kirchhoff's-law–Johnson-noise secure key exchange", *Fluct. Noise Lett.* **13**, 1450024 (2014).
- ²⁰ R. Mingesz, Z. Gingl, L.B. Kish, "Johnson-like-noise–Kirchhoff-loop based secure classical communicator characteristics, for ranges of two thousand kilometers, via model-line", *Phys. Lett. A* **372**, 978–984 (2008).
- ²¹ L.J. Gunn, A. Allison, D. Abbott, "A directional wave measurement attack against the Kish key distribution system", *Sci. Reports* **4**, 6461 (2014).
- ²² H.P. Chen, L.B. Kish, C.G. Granqvist, G. Schmera, "Do electromagnetic waves exist in a short cable at low frequencies? What does physics say?" *Fluct. Noise Lett.* **13**, 1450016, (2014).
- ²³ H.P. Chen, L.B. Kish, C.G. Granqvist, G. Schmera, "On the 'cracking' scheme in the paper 'A directional coupler attack against the Kish key distribution system' by Gunn, Allison and Abbott", *Metrol. Meas. Syst.* **21**, 389–400 (2014).
- ²⁴ L.B. Kish, Z. Gingl, R. Mingesz, G. Vadai, J. Smulko, C.G. Granqvist, "Analysis of an attenuator artifact in an experimental attack by Gunn-Allison-Abbott against the Kirchhoff-law–Johnson-noise (KLJN) secure key exchange system", *Fluct. Noise Lett.* **14**, 1550011 (2015).
- ²⁵ P.L. Liu, "A key agreement protocol using band-limited random signals and feedback", *IEEE J. Lightwave Tech.* **27** (2009) 5230–5234.
- ²⁶ L. Gunn, A. Allison, D. Abbott, to be published.

Rates of rare events: scaling, fragility, and delay effects

Mark I. Dykman¹

¹*Department of Physics and Astronomy, Michigan State University, East Lansing, MI 48824, USA*
e-mail address: dykman@pa.msu.edu

I. INTRODUCTION

We consider the tails of the probability distribution and the escape rates in classical and quantum systems away from thermal equilibrium. These characteristics and the very mechanisms of the appropriate large rare fluctuations display features, which have no analogs in equilibrium systems. An example is switching between coexisting stable periodic states due to quantum fluctuations via the mechanism, which we call quantum activation and which is neither tunneling nor classical activation.¹ Despite the fact that there are no known general principles, which would describe the rates of rare events, these rates display some universal features. In particular, they display scaling behavior near bifurcation points where the number of the stable states changes. We will describe this behavior and provide a comparison with the experiment. We will also discuss the effect of fragility of the switching rates. This effect consists in the nonanalytic dependence of the logarithms of the rates on the system parameters in the relevant limit. It has been found in such diverse problems as population dynamics and nonequilibrium quantum fluctuations. However, the general nature of the fragility remains elusive, this is an unsolved problem of noise. We will also outline the results on rare fluctuations in classical systems with delayed dissipation. In such systems, the most probable paths followed in fluctuations to a given state or in switching are given by acausal equations. This leads to nontrivial consequences and a strong modification of the rates even for small delay.

II. QUANTUM ACTIVATION

A reliable platform for studying quantum phenomena away from thermal equilibrium is provided by resonantly modulated vibrational systems, such as modes of superconducting cavities or plasma vibrations of Josephson junctions. These modes (oscillators) have a small decay rate Γ compared to the eigenfrequency ω_0 and weak nonlinearity. When driven close to ω_0 or parametrically modulated close to $2\omega_0$, they display almost sinusoidal vibrations. However, when the driving amplitude F is not too small, because of the interplay between the weak nonlinearity and slow decay, they can have several coexisting vibrational states.

The coupling of a driven oscillator to a thermal reservoir leads to quantum noise. This noise and the motion of the oscillator as a whole can be conveniently described in the rotating wave approximation (RWA). For fairly general assumptions about the coupling, on times slow

compared to the vibration period $2\pi/\omega_0$ one can derive a quantum Langevin equation for the scaled dimensionless coordinate Q and momentum P in the rotating frame. It can be written as

$$\begin{aligned}\dot{Q} &= -i\tilde{\hbar}^{-1}[Q, \hat{g}] - Q + \hat{f}_Q(\tau), \\ \dot{P} &= -i\tilde{\hbar}^{-1}[P, \hat{g}] - P + \hat{f}_P(\tau).\end{aligned}\quad (1)$$

Here, $\tilde{\hbar}$ is the scaled dimensionless Planck constant and \hat{g} is the Hamiltonian of the driven oscillator in the rotating frame. It does not depend on time in the RWA. The explicit form of $\tilde{\hbar}$ and \hat{g} is given in Ref. 1. The eigenvalues of the operator \hat{g} give the scaled quasienergy of the periodically driven oscillator.

In Eq. (1), $\hat{f}_{Q,P}$ are quantum noise operators. The noise is δ -correlated in slow time,

$$\begin{aligned}\langle \hat{f}_Q(\tau) \hat{f}_Q(\tau') \rangle &= \langle \hat{f}_P(\tau) \hat{f}_P(\tau') \rangle = \tilde{\hbar}(2\bar{n} + 1)\delta(\tau - \tau'), \\ \langle [\hat{f}_Q(\tau), \hat{f}_P(\tau')] \rangle &= 2i\tilde{\hbar}\delta(\tau - \tau');\end{aligned}\quad (2)$$

$\bar{n} = [\exp(\hbar\omega_0/k_B T) - 1]^{-1}$ is the oscillator Planck number.

Equations (1) simplify for the values of the driving field F and its frequency ω_F close to the bifurcation points where the number of the stable states changes. Here, one of the motions in the system becomes slow, there emerges a soft mode with coordinate \tilde{Q} , which is a linear combination of Q and P . The dynamics of this mode is essentially classical, since it commutes with itself, with equation of motion of the form $\dot{\tilde{Q}} = -\partial_{\tilde{Q}}U(\tilde{Q}) + f_{\tilde{Q}}(\tau)$. The only signature of the quantumness is the noise intensity $f_{\tilde{Q}}$, which is given by Eq. (2) and explicitly contains $\tilde{\hbar}$, whereas the form of $U(\tilde{Q})$ is determined by the type of the bifurcation point. The problem of switching is then mapped on the Kramers problem of escape of an overdamped particle. The escape rate is

$$W_{\text{sw}} = \Omega_{\text{sw}} \exp(-R_A/\tilde{\hbar}).\quad (3)$$

The quantum activation energy is $R_A = \Delta U/(\bar{n} + 1/2)$, where ΔU is the height of the barrier to be overcome in escape; Ω_{sw} is the Kramers prefactor. Both for the saddle-node and pitchfork bifurcation points, which are of interest for driven oscillators, R_A and Ω_{sw} scale as powers of the distance to the bifurcation point.¹

Of significant interest for the current experiments on parametrically driven quantum oscillators is the vicinity of the critical point $F = F_c, \omega_F = 2\omega_0$ where there first emerge period-two vibrations for parametric driving. The dynamics in this parameter range is significantly different from that near simple (co-dimension one) bifurcation points. We have now developed a method to analyze

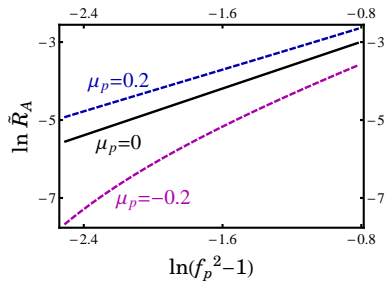


FIG. 1. Scaling of the quantum activation energy $\tilde{R}_A = (\bar{n} + 1/2)R_A$ with the relative driving field amplitude $f_p = F/F_c$ for transitions between the parametrically excited period-two vibrational states with opposite phases. In the shown range $1.04 < f_p < 1.2$ the scaled frequency detuning $\mu_p \propto (\omega_F - 2\omega_0)/\omega_F$ is such that the period-two vibrations are the only stable states of the oscillator.

this dynamics. There is no simple single scaling law that would describe the behavior of R_A . The results obtained for R_A are shown in Fig. 1.

Of significant interest is the parameter range where the motion of the oscillator in the rotating frame is underdamped. With no dissipation, the oscillator would stay in a state with given quasienergy or in a superposition of such states. Dissipation leads to drift over quasienergy toward its value in the classically stable vibrational state. However, it also leads to diffusion over quasienergy. Such diffusion occurs even for $T = 0$ and is of purely quantum origin. It results in a stationary distribution ρ_n over quasienergy states $|n\rangle$ of the Boltzmann type, $\rho_n \propto \exp[-R_n/\hbar]$. For small \hbar one has $R_n \equiv \int_{g_{st}}^{g_n} dg R'(g)$, where $g_n = \langle n|\hat{g}|n\rangle$ and g_{st} is the value of \hat{g} at the stable state. Function $R'(g)$ plays the role of the reciprocal effective temperature, which depends on g .

Remarkably, the small- \hbar approximation breaks down where $T \rightarrow 0$. The value of R' obtained for $T = 0$ and $T \rightarrow 0$ are different. We have recently shown² that the quasi-Boltzmann form of the distribution does not apply in a narrow temperature range $T_{c1} < T < T_{c2}$, where the critical temperatures are $T_{c1} \propto \hbar^2$ and $T_{c2} \propto \hbar/|\log \hbar|$. One can say that $R'(g)$ has a kink. Such kink is shown in Fig. 2.²

We will discuss the general conditions for the onset of fragility and provide an analytical theory of the kink of $R'(g)$. We will also compare the onset of fragility in a quantum system and in several models of population dynamics. So far the effect has been seen in systems with discrete states, like quasienergy states or the numbers of species. An important open question is whether fragility

also emerges in continuous systems.

III. SWITCHING IN SYSTEMS WITH DELAY

Delay naturally arises in dissipative dynamical systems. In such systems, dissipation results from the coupling to a reservoir: motion of the system causes changes in the reservoir, which in turn affect the motion. The underlying reaction of the reservoir is generically delayed. Along with the dissipative force, the reservoir exerts a random force on the system. If dissipation is delayed, the random force has a finite correlation time.

We will discuss our recent results³ on the probability distribution and switching rates in systems with delay. They are related to systems where chaotic motion in the absence of noise does not play a role. There are several key elements here. First, even though to find a dynamical trajectory without noise one has to know the whole dynamical history of the system, the trajectory, which is most likely to be followed in a large fluctuation to a given state, is well defined. It is well-defined also for the problem of escape from a metastable state. The “price” for having delay is that the functional, which we obtain and which determines the distribution of fluctuational trajectories, is nonlocal in time. Therefore the equations for the most probable trajectories, which are the extremals of this functional, are acausal.

We will present explicit results for the switching rates close to bifurcation points of the system, and also for the case of small delay compared to the system relaxation time. The effect of the finite correlation time of the noise will be also discussed.

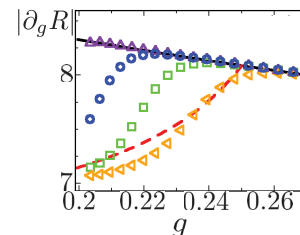


FIG. 2. Effective reciprocal temperature $|\partial_g R|$ calculated numerically from $\ln(\rho_n/\rho_{n-1})$. The results refer to three temperatures in the range $T_{c1} < T < T_{c2}$. The total number of localized quasienergy states in the basin of attraction of the small-amplitude state of a resonantly driven oscillator is $M = 20$. The solid and dashed lines show $|\partial_g R|$ for $\bar{n} = 0$ and for $\bar{n} \rightarrow 0$ but $T > T_{c2}$, respectively.²

¹ M. I. Dykman, in *Fluctuating Nonlinear Oscillators: from Nanomechanics to Quantum Superconducting Circuits*, ed. by M.I. Dykman (OUP, Oxford, 2012), p. 165.

² L. Guo, V. Peano, M. Marthaler, and M. I. Dykman, Phys.

Rev. A, **87**, 062117 (2013).

³ M. I. Dykman and I. B. Schwartz, Phys. Rev. E **86**, 031145 (2012); I. B. Schwartz et al., *ibid.* **91**, 012139 (2015).

Stochastic resonance and diversity-induced resonance in complex systems

Marco Patriarca,¹ Els Heinsalu,¹ Emilio Hernández-García,² and Raúl Toral²

¹NICPB–National Institute of Chemical Physics and Biophysics, Rõvala 10, 15042 Tallinn, Estonia
e-mail addresses: marco.patriarca@kbfi.ee; els.heinsalu@kbfi.ee

²IFISC–Instituto de Física Interdisciplinar y Sistemas Complejos (CSIC-UIB), E-07122 Palma de Mallorca, Spain
e-mail addresses: emilio@ifisc.uib-csic.es; raul@ifisc.uib-csic.es

Complex systems theory is a conceptual framework for understanding many phenomena from the nano-scaled condensed matter to the macroscopic social scale, characterized by emergent properties produced by the non-linear interactions between the constituent units, in general surprisingly different from those of the units themselves. Among the many examples known, such as synchronization, phase transitions, and pattern formation, here we explore some instances of emergent phenomena induced by disorder. Disorder can mean both *noise*, i.e. time-dependent disorder in the form of e.g. a random force acting on a particle, a noisy background, or random fluctuations of some parameter, and *heterogeneity*, i.e. quenched disorder affecting some features of the units composing the system, related to e.g. the different ion-channels in a cell, neurons with heterogeneous parameters in a neuronal network, different individuals in a social group, heterogeneous economic agents in a market economy, or species with different fitness in an ecological system.

The subject of this study is the effect resulting by the interplay between noise and diversity. For this reason the focus is on systems that present both stochastic resonance, that takes place at intermediate amplitudes of noise¹, and diversity-induced resonance, that appears for a suitable (i.e. neither too high nor too low) level of quenched disorder in the form of heterogeneity of the constituent units²⁻⁴. Previous investigations have concen-

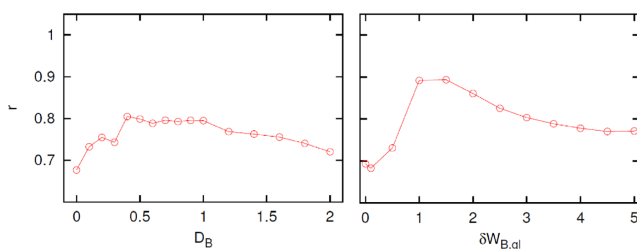


FIG. 1. The coefficient r providing a quantitative estimate of the quality of a sleep-wake cycle⁵ presents both a stochastic resonance when studied in *versus* the noise amplitude (left) and diversity-induced resonance *versus* the diversity level of the neuronal activation thresholds (right), see Ref. [5] for further details.

trated on the study of noise and diversity treated as independent phenomena. For instance, some of the authors showed that a multi-neuronal model of the wake-sleep cycle presents stochastic resonance as well as diversity-

induced resonance (with a clear evidence of diversity-induced resonance and a milder level of stochastic resonance)⁵, see the example in Fig. 1. On the other hand, here we consider the actual interplay between noise and diversity.

A first question that we consider and try to answer is related to the way noise and diversity should interact with each other in order to produce the optimal response of a system, e.g. which parameters it is best to diversify and which parts of the system should undergo random fluctuations. In turn this depends on the specific type of dynamical system under study. To this aim we review previous work on this topic and presents the results of numerical studies of multicomponent systems with bistable, excitable, and other types of constituent units.

A second question is whether there exists a general connection between stochastic resonance and diversity-induced resonance, enabling one to predict the possible appearance of diversity-induced resonance in a system when the (corresponding noisy single-particle version of the) system is known to present stochastic resonance.

At a general level, this research is motivated by the well known fact that an appreciable level of both noise and quenched disorder is naturally present in all biological and social systems. It is a natural question to ask whether there is a reason for the evolution of different types of system toward a similar state with a combined level of noise and diversity, that are both known to be able to play a relevant role in e.g. improving the response, resilience, or performance of a system subject to external perturbations and interactions⁴.

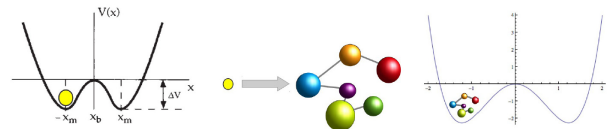


FIG. 2. The prototypical diversity-induced resonant system² (right) can be considered as a generalization of the prototypical stochastic resonant system¹ (left) obtained by replacing the Brownian particle by a heterogeneous polymer.

Finally, this work is related to and extends the implications of the links between stochastic resonance and diversity-induced resonance that have been pointed out or implicitly demonstrated by different authors. The original introduction of the concept of diversity-induced resonance is in fact in the perspective of an analogy with a stochastic resonant system². The analogy can be vi-

sualized by constructing the diversity-induced resonant system from the famous example of a stochastic resonant system of a Brownian particle in a quartic bistable potential through the replacement of the Brownian particle by a heterogeneous polymer, see Fig. 2. As a different example, the studies of the phenomenon of supra-threshold stochastic resonance⁶ employed some particular model of multi-component system that can be re-interpreted as a heterogeneous systems that in principle presents diversity-induced resonance, see Fig. 3.

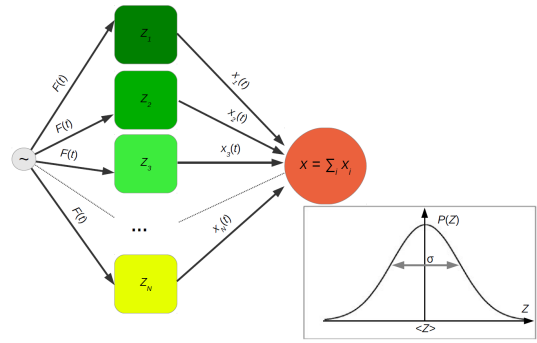


FIG. 3. This supra-threshold stochastic resonant system⁶ with input signal $F(t)$ and output signal $x = \sum_i \Theta(F(t) - Z_i)$, where $\Theta(\cdot)$ is the step function, can represent a stochastic resonant or a diversity-induced resonant system depending whether the thresholds Z_i are assumed to be diversified by independent noises $\xi_i(t)$, $Z_i = \langle Z \rangle + \xi_i(t)$, or extracted from a suitable distribution $P(Z)$.

¹ L. Gammaitoni, P. Hänggi, P. Jung, F. Marchesoni, Stochastic Resonance, Rev. Mod. Phys. **70**, 223 (1998).
² C.J. Tessone, C.R. Mirasso, R. Toral, J.D. Gunton: Diversity-induced resonance, Phys. Rev. Lett. **97**, 194101 (2006).
³ R. Toral, C. J. Tessone, J. Viana Lopes, Collective effects induced by diversity in extended systems, Eur. Phys. J.-Special Topics **143**, 59 (2007).
⁴ L.F. Lafuerza, R. Toral, On the effect of heterogeneity in stochastic interacting-particle systems, Sci. Rep. **3**, 1189

(2013).
⁵ M. Patriarca, S. Postnova, H.A. Braun, E. Hernandez-Garca, R. Toral, Diversity and Noise Effects in a Model of Homeostatic Regulation of the Sleep-Wake Cycle, PLoS Comput. Biol. **8** (8), e1002650 (2012).
⁶ M.D. McDonnell, N.G. Stocks, C.E.M. Pearce, D. Abbott, Stochastic Resonance. From supra-threshold Stochastic Resonance to Stochastic Signal Quantization, Cambridge University Press (2008).

Non-hermitian diffusion

Maciej A. Nowak¹

¹*M. Smoluchowski Institute of Physics and Mark Kac Complex Systems Research Center,
Jagiellonian University, 30-348 Kraków, S. Łojasiewicza 11, Poland
e-mail address: nowak@th.if.uj.edu.pl*

I. HISTORICAL INSPIRATION

In 1962 Dyson suggested an inspiring way to understand the joint probability distribution (jpd) of the eigenvalues of random matrices. In order to find the jpd, he was inventing an auxiliary dynamics undergoing in some fictitious "time", which, at the static limit, will lead to the stationary state (Gibbs state), representing the desired jpd. As he pointed¹, *"after considerable and fruitless efforts to develop a Newtonian theory of ensembles, we discovered that the correct procedure is quite different and much simpler. The x_i [eigenvalues] should be interpreted as positions of particles in Brownian motion.* The resulting stationary distributions (originally for hermitian or for unitary random matrices) were obtained as an effect of Ornstein-Uhlenbeck diffusion with a drift force coming from electrostatic-like repulsion of eigenvalues. The success of this description has contributed to multiple applications of random matrix models in practically all branches of science. The notion of "time" has evolved as well, so nowadays the "time" can be a physical dynamical parameter, representing either the real time or, e.g., the length of the mesoscopic wire, area of the string or external temperature. The idea of noisy walk of eigenvalues led also recently to such concepts as the study of determinantal processes, Loewner diffusion, fluctuations of non-intersecting interfaces in thermal equilibrium and the emergence of pre-shock spectral waves and universal scaling at the critical points of several random matrix models.

Three years after Dyson, Ginibre² has considered for the first time strictly non-hermitian random matrix modes, whose spectrum does not need to be confined either to real line (hermitian operators) or to unit circle (unitary operators), but can be located on the two-dimensional supports on the complex plane. Original motivation for the study of complex, random spectra was purely academic. Today, however, non-hermitian random operators play role in quantum information processing, in financial engineering (when lagged correlations are discussed) or in identifying clusters in social or biological networks using non-backtracking operators, to name just a few recent applications. Additionally, statistical properties of eigenvectors of non-hermitian operators contribute to understanding scattering problems in open chaotic cavities and random lasing.

II. MAIN RESULTS

In this contribution, following our recent work³, we combine the original ideas of noisy random walk with the strict non-hermiticity of the operators, studying an evolution of Ginibre matrices whose elements undergo Brownian motion. The non-hermitian character of the Ginibre ensemble binds the dynamics of eigenvalues to the evolution of eigenvectors in a non-trivial way, leading to a system of coupled nonlinear equations resembling those for turbulent systems. We formulate a mathematical framework allowing simultaneous description of the flow of eigenvalues and eigenvectors, and we unravel a hidden dynamics as a function of new complex variable, which in a standard description is treated as a regulator only. We solve the evolution equations for large matrices and demonstrate that the non-analytic behavior of the Green's functions is associated with a shock wave stemming from a Burgers-like equation describing correlations of eigenvectors.

III. CONCLUSIONS AND OPEN PROBLEMS

We have proven that a consistent description of non-hermitian Gaussian ensemble requires the knowledge of the detailed dynamics of co-evolving eigenvalues and eigenvectors. Moreover, the dynamics of eigenvectors plays the superior role and leads directly to the inference of the spectral properties. This is dramatically different scenario comparing to the standard random matrix models, where the statistical properties of eigenvalues are of primary importance, and the properties of eigenvectors are basically trivial due to their decoupling from the spectra. We conjecture that the discovered by us hidden dynamics of eigenvectors, that we have observed for the Ginibre ensemble, is a general feature of all non-hermitian random matrix models.

Our formalism could be exploited to expand the area of application of non-Hermitian random matrix ensembles within problems of growth, charged droplets in quantum Hall effect and gauge theory/geometry relations in string theory beyond the subclass of complex matrices represented by normal matrices.

One of the challenges is an explanation, why, despite being so different, Smoluchowski-Fokker-Planck equations for hermitian and non-hermitian random matrix models exhibit structural similarity to simple models of turbulence, where so-called Burgers equation plays the vital role, establishing the flow of the spectral density of eigenvalues in the case of the hermitian or unitary en-

sembles and the flow of certain eigenvector correlator in the case of non-hermitian ensembles.

We believe that our findings will contribute to understand several puzzles of non-hermitian dynamics, alike extreme sensitivity of spectra of non-hermitian systems to perturbations^{4,5}.

ACKNOWLEDGMENTS

This contribution summarizes some recent results³ worked out in the collaboration with Zdzisław Burda,

Jacek Grela, Wojciech Tarnowski and Piotr Warchol. Additionally to the above-mentioned coauthors, MAN appreciates collaboration and/or discussions with Jean-Paul Blaizot, Neil O'Connell, Ewa Gudowska-Nowak, Romuald Janik, Jerzy Jurkiewicz, Dima Savin and Oleg Zaboronski. This work was supported by the Grant DEC-2011/02/A/ST1/00119 of the National Centre of Science.

¹ F.J. Dyson, J. Math. Phys. **3**, 1192 (1962).

² J. Ginibre, J. Math. Phys. **6**, 440 (1965).

³ Z. Burda, J. Grela, M.A. Nowak, W. Tarnowski and P. Warchol, Phys. Rev. Lett. **113**, 104102 (2014).

⁴ J.T. Chalker and B. Mehlige, Phys. Rev. Lett. **81**, 3367 (1998).

⁵ Y.V. Fyodorov and D.V. Savin, Phys. Rev. Lett. **108**, 184101 (2012).

From cell membranes to ultracold gases: classical and quantum diffusion in inhomogeneous media

Pietro Massignan,^{1,*} John Lapeyre,^{1,2} Carlo Manzo,¹ Juan A. Torreno-Pina,¹
Aniello Lampo,¹ Jan Wehr,³ Maria F. García-Parajo,¹ and Maciej Lewenstein¹

¹*ICFO-Institut de Ciències Fotòniques, Mediterranean Technology Park, Castelldefels (Barcelona), Spain*

²*Instituto de Diagnóstico Ambiental y Estudios del Agua (IDAEA-CSIC), Barcelona, Spain*

³*Department of Mathematics, University of Arizona, Tucson, Arizona, USA*

I. INTRODUCTION

Brownian motion is one of the most fundamental phenomena of physics, and its discovery and study contributed to the birth of contemporary statistical physics and theory of stochastic processes. It finds wide applications in many branches of science, including physics, chemistry, biology and economics.

A long series of studies, however, indicates that transport in condensed matter and living systems is often far from random. As an example, many cellular components exhibit anomalous diffusion, i.e., a mean-squared displacement $\text{MSD} \sim t^\beta$ with $\beta \neq 1$, and recent works even evidenced clear signatures of nonergodic behavior. Presently open are many questions on what are the physical mechanisms generating non-ergodicity, what are the implications of anomalous diffusion for biological function, and more generally how complex environments affect Brownian motion.

II. CLASSICAL BROWNIAN MOTION

A celebrated model yielding anomalous, subdiffusive and nonergodic dynamics, widely used in biology and condensed matter is the so-called Continuous-Time Random Walk (CTRW), whose underlying assumption is that particles, while diffusing, wait at random positions for anomalously long times. However, transient trapping is not the only possible source of transport anomalies, as spatial and temporal disorder may have important consequences in this direction.

In a recent theoretical work, we introduced models which describe particles diffusing in a complex and inhomogeneous medium consisting of patches with random sizes and random diffusivities¹. The particles are never trapped, but rather perform continuous Brownian motion with the local diffusion constant. Under simple assumptions on the distribution of diffusivities D in each patch, such as

$$P_D(D) = \frac{D^{\sigma-1} e^{-D/b}}{b^\sigma \Gamma(\sigma)}, \quad (1)$$

and of the traversal times τ of each patch, such as

$$P_\tau(\tau|D) = \frac{D^\gamma}{k} e^{-\tau D^\gamma/k}, \quad (2)$$

with b and k appropriate dimensionful constants, we find that the mean squared displacement displays subdiffusion

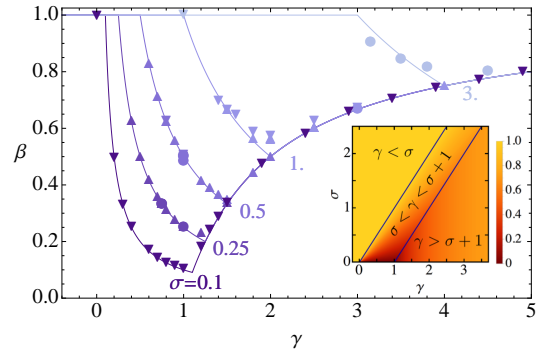


FIG. 1. **Subdiffusion exponent** β . Lines are the analytic predictions for different values of σ . Symbols are numerical simulations of various annealed models with spatial or temporal disorder. Lines and symbols vary from dark to light with increasing σ . The inset shows a density plot of β vs. both γ and σ .

due to non-ergodicity for both annealed and quenched disorder, see Fig. (1). Our model is formulated as a walk continuous in both time and space, similar to the Lévy walk.

In a complementary experimental work, we used single particle tracking on living cells to demonstrate that the motion of the transmembrane receptors DC-SIGN reveals nonergodic subdiffusion on living cell membranes, see Fig. (2). In contrast to previous studies, this behavior resulted incompatible with transient immobilization, and therefore it can not be interpreted according to continuous time random walk theory. We show instead that receptors undergo changes of diffusivity, consistent with the current view of the cell membrane as a highly dynamic and diverse environment. Simulations based on the above mentioned theoretical model of ordinary random walk in an inhomogeneous medium quantitatively reproduce all our observations, pointing towards diffusion heterogeneity as the cause of DC-SIGN anomalous behavior. By studying different receptor mutants, we further correlated receptor motion to its molecular structure, thus establishing a strong link between nonergodicity and biological function. Our results highlight the fundamental role of disorder in cell membranes, and its connection with function regulation.

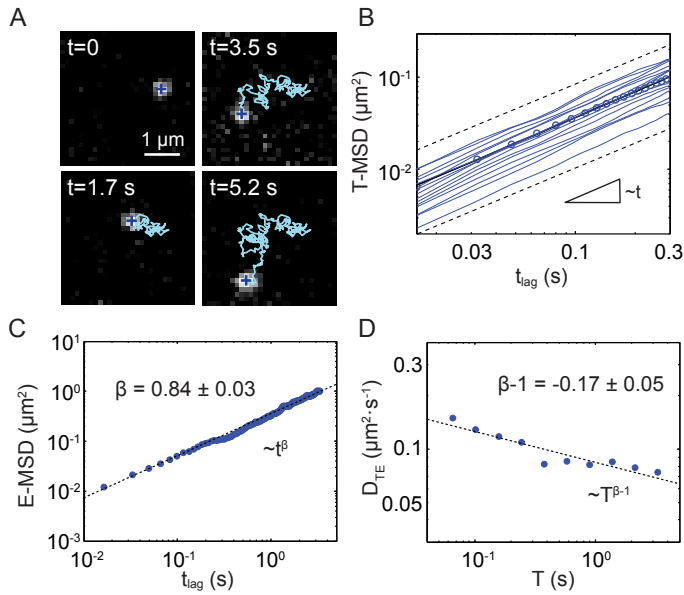


FIG. 2. DC-SIGN diffusion shows weak ergodicity breaking and aging. (A) A quantum-dot-labeled wtDC-SIGN molecule diffusing on the cell membrane. (B) The time-averaged MSD for individual trajectories scales linearly in time, compatibly with pure Brownian motion. (C) The ensemble-averaged MSD shows marked subdiffusion. (D) The time-ensemble-averaged diffusion coefficient shows non-stationarity (aging) of the process as a function of the total observation time T .

III. QUANTUM BROWNIAN MOTION

Quantum Brownian motion, although studied since half a century, has not yet found convincing experimental realizations and observations. Recent experiments on trapped ultracold atomic gases provide unprecedented precision and control that allow us to hope to observe effects of quantum Brownian motion in a very near future. But the presence of the external trapping potential introduces a novel complexity level into the well studied problem. In a recently published work, we revise the standard theory of quantum Brownian motion and consider in detail the case when a quantum Brownian

particle is moving in a spatially inhomogeneous environment, such as the one provided by a trap³. This leads to spatially dependent diffusivity and, consequently, to spatially dependent decoherence and damping rates. As a result of these intrinsically nonlinear relations novel quantum effects occur: the interaction of the quantum Brownian particle with such environment might induce effective cooling of its state, and even squeezing of the fluctuations of its motion, see Fig. (3).

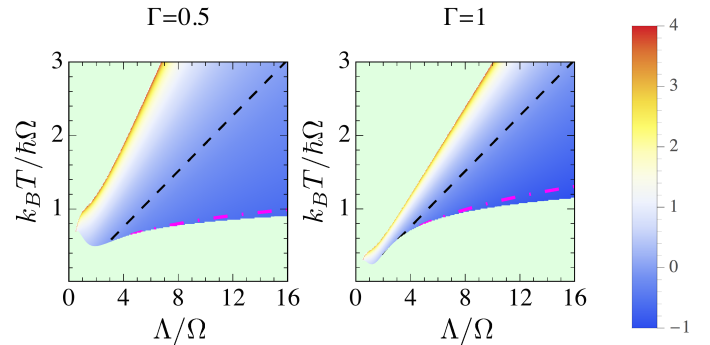


FIG. 3. Shape of the stationary distributions. Aspect ratio of the impurity wavefunction, $\ln(\delta_x^2/\delta_p^2)$, for the case of a quadratic coupling with the environment, as a function of spectral density cut-off Λ and temperature T ; left (right): weak (strong) damping. The impurity shows “cooling” (i.e., $\delta_x^2 < \delta_p^2$) below the black dashed line, and “quantum squeezing” (i.e., $\delta_x^2 < 1$) below the magenta dotted-dashed line.

ACKNOWLEDGMENTS

This work was supported by Fundació Cellex, Generalitat de Catalunya (2009-SGR-597), the European Commission (FP7-ICT-2011-7, 288263), the HFSP (RGP0027/2012), ERC Advanced Grant Osyris, EU IP SIQS and STREP EQuaM, John Templeton Foundation, the Spanish Ministry of Science and Innovation (FIS2008-00784, MAT2011-22887, and Plan Nacional FOQUS). P.M. acknowledges funding from a Spanish “Ramón y Cajal” fellowship.

* pietro.massignan@icfo.es

¹ P. Massignan, C. Manzo, J. A. Torreno-Pina, M. F. García-Parajo, M. Lewenstein, and G. J. Lapeyre Jr, *Non-ergodic subdiffusion from Brownian motion in an inhomogeneous medium*, Phys. Rev. Lett. **112**, 150603 (2014).

² C. Manzo, J. A. Torreno-Pina, P. Massignan, G. J. Lapeyre Jr., M. Lewenstein, and M. F. García Parajo, *Weak ergodicity breaking of receptor motion in living cells stemming from random diffusivity*, Phys. Rev. X **5**, 011021 (2015).

³ P. Massignan, A. Lampo, J. Wehr, and M. Lewenstein, *Quantum Brownian motion with inhomogeneous damping and diffusion*, Phys. Rev. A, in press (2015); arXiv:1410.8448.

A motor that detects the length of DNA by using chain fluctuation

Ana Maria Florescu¹ and Kuni H Iwasa²

¹Max Planck Institute for Physics of Complex Systems, Nöthnitzer Str. 38 Dresden, D-01187 Germany
e-mail address: aflorescu@sissa.it

²Max Planck Institute for Physics of Complex Systems, Nöthnitzer Str. 38 Dresden, D-01187 Germany
and National Institutes of Health, Bethesda, Maryland 20892, USA
e-mail address: iwasa@mailaps.org

I. INTRODUCTION

Chromatin remodeling motors translocate nucleosome, with which they are associated, on DNA¹. A class of these motors translocate nucleosomes in the direction either the chain length of the DNA is longer or shorter. In order to accomplish such a translocation, these motors need to detect the length of the DNA strands to the neighboring nucleosomes.

One such mechanism could be to use a molecular scale. That appears to be the case for the yeast ISW1a chromatin remodeler². This remodeler places itself between two nucleosomes. Another mechanism must be at work for the human ACF complex because its dimer is closely associated with a single nucleosome³. It has been shown that this motor can detect the length of DNA and moves the nucleotide to the center, using a system in which a single nucleosome is associated with a single DNA molecule³. What is the biophysical basis for such a sensitivity?

The simplest possible mechanism would be that the motor makes contact with the end of the DNA strand. However, that is unlikely because the persistence length of DNA is about 50 to 60 nm, much larger than the dimension of the motor. Thus, it must detect the differences in the local property of DNA, which depends of the chain length. We hypothesize that local fluctuation of DNA near the motor provides information on the DNA chain attached.

These motors are large dimers, covering the surface of histone octamers. These subunits may interact each other rather than fighting each other in such a way that they do not waste energy. Here we focus only on the way how these molecules can detect the length of DNA and do not address how two subunits need to interact each other.

II. CHAIN FLUCTUATION

The binding of DNA to a nucleosome is not static but undergoes thermal fluctuation⁴. Given the stiffness of DNA chain, this mode of motion corresponds to a pivoting motion of the DNA chain if the chain length is less than the persistence length of about 50 nm. To describe such a motion in a simple manner, it would be useful to assume a quadratic potential well with respect to the relative orientation of the chain formed by a holding spring with relatively shallow local minima at two positions off

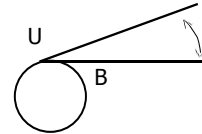


FIG. 1. Pivoting motion of DNA chain on a nucleosome

center.

If these local minima are shallower than the thermal energy, pivoting motion of the polymer is described by the stiffness of the holding spring, which in turn determines the transition rates between two states, one of which is “bound” and “unbound.” These states are associated with wrapping and unwrapping of DNA on a nucleosome. If one of these states is a starting point of an ATP-dependent sliding motion between the DNA and nucleosome, movement of the nucleosome on the DNA is realized. The dependence on the chain length is introduced through the drag on the chain during transitions between “bound” and “unbound” states, which require movement of the chain assuming that the nucleosome is stationary. The angular fluctuation amplitude shows little length dependence. If the rotational drag of the nucleosome is smaller than that of the DNA, those transitions take place mainly by a rotation of the nucleosome, insensitive to the chain length of DNA.

Rotational diffusion coefficient D_r of short DNA chains is well approximated by assuming short DNA chains as a rod-like conformation⁵. The analytical expression is

$$\pi\eta L^3 D_r / (3k_B T) = \ln(L/2r) + \delta \quad (1)$$

where $\delta \approx -0.7 + O(2r/L)$. The rotational drag coefficient ζ_r of a DNA chain is thus,

$$\zeta_r \approx \frac{1}{3} \pi \eta L^3 / (\ln(L/2r) - 0.7), \quad (2)$$

using Einstein’s relationship. The terms $O(2r/L)$ could be ignored if $L \gg 2r$.

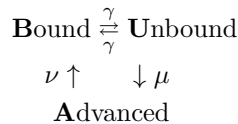
For the chain length of the DNA to be important for angle fluctuation at the supporting point, the rotational motion of the nucleosome must be less than chain fluctuation of the DNA, namely the rotational drag of the nucleosome must be larger than that of DNA chain. We can show that this factor imposes a detection limit.

III. THE MODEL

We have already discussed two states, “unbound” and “bound.” For describing a motor, we need to provide another state that describes motile activity. The proposed model consists of the following assumptions.

1. The binding site of the motor has three states, bound (B), unbound (U), and advanced (A).
2. Transitions between B and U depends on the contact of DNA to the site and thus depends on the movement of DNA.
3. Transitions from U to A and from A to B involves ATP binding and hydrolysis. For this reason these transitions are unidirectional.
4. Transition from U to A produces unidirectional movement of DNA relative to the nucleosome.

The transitions between these three states are represented schematically:



The transition rates between U and B are γ and in both directions because this reflects fluctuation of the DNA. The rate γ is a decreasing function of the chain length L . The differential equations that govern the transitions between these states are,

$$\frac{dB}{dt} = -\gamma B + \gamma U + \nu A, \quad (3)$$

$$\frac{dU}{dt} = \gamma B - (\mu + \gamma)U, \quad (4)$$

$$\frac{dA}{dt} = \mu U - \nu A, \quad (5)$$

where μ and ν are transitions, in which ATP binding and its hydrolysis are involved. The rotation rate of the motor is proportional to νA for normalized A, i.e. $B+U+A = 1$.

The eigenvalues are 0 and $1/2 - (2\gamma - \mu - \nu) \pm \sqrt{4\gamma^2 + (\mu - \nu)^2 - 4\gamma\nu}$. The eigenvalues other than 0 correspond to transient modes. The eigenvector for

eigenvalue 0 is then given by $(\gamma + \mu, \gamma, \gamma\mu/\nu)$. After normalization of this vector, we obtain for the rotation rate of the motor,

$$\nu A = \frac{\gamma\mu}{\sqrt{\gamma^2 + (\gamma + \mu)^2 + (\gamma\mu/\nu)^2}}. \quad (6)$$

The last term of the denominator diminishes for large ν . If u is the unit distance the motor travels per cycle, the speed of the motor, which is expressed as νAu , is an increasing function of γ expect for large values of ν , where it behaves as a constant.

If we assume $\gamma \sim L^{-2}$, the advance of the motor has the dependence of the chain length as shown in Fig. (2).

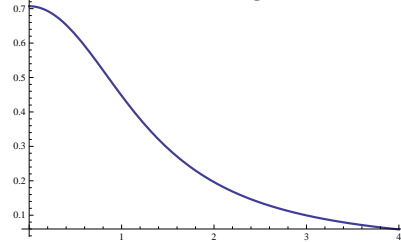


FIG. 2. The advance νA of the motor plotted against the chain length L for $\mu = 1$ and $\nu \rightarrow \infty$.

IV. DISCUSSION

The present model predicts that the speed of the motor is an increasing function of the frequency, at which DNA chain “breathes” near the nucleosome. Since shorter polymer chain oscillates at a higher frequency than longer ones, a shorter chain produces a greater speed of uncoiling. In other words, the direction is away from the short end, consistent with the experimental observation.

The saturating behavior to chain length is obvious from Fig. 2. In addition, for long chains, the rotational drag of nucleosome becomes comparable to that of the DNA chain, reducing the dependence on the chain length.

The motor is unable to function if the DNA is too short. This could be explained by the reduced slope at small L . Since the motor is a dimer and works in a pair, the difference in the preference is small for short chains. This may lead to the insensitivity of the motor for detecting the difference in length of short DNA chains, in addition to the detection limit imposed by the rotational diffusion of the nucleosome.

¹ C. R. Clapier and B. R. Cairns, *Annu Rev Biochem* **78**, 273 (2009).

² K. Yamada, T. D. Frouws, B. Angst, D. J. Fitzgerald, C. DeLuca, K. Schimmele, D. F. Sargent, and T. J. Richmond, *Nature* **472**, 448 (2011).

³ L. R. Racki, J. G. Yang, N. Naber, P. D. Partensky, A.

Acevedo, T. J. Purcell, R. Cooke, Y. Cheng, and G. J. Narlikar, *Nature* **462** 1016 (2009).

⁴ G. Li, M. Levitus, C. Bustamante, and J. Widom, *Nat Struct Mol Biol* **12**, 46 (2005).

⁵ M. M. Tirado, C. L. Martínez, and J. G. de la Torre, *J Chem Phys* **81**, 2047 (1984).

Model and parameter determination for molecular motors from single molecule experiments

Francisco J. Cao¹

¹Universidad Complutense de Madrid. Facultad de Ciencias Físicas. Departamento Física Atómica, Molecular y Nuclear, Av. Complutense s/n. 28040 Madrid. Spain.
franco@fis.ucm.es

I. INTRODUCTION

In the last decades new experimental techniques have allowed the study of single molecule processes^{1,2,3}. This allows in particular to explore in real time the operation of molecular motors. Molecular motors are proteins that are able to do work, and they operate to perform different task in the cell, which range from DNA replication to transport of compounds inside the cell, or even transport of the whole cell.

Stochastic processes are very present in single molecule experiments with molecular motors. Molecular motors have stochastic dynamics, with binding energies, typically, of the order of the energy of thermal fluctuations, $k_B T$, or only an order of magnitude greater. In addition, thermal fluctuations also affect the measurement adding unwanted thermal noise, which partially mask the signal of the system dynamics.

In addition, single molecule experiments allow only to monitor one or a few distances of the system, and from the limited information contained in these distances and their time evolution one has to infer which the system dynamics was, determining the correct model and its parameter values. We will review all these questions with examples from our recent works in this field.

II. DETERMINATION OF DNA REPLICATION SPEED MASKED BY PAUSES

A mutated DNA polymerase (a molecular motor that replicates DNA) was observed to have a lower replication speed than its wild type counterpart (the one present in nature).

Our study of experimental polymerase trajectories for different forces applied to separate the two strands of DNA showed that the mutation induced additional pauses in the replication^{4,5}, see Fig. (1). The lower speed was due to the transition of the polymerase to a long pause state, while during the polymerization state the speed was the same. The force dependency of the entry and exit rates to this pause state, which we determined, were compatible with a transition to the long pause state induced by the interaction of the polymerase with the DNA fork, where the two strands of DNA merge.

This example shows how the detailed analysis of the single molecule trajectories can help to determine the mechanism underlying some effect, as in this case was the speed reduction.

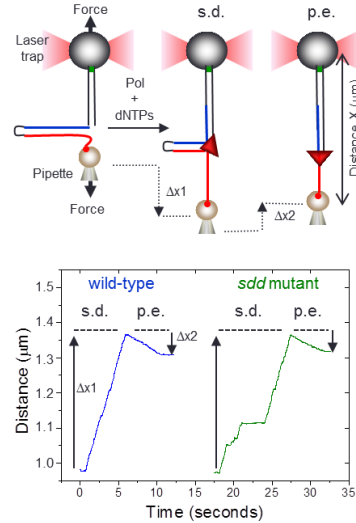


FIG. 1. **Top diagram** shows experimental configuration, in this configuration the force aids the separation of the two strands of DNA. At the left, previous to polymerase addition; at the center, on the strand displacement (s.d.) phase where the polymerase both unwinds the double strand of DNA and replicates one of the strands; and at the right, during the primer extension (p.e.) phase where the polymerase only replicates the remaining single strand of DNA. **Bottom plot** shows typical trajectories for the wild type and strand displacement deficient (ssd) mutant during both the s.d. and the p.e. phases of the dynamics. Sdd mutant trajectories clearly show the appearance of long pauses during the s.d. phase.

III. DETERMINATION OF STEPPING PROCESS IN THE DNA REPLICATION CYCLE

We have studied the experimental trajectories of a DNA polymerase in the presence of aiding and opposing forces and for different abundances in the solution of the nucleotides needed for the replication⁶, see Fig. (2). Our analysis shows that experimental results are incompatible with any of the two chemical steps that can lead to power stroke mechanisms leading the stepping process, while they are compatible with a Brownian ratchet mechanism for the polymerase advance.

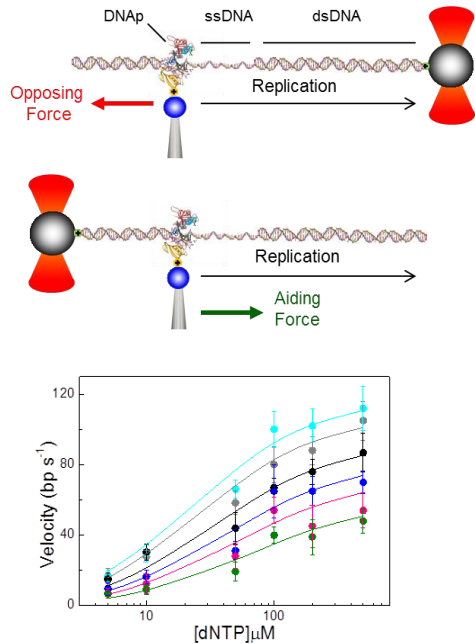


FIG. 2. **Top diagram** shows experimental configuration, in this configuration the force acts directly on the polymerase aiding or opposing the displacement associated with replication. **Bottom plot** shows replication velocity as a function of nucleotide concentration in the solution, for forces of 20, 5, -5, -10, -15 and -20 pN (from top to bottom curve, positive forces are aiding forces).

IV. OPEN PROBLEMS

We also want to point examples of open problems that are expected to be solved through appropriate analysis of experimental trajectories combined with an appropriate experimental design:

- Determination of the step size when it is below the experimental resolution. We have a proposal to solve this problem which is expected to work for certain polymerases.
- Determination of possible transitions between fast and slow pause states, for the ssd mutant studied or for other molecular motors with two pause states.
- Detailed determination of whether stepping distributed among several of the processes in the chemical cycle can

- ¹ K. Visscher, M. J. Schnitzer, and S. M. Block, *Single kinesin molecules studied with a molecular force clamp*, *Nature* **400**, 184 (1999).
- ² J. R. Moffitt, Y. R. Chemla, S. B. Smith, and C. Bustamante, *Recent Advances in optical tweezers*, *Annu. Rev. Biochem.* **77**, 205 (2008).
- ³ C. Bustamante, W. Cheng, Y. X. Meija, and Y. X. Meija, *Revisiting the central dogma one molecule at a time*, *Cell* **144**, 480 (2011).
- ⁴ J. A. Morin, F. J. Cao, J. M. Lázaro, J. R. Arias-Gonzalez, J. M. Valpuesta, J. L. Carrascosa, M. Salas, B. Ibarra, *Active DNA unwinding dynamics during processive DNA replication*, *Proc. Natl. Acad. Sci. U. S. A.* **109**, 8115 (2012).

be excluded and in which cases, for the DNA polymerase studied or for other molecular motors.

The two last points share in common that they imply the introduction of additional parameters in the model making more difficult to determine their values, and giving rise to degeneracies, *i.e.*, several sets of values or even a region of the parameter space lead to good fits to the experimental data. Application of statistical inference methods can help to extract further information from the physical trajectories, and to combine the information of different experiments in a rigorous way. This combination of different experiments has already been done successfully in other fields of Science, as Cosmology, to successfully determine the values of models with a large number of parameters⁷.

V. CONCLUSIONS

Single molecule experiments provide very detailed information of one or several of the distances involved in the system dynamics. From this partial information a lot of knowledge can be extracted mainly because it contains the temporal evolution of the distance which reflects transition processes.

Close and strong collaboration with biochemists and biologist is recommended to be able to do relevant contributions, structural details and bulk experiments give additional constraints to models, complementing the information from single molecule experiments. (Bulk experiments are traditional experiments performed in the test tube involving a macroscopic number of the molecules under study, in this case molecular motors.)

Molecular motors have a rich stochastic dynamics and its understanding challenge statistical physicist and stochastic dynamics mathematicians. Biochemists provide their ability to completely inhibit certain processes or to block them with a certain probability, providing experimental data with more information in particular aspects of the involved dynamics. This provides abundant data to challenge our modelling ability and our statistical physics understanding.

We expect with this talk to attire more interest from the stochastic dynamics community to this area, where relevant and challenging problems are waiting for solutions, and will have a fast and strong impact in the development of Science.

ACKNOWLEDGEMENTS

F.J.C. acknowledges financial support from Ministerio de Ciencia e Innovación (Spain) through Grant No. FIS2010-17440.

- ⁵ J. A. Morin, F. J. Cao, J. M. Valpuesta, J. L. Carrascosa, M. Salas, and B. Ibarra, *Manipulation of single polymerase-DNA complexes: A mechanical view of DNA unwinding during replication*, *Cell Cycle* **11**, 2967 (2012).
- ⁶ J. A. Morin, F. J. Cao, J. M. Lázaro, J. R. Arias-Gonzalez, J. M. Valpuesta, J. L. Carrascosa, M. Salas, B. Ibarra, *Mechano-chemical kinetics of DNA replication: identification of the translocation step of a replicative DNA polymerase*, to appear in *Nucleic Acids Res.* (2015).
- ⁷ S. Dodelson, *Modern Cosmology*, Elsevier (2003).

Free energy measurement of ligands binding nucleic acids using fluctuation theorems

Joan Camunas-Soler,¹ Anna Alemany,¹ and Felix Ritort^{1,2,3}¹*Departament de Física Fonamental, Universitat de Barcelona, Diagonal 647, 08028 Barcelona, Spain*²*CIBER de Bioingeniería, Biomateriales y Nanomedicina, Instituto de Salud Carlos III, Madrid, Spain*³*fritort@gmail.com*

Fluctuation theorems allow to relate the work performed along non-equilibrium processes to thermodynamic free-energy differences. In the past years, fluctuation theorems have been used to obtain the free-energy of formation of DNA and RNA structures from force-spectroscopy measurements¹. More recently, an extended version of the Crooks fluctuation relation has been used to recover free-energies of intermediate and misfolded structures^{2,3}. However, so far this method has only been applied to unimolecular reactions. In this work, we have developed a novel methodology based on fluctuation relations to determine the free energy of binding of peptides and proteins to nucleic acids, so essential in many regulatory processes and drug targeting. We performed pulling experiments of DNA hairpins containing a binding site for a given DNA binding ligand (Figure 1) and measured the irreversible work done in the experiments. We then used a new fluctuation theorem to extract the affinity of binding of the ligands (i.e. single DNA peptides, DNA restriction enzymes, and an RNA binding protein), finding a new method to extract chemical potentials. Using this fluctuation relation we have also measured the binding energy of low solubility compounds difficult to characterize with bulk techniques and that find application as anticancer agents⁴. Finally, this methodology should also be useful to determine the bind-

ing affinities of protein-protein interactions, so essential in multiprotein assembly.

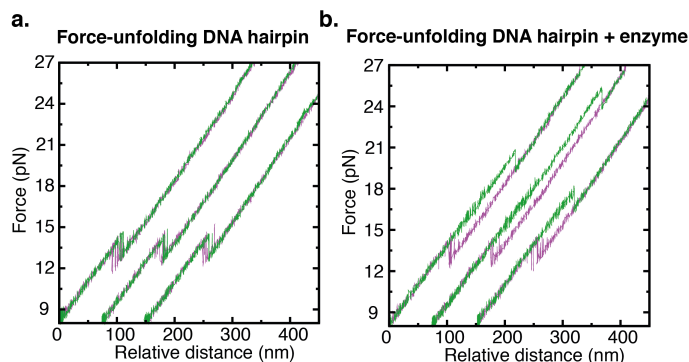


FIG. 1. Detection of binding events one-at-a-time (a) Pulling curves of a DNA hairpin in the absence of binding enzyme. Hairpin unfolding (green) and refolding (purple) is reversible and happens at a force range 13-14 pN. (b) Pulling curves of a DNA hairpin in the presence of an enzyme that binds at the hairpin stem. In the presence of protein the unfolding of the hairpin happens at a much higher force range of 21-26 pN due to the stabilizing effect of protein binding. When the force is released, the hairpin refolds at the typical hairpin coexistence force of 13 pN.

¹ F. Ritort, *Advances in Chemical Physics* **137**, 31–123 (2008).

² I. Junier *et al.*, *Physical Review Letters* **102**, 070602 (2009)

³ A. Alemany *et al.*, *Nature Physics* **8**, 688–694 (2012).

⁴ J. Camunas-Soler *et al.*, *ACS Nano*. **7**, 5102–5113 (2013).

Is it possible to detect long-range interactions among biomolecules through noise and diffusion?

I. Donato¹, M. Gori¹, I. Nardecchia¹, M. Pettini¹,
J. Torres² and L. Varani²

¹Centre de Physique Théorique, Aix-Marseille University, 13288 Marseille, France

²Institut d'Electronique et Systèmes, Montpellier University, 34095 Montpellier, France

Abstract

Fluctuation phenomena in biological systems are mainly related to diffusion phenomena inside living cells. Brownian diffusion of freely moving biomolecules is usually considered to drive the dynamics of the molecular machinery maintaining cellular functions and thus life. However, the high efficiency and rapidity of the encounters between cognate partners of biochemical reactions inside living cells calls for a more convincing explanation with respect to purely thermal-fluctuations-driven random walk. In fact, it has been surmised that a suitable interplay between Brownian diffusion and selective electrodynamic interactions acting at a long distance (up to thousands Angstroms) could make the job of significantly accelerating the encounter times of interacting biomolecules in living matter[1].

The present contribution consists of a report on ongoing experimental proof of concept of the possibility of activating the mentioned electrodynamic interactions between biomolecules, and that the excitation level can be sufficient to compete with Brownian diffusion. The ongoing experiments are performed in vitro by studying how diffusion is affected by the alleged activation of electrodynamic

interactions. Diffusion is detected by means of Fluorescence Correlation Spectroscopy.

This kind of experiments are crucially complemented by TeraHertz spectroscopic studies of the activation of collective oscillations of the biomolecules used in the Fluorescence Correlation Spectroscopy experiments; these collective molecular oscillations are accompanied by large dipole moment vibrations entailing the activation of electrodynamic long-range interactions [2].

References

- [1] I. Nardecchia, L. Spinelli, J. Preto, M. Gori, E. Floriani, S. Jaeger, P. Ferrier, and M. Pettini, *Experimental detection of long-distance interactions between biomolecules through their diffusion behavior: Numerical study*, Phys. Rev. E **90**, 022703 (2014).
- [2] J. Preto, M. Pettini, and J. Tuszynski, *Possible role of electrodynamic interactions in long-distance biomolecular recognition*, Phys. Rev. E **91**, 052710 (2015).

Electrochemical noise analysis to probe ion transport mechanisms in a membrane channel

Maria Queralt-Martin¹, M. Lidón López² and Antonio Alcaraz³

Universitat Jaume I, Department of Physics, Av. de Vicent Sos Baynat s/n 12071 Castelló de la Plana (Spain)

¹ e-mail address: mqueralt@uji.es

² e-mail address: lopezp@uji.es

³ e-mail address: alcaraza@uji.es

I. INTRODUCTION

Electrochemical noise (EN) analysis, defined as the evaluation of the spontaneous fluctuations of current generated by electrochemical processes¹, has been used over the years to study kinetic effects in biological systems like neuronal networks² or biomembranes³. In particular, EN has been successfully employed in protein ion channels to investigate the transport mechanisms that control the channel function^{2,4,5}. In this work we use EN to assess the different transport mechanisms occurring in the bacterial porin OmpF, a wide and weakly selective channel in the outer membrane of *E. coli*.

Noise analysis has been previously used in OmpF to investigate the pH titration of the channel residues⁴. It was shown that the power spectral density could be represented by a sum of Lorentzians plus the background spectrum, demonstrating that the conductance dynamics follow a two-state Markov process. Although the use of simple Markov models provides in principle all the kinetic constants and the number of independent residues participating in the process^{6,7}, the study in this case was seriously complicated by the pH dependence of the current steps between substates, which should be constant to allow this kind of analysis.

Here we follow a complementary approach based on the noise studies of Hoogerheide et al. in synthetic nanopores⁸. We pay attention to the appearance of an additional white noise in the low frequency range, as shown in Fig. (1). The level of this constant region changes with the applied voltage bias so that higher potentials yield higher values of the white noise. The current fluctuations S_I obtained from the framed region of the PSD in Fig. (1) (right) can be related to the conductance fluctuations, S_G , by $S_I = (S_G/G^2) \cdot I^2$. The parabolic coefficient S_G/G^2 contains relevant physicochemical information of the intrinsic system fluctuations. In particular, it has been related to the number of particles that fluctuates at the pore walls⁸.

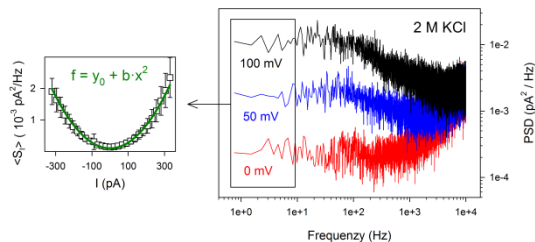


FIG. 1. Right: Power spectral density (PSD) calculated from single-channel current recordings at 2 M KCl electrolyte solution and different voltages. Left: parabolic dependence of the averaged PSD with current (open squares) obtained from the low frequency region (0 - 20 Hz band) framed in the right. The parabolic coefficient S_G/G^2 is obtained from a parabolic fit (solid line).

Consequently, we performed a parabolic fit of the averaged low frequency noise S_I plotted versus the current I (Fig. (1), left) to obtain the parabolic coefficient S_G/G^2 from each EN analysis. We performed this analysis with different electrolytes and studied how these fluctuations, altogether with the measured conductance, depend on ionic concentration to disclose the different transport mechanisms occurring in the OmpF channel.

II. MATERIAL AND METHODS

We analyze the current fluctuations from single-channel measurements performed using the V-clamp technique. The detailed experimental protocol can be found elsewhere⁴. The lipid membrane was created with 1,2-diphytanoyl-sn-glycero-3-phosphocholine (DPhPC) lipid. The electrolyte (monovalent or divalent) solution was kept at pH 6. The bacterial porin OmpF was kindly provided by Dr. S. M. Bezrukov (NIH, Bethesda, USA). Single-channel current recordings were obtained using an Axopatch 200B amplifier (Molecular Devices, Sunnyvale, CA) with an in-line low-pass Bessel filter at 10 kHz. Data were digitalized with a sampling frequency of 50 kHz using a Digidata 1440 (Molecular Devices, Sunnyvale, CA). The chamber was isolated from external noise sources with a double metal screen (Amuneal Manufacturing Corp., Philadelphia, PA).

III. RESULTS AND DISCUSSION

Fig. (2) displays the results obtained for both the (normalized) conductance (a) and the parabolic coefficient (b) as a function of ion activity, for the different electrolytes used. The use of electrolyte activity instead of concentration is necessary to separate the role of the channel from the intrinsic properties of the electrolyte that become important for salts of divalent cations at high molarity⁹. Fig. (2a) demonstrates that the channel conductance measured in salts of monovalent and divalent cations displays common trends. This is consistent with the lack of specificity of the OmpF channel reported in previous studies⁴. In all electrolytes under study the conductance scales as $G \sim a^{3/4}$ for low activities. In the high activity regime we find saturation or even a slightly decrease in conductance that scales as $G \sim a^{-1/4}$. In the case of KCl this late regime is not attained because of the solubility limit. To rationalize these results, we used a simple theoretical model that accounts for: *i*) The effect of the charged residues of the pore walls -that induces the accumulation of counterions and the exclusion of coions to preserve local electroneutrality-, through the Donnan formalism. *ii*) The experimental dependence of diffusion coefficients on ion activity, which shows different variants distinctive of each electrolyte⁹. *iii*) The variation in the concentration of mobile ions inside the channel due to adsorption processes, using the Langmuir adsorption isotherm¹⁰.

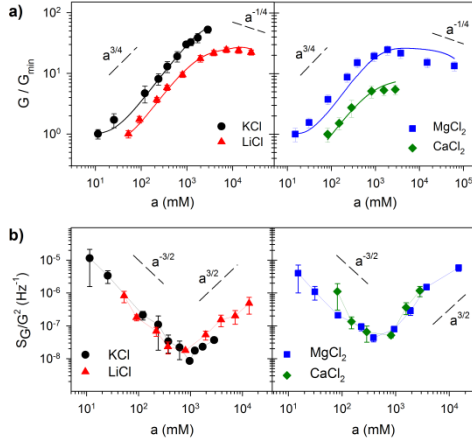


FIG. 2 a) Normalized OmpF channel conductance versus electrolyte activity for different salts. The dashed lines show the qualitative trends observed. The solid lines are calculated applying a theoretical model as described in the main text. b) Dependence of the parabolic coefficient S_G/G^2 on electrolyte activity, for different salts. The dashed lines show the two regimes observed. The solid lines are drawn to guide the eye.

The existence of adsorption processes in OmpF has been suggested by a number of different approaches that pointed to the existence of a binding site for cations located around the central constriction of the OmpF channel¹¹. In spite of all this information, the functional role of that binding site remained unclear since no blocking events have been observed and the channel displays Ohmic conduction in all conditions studied.

The theoretical model developed has only two free parameters: the channel fixed charge concentration, X , and the binding constant K_d of the binding model. Despite the simplicity of this approach, the model reproduces the two trends observed in the experiments, as reported in Fig. (2a) (solid lines). The parameters used for the calculation, $X \sim 50\text{--}100$ mM and $K_d \sim 70$ M, are of the order of magnitude expected. In any case, the qualitative message is clear: the fixed charge of the pore exerts a control of the ion transport and this control is enough to explain the behavior of conductance at the low activity regime, regardless the type of ions present in the system. In addition, the existence of a binding site for cations, altogether with the solution effects, explains the trend at high activities.

The information obtained from the parabolic coefficient, shown in Fig. (2b), can be understood using the same theoretical approach. For all electrolytes under study, the parabolic coefficient exhibits two different regimes, $S_G/G^2 \sim a^{-3/2}$ at low activities and $S_G/G^2 \sim a^{3/2}$ at high activities. Interestingly, the inflection point is observed around $a \sim 1$ M, similarly to the onset of conductance saturation in Fig. (2a). From S_G/G^2 we calculated the number of particles that contribute to the conductance noise, S_G , yielding $S_G \sim a^0$ at the low activity regime. This means that the number of fluctuating particles remains constant when increasing the activity. Having in mind that only for surface-bound fluctuations does the parabolic coefficient S_G/G^2 scale as $a^{-3/2}$ ⁸, the fluctuating particles could be just the counterions screening the channel charges located in the pore surface as explained by Donnan equilibrium. This result is consistent with a transport regime in which the electroneutrality requirements arising from the channel fixed charge dictate the channel conductance. In the

case of high activities, $S_G \sim a^1$. This result can be understood invoking again the binding processes that dominate the channel conductance in the high activity regime as shown in the analysis of Fig. (2a). We can assume that the fraction of occupied sites is directly related to the quantity of fluctuating particles that contributes to the noise. Using the Langmuir adsorption isotherm¹⁰ to account for that binding, the fraction of occupied sites varies linearly with solution activity when the activity of cations is lower than the effective dissociation constant K_d . Accordingly, the conductance fluctuations are expected to follow $S_G \sim a^1$, which is what we actually observe in Fig. (2b). This explanation is consistent with the high K_d values obtained.

Therefore, by means of a particular EN analysis technique combined with conductance experiments we have demonstrated the existence of two main ion transport regimes in the OmpF channel, both for salts of monovalent and divalent cations.

IV. CONCLUSIONS

The analysis of EN provides direct functional evidence of the transport mechanisms occurring in the protein channel OmpF showing features that may appear undetected in the current traces. This is especially evident at high salt concentration. In contrast to conductance experiments, EN analysis show a well-defined common trend clearly visible in all electrolytes under study. The adsorption processes related to the binding site for cations that are hardly visible in conductance experiments can be detected and elucidated using EN analysis.

ACKNOWLEDGEMENTS

We wish to acknowledge the support from the Spanish Ministry of Economy and Competitiveness (MINECO Project FIS2013-40473-P) and the Fundació Caixa Castelló-Bancaixa (Project no. P1-1B2012-03).

- ¹ B. Legros, P.-X. Thivel, Y. Bultel, and R.P. Nogueira, *Electrochem. Commun.* **13**, 1514 (2011).
- ² S.M. Bezrukov, *Fluct. Noise Lett.* **4**, L23 (2004).
- ³ L.J. DeFelice, *Introduction to Membrane Noise* (Springer US, Boston, MA, 1981).
- ⁴ E.M. Nestorovich, T.K. Rostovtseva, and S.M. Bezrukov, *Biophys. J.* **85**, 3718 (2003).
- ⁵ P.A. Gunev, D. Harries, V.A. Parsegian, and S.M. Bezrukov, *J. Physics. Condens. Matter* **22**, 454110 (2010).
- ⁶ S.M. Bezrukov and J.J. Kasianowicz, *Phys. Rev. Lett.* **70**, 2352 (1993).
- ⁷ J.J. Kasianowicz and S.M. Bezrukov, *Biophys. J.* **69**, 94 (1995).
- ⁸ D.P. Hoogerheide, S. Garaj, and J.A. Golovchenko, *Phys. Rev. Lett.* **102**, 256804 (2009).
- ⁹ R.A. Robinson and R.H. Stokes, *Electrolyte Solutions: Second Revised Edition* (Dover Publications, 2002).
- ¹⁰ B. Hille, *Ion Channels of Excitable Membranes*, Third Ed. (Sinauer Associates Inc, Sunderland, MA, 2001).
- ¹¹ A. Alcaraz, M. Queralt-Martín, E. García-Giménez, and V.M. Aguilera, *Biochim. Biophys. Acta-Biomembranes* **1818**, 2777 (2012).

Coulomb Blockade of Stochastic Permeation in Biological Ion Channels

W.A.T. Gibby,¹ I.Kh. Kaufman,¹ D.G. Luchinsky,¹ P.V.E. McClintock,¹ and R.S. Eisenberg²

¹*Department of Physics, Lancaster University, Lancaster LA1 4YB, UK*
e-mail address: p.v.e.mcclintock@lancaster.ac.uk

²*Department of Molecular Biophysics, Rush University, Chicago, USA*
e-mail address: beisenbe@rush.edu

I. INTRODUCTION

Although the passage of ions through ion channels¹ in the bilipid membranes of biological cells clearly involves thermally-driven Brownian diffusion in an electrostatic field, there remain many unsolved problems of long standing. The central conundrum is that a channel's powerful selectivity – whereby it may allow a particular ion species to pass while barring others by a factor of up to 1000:1 – is combined with a speed of passage comparable to the rate of free diffusion, i.e. as though the channel were just an open hole.

Other unsolved problems include: (i) the role played by the fixed charge Q_f known to exist inside the channel at its selectivity filter; (ii) why mutations that change Q_f can alter the selectivity (e.g. convert a Na^+ to a Ca^{2+} channel) or eliminate conduction altogether; (iii) the anomalous mole fraction effect (AMFE), whereby Na^+ ions can pass easily through a Ca^{2+} channel in a pure NaCl electrolyte, but are blocked by tiny traces of Ca^{2+} in the bath. Brownian dynamics simulations of a very simple model of the permeation process reveal² that the current and selectivity exhibit the unexpected pattern of conduction bands and stop bands as a function of Q_f shown in Fig. 1(a).

We now propose that the conduction bands and, quite generally, the permeation and selectivity of biological ion channels may be governed by ionic Coulomb blockade³, an electrostatic phenomenon closely analogous to its electronic counterpart in quantum dots^{4,5}, but with stochastic dynamics rather than quantum tunnelling as the underlying mechanism, and we show that several hitherto unsolved problems of ion channel conduction can apparently be explained on this basis. We will refer to Ca^{2+} ion channels, but the underlying ideas can have wider applicability.

II. MODEL TO BE ANALYSED

We analyse the properties of a self-consistent electrostatic model² of the selectivity filter of a generic calcium channel considered as a negatively-charged, axisymmetric, water-filled, cylindrical pore through a protein hub in the cellular membrane. The pore is taken to be of radius $R = 0.3$ nm, length $L = 1.6$ nm, and the x -axis coincides with the channel axis, with $x = 0$ at the center of the channel. A centrally-placed ring of fixed negative charge $0 \leq |Q_f| \leq 7e$ is embedded in the wall at $R_Q = R$. A potential difference of 0 – 75 mV is applied between the

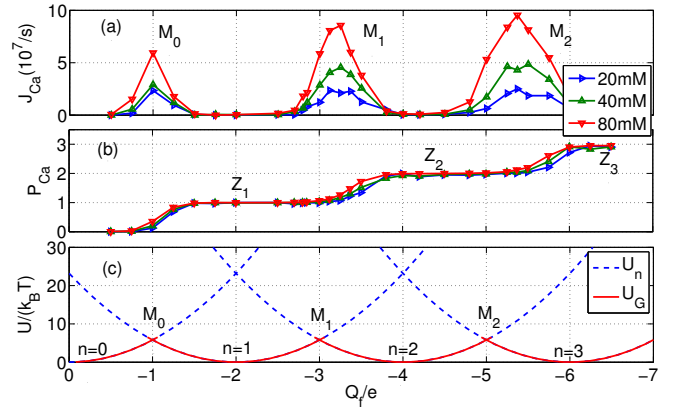


FIG. 1. Brownian dynamics simulations of multi-ion Ca^{2+} conduction and occupancy in the $\text{Ca}^{2+}/\text{Na}^+$ channel model *vs.* the effective fixed charge Q_f ; (a),(b) are reworked from². (a) Plots of the Ca^{2+} current J_{Ca} for pure Ca^{2+} baths of concentration 20, 40 and 80mM. (b) The occupancy P_{Ca} . (c) Plots of electrostatic energy U_n (blue, dashed) and resulting oscillations of ground state energy (red, solid) *vs.* Q_f for channels with $n = 0, 1, 2$. Ca^{2+} ions inside. The conduction bands M_0, M_1, M_2 stop bands Z_1, Z_2, Z_3 (indicated by labels) are discussed in the text.

left and right channel boundaries to represent the membrane potential. The mobile Ca^{2+} ions are described as charged spheres of radius $R_i \approx 0.1$ nm, with a diffusion coefficient⁶ of $D_{\text{Ca}} = 0.79 \times 10^{-9}$ m²/s. We assume an asymmetrical ionic concentration: $C_L > 0$ on the left, and $C_R = 0$ on the right and take both the water and the protein to be homogeneous continua describable by relative permittivities $\epsilon_w = 80$ and $\epsilon_p = 2$, respectively, together with an implicit model of ion hydration the validity of which is discussed elsewhere. The Brownian dynamics simulations (Fig. 1) involved the self-consistent numerical solution of Poisson's equation for this model, coupled with a Langevin equation for the moving ions.

III. IONIC COULOMB BLOCKADE

The alternating conduction and stop bands as Q_f is increased (Fig. 1(a)) can be considered as oscillations. We propose that both they and the occupancy steps (Fig. 1(b)) are attributable to ionic Coulomb blockade³, an electrostatic phenomenon closely similar to electronic Coulomb blockade in quantum dots⁵.

The discreteness of the charge allows us to introduce

exclusive “eigenstates” $\{n\}$ of the channel for fixed integer numbers of ions inside its selectivity filter, with total electrostatic energy U_n . The transition $\{n\} \rightarrow \{n+1\}$ corresponds to entry of a new ion, whereas $\{n\} \rightarrow \{n-1\}$ corresponds to escape of a trapped ion. The n eigenstates form a discrete exclusive set of $\{n\}$ -states:

$$n = \{0, 1, 2, \dots\} \quad \sum_n \theta_n = 1; \quad P_c = \sum_n n\theta_n, \quad (1)$$

where θ_n is the occupancy of the state $\{n\}$ and P_c is the average selectivity filter occupancy. In equilibrium an *electrostatic exclusion principle* (1) leads to Fermi-Dirac statistics for θ_n (and P_c):

$$\theta_n = \left(1 + \exp\left(\frac{U_n - \mu}{k_B T}\right) \right)^{-1}, \quad (2)$$

where μ is the chemical potential. The total energy U_n for a channel in state $\{n\}$ is $U_n = U_{n,s} + U_{n,a} + U_{n,int}$, where $U_{n,s}$ is the self-energy, $U_{n,a}$ is the energy of attraction, and $U_{n,int}$ is the ions’ mutual interaction energy. We approximate U_n as the dielectric self-energy $U_{n,s}$ of the excess charge Q_n , assuming that both the ions and Q_f are within the central part of the selectivity filter, leading to a quadratic dependence of U_n on Q_f ,

$$U_n = \frac{Q_n^2}{2C_s} \quad (\text{Electrostatic energy}) \quad (3)$$

Here, C_s is the geometry-dependent channel self-capacitance and $Q_n = zen + Q_f$ is the excess charge.

With (3) we arrive at the electronic Coulomb blockade equation and our further consideration follows standard Coulomb blockade theory⁴. Remarkably, however, the ionic version of phenomenon exhibits valence selectivity.

Strong Coulomb blockade oscillations appear in low-capacitance systems on account of quantization of the quadratic energy in (3) on a grid of discrete states (1), provided that the ground state $\{n_G\}$ is separated from its neighbouring $\{n_G \pm 1\}$ states by large Coulomb energy

gaps $\Delta U = z^2 e^2 / (2C_s) \gg k_B T$. This is the applicability condition for the strong electrostatic exclusion principle.

Fig. 1(c) shows the ground state energy $U_G(Q_f) = \min_n(U_n(Q_f, n))$, as functions of Q_f . It follows from (3) that U_n vs. Q_f for given z is described by an equidistant set of identical parabolæ of period equal to the ionic charge ze , providing oscillations in U_G . We note that $U_G(Q_f)$ exhibits two different kinds of ground state singular points, marked as M_n and Z_n . The positions of these singular Q_f points can be written as:

$$Z_n = -zen \quad (\text{Coulomb blockade}) \quad (4)$$

$$M_n = -ze(n + 1/2) \quad (\text{Resonant conduction}) \quad (5)$$

We propose that the stop bands in Fig. 1(a) correspond to neutralisation points Z_n where the total charge at the selectivity filter $Q_n = 0$, while the conduction bands correspond to crossover points M_n allowing barrier-less conduction between different n -states. The occupancy plots in Fig. 1(b) can therefore be interpreted as a Coulomb staircase.

IV. CONCLUSIONS

Our identifications of the Brownian dynamics-simulated conduction bands (Fig. 1(a)) that appear with increasing $|Q_f|$ as Coulomb blockade conductance oscillations⁴, and of the corresponding occupancy steps (Fig. 1(b)) as a Coulomb staircase⁵, represent a fresh vision of conduction in biological ion channels. It offers immediate explanations of the fast conduction and mutation shifts and, because the pattern is valence-dependent, it can also account for valence selectivity and AMFE.

We point out that the Coulomb blockade model should also be applicable to other ion channels as well as to artificial nanopores.

ACKNOWLEDGMENTS

The research was supported by the Engineering and Physical Sciences Research Council UK (grant No. EP/M015831/1).

¹ B. Hille, *Ion Channels Of Excitable Membranes*, 3rd ed. (Sinauer Associates, Sunderland, MA, 2001).

² I. K. Kaufman, D. G. Luchinsky, R. Tindjong, P. V. E. McClintock, and R. S. Eisenberg, *Phys. Biol.* **10**, 026007 (2013).

³ M. Krems and M. Di Ventra, *J. Phys. Condens. Matter* **25**, 065101 (2013).

⁴ C. W. J. Beenakker, *Phys. Rev. B* **44**, 1646 (1991).

⁵ K. K. Likharev, *Nano et Micro Tech.* **3**, 71 (2003).

⁶ B. Corry, T. W. Allen, S. Kuyucak, and S. H. Chung, *Biophys. J.* **80**, 195 (2001).

Antipersistent Random Walk in a Two State Flashing Magnetic Potential

Pietro Tierno¹, Francesc Sagués², Tom H. Johansen,^{3,4} and Igor M. Sokolov⁵

¹*Estructura i Constituents de la Matèria, Universitat de Barcelona, Avenida Diagonal 647, 08028 Barcelona, Spain*

²*Departament de Química Física, Universitat de Barcelona, Avenida Diagonal 647, 08028 Barcelona, Spain*

³*Department of Physics, University of Oslo, P. O. Box 1048, Blindern, Norway*

⁴*Centre for Advanced Study at The Norwegian Academy of Science and Letters, 0271 Oslo, Norway*

⁵*Institut für Physik, Humboldt-Universität zu Berlin, Newtonstrasse 15, 12489 Berlin, Germany*

e-mail address: ptierno@ub.edu

I. ABSTRACT

Self-diffusion of colloidal particles arises due to continuous transfer of momentum by the solvent molecules, and it is characterized by a mean square displacement (MSD) proportional to time.¹ In complex environments, like in crowded suspensions of hard spheres, granular materials, viscoelastic media, and in many biological systems, diffusion is often anticipated by subdiffusion, where the exponent of the power law in the MSD is less than one. Subdiffusion is usually attributed to trapping or obstruction, and understanding its origin is crucial in both fundamental and applied research.

When dealing with individual colloids in simple fluids, the absence of interacting neighbors excludes subdiffusion a priori, which, however, can be observed by placing traps or obstacles along the particle path via chemical modification or physical actuation. In the first case, for instance, one can functionalize the particle surface and a nearby substrate with complementary strands of DNA making them “sticky” at a temperature close to the melting of the DNA.² On the other hand, there are many ways to manipulate colloidal particles via external fields that may be employed to confine or release the particles via remote control. In particular, magnetically patterned substrates have shown such capabilities with magnetic colloids,³ opening up the possibilities to induce anomalous kinetics in systems showing otherwise conventional diffusion.

In this talk I will report on the (sub-)diffusive behavior of paramagnetic colloids moving through a flashing potential obtained via external modulation of the stray field of a magnetic bubble lattice. Depending on the applied field parameters, we observe different regimes of motion ranging from trapping to enhanced (non-thermal) diffusion. In particular, we observe robust subdiffusive motion, with MSD growing as \sqrt{t} and lasting in some cases, up to three orders of magnitude in time. In the subdiffusive regime, the particles perform an antipersistent random walk with an astonishing similarity to the random walk on a random walk (RWRW) model introduced in,⁴ as a nontrivial example of correlated RW. Our results also demonstrate that flashing potentials, which often have been employed to ratchet molecules and colloids in the presence of non-negligible thermal fluctuations, can be used to induce and conveniently control the diffusive properties of the particles.⁵

ACKNOWLEDGEMENTS

P. T. was supported by the “Ramon y Cajal” program (RYC-2011-07605) and by the European Research Council via Starting Grant Dynamo (Proj. no. 335040). T. H. J. by The Research Council of Norway.

¹ A. Einstein, *Ann. Phys.* (Leipzig) 322, 549 (1905)

² Q. Xu, L. Feng, R. Sha, N. C. Seeman, and P. M. Chaikin, *Phys. Rev. Lett.* 106, 228102 (2011).

³ P. Tierno, T. H. Johansen, and T. M. Fischer, *Phys. Rev. Lett.* 99, 038303 (2007).

⁴ K.W. Kehr and R. Kutner, *Physica* (Amsterdam) 110A, 535 (1982).

⁵ P. Tierno, F. Sagués, T. H. Johansen, and I. M. Sokolov, *Phys. Rev. Lett.* 109, 070601 (2012).

Giant acceleration of diffusion observed in a single-molecule experiment on F_1 -ATPase

Kumiko Hayashi¹

¹Department of Applied Physics, School of Engineering, Tohoku University, Sendai, Japan
e-mail address: kumiko@camp.apph.tohoku.ac.jp

I. ABSTRACT

The giant acceleration (GA) of diffusion is one of the modern diffusion theories in the field of non-equilibrium statistical mechanics, and was predicted by the theoretical analysis given in Ref. [P. Reimann *et al.*, Phys. Rev. Lett. 2001]. In this study, we applied the theory of the GA of diffusion to a single-molecule experiment on a rotary motor protein, F_1 , which is a component of F_0F_1 adenosine triphosphate (ATP)-synthase. The energetic properties of F_1 were discussed on the basis of the above mentioned theory and the high energy barrier of the rotary potential was estimated to be $20k_B T$ for the first time, with the condition that the adenosine diphosphates (ADPs) were tightly bound to the F_1 catalytic sites.

II. INTRODUCTION

The diffusion phenomena of microscopic particles, heat energy, electrons, etc., are common mechanisms that are routinely observed. They occur in solids, liquids, gases, and even in supercritical fluids, as a result of the thermal motion of the atoms and molecules which constitute these media. Many diffusion theories exist in the field of non-equilibrium statistical mechanics, one of which is the giant acceleration (GA) of diffusion [1-3]. According to Ref. [1], when a constant force is applied to a colloidal particle in a periodic potential, the diffusion of the particle is greatly enhanced. An increase of up to 14 orders of magnitude can occur, compared to free thermal diffusion for a realistic experimental setup. The diffusion coefficient as a function of an applied force exhibits a resonance peak at the force value near the critical tilt of the potential, which becomes increasingly pronounced as the environmental temperature decreases or as the energy barrier (Δ_E) of the periodic potential rises (Fig. 1(a)(b)). Previously, giant enhancement of the free thermal diffusion has been observed in an experiment on metal nanoparticles in the force field of an optical vortex lattice [4].

In this study, we present an effective application of the GA of diffusion to a single-molecule experiment on a rotary motor protein, F_1 -ATPase (F_1), which is a component of F_0F_1 -adenosine triphosphate (ATP) synthase [5].

The minimum complex in F_1 that can act as a motor is the $\alpha_3\beta_3\gamma$ -subcomplex (Fig. 2(a)). When F_1 is isolated from F_0 , the γ -subunit (rotor) rotates in the $\alpha_3\beta_3$ -subunit (ring), hydrolyzing ATP

into ADP (adenosine diphosphate) and Pi (phosphate). In a cell, F_1 is forced to rotate in the reverse direction by the F_0 -motor to synthesize ATP from ADP and Pi. In order to enhance the efficiency of the ATP synthesis, F_1 has a mechanism, such as ADP inhibition, to inhibit the ATP hydrolysis caused by the spontaneous rotation of F_1 itself [6]. In fact, we often observe long pauses during a single-molecule assay during which F_1 falls into the ADP inhibition state. At this point, ADP is tightly attached to a catalytic site of F_1 and is not released.

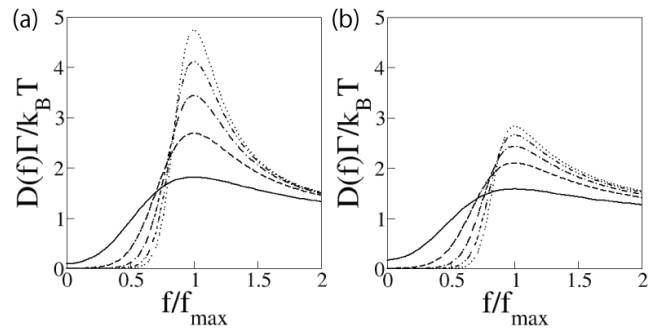


FIG.1. Theoretical results obtained in Ref. [1] and applied to our F_1 experiments. The dimensionless expression of the diffusion coefficient $D(f)\Gamma/k_B T$ as a function of f/f_{\max} for (a) a sinusoidal potential and for (b) a triangle potential with the energy barrier height $\Delta_E=5, 10, 15, 20,$ and $25 k_B T$ (from bottom to top). f_{\max} is the force at which $D(f)$ reaches its peak.

In our study, the application of the GA of diffusion to F_1 made it possible to estimate the high energy barrier of the rotary potential for the first time, under the condition that the ADPs were tightly attached to the catalytic sites of F_1 . We forced a rigid F_1 to rotate by applying an external torque using a single-molecule technique (Fig. 2(b)), and found that the diffusion coefficient of a probe attached to F_1 (as a function of the external torque) shows a resonance peak. The energy barrier was estimated from this peak and found to be approximately $20 k_B T$ at $25^\circ C$ (where k_B is the Boltzmann constant and T is the environmental temperature).

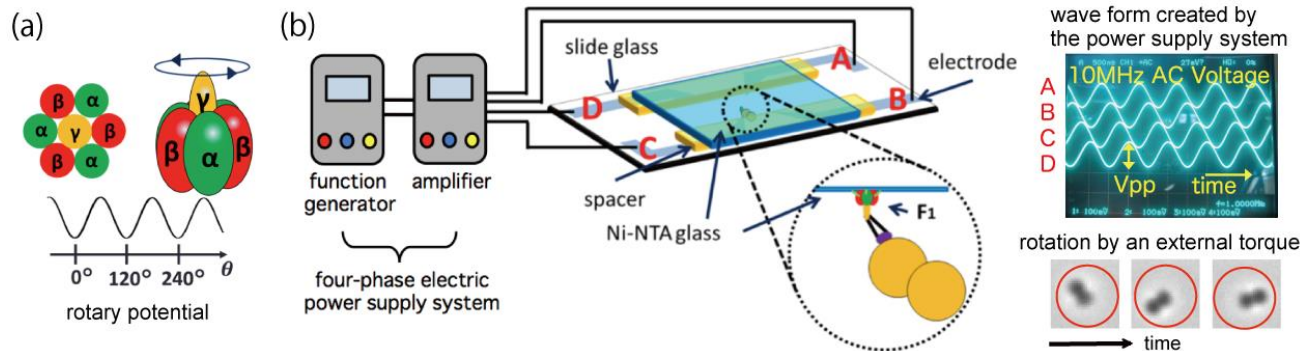


FIG. 2. (a) Because the structure of F_1 has three-fold symmetry, its rotary potential has a period of 120° . (b) Electro-rotation method [7]. A duplex of polystyrene beads (460-nm diameter), which is a dielectric, is attached to the γ -subunit of F_1 . F_1 is fixed on the top glass surface (Ni-NTA-coated coverslip). At the center of the four electrodes, a rotating electric field with the frequency of 10 MHz is generated by applying sinusoidal voltages with a $\pi/2$ phase shift. The phase delay between the electric field and the dielectric moment of the duplex generates a constant torque, N_{ex} .

III. THE CONFERENCE GOAL

In the conference, we would like to offer the opportunity to discuss the way to extract energetic information from noise, which is useful for single-molecule experiments. Because biomolecules work subject to thermal noise, the measurement method based on a noise analysis is significant for single-molecule experiments. A development of methods using a new theory on noise is surely an open problem.

ACKNOWLEDGEMENTS

We thank R. Hayashi, K. Sasaki, S. Nakamura, S. Kudo, Y. Inoue and H. Noji for their contribution to the work. This work was supported by Grants-in-Aid for Scientific Research to K. H. from the MEXT (Nos. 23107703 and 26104501). We also thank the members of the A. Ishijima and S. Takahashi laboratories for their helpful discussions, and Dr. S. Enoki, Dr. M. Tanigawara, and Dr. M. K. Sato for assistance with technical details of the experiments.

- ¹ P. Reimann, C. Vanden Broeck, H. Linke, P. Hanggi, J. M. Rubi and A. Perez-Madrid, *Phys. Rev. Lett.* **87**, 010602 (2001).
- ² P. Reimann, C. Vanden Broeck, H. Linke, P. Hanggi, J. M. Rubi and A. Perez-Madrid, *Phys. Rev. E* **65**, 031104 (2002).
- ³ G. Costantini and F. Marchesoni, *Europhys. Lett.* **48**, 491 (1999).
- ⁴ S. Albaladejo, M. I. Marques, F. Scheffold and J. J. Saenz, *Nano Letters* **9**, 3527 (2009).
- ⁵ D. Okuno, R. Iino and H. Noji, *J. Biochem.* **149**, 655 (2011).
- ⁶ E. I. Sunamura, H. Konno, M. Imashimizu-Kobayashi, Y. Sugano, T. Hisabori, *Plant Cell Physiol.* **51**, 855 (2010).
- ⁷ T. Watanabe-Nakayama, S. Toyabe, S. Kudo, S. Sugiyama, M. Yoshida and E. Muneyuki, *Biochem. Biophys. Res. Commun.* **366**, 951 (2008).

The role of temperature in different thermodynamic ensembles

Peter Hänggi¹

¹*Institut für Physik, Universitätsstr. 1, D-86135 Augsburg
e-mail address: hanggi@physik.uni-augsburg.de*

I. INTRODUCTION

Let us elaborate on the notion of thermodynamic entropy S (Clausius 1865) and its consequences within its statistical mechanical description¹. The celebrated Clausius relation identifies the inverse thermodynamic temperature T as the integrating factor for the second Law in the form that $dS = \delta Q/T$, with δQ being the quasi-static and reversible infinitesimal heat exchange. We first address the most fundamental statistical equilibrium ensemble, namely the microcanonical ensemble (MCE). Please bear in mind that the canonical and the grand canonical ensemble follow from this MCE. – It was J.W. Gibbs who first put forward two notions of thermodynamic entropy for an isolated MCE-system that I commonly will refer to as (i) *volume entropy*, i.e.

$$S_{\text{volume}} := S_G = k_B \ln \Omega(E, Z), \quad (1)$$

where k_B is the Boltzmann constant and the dimensionless quantity $\Omega(E, Z)$ is the integrated, non-negative valued density of states (DoS) $\omega(E, Z)$ over energies not exceeding E . Z denotes the set of external control parameters such as the available volume, particle numbers, magnetic field, etc.. Note that within classical statistical mechanics $\Omega(E, Z)$ equals the properly normalized, dimensionless total available phase space volume up to the energy E . In this context, Gibbs also considered a second expression, namely the (ii) *surface entropy*, reading

$$S_{\text{surface}} := S_B = k_B \ln[\epsilon \omega(E, \lambda)]. \quad (2)$$

This entropy expression is also known (incorrectly) as the Boltzmann entropy. Here ϵ denotes a small energy constant required to make the argument of the logarithm dimensionless. The fact that the definition of S_B requires an additional energy constant ϵ is conceptually displeasing, but bears no relevance for physical quantities that are related to derivatives of S_B .

Historically¹, Boltzmann's tombstone famously carries the formula $S = k_B \log W$, although, following the discussion by Sommerfeld in his book [reprinted, Vorlesungen über Theoretische Physik (volume V): Thermodynamik und Statistik (Verlag Harri Deutsch, Frankfurt am Main, 2011), pp. 181 - 183] it was Planck, and not Boltzmann, who established this equation. As described in many textbooks, the entropy expression S_B defined in Eq. (2) is heuristically obtained by identifying $\log = \ln$ and interpreting $W = \epsilon \omega(E, Z)$ as the number of microstates accessible to a physical system at energy E . Perhaps it is for this reason that the entropy S_{surface} is commonly termed 'Boltzmann entropy' nowadays.

The problem thus arises: **Which entropy should we use?** The consistency with the thermodynamics of isolated systems yields a unique answer: The validity for the celebrated 0-th, 1-st and 2-nd thermodynamic Law then uniquely singles out the microcanonical Gibbs entropy S_G ¹. A different reasoning² yielding this very same finding uses the two thermodynamic pillars that for the validity of the (i) Clausius relation as an exact differential the inverse temperature of the (ii) ideal gas law must fix the integrating factor. A profound recent finding is that any microcanonical entropy expression other than the Gibbs volume entropy, – such as for example the Boltzmann entropy –, can lead to thermodynamical inconsistencies^{1,2}.

The thermodynamic temperature is a *derived* quantity: Given an entropy expression it is given by

$$T^{-1} = \partial S / \partial E. \quad (3)$$

J.W. Gibbs considered yet another entropy expression $S_N = -k_B \text{Tr}[\rho \ln \rho]$, where ρ is the corresponding thermal equilibrium density function for a N -particle system. One should stress here that Gibbs used this definition mainly when describing systems weakly coupled to a heat bath within the framework of the canonical ensemble. Nowadays, S_N is commonly referred to as the *canonical* Gibbs entropy in classical statistical mechanics, as von Neumann entropy in quantum statistics, or as Shannon entropy in information theory.

The most salient results in Ref. [1] and in Ref. [2] are:

- Demanding additivity of S under *factorization* of $\Omega(E, Z)$ (which in turn implies energetically decoupled systems that prevent an energy exchange) uniquely selects the logarithm \ln to yield the microcanonical Gibbs temperature T_G , reading

$$k_B T_G(E, Z) = k_B [\partial S_G / \partial E]^{-1} = \Omega(E, Z) / \omega(E, Z). \quad (4)$$

Because the DoS $\omega(E, Z)$ is non-negative, the 'volume' $\Omega(E, Z)$ is a monotonically increasing function of E . Thus, the Gibbs temperature necessarily has a definite sign, being always non-negative!

- Only for the Gibbs entropy S_G does the thermodynamic temperature obey classical equipartition; i.e., $k_B T = [\partial S_G / \partial E]^{-1} = \langle \xi_k \partial H / \partial \xi_k \rangle$ with ξ_k a phase space degree and H the microscopic Hamiltonian. This feature rules out already the Boltzmann expression S_B as a consistent thermodynamic entropy. The same remark applies to the thermodynamic generalized forces p_i . These must obey the consistency relation

$$p_i := T_G \left(\partial S_G / \partial Z_i \right)_E \stackrel{!}{=} - \left\langle \partial H / \partial Z_i \right\rangle_E, \quad (5)$$

for any system of arbitrary size. This consistency relation is violated for the Boltzmann entropy. For a elucidative demonstration of this breakdown of consistency for S_B see the results for the magnetization of a system of $N \gg 1$ distinguishable and non-interacting spin 1/2 systems in Ref.²

- Although S_G and S_B and other entropy candidates often yield practically indistinguishable predictions for the thermodynamic properties of *normal* systems (see in: R. Kubo, *Statistical Mechanics: An Advanced Course with Problems and Solutions* (Elsevier B. V., Amsterdam, 1965), Sec. 1.6 therein), such as quasi-ideal gases with macroscopic particle numbers, they can produce substantially different predictions for mesoscopic, finite systems and ad hoc truncated Hamiltonians with upper energy bounds. This being so, the microcanonical description is thus generally not equivalent with a canonical description.
- Neither the Gibbs temperature nor the Boltzmann temperature do predict the energy flow between weakly coupled systems which were prepared before coupling at initially different temperatures. The naive formulation of the second law that heat always flows from ‘hot’ to ‘cold’ is thus in general not valid; i.e., it does not always (for example, with the DoS exhibiting local maxima) present a strict formulation of the second Law of thermodynamics.

II. FINITE SYSTEMS: INEQUIVALENCE OF ENSEMBLES AND OPEN PROBLEMS

Shortcomings that relate to the thermodynamics of isolated *small* systems are illustrated when sticking to the (Boltzmann)-surface entropy^{3,4}. Most of all, the uncritical use of Boltzmann entropy for microcanonical systems may formally yield negative values for the absolute temperatures. This is not only physically incorrect for the concept of an absolute temperature, but also would violate thermodynamic stability if the system is brought into (weak) contact with an omnipresent sort of environment of radiation source or otherwise with no upper bound in energy.

We further address canonical ensemble entropy for

quantum systems that interact *strongly* with an environment. Then, the *canonical* (!) specific heat can assume *negative* values away from absolute zero temperature⁵. Likewise, the thermodynamic entropy for a strongly coupled system, assuming a form close to the quantum conditional entropy, but *not* quite, can be negative away from absolute $T = 0$ ⁶.

One unsolved problem is the case for quantum systems with discrete spectra. Here too the volume $\Omega(E, Z)$ is well defined as the sum over the number of energy eigenvalues, accounting also for the degeneracy of corresponding eigenstates E_n , so that the quantum Gibbs entropy has a well defined meaning. A small grain of salt occurs nevertheless: All the considerations thus far relied on the technical assumption that the integrated density of states $\Omega(E, Z)$ is continuous and piecewise differentiable, the latter assumed particularly so with respect to energy E . As a working principle one may use analytic continuations of the discrete level counting functions $\Omega(E_n, Z)$ and $\omega(E_n, Z)$ that are, however, defined strictly speaking only on the discrete set E_n of isolated points of the spectrum¹. This procedure yields in parts astonishingly reasonable results. As temperature approaches zero, however, difficulties occur, such as the failure of microcanonical specific heat not approaching zero as $T \rightarrow 0$, this despite the fact that S_G does obey the 3-rd Law at its lowest energy $E = E_{groundstate}$. In distinct contrast, coupling the system weakly to a heat bath yields the canonical description of these quantum systems for which the canonical partition function $Y(\beta, Z)$, i.e. the Laplace transform of the DoS at the canonical parameter $\beta := (k_B T_{can})^{-1}$ (being the corresponding integrating factor²) becomes well defined at all temperatures. The corresponding canonical specific heat values now vanish for $T \rightarrow 0$. This again reflects the non-equivalence between the two ensemble descriptions for finite size quantum systems.

ACKNOWLEDGMENTS

I like to thank my collaborators Michele Campisi, Jörn Dunkel, Stefan Hilbert, Gert-Ludwig Ingold and Peter Talkner for numerous (almost countless) mutually constructive discussions on these topics over the last ten years. PH also acknowledges support from the cluster of excellence Nanosystems Initiative Munich (NIM).

¹ S. Hilbert, P. Hänggi, and J. Dunkel, *Thermodynamic Laws in Isolated Systems*, Phys. Rev. E **90**, 062116 (2014).

² M. Campisi, *Construction of microcanonical entropy on thermodynamic pillars*, arXiv:1411.2425v3.

³ J. Dunkel and S. Hilbert, *Phase transitions in small systems: microcanonical vs. canonical ensembles*, Physica A **370**, 390 (2006).

⁴ M. Campisi, *On the mechanical foundations of thermodynamics: The generalized Helmholtz theorem* *Studies in History and Philosophy of Modern Physics* **36**, 275 (2005).

⁵ P. Hänggi, G.L. Ingold, and P. Talkner, *Finite quantum dissipation: the challenge of obtaining specific heat*, New J. Phys. **10**, 115008 (2008); *ibid*, *Specific heat anomalies of open quantum systems*, Phys. Rev. E **79**, 061105 (2009).

⁶ M. Campisi, P. Talkner, and P. Hänggi, *Thermodynamics and fluctuation theorems for a strongly coupled open quantum system: an exactly solvable case*, J. Phys. A: Math. Theor. (Fast Track) **42**, 392002 (2009).

Adiabatic Passage and Noise in Quantum Dots

Sigmund Kohler¹

¹*Instituto de Ciencia de Materiales de Madrid, CSIC, Cantoblanco, 28049 Madrid, Spain*
e-mail address: sigmund.kohler@icmm.csic.es

I. INTRODUCTION

The dynamics at avoided level crossing is an intriguing topic since the early days of quantum mechanics. As early as in 1932, Landau, Zener, Stückelberg, and Majorana independently of each other derived the well-known formula for the corresponding transition probability. Today in the realm of quantum dots, adiabatic transitions motivated both theoretical and experimental investigations on the control of solid state qubits. Here we discuss two applications for which noise plays a crucial role: In the first one, shot noise of an electric current is used as signal; in the second one, we analyze how quantum noise stemming from substrate phonons influences of repeated adiabatic passages.

II. COHERENT TRANSFER BY ADIABATIC PASSAGE

Adiabatic passage of an electron in a triple quantum dot from the first to the last dot without ever occupying the middle dot recently attracted much attention. This coherent transfer by adiabatic passage (CTAP) represents an all-electronic version of stimulated Raman adiabatic passage. A major experimental obstacle for the implementation of this protocol is the impossibility of directly measuring the non-occupation of the middle dot, because the unavoidable backaction would influence the effect that it should substantiate. It will be shown that an indirect verification is possible by attaching electron

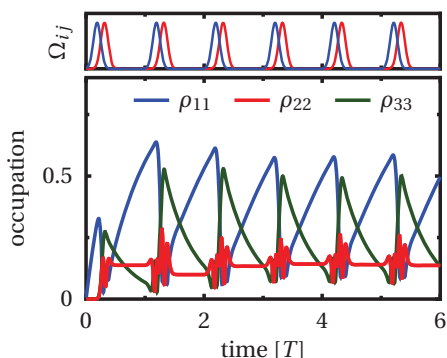


FIG. 1. Upper panel: Sequence of Gauss pulsed tunnel matrix elements that induce adiabatic electron transfer from the first to the third quantum dot¹. Lower panel: Resulting occupation of each quantum dot. The middle dot (dot no. 2) exhibits only a small occupation which changes considerably less than the occupation of dots 1 and 3.

source and drain to the triple dot. Then the protocol can be repeated such that a steady state current flows. The noise properties of this current hint on the proper course of the protocol.

III. LANDAU-ZENER INTERFEROMETRY

Quantum dots with long coherence times also allow the implementation of tunnel phenomena under the influence of AC driving. In a comprehensive picture, one may study the average current as function of the static level detuning and the driving amplitude. This yields a so-called Landau-Zener-Majorana-Stückelberg (LZSM) interference pattern similar to one found with superconducting qubits. The experimentally observed fading of this interference pattern with increasing temperature is explained in terms of a transport calculation for which a Caldeira-Leggett-like coupling to bulk phonons is considered. The comparison with experimental data allows one to determine the parameters of the system-bath model and to draw conclusions on the coherence time of charge qubits.

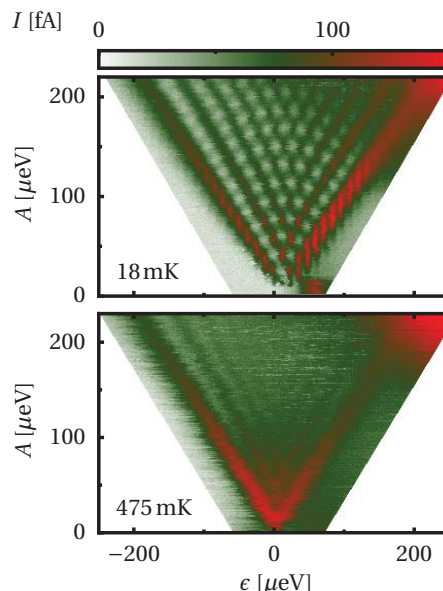


FIG. 2. Measured LZSM pattern as a function of the DQD detuning and the driving amplitude for two different temperatures². A comparison with corresponding theoretical data allows one to determine the coherence times T_2 and T_2^* .

IV. ADIABATIC PASSAGE IN THE PRESENCE OF A CHARGE MONITOR

Many recent realizations of quantum dots include a charge monitor, i.e., a quantum point contact whose conductivity is affected by the capacitive interaction with the dot electrons. Measuring the current through the point contact implies monitoring the dot occupation. In the case of coherently coupled quantum dots, such measurement entails backaction on delocalized quantum dot states. It can be shown³ that if the measurement is sufficiently strong to provide useful information, the inter-dot tunneling becomes essentially classical. Since adiabatic passages rely on quantum coherence, one must assume that it is strongly affected by such detector backaction. So far, only the basic measurement effects have been investigated, while the impact of the charge monitor on

a more complex quantum dynamics such as CTAP or LZSM interference requires the development of a proper formalism for the full setup including the monitor. This is particularly challenging for a point contact with transmission close to unity, because it must combine a formalism suited for quantum dots (weak dot-lead coupling, strong interaction) with a scattering formalism which addresses the opposite limit. This would also allow testing fluctuation theorems along the lines of Ref. 4, but beyond the regime of intermediately strong wire-lead coupling.

ACKNOWLEDGMENTS

This work was supported by the Spanish Ministry of Economy and Competitiveness via the grant MAT2011-24331 and MAT2014-58241-P.

¹ J. Huneke, G. Platero, and S. Kohler, *Steady-state coherent transfer by adiabatic passage*, Phys. Rev. Lett. **110**, 036802 (2013).

² F. Forster, G. Petersen, S. Manus, P. Hänggi, D. Schuh, W. Wegscheider, S. Kohler, and S. Ludwig, *Characterization of qubit dephasing by Landau-Zener-Stückelberg-Majorana interferometry*, Phys. Rev. Lett. **112**, 116803

(2014).

³ R. Hussein, J. Gómez-García, and S. Kohler, *Monitoring quantum transport: Backaction and measurement correlations*, Phys. Rev. B **90**, 155424 (2014).

⁴ R. Hussein and S. Kohler, *Quantum transport, master equations, and exchange fluctuations*, Phys. Rev. B **89**, 205424 (2014).

Non-zero probability of detecting identical electrons at the same position: How does it affect the Landauer-Büttiker noise expression at high temperatures?

Enrique Colomés,¹ Damiano Marian,¹ and Xavier Oriols¹

¹*Departament d'Enginyeria Electrònica, Universitat Autònoma de Barcelona, Bellaterra 08193, Spain
e-mail address: xavier.oriols@uab.es*

I. INTRODUCTION

Is it possible to detect two electrons at the same position with the same energy? Initially one would answer negatively due to the Pauli principle¹. However, strictly speaking the Pauli principle, which is just a consequence of the exchange interaction (for the indistinguishability of quantum particles), only forbids common positions when electrons share exactly the same state. Therefore, if two particles are described by slightly different states, one cannot neglect the possibility of detecting both at the same location.

The modeling of quantum noise in mesoscopic systems is normally studied within the (energy) scattering (eigen)states², where only one state is available for each energy, precluding the detection of two particles at the same position. However, in this conference we show that quasi-particle wave packets do not preclude such possibility. The detection of two particles with identical energies at the same position are possible with such time-dependent states, because transmitted and reflected wave packets are not exactly identical. These new two-particle scattering probabilities leads to new terms in the usual Landauer-Büttiker² quantum noise expression.

II. TWO-PARTICLE SCATTERING

A new quantum noise formalism is developed for many-electron systems described by quasi-particle wave packets. For simplicity, the relevant effects are discussed in the two-particle scenario depicted in Fig. 1. The generalization to a realistic many-particle system will be mentioned in the conclusions. We analyze two identical wave packets that are located at each side of the barrier (at the same distance) and with opposite momentum (i.e. same central energy). During the interaction with the barrier, the initial wave packets split into a transmitted and a reflected part. At the final time, apart from the obvious probabilities of detecting a particle at each side of the barrier (see Fig. 1a and b), the time-dependent numerical solution constructed from quasi-particle wave packets shows that it is possible to find both electrons at the same place, i.e. both at the left side or at the left side (see Fig. 1c and d). The ultimate reason of these unexpected probabilities is the fact that the reflected and transmitted wave packets are not equal at the final time, even if they have identical energy at the initial time^{3,4}. It is remarkable that our many-particle wave packet formalism provides simple physical explanations for some relevant and still unexplained experimental results^{5,6}.

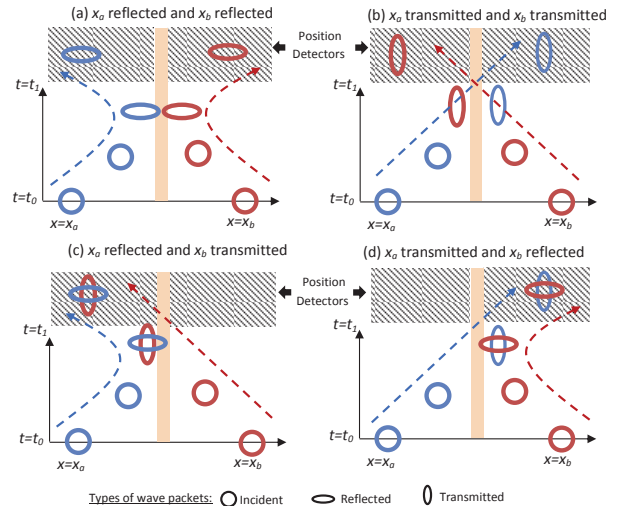


FIG. 1. Two identically injected wave packets from the left x_a and from the right x_b of a scattering barrier. Solid regions represent the barrier region and shaded regions represent the particle detectors. (a) and (b) each particle is detected on a different side of the barrier at final time t_1 when the interaction with the barrier has almost finished. (c) and (d) both particles are detected on the same side of the barrier.

For example, the possibility of finding both quasi-electrons at the left side ($\mathcal{P}_{\mathcal{L}\mathcal{L}}$) is

$$\mathcal{P}_{\mathcal{L}\mathcal{L}} = \int_{-\infty}^0 dx_1 \int_{-\infty}^0 dx_2 |\Phi|^2 = R_a T_b - |I_{a,b}^{r,t}|^2. \quad (1)$$

where Φ is the antisymmetric two-particle wave function. R_a and T_b are the reflection and transmission coefficients of the single wave packets. The term $|I_{a,b}^{r,t}|^2$ accounts for the overlapping among the reflected wave packet a and the transmitted wave packet b .

As mentioned above, the probabilities $\mathcal{P}_{\mathcal{L}\mathcal{L}}$ and $\mathcal{P}_{\mathcal{R}\mathcal{R}}$ are different from zero and their values fluctuate between $\mathcal{P}_{\mathcal{L}\mathcal{L}} = 0$ and $\mathcal{P}_{\mathcal{L}\mathcal{L}} = RT$. This is seen in Fig. 2, where the usual zero probability is recovered for large spatially extended wave packets (close to time-independent scattering states) with energies far from the resonant energy. On the contrary, the maximum values of $\mathcal{P}_{\mathcal{L}\mathcal{L}}$ are achieved for not infinitely-extended wave packets with energies closer to the resonance.

Obviously, in scenarios with more scattering probabilities (the ones showed in Fig. 1c and d for both electrons at the same place), the quantum noise is enlarged. This

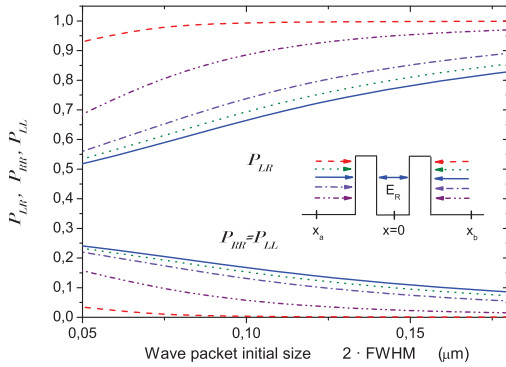


FIG. 2. Probability of detecting two electrons at the same side of the barrier ($\mathcal{P}_{\mathcal{L}\mathcal{L}}$ and $\mathcal{P}_{\mathcal{R}\mathcal{R}}$) and of detecting one electron at each side ($\mathcal{P}_{\mathcal{L}\mathcal{R}}$) depending on the wave packet initial size for three different energies.

is reflected in the following expression for quantum noise which has a new term in our two-particle scenario (in a many-particle scenario more terms are added):

$$\langle S \rangle = \frac{4q^2}{h} \int_0^\infty dE \{ T[f_a(1-f_a) + f_b(1-f_b)] + T(1-T)(f_a - f_b)^2 + 2\mathcal{P}_{\mathcal{L}\mathcal{L}}f_af_b \}. \quad (2)$$

The new term $2\mathcal{P}_{\mathcal{L}\mathcal{L}}f_af_b$ shows that the well-established Landauer-Büttiker² expression (obtained using scattering states) can be violated in same scenarios. On the contrary, when wave packets are close to scattering states, then $\mathcal{P}_{\mathcal{L}\mathcal{L}} = 0$, and usual results are recovered.

III. CONCLUSIONS AND DISCUSSIONS

We generalize the Landauer-Büttiker noise expression by considering many-particle states constructed from an antisymmetric combination of quasi-particle wave packets. In the particular two-particle scenario, the results in equation (2) recover also the usual scattering states results when using infinitely-extended states.

A realistic scenario for quantum transport implies the consideration of a many-particle case. Then, new more terms appear in the quantum noise expression accounting for two-, three-, etc wave packets correlations. At

low temperatures, when the phase-space is full, the mentioned new terms added in the quantum noise expression tends to zero (see Fig. 3) and the quantum noise is zero, satisfying the fluctuation-dissipation theorem^{7,8}. Nevertheless, at high temperatures, these news terms can not be neglected and quantum noise is increased over what is usually predicted. We emphasize that the formalism presented in this conference provides a physical explanation for surprising experimental results^{5,6}, which are normally attributed to spurious effects. Finally, we remark that the increment of quantum noise discussed here is very robust and it is present (even magnified) when time-dependent potentials or (non-separable) Coulomb interactions are considered³.

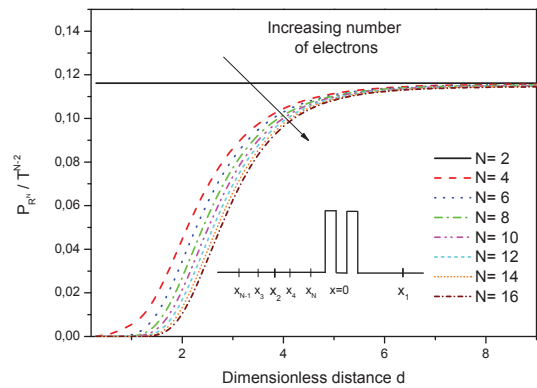


FIG. 3. Each curve reflects the new term added in the quantum noise expression for different number of involved electrons. The phase space gets filled as we increase the number of electrons and we decrease the dimensionless distance d . We see how probabilities decrease.

ACKNOWLEDGMENTS

This work has been partially supported by the “Ministerio de Ciencia e Innovación” through the Spanish Project TEC2012-31330 and by the Grant agreement no: 604391 of the Flagship initiative “Graphene-Based Revolutions in ICT and Beyond”.

¹ W. Pauli, Physik **31** 765 (1925).

² M. Blanter and M. Büttiker, Phys. Rep. **336**, 1 (2000).

³ D. Marian, E. Colomé and X. Oriols, J. Phys. Condens. Matter **27**, 245302 (2015).

⁴ http://europe.uab.es/xoriols/two_identical_electrons.mov

⁵ R. C. Liu, B. Odom, Y. Yamamoto and S. Tarucha, Nature **391**, 263 (1988).

⁶ E. Bocquillon, V. Freulon, J. M. Berroir, P. Degiovanni, B. Plaçais, A. Cavanna, Y. Jin and G. Fève, Science **339**, 1054 (2013).

⁷ H. Nyquist, Phys. Rev. **32**, 110 (1928).

⁸ J. Johnson, Phys. Rev. **32**, 97 (1928).

Dissipative dynamics of a quantum particle strongly interacting with a super-Ohmic heat bath

Luca Magazzù,^{1,2} Davide Valenti,¹ and Bernardo Spagnolo^{1,2,3}

¹*Dipartimento di Fisica e Chimica, Università di Palermo, Interdisciplinary Theoretical Physics Group, Università di Palermo and CNISM, Unità di Palermo, Viale delle Scienze, Edificio 18, 90128 Palermo, Italy*

²*Radiophysics Department, Lobachevsky State University, 23 Gagarin Avenue, 603950 Nizhniy Novgorod, Russia*

³*Istituto Nazionale di Fisica Nucleare, Sezione di Catania, Via S. Sofia 64, I-90123 Catania, Italy*

I. INTRODUCTION

Realization of devices displaying quantum behavior is within the reach of present day experimental capabilities. Experimental and theoretical results on superconducting quantum devices has made them among the main candidates for the realization of quantum computing¹. In these devices the magnetic flux quantum associated to the current of the superconducting circuit is usually subject to a bistable potential. Bistability is also present in systems such as single high-spin molecule magnets². These molecules tunnel through the potential barrier of the effective bistable potential given by the interaction of the spin with the molecular field. Both single molecule magnets and superconducting devices are subject to environmental fluctuations. In quantum regime the dynamics of a particle interacting with the environment can be described by the celebrated Caldeira-Leggett model³, which allows to analyze the dynamics of a particle coupled by a linear interaction to a reservoir of N independent quantum harmonic oscillators. The interaction with the bath can affect the system dynamics in a significant way since, even if the coupling with the individual oscillator is weak, the dissipation regime may be strong. In the thermodynamical limit $N \rightarrow \infty$ the reservoir is called a *heat bath* and its spectral density function $J(\omega)$, describing the frequency dependence of the coupling to the system, is taken to be of the form $J \propto \omega^s$, with a high-frequency cut-off. The special case $s = 1$ describes the so-called Ohmic dissipation. The quantum Langevin equation for the particle's coordinate in the Ohmic case is characterized by a memoryless damping kernel (frequency independent friction) and in the classical limit $\hbar \rightarrow 0$ corresponds to the case of white noise source.

Despite the circumstance that in most cases the Ohmic dissipation gives a good description of the effects exerted by the thermal bath, super-Ohmic environments ($s > 1$) are of interest on both the theoretical and the experimental point of view. Moreover, the system dynamics can be significantly affected by the value of the cut-off frequency present in $J \propto \omega^s$.

In this work we intend to answer two questions: i) how the dynamics of a M -level quantum particle changes when a heat bath with a super-Ohmic spectral density is present instead of an Ohmic reservoir; ii) how varying the cut-off frequency in the spectral density function affects the system dynamics. The study is carried out by using

an integro-differential equation within the path integral formalism, following the approach used in Refs.^{4,5}.

II. THE MODEL

The model of dissipation used here is the Caldeira-Leggett model. It allows for a *microscopic* derivation of dissipation in the reduced dynamics. The system, a particle of mass M , coordinate \hat{q} , and momentum \hat{p} subject to a potential V_0 , is linearly coupled to the environment, a reservoir of N independent quantum harmonic oscillators of masses m_j , frequencies ω_j , coordinates \hat{x}_j , and momenta \hat{p}_j . The reservoir is also called, in the thermodynamical limit $N \rightarrow \infty$, bosonic *heat bath*, since its excitations obey the Bose-Einstein statistics. The full Hamiltonian is the sum of a free system term, a free reservoir term and a system-reservoir interaction term

$$\hat{H} = \frac{\hat{p}^2}{2M} + V_0(\hat{q}) + \sum_{j=1}^N \frac{1}{2} \left[\frac{\hat{p}_j^2}{m_j} + m_j \omega_j^2 \left(\hat{x}_j - \frac{c_j}{m_j \omega_j^2} \hat{q} \right)^2 \right]. \quad (1)$$

The bistable asymmetric potential V_0 used in this work is depicted in Fig. 1. In the general case of continuous bath the spectral density function is modeled as a power of ω , characterized by the exponent s , with an exponential cutoff at ω_c

$$J(\omega) = M \gamma \omega_{\text{ph}}^{1-s} \omega^s e^{-\omega/\omega_c}. \quad (2)$$

The bath is said sub-Ohmic for $0 < s < 1$, Ohmic for $s = 1$ and super-Ohmic for $s > 1$. The so-called *damping constant* γ is a measure, in the continuous limit, of the system-bath coupling. The *phonon* frequency ω_{ph} is introduced in such a way that γ has the dimension of a frequency also in the non-Ohmic case ($s \neq 1$).

The dynamics of the reduced density matrix (RDM) $\rho_{qq'}$ = $\langle q | \rho | q' \rangle$ is given by the exact formal expression

$$\rho_{qq'}(t) = \int dq_0 \int dq'_0 G(q, q', t; q_0, q'_0, t_0) \rho_{q_0 q'_0}(t_0), \quad (3)$$

where the propagator G is a double path integral in the left/right coordinate q/q' . The amplitudes in this sum-over-paths are weighted by the Feynman-Vernon influence functional \mathcal{F}_{FV} , which accounts for the effects of the environment.

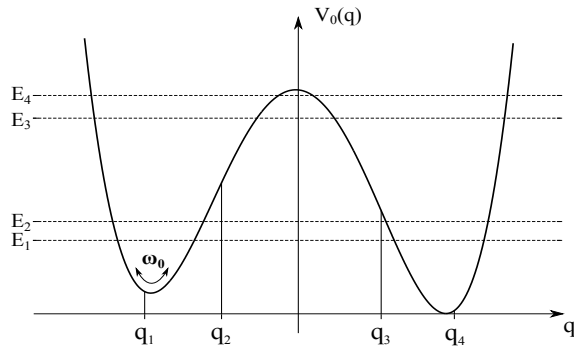


FIG. 1. Potential V_0 , energy levels considered, and position eigenstates. The frequency ω_0 is the oscillation frequency around the minima and is of the order of the average inter-doublet spacing: $\hbar\omega_0 \sim (E_4 + E_3 - E_2 - E_1)/2$.

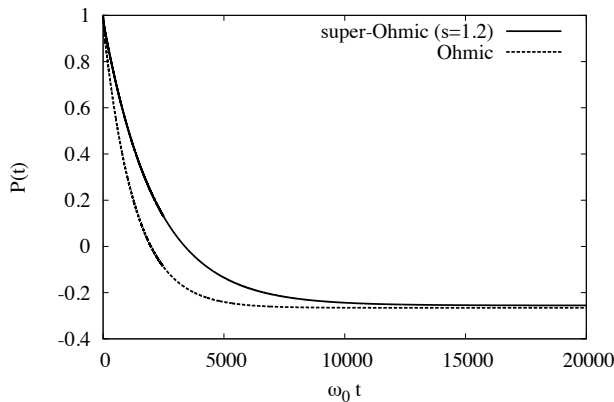


FIG. 2. Population difference $P(t) = P_R - P_L$, where $P_L = \rho_{11} + \rho_{22}$ and $P_R = \rho_{33} + \rho_{44}$ at damping strength $\gamma = 0.1 \omega_0$ and temperature $T = 0.2 \hbar\omega_0/k_B$. Comparison between the Ohmic and the super-Ohmic ($s = 1.2$) regime.

Here we consider the so-called *double-doublet* system, where only the first 4 levels of the potential V_0 are considered. The continuum of position states turns into a discrete set of states localized around a grid of 4 position eigenvalues q_1, \dots, q_4 , where $\hat{q}|q_j\rangle = q_j|q_j\rangle$. The set $\{q_i, |q_i\rangle\}$ constitutes the discrete variable representation (DVR). The system dynamics is studied through the time evolution of the populations $\rho_{ii} = \langle q_i|\rho|q_i\rangle$. Finally, within a NIBA-like approximation scheme the generalized master equation (GME) for the populations in the

DVR reads⁴

$$\dot{\rho}_{ii}(t) = \sum_{j=1}^4 \int_{t_0}^t dt' K_{ij}(t-t') \rho_{jj}(t'). \quad (4)$$

Solving Eq. (4) in the intermediate temperature/damping regime, with the initial condition $\rho_0 = |q_1\rangle\langle q_1|$, we obtain the results shown in Fig 2 (Ohmic and sub-Ohmic case with a high frequency cutoff at $\omega_c = 50\omega_0$) and Fig. 3 (Ohmic regime for different cutoff frequencies). We notice that the equilibrium configuration in the super-Ohmic case is reached later with respect to the Ohmic case, even if the time evolution of the individual populations (not shown) displays similar features (transient intra-well oscillations and incoherent tunneling). Changing the cutoff frequency in the Ohmic regime has an influence both on the relaxation dynamics and on the stationary configuration.

A major unsolved problem in the context of the influence of quantum noise on multi-state systems is the description of the decoherence in this intermediate dissipation regime, using a fully non-Markovian approximation scheme.

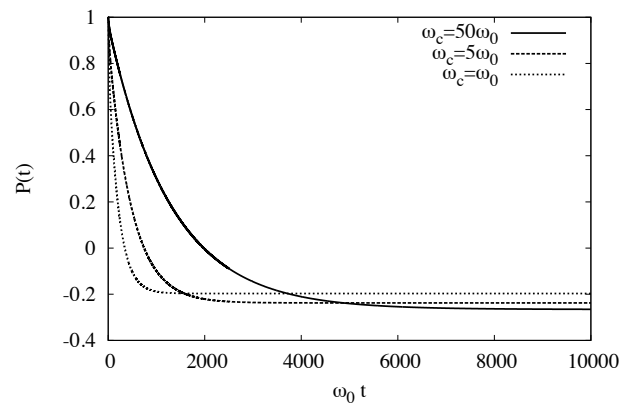


FIG. 3. Population difference $P(t) = P_R - P_L$, where $P_L = \rho_{11} + \rho_{22}$ and $P_R = \rho_{33} + \rho_{44}$ at damping strength $\gamma = 0.1 \omega_0$ and temperature $T = 0.2 \hbar\omega_0/k_B$. Ohmic regime with different cutoff frequencies.

ACKNOWLEDGMENTS

This work was supported by MIUR through Grant. No. PON02_00355_3391233, "Tecnologie per l'ENERGIA e l'Efficienza enerGETICa - ENERGETIC".

¹ M. H. Devoret and R. J. Schoelkopf, Science **339**, 1169 (2013).

² C. Schlegel, *et al.*, Phys. Rev. Lett. **101**, 147203 (2008).

³ A. O. Caldeira and A. J. Leggett, Phys. Rev. Lett. **46**, 211 (1981).

⁴ M. Thorwart, M. Grifoni, and P. Hänggi, Ann. Phys. **293**, 15 (2001).

⁵ L. Magazzù, D. Valenti, B. Spagnolo, and M. Grifoni, arXiv:1412.7467v1 (2014).

Fractional quantum Hall spectroscopy investigated by a resonant detector

Alessandro Braggio,¹ Matteo Carrega,¹ Dario Ferraro,^{2,3} and Maura Sassetti^{4,1}

¹*SPIN-CNR, Via Dodecaneso 33, 16146 Genova, Italy*

²*Aix Marseille Université, Université de Toulon,*

CNRS, CPT, UMR 7332, 13288 Marseille, France

³*Département de Physique Théorique, Université de Genève,*
24 quai Ernest Ansermet, CH-1211 Geneva, Switzerland

⁴*Dipartimento di Fisica, Università di Genova, Via Dodecaneso 33, 16146 Genova, Italy*

I. INTRODUCTION

In recent years a great attention has been devoted to the study of strong correlations in low dimensional systems. Among them the fractional quantum Hall effect (FQHE) plays a major role, in which correlations can induce the emergence of excitations with fractional charges and fractional statistics.^{1,2} Several works focussed on the experimental detection of these peculiar features. In particular, fractional charges can be revealed by means of shot noise measurements in a quantum point contact (QPC) geometry.³ Indeed, the zero frequency current-current correlation, in the weak-backscattering regime, is predicted to be proportional to the induced backscattering current via the fractional charge associated to the tunnelling excitation between the opposite edges of the Hall bar. Clear experimental signatures of this fact have been reported for the Laughlin sequence. In the case of composite edges, such as in the Jain sequence the situation is more involved since at low energies, various excitations with different fractional charges can contribute to the transport.^{4,5} Moreover, zero frequency noise may be not enough in order to extract in a univocal way the values of the fractional charges when many of them contribute, with comparable weight to QPC transport. A possible way to overcome this limitation is to look at the finite frequency (f.f.) properties.⁶⁻⁸ In particular, for quantum Hall QPC transport, the f.f. noise is predicted to show resonances in correspondence of Josephson frequencies, which are proportional to the fractional charges.

II. PROPOSED DETECTION SCHEME

In the context of current-current correlations Lesovik and Loosen⁹ introduced a model based on a resonant LC circuit as prototypical scheme for f.f. noise measurement. It has been shown that the measured quantity for the LC detector setup can be expressed in terms of the non-symmetrized f.f. noise which reflects the emission and adsorption contributions of the active system under investigation, *i.e.* the QPC. The non-symmetrized noise has been considered in literature for different systems as the ultimate source of information of quantum noise properties.¹⁰⁻¹² Here¹³ we consider the f.f. detector output power of a resonant circuit coupled to a QPC in the fractional

quantum Hall regime. A schematic view of the proposed setup is shown in Fig.(1). The measurable quantity, in

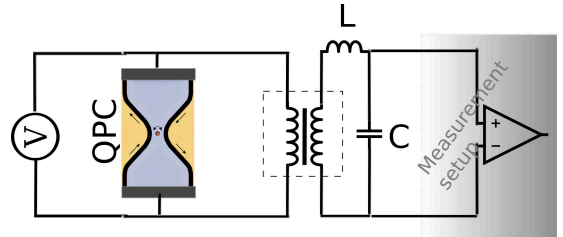


FIG. 1. Schematic view of the proposed setup.

this scheme, is the variation of the energy (at frequency $\omega = \sqrt{1/LC}$) stored in the LC circuit before and after the switching on of the LC-QPC coupling, *i.e.* the circuit element in the dashed line of Fig.(1). We will indicate it as measured noise S_{meas} . At lowest perturbative order in the coupling $K \ll 1$ it can be expressed in terms of the non-symmetrized noise spectrum of the QPC.^{9,10} Finally, this quantity may be eventually expressed in terms of the difference of the output LC power, at finite bias V , subtracted with the same quantity measured at equilibrium, $V = 0$.¹³

III. RESULTS

Hereafter we will discuss this detector model coupled with a QPC kept in the fractional Hall regime in the limit of weak back-scattering. This realistically measurable noise power will be analyzed, at fixed frequency ω , as a function of QPC bias V , measured in terms of the Josephson frequency $\omega_0 = e^*V/\hbar$ associated to the fundamental fractional charge e^* of the considered Hall state. We will assume that the temperature T_c of the detector could be controlled and kept, eventually, at different temperature from the QPC circuit T . We will mainly consider the quantum limit for the detector, $\hbar\omega \gg k_B T_c$, where the output power is proportional to the non-symmetrized noise. The QPC, will be investigated by scanning the bias out of equilibrium (shot noise limit $e^*V \gg k_B T$). These limits represent the best conditions to extract information about fractional multiple quasiparticles (qps), in particular, their charge me^* and their scaling properties.¹⁴

First of all, we will analyze the well known case of non-

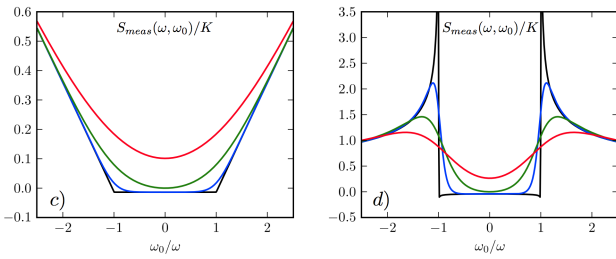


FIG. 2. Measured noise S_{meas} as a function of external bias for $\nu = 1$ (left panel) and $\nu = 1/3$ (right panel) (in units of $S_0 = e^2|t_1|^2/(2\pi\alpha)^2\omega_c$). Bias measured as ω_0/ω , with $\omega_0 = e^*V$. Temperatures are: $T = 0.1$ mK (black), $T = 5$ mK (blue), $T = 15$ mK (green) and $T = 30$ mK (red). Other parameters are: $T_c = 15$ mK, $\omega = 7.9$ GHz (60 mK), $\omega_c = 660$ GHz (5 K).

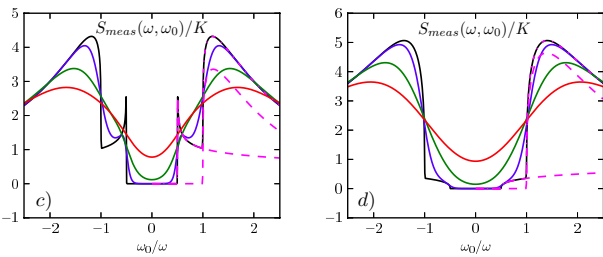


FIG. 3. Measured noise S_{meas} as a function of ω_0/ω for $\nu = 2/5$ (left panel) and $\nu = 2/3$ (right panel). All quantities are in units of S_0 . The temperatures are the same of Fig.2. Other parameters are: $\omega = 7.9$ GHz (60 mK), $T_c = 0.1$ mK, $\omega_n = 6.6$ GHz (50 mK), $\omega_c = 660$ GHz (5 K). The dashed lines correspond to the rate contributions of the 2-agglomerate and the single-qp for $T = 0.1$ mK. They are calculated separately and fitted only by changing their prefactors. The dashed-dotted line is the sum of the two contribution and returns exactly the behaviour of S_{meas} .

interacting Fermi liquid ($\nu = 1$) and Laughlin ($\nu = 1/3$) to show some important and useful properties of the measurement setup. Differently from what usually considered in other theoretical papers, where the noise is shown at finite bias as a function of the frequency, here we will discuss the opposite case in which the bias is moved at fixed frequency. This allows us to be closer to realistic exper-

imental situations representing by far the simplest measurement protocol for the system. We discuss in details the advantages of considering this measurement scheme in comparison to the simpler symmetrized noise.

In Fig.(2). we report the measured noise S_{meas} for the cases $\nu = 1$ (left panel), $1/3$ (right panel) for different temperatures. It is easy to recognise in the behaviour of the output power directly the shape of tunnelling rates for the dominant excitation e (electron) and single-qp $e^* = \nu e$ (single-qp). Indeed in the Laughlin case the line-shape return immediately information of the investigated excitation, such as the scaling dimension from the shape of the peaks centred at ω_0 . This information can be accessed in this setup and it may be crucial in order to validate the edge states theories.

The detector response will give the unique possibility to selectively address the emission contribution of QPC noise or its adsorptive part only by acting on the detector temperature. We also discuss the range of the detector temperatures in order to access the non-symmetrized noise contributions. In particular it is convenient that T_c is smaller than the considered frequency ω .

Finally, see Fig.(3), we apply the previous concepts to the measurement of multiple qps for two values of the Jain sequence ($\nu = 2/5$ and $\nu = 2/3$). In all cases we demonstrate how this setup is able to clearly address the different qps contributions separately and to quantitatively validate the hierarchical edge state models. In such cases we could distinguish the contribution of single-qp (e^*) or 2-agglomerate ($2e^*$) from the position of the corresponding Josephson resonances. From this we can separately address the contribution of the two excitations fitting their tunnelling rates and identifying their fundamental properties, such as the scaling dimensions. From these knowledges it is possible to validate various edge state models which in general differ in the prediction of these quantities. This possibility to separately address the different excitation contribution on the base of their different charges is unique resource of this setup and is deeply connected to the fact that analysis is done at finite bias (out-of-equilibrium) and at finite frequencies.

The same analysis can be repeated for other fractions, such as $\nu = 5/2$, with the factual possibility to identify which edge state model apply to the observed Hall state (Abelian, Pfaffian or anti-Pfaffian).^{7,8}

¹ R. Laughlin Phys. Rev. Lett. **50** 1395(1983).

² J. K. Jain Phys. Rev. Lett. **63** 199 (1989).

³ R. de Picciotto *et al.* Nature **389** 162 (1997).

⁴ Y. C. Chung, M. Heiblum, and V. Umansky Phys. Rev. Lett. **91** 216804 (2003); A. Bid *et al.* Phys. Rev. Lett. **103** 236802 (2009); M. Dolev, *et al.* Phys. Rev. B **81** 161303 (2010).

⁵ D. Ferraro *et al.* Phys. Rev. Lett. **101** 166805 (2008).

⁶ C. Chamon *et al.* Phys. Rev. B **51** 2363 (1995); C Chamon *et al.* Phys. Rev. B **53** 4033 (1996).

⁷ M. Carrega *et al.* Phys. Rev. Lett. **107** 146404 (2011).

⁸ M. Carrega *et al.* New J. Phys. **14** 023017 (2012).

⁹ G. B. Lesovik and R. Loosen JETP Lett. **65** 295(1997).

¹⁰ U. Gavish *et al.* Phys. Rev. B **67** 10637 R (2000); U. Gavish *et al.* Phys. Rev. Lett. **93** 250601 (2004); D. Chevallier *et al.* Phys. Rev. B **81** 205411 (2010)

¹¹ A. Bednorz *et al.* Phys. Rev. Lett. **110** 250404 (2013).

¹² R. Aguado and L. P. Kouwenhoven Phys. Rev. Lett. **84**, 1986 (2000).

¹³ D. Ferraro, M. Carrega, A. Braggio, and M. Sassetti New J. Phys. **16** 043018 (2014).

¹⁴ A. Braggio *et al.* New J. Phys. **14** 093032(2012).

Thermal and mechanical noise in gravitational wave detectors

Gianpietro Cagnoli¹

¹*Laboratoire des Matériaux Avancés (LMA), IN2P3/CNRS,
Université de Lyon, F-69622 Villeurbanne, Lyon, France
e-mail address: g.cagnoli@lma.in2p3.fr*

I. INTRODUCTION

Gravitational Waves detectors based on laser interferometry like Advanced Virgo, Advanced LIGO and KAGRA, are expected to be limited by mechanical thermal noise in the frequency band where the sensitivity is the highest. A first series of detectors, based on mechanical resonators, have been developed in the forty years after the pioneering work of Josef Weber in 1960. The current generation is based on the laser interferometry used to monitor the length changes on a Michelson interferometer arms. These detectors have an optical readout able to measure displacements of the order of 10^{-20} m/ $\sqrt{\text{Hz}}$ from 10 Hz to 10 kHz. With such performance they can be seen as gigantic amplifiers of mechanical and thermal noises and actually these noises are thought to be limiting the detection of GW in the advanced detectors. During the 30 years of interferometric detector developments many sources of noises have been studied, some of them have led to other questions, some other have not completely explained or investigated yet. A view on these standing challenges on GW detector noise will be given.

II. THE MECHANICAL NOISES

The Seismic Noise is the first of all the mechanical noises to cure in a GW detector. Its typical amplitude is 10^{-7} m/ $\sqrt{\text{Hz}}$ at 1 Hz and falls roughly as $1/f^2$ up to few tens of Hz. The seismic noise is able to shortcut the suspension system designed to filter the Earth vibrations before they reach the mirrors: the density fluctuations of the soil are directly coupled to the mirrors through the Newtonian law of gravity. The effect is irrelevant in most of the experiments but in future GW detectors which are designed to work at frequencies as low as 1 Hz. Following some models, this noise could be detected even by the present generation of detectors. What is still under discussion is how to mitigate the effect of this noise: will the measurement of the seismic motion by an array of accelerometers be a solution good enough to mitigate this noise or the underground operation is an avoidable caveat for the third generation of GW detectors?

One of the most long standing question in the mechanical noise domain is whether or not stress in structures can trigger sudden relaxations of elastic energy that can be seen as either burst signals or a continuous shot noise on the GW detectors. In the GW community such noise is called *creep noise* or *cracking noise*. Relatively high

stress that is able to trigger relaxations close enough to the test masses (i.e. the mirrors) is present on the metal cantilever blades used to vertically filter the seismic noise, on the mirror suspension fibres made of silica and on the silicate bonding layer used to attach the connecting elements between the thin fibres and the large mirrors. In the latter the stress is not particularly high (few MPa) but the bonding layer is thought to have plenty of relaxation centres. An overview of the investigations conducted and ongoing around this subject will be given.

III. THE THERMAL NOISES

Thermal noise is indeed the most reach source of "troubles", and hence of research interest, among all the fundamental noises in GW detectors all along the history of their development. In the first generation of GW detectors suspension thermal noise was the most severe limit to the instrument sensitivity but in the last 15 years, since the technology of fused silica suspension replaced the one based on steel wires, the focus has moved onto the mirror coatings thermal noise: any tiny reduction of this noise level is translated in an equivalent increase of the maximum distance at which a GW detection can be made.

The observable, whose fluctuations are picked up by the interferometer output, is the phase of the laser beam reflected by the Bragg structure of coatings deposited on each mirror. This fact together with the uncorrelated fluctuations of temperature and density make the study of coating thermal noise rather complicated and at the same time reach of phenomena.

The materials used so far are amorphous (glasses) in both the forms of bulk and thin films. The greatest unsolved problem in this subject is to understand the origin of structural relaxations that represent the highest source of thermal noise in coatings. A review of the structural studies and modeling of glasses will be given.

In recent years people have started to develop Bragg reflectors made of III-V semiconductors. These materials have shown a considerable reduction of thermal noise level as compared to the amorphous counterpart. A brief description of the new type of thermal noise mechanisms affecting these devices will be presented.

IV. OTHER WELL KNOWN UNSOLVED PROBLEMS

As a possible way to reduce thermal noise, a design of a detector operated at cryogenic temperatures has been made¹. In this design the mirror suspension fibres work with a large thermal gradient. The mirrors itself have a thermal gradient due to the laser power dissipated in the mirror substrates or on the coatings. These facts triggered the interest on studying the thermal noise under steady state heat flux. No theory has been made that is able to treat systems like those and only very few peo-

ple in the GW community have done an investigation on that. In the near future the situation might change.

ACKNOWLEDGMENTS

The authors are grateful to the LABEX Lyon Institute of Origins (ANR-10-LABX-0066) of the Universit de Lyon for its financial support within the program "Investissements d'Avenir" (ANR-11-IDEX-0007) of the French government operated par the National Research Agency (ANR).

¹ The ET Science Team, technical note ET-0106C-10, <http://www.et-gw.eu/etdsdocument>

This large document contains the majority of the relevant publications in the field of GW detectors development.

The quest for the missing noise in a micro-mechanical system out of equilibrium

Mickael Geitner,¹ Felipe Aguilar Sandoval,^{1,2} Éric Bertin,³ and Ludovic Bellon¹

¹Université de Lyon & CNRS, Laboratoire de Physique ENS Lyon (France)
e-mail address: Ludovic.Bellon@ens-lyon.fr

²Universidad de Santiago de Chile, Laboratorio de Física non lineal

³Université Joseph Fourier & CNRS, Laboratoire interdisciplinaire de Physique (Grenoble, France)

I. INTRODUCTION

Equipartition principle plays a central role in the understanding of the physics of systems in equilibrium: the mean potential and kinetic energy of each degree of freedom equilibrates to $k_B T/2$, with k_B the Boltzmann constant and T the temperature. This equality is linked to the fluctuation-dissipation theorem: fluctuations of one observable are proportional to the temperature and dissipation in the response function associated to that observable. In non equilibrium situations however, such relations between fluctuations and response are not granted, and *excess* noise is usually expected to be observed with respect to an equilibrium state³.

In this presentation, we show that the opposite phenomenon can also be experimentally observed: a system that fluctuates *less* than what would be expected from equilibrium! Indeed, when we measure the thermal noise of the deflexion of a micro-cantilever subject to a strong stationary temperature gradient (and thus heat flow), fluctuations are much smaller than those expected from the system mean temperature.

We first present the experimental system, an atomic force microscope (AFM) micro-cantilever in vacuum heated at its free extremity with a laser. We show that this system is small enough to have discrete degrees of freedom but large enough to be in a non-equilibrium steady state (NESS). We then estimate its temperature profile with the mechanical response of the system, and observe that equipartition theorem can not be applied for this NESS: the thermal noise of the system is roughly unchanged while its temperature rises by several hundred degrees! We conclude with a widely open question of the origin of this missing noise.

II. EXPERIMENT

Using a differential interferometer², we measure the thermal noise induced flexural deflexion of an AFM cantilever, a micro-mechanical beam clamped at one extremity and free at the other – see sketch in the inset of Fig. (1). No external forces are applied to the 500 μm long cantilever. As illustrated in Fig. (1), the power spectrum density (PSD) of the deflexion in vacuum is characteristic of a collection of independent quasi-harmonic oscillators corresponding to the normal modes of the cantilever. The resonance frequencies and spacial mode shapes are well described by an Euler-Bernoulli model for an elastic beam¹. In equilibrium, the amplitude of the thermal

noise can be used to deduce the stiffness k_n of each mode n using equipartition:

$$\frac{1}{2}k_n \langle d_n^2 \rangle = \frac{1}{2}k_B T \quad (1)$$

with $\langle d_n^2 \rangle$ the mean square deflexion measured for that mode (integral of the PSD around the resonance).

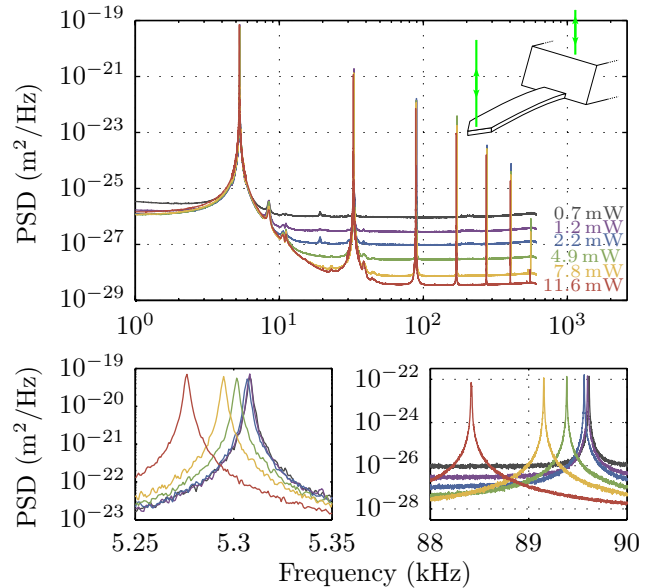


FIG. 1. Power spectrum density (PSD) of thermal noise induced deflection of a silicon micro-cantilever as a function of frequency, for various incident light power I on the lever in vacuum. The flat base line of the PSD is due to the shot noise on the photodetectors, it decreases for larger I . All the resonant frequencies of the cantilever decrease when I grows, as illustrated in the 2 bottoms figures for modes 1 and 3. The inset of the top figure illustrate the principle of the measurement: the fluctuations of deflection are recorded through the interference of two laser beams, one reflected on the cantilever free end, the other on the chip holding the cantilever².

To lower the contribution of the shot noise of the photodetectors to the measured spectrum, we increase the laser intensity. The sought noise reduction is obtained as illustrated in Fig. (1), but we also observe a lowering of the resonant frequencies of the normal modes. A simple argument can be used to understand this red shift: each mode can be pictured as an harmonic oscillator of mass m , whose stiffness k_n is proportional to the Young's modulus E of silicon (the cantilever material). The increase of temperature, due to light absorption, induces a

softening of the cantilever: the temperature coefficient of E is negative

$$\alpha_E = \frac{1}{E} \frac{dE}{dT} \approx -64 \times 10^{-6} \text{ K}^{-1} \quad (2)$$

The resonant frequencies f_n of the normal modes should therefore decrease as light intensity I increases:

$$2\pi f_n = \sqrt{\frac{k_n}{m}} \propto E^{1/2} \quad (3)$$

$$\frac{\Delta f_n}{f_n} \approx \frac{1}{2} \frac{\Delta E}{E} \approx \frac{1}{2} \alpha_E \Delta T \propto I \quad (4)$$

In the presentation, a careful treatment of the interplay between the temperature profile and the spatial shape of the modes will show how we deduce from the frequency shifts the temperature gradient in the cantilever.

The deduced temperature at the free end of the cantilever is plotted in Fig. (2): we reach huge temperature gradients for a few tens of mW of the measuring laser. We could even melt silicon cantilevers in vacuum for $I = 20$ mW, when the melting point of silicon is 1410°C !

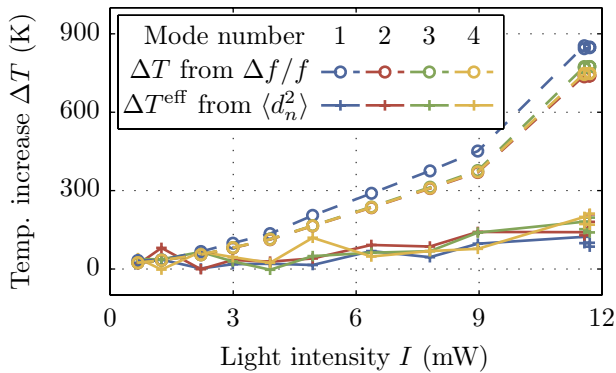


FIG. 2. Temperature increase at the free end of the cantilever deduced by two methods: upper curves (dashed) from the frequency shift of the resonances (Eq. 4), lower curves (plain) from an extension of the equipartition theorem to this NESS (Eq. 5). The latter is clearly under evaluated.

III. EFFECTIVE TEMPERATURE

Though the cantilever is in a NESS due to the heat flowing along its length, it is tempting to extend equipartition as in Eq. (1) to define an effective temperature of each mode. Indeed, the mean square deflection can be measured from the PSD, and the stiffness of the modes is known from a calibration in equilibrium and the frequency shift already discussed. We may thus extend Eq.

(1) to define an effective temperature T_n^{eff} of each mode:

$$T_n^{\text{eff}} = \frac{k_n}{k_B} \langle d_n^2 \rangle \quad (5)$$

Again, in the presentation, a careful treatment of the interplay between the temperature profile and the spatial shape of the modes will show how to define the effective temperature gradient in the cantilever from the measured thermal noise.

The deduced effective temperature at the free end of the cantilever is plotted in Fig. (2): though T^{eff} rises with I , its value is far smaller than that inferred from the response of the cantilever (frequency shift). The equipartition clearly fails for this NESS, but in a completely unexpected way: the level of noise is below what one would expect. And indeed, the area under the resonance peaks in the thermal noise spectra in Fig. (1) looks constant while the maximum temperature in the lever increases from 300 K to 1100 K. On the contrary, one would expect the fluctuations to rise even more due to the non equilibrium situation.

IV. OPEN PROBLEMS

Our system offers a nice and carefully controlled out of equilibrium system, where fluctuation and response can be measured with a high accuracy for several independent degrees of freedom. We demonstrate that in such a NESS, the thermal noise of all modes is close to the one expected for the lower temperature of the system, when one would expect it to be higher (of at least equal) to that of its mean temperature. This result is in strong contradiction with other experiments of mechanical systems subject to a stationary heat flow, where excess noise is observed³.

In our quest for this missing noise, we have identified a few leads that will be discussed during the presentation, for instance:

- > effect of a spatially non-uniform damping mechanism ?
- > absence of coupling between longitudinal heat transport and flexural deflexion ?

Other suggestions will be welcomed during the discussion !

ACKNOWLEDGMENTS

We acknowledge the support of ERC project OutE-FLUCOP and ANR project HiResAFM.

¹ P. Paolino, B. Tiribilli and L. Bellon, Journal of Applied Physics **106**, 094313 (2009)

² P. Paolino, F. Aguilar Sandoval and L. Bellon, Rev. Sci. Instrum. **84**, 095001 (2013)

³ L. Conti, P. De Gregorio, G. Karapetyan, C. Lazzaro, M. Pegoraro, M. Bonaldi and L. Rondoni, J. Stat. Mech.,P12003 (2013)

Noise Thermal Impedance: a way to access electron dynamics.

E. Pinsolle¹ and B. Reulet¹

¹*Université de Sherbrooke department of physics,
2500 boulevard de l'université, Sherbrooke (Québec), Canada J1K 2R1
edouard.pinsolle@usherbrooke.fr*

I. INTRODUCTION

In good conductors the frequency dependence of the conductance and the noise is given only by charge screening. To have access to inelastic processes or diffusion times in such samples one need to measure small quantum corrections to the conductance¹ or tunneling properties on materials with which tunnel junction can be made². Those are indirect measurements of interactions and diffusion time and are sometimes hard to access. Recently B. Reulet and D.E. Prober have proposed a new technique based on Johnson noise measurement to directly access the dynamic of electrons in normal metals³. They named it Noise Thermal Impedance (NTI).

II. EXPERIMENTAL PRINCIPAL AND RESULTS

In the case of Johnson noise the current noise density S_2 is determined directly by the electron gas temperature T by: $S_2 = 4k_B T G$. It's interesting to generalize this link by defining the noise temperature $T_N = S_2 / (4k_B G)$. The NTI measure the fluctuations of the noise temperature δT_N^ω of an electron gas heated by an oscillating power δP_j^ω at frequency ω . This complex response function is define as $R(\omega) = \delta T_N^\omega / \delta P_j^\omega$.

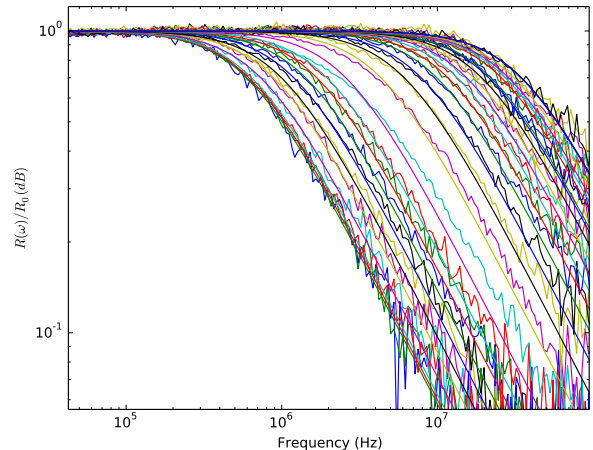
B. Reulet and D.E Prober calculated³ the expected form of this response function for a metallic diffusive wire for several limiting cases. In those kind of samples one can distinguish between three regimes depending on the sample length and the temperature. For long sample $L \gg L_{e-ph}$ the energie relaxation of the electron gas is dominated by electron-phonon interactions, this is called the macroscopic regime. In this case the energie relaxation occurs in a time τ_{e-ph} given by the mean electron-phonon interaction time and the NTI have the form:

$$R(\omega) = \frac{\delta T_e^\omega}{\delta P_j^\omega} = \frac{G_{e-ph}^{-1}}{(1 + i\omega\tau_{e-ph})} \quad (1)$$

For smaller samples $L \ll L_{e-ph}$ electron-phonon processes are inefficient and the energie relaxation is dominated by diffusion of hot electrons into the leads. The time scale associated is given by the diffusion time τ_D . In this length scale one can discriminate between a case $L_{e-e} \ll L$ where electrons exchange energie, called hot electron regime, and a case where electrons don't interact with each others, called independent electron regime. In those two regimes the time scale of energie

relaxation is given by the diffusion time τ_D . We have applied this technique to different metallic wires to measure directly the electron-phonon interaction times and the diffusion time in function of temperature and length to go throught hot electron regime to macroscopic regime.

"In Fig. (1)" we present the noise thermal impedance for a $50 \mu m$ long aluminum wire at different temperatures. Those curves are in good agreement with the equation 1 superposed to the experimental data. We have repeted this experiment for different wire lenghtes from $5 \mu m$ to $50 \mu m$ and extract the cutoff frequencies.

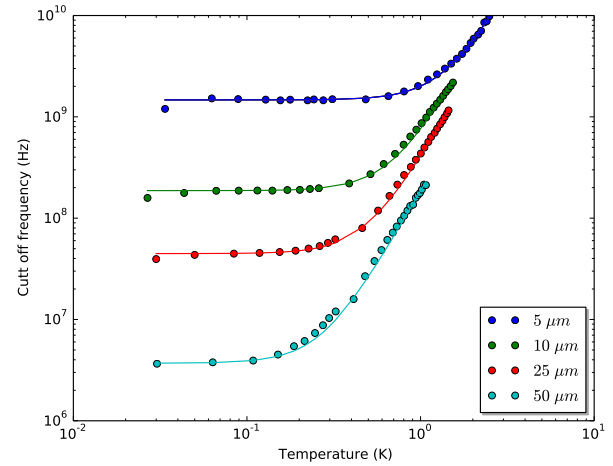


"FIG. 1. Amplitude of the normalised noise thermal impedance in function of frequency for a $50 \mu m$ long aluminum wire. The different curves correspond to different electron noise temperatures from around $30 mK$ to $1.5 K$. Those curves are fitted with the equation 1 which permit to extract a cutoff frequency "

"In Fig. (2)" we present those cutoff frequencies in function of temperature for the different wires. At high temperature we observe a power law characteristic of an electron-phonon interaction time ($\tau_{e-ph}^{-1} = A * T^3$)⁴. When we decrease the temperature we access a regime where the energie relaxation is dominated by diffusion. As we expected, this diffusion time is independant of temperature which gives rise to a plateau at low temperature. The different curves as been fitted by assuming that, in presence of different relaxation processes, the frequencies add up $\tau_{relaxation}^{-1} = \tau_D^{-1} + \tau_{e-ph}^{-1}$. We checked that the diffusion time is proportionnal to the sample length in

agreement with a diffusion law $L^2 = D\tau_D$. This permit us to extract the diffusion coefficient.

This experiment demonstrate that a NTI measurement is of great interest to access dynamics of electron gazes. This could be applied to probe diffusion times in new materials such as h-graphene or to investigate electron-phonon interaction in High T_c superconductors. One could also imagine to study diffusion law in more fancy sample with a fractal dimation⁵.



“FIG. 2. Energy relaxation frequencies in function of electron noise temperature for aluminum wires of different lengths.”

¹ D.E. Prober et al., Phys. Rev. B **29**, 6 (1984).

² H. Pothier et al., Phys. Rev. Lett. **79**, 3490 (1997).

³ B. Reulet and D.E. Prober, Phys. Rev. Lett **95**, 066602 (2005).

⁴ W.E. Lawrence and A.B. Meador, Phys. Rev. B **18**, 1154 (1978).

⁵ I.M. Sokolov, Mathematics of Complexity and Dynamical Systems, p.13-25 (2011).

Towards an information-theoretic model of the Allison mixture

Lachlan Gunn,¹ François Chapeau-Blondeau,² Andrew Allison,³ and Derek Abbott⁴

¹*School of Electrical and Electronic Engineering, The University of Adelaide, SA 5005, Australia
e-mail address: lachlan.gunn@adelaide.edu.au*

²*Laboratoire Angevin de Recherche en Ingénierie des Systèmes (LARIS),
University of Angers, 62 avenue Notre Dame du Lac, 49000 Angers, France.
e-mail address: chapeau@univ-angers.fr*

³*School of Electrical and Electronic Engineering, The University of Adelaide, SA 5005, Australia
e-mail address: andrew.allison@adelaide.edu.au*

⁴*School of Electrical and Electronic Engineering, The University of Adelaide, SA 5005, Australia
e-mail address: derek.abbott@adelaide.edu.au*

I. INTRODUCTION

The Allison Mixture¹ is a process formed by random sampling of two parent processes, and which can have the unintuitive property of being autocorrelated, despite all its values being drawn from uncorrelated processes. However, this correlation vanishes if the parent processes are of equal mean, suggesting the use of autoinformation^{2,3} as an alternative to correlation, providing a canonical measure of the strength of the memory of the Allison mixture. We apply this measure to the Allison mixture, producing analytic expressions for the k -step autoinformation of its sampling process.

II. THE ALLISON MIXTURE

The Allison mixture¹ is a process in which samples are drawn from one of two distributions, the choice determined by the state of a Markov chain, shown in Fig. (1). The marginal distribution of this process is a mixture of the two source distributions, the mixing constant determined by the stationary distribution of the Markov chain.

Definition II.1 (Allison mixture¹). *An Allison mixture X_t of two processes U_t and V_t is given by*

$$X_t = S_t U_t + (1 - S_t) V_t \quad (1)$$

where the sampling process S_t is a Markov chain, shown in Fig. (1), having states $\{0, 1\}$ and transition probabilities α_0 and α_1 when in states 0 and 1 respectively.

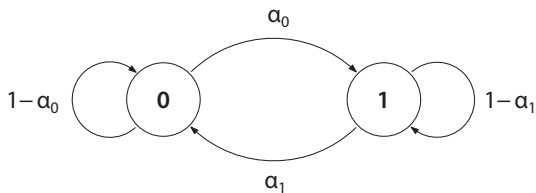


FIG. 1. The Markov chain defining the sampling process S_t of the Allison mixture. It is parametrised by the probabilities α_0 and α_1 of leaving states 0 and 1 respectively.

The stationary distribution of S_t is given by

$$\pi_0 = \frac{\alpha_1}{\alpha_0 + \alpha_1} \quad (2)$$

$$\pi_1 = \frac{\alpha_0}{\alpha_0 + \alpha_1}. \quad (3)$$

We use a spectral decomposition of the transition matrix P in order to compute the k -step probability matrix P^k and so the k -step transition probabilities $\alpha_{0,k}$ and $\alpha_{1,k}$.

Theorem II.1. *The sampling process S_t has k -step transition probabilities*

$$\alpha_{0,k} = \pi_0 [1 - (1 - \alpha_0 - \alpha_1)^k] \quad (4)$$

$$\alpha_{1,k} = \pi_1 [1 - (1 - \alpha_0 - \alpha_1)^k]. \quad (5)$$

III. AUTOINFORMATION OF THE ALLISON MIXTURE SAMPLING PROCESS

The autoinformation function is an alternative to the autocovariance function as a measure of dependence, defined as follows:

Definition III.1 (Autoinformation function³). *The autoinformation function of a stochastic process S_t is the mutual information*

$$I_{xx}[t, k] = I(S_t, S_{t-k}) \quad (6)$$

$$= H(S_t, S_{t-k}) - H(S_t) - H(S_{t-k}). \quad (7)$$

If S_t is stationary, then we may omit t as a parameter, leaving us with

$$I_{xx}[k] = I(S_t, S_{t-k}) \quad (8)$$

$$= H(S_t, S_{t-k}) - 2H(S_t). \quad (9)$$

The autoinformation improves on the autocovariance function as a measure of dependence by providing a condition both sufficient and necessary—whereas a lack of correlation does not necessarily indicate independence, two variables will have zero mutual information only if they are statistically independent; this is vital when the processes U_t and V_t of the system being modelled have identical means but differing variances, such as particle velocities in statistical mechanics.

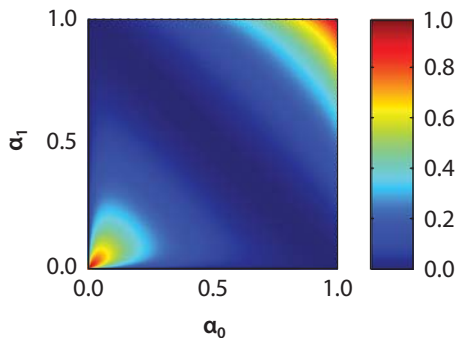


FIG. 2. Single-step autoinformation of the Allison mixture sampling process as a function of α_0 and α_1 . Note the lines of zero autoinformation along $\alpha_0 = 0$, $\alpha_1 = 0$, and $\alpha_0 + \alpha_1 = 1$.

Lemma III.1. *Let S_t be a binary-valued random process with transition probabilities and a stationary distribution equal to that of the Markov chain in Definition II.1. Then, in the fully-mixed regime the single-step autoinformation is given by*

$$I_{xx}[1] = \frac{\alpha_1(1 - \alpha_0) \log_2 \frac{1 - \alpha_0}{\alpha_1}}{\alpha_0 + \alpha_1} + \frac{\alpha_0(1 - \alpha_1) \log_2 \frac{1 - \alpha_1}{\alpha_0}}{\alpha_0 + \alpha_1} + \log_2(\alpha_0 + \alpha_1), \quad (10)$$

where both α_0 and α_1 are nonzero, zero if exactly one of α_0 and α_1 is equal to zero, and undefined if both are equal to zero.

Thus the autoinformation is equal to zero when $\alpha_0 = 0$, $\alpha_1 = 0$, or $\alpha_0 + \alpha_1 = 1$, and so these previously-described¹ conditions for decorrelation of the sampling process imply zero mutual information and therefore genuine independence.

Importantly, we have not assumed the Markov property, instead directly demanding that the formulae for the stationary probabilities hold. This weakening is intended to allow us later to generalise to the Allison mixture proper.

The mutual information as a function of (α_0, α_1) is shown in Fig. (2). As one would expect, we see a peak near $(\alpha_0, \alpha_1) = (0, 0)$, where consecutive states are highly dependent. Similarly, we see a large autoinformation near $(1, 1)$, where the strong anticorrelation makes consecutive states highly predictable. Between these two extremes lies a valley, its nadir falling along the line

$\alpha_0 + \alpha_1 = 1$; along this line, consecutive states of the sampling process are completely independent.

Theorem III.1. *The k -step autoinformation of a fully mixed two-state Markov chain with exit probabilities α_0 and α_1 , as in Fig. (1), is given by Lemma III.1 under the substitution*

$$\alpha_0 \longrightarrow \pi_0 [1 - (1 - \alpha_0 - \alpha_1)^k] \quad (11)$$

$$\alpha_1 \longrightarrow \pi_1 [1 - (1 - \alpha_0 - \alpha_1)^k]. \quad (12)$$

This final theorem allows us to extend our single-step results to arbitrary time-lags, completing our characterisation of the Allison mixture sampling process.

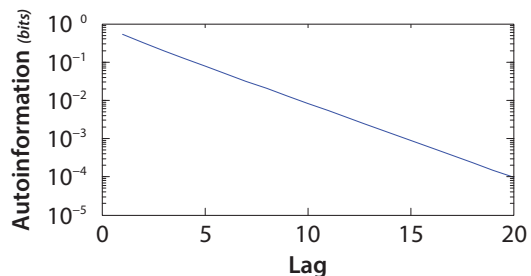


FIG. 3. Exponentially-decaying autoinformation of an Allison mixture sampling process with $\alpha_0 = 0.1$, $\alpha_1 = 0.1$.

We show the autoinformation in Fig. (3) as a function of lag; it can be seen to decay at a roughly exponential rate.

IV. OPEN QUESTIONS

The theorems that we have presented allow computation of the autoinformation function of the Allison mixture sampling process, and can be readily extended to binary-valued Allison mixtures. However, many physical systems are described by continuous-valued processes, and their autoinformation cannot be calculated by Lemma III.1. It remains to be seen whether the autoinformation can be computed by transformation of the sampling process autoinformation in a similar fashion to that of the autocovariance function¹.

Furthermore, the information-theoretic approach that we have presented provides the starting point for an investigation of the transfer entropy⁴ between the sampling process and the Allison mixture; previous works on transfer entropy have focussed on complex systems, leaving room for the analysis of simpler and analytically tractable models in order to better probe its properties.

¹ L. J. Gunn, A. Allison, and D. Abbott, International Journal of Modern Physics **33**, 1460360 (2014).

² G. A. Darbellay, Physica A **287**, pp. 429–439 (2000).

³ F. Chapeau-Blondeau, Physica A **380**, pp. 1–18 (2007).

⁴ T. Schreiber, Physical Review Letters **85**, pp. 461–464 (2000).

How a player with finite memory can win by switching in a sequence of Parrondo Games?

Ka Wai CHEUNG, Ho Fai MA, Degang Wu, Ga Ching LUI, Kwok Yip Szeto¹

Department of Physics, The Hong Kong University of Science and Technology, Clear Water Bay, Hong Kong, HKSAR, China
¹e-mail address: phszeto@ust.hk

I. INTRODUCTION

Smoluchowsky¹ proposed the concept of Brownian Ratchets about a century ago as nonequilibrium devices where fluctuations can be rectified to produce directional transport of particles along a periodic asymmetric potential. Later, Feynman, in his famous lecture on the ratchet-and-pawl setup, discussed the Brownian motor, which is a Brownian ratchet with a load^{2,3}. About 20 years ago, the flashing ratchet with scheduled On/Off switching of an asymmetric potential was discussed^{4,7}. Later the flashing ratchet inspired the invention of Parrondo's game⁸ in which two losing games can be combined to become a winning game. Since then, much research has been conducted on different switching strategies for Parrondo Game. The optimal periodic sequence that maximizes the expected payoff was computed by Dinis⁹, and more complex sequences by Tang *et al.*¹⁰ and for long sequence by Wu and Szeto¹¹ using Genetic Algorithm. Other types of Parrondo Games have also been constructed, such as the Quantum Parrondo Game and history dependent games^{12,13}. Here we address the possible gain by player with finite memory in various switching strategies when playing the original Parrondo Game. We expect player with memory can implement a feedback control so as to switch his game plan at appropriate time to improve his gain, since in control theory the feedback control can generally improve the performance of an open-loop system. We find for player with one-step memory, certain switching strategy can lead to optimal winning.

II. ORIGINAL PARRONDO GAMES

The original Parrondo Game contains two independent games: A and B. Game A can be thought as a coin-tossing game, which has probability $p=1/2-\varepsilon$ to win, where ε is a small nonnegative number. If the average yield of a game is $\langle X(t) \rangle$, then the expected gain is $g=\langle X(t+1) \rangle-\langle X(t) \rangle$ and for a long sequence of A game, it is $\langle X(t+1) \rangle=\langle X(t) \rangle+2p-1$. Thus, game A is fair if ε is zero, and is a losing game if ε is larger than zero. Game B can be thought of as a complicated game with two biased coins: a good coin and a bad coin. The good coin's winning probability is $p_g=0.75-\varepsilon$, and the bad coin's winning probability is $p_b=0.1-\varepsilon$. If the player's capital is multiple of 3, the bad coin is used, otherwise the good coin is used. Therefore the expected capital gain for game B is $\langle X(t+1) \rangle=\langle X(t) \rangle+2(\pi_0(t)p_b+(1-\pi_0(t))p_g)-1$, where $\pi_0(t)$ is the probability that the player's capital is multiple of 3 at time t . We can find the values of $\pi_0(t)$ by using discrete Markov Chain, and define the probability vector as $\pi(t)=(\pi_0(t),\pi_1(t),\pi_2(t))$, where $\pi_1(t)$ and $\pi_2(t)$ is the probability

that player's capital is multiple of 3 plus 1 and plus 2 respectively, therefore we can write the transition matrix of Game A and B as

$$\mathbf{\Pi}_A = \begin{pmatrix} 0 & p & -p+1 \\ -p+1 & 0 & p \\ p & -p+1 & 0 \end{pmatrix}; \quad \mathbf{\Pi}_B = \begin{pmatrix} 0 & p_b & -p_b+1 \\ -p_g+1 & 0 & p_g \\ p_g & -p_g+1 & 0 \end{pmatrix} \quad (1)$$

A stochastic mixture of A and B game can be represented as

$$\mathbf{\Pi} = \gamma \cdot \mathbf{\Pi}_A + (1-\gamma) \cdot \mathbf{\Pi}_B \quad (2)$$

where γ is the probability of playing game A. The time evolution of the probability vector is $\pi(t+1)=\pi(t)\mathbf{\Pi}$.

III. PARRONDO GAME WITH ONE TIME STEP MEMORY

If the player has one-step memory, he has some extra information in his decision of game to be played, rather than random switching or deterministic switching in a preset sequence. This extra information from his memory of the result of the last game enables him to make a more informed decision, which hopefully yields better performance in the long run. This is the feedback control implemented by the player due to his ability to remember. Note that during the whole process, the player does not know which game he played is A or B, otherwise the problem is trivial. He can simply play game A if his capital is multiple of 3 and play game B otherwise, so as to maximize his payoff. In the setting of our Parrondo game, we assume that the player has one step memory, and plays two kinds of game, call C and D, without knowing whether C is A or D is A, while the other is B. The finite memory of the player in general cannot be used to identify the nature of game C and D. The state of the player is represented by the vector $\mathbf{U}(t)=(C_0(t),C_1(t),C_2(t),D_0(t),D_1(t),D_2(t))$, here C/D means that the player play game C/D at time t . The subscripts 0, 1, 2 denote that the player's capital being a multiple of 3 plus 0, 1, 2 respectively. Thus, $C_0(t)$ means that the player's current capital is multiple of 3 and he will play game C for at time t . For one step memory, we need only to consider the conditional probability $P(G_t|G_{t-1})$ for switching, as defined below,

$$P(D_t|C_{t-1})=\alpha; \quad P(C_t|C_{t-1})=1-\alpha \quad (3)$$

$$P(C_t|D_{t-1})=\beta; \quad P(D_t|D_{t-1})=1-\beta$$

Here α, β are the probabilities of switching as illustrated in Fig.1.

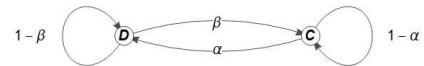


FIG. 1. At each time step, the player switch from C to D with probability α and switch from D to C with probability β .

Under this hypothesis of conditional probability for one step memory and using the switching scheme in Fig.1, we can

represent the game for player with one step memory by a 6×6 transient matrix Π_s , with element written as $P(G_i|G_{i-1})P_{win}(G_i)$ and $P(G_i|G_{i-1})(1-P_{win}(G_i))$ if the game is winning or losing separately and G_i is one of the six elements in $\mathbf{U}(t)$. An illustration of the expected gain for particular sets of winning probability is shown in Fig.2. One of the interesting results we derive and verified numerically is that the stochastic mixture of game C and game D with the mixing parameter γ in Eq. (2) can be related to player with one-step memory playing games with the special switching parameter α, β when $\alpha=1-\gamma$ and $\beta=\gamma$.

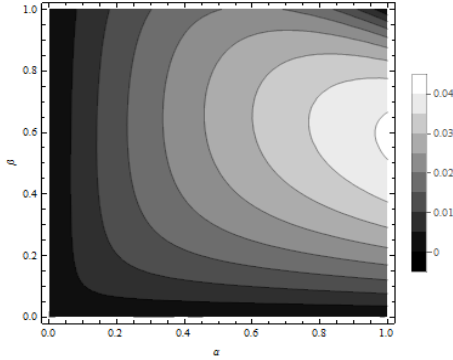


FIG. 2. Contour plot for the expected capital gain (in grey code) for the original Parrondo game. The parameters are $p=0.5-\varepsilon$, $p_g=0.75-\varepsilon$, $p_b=0.1-\varepsilon$, and $\varepsilon=0.003$. The optimal value of α and β for this set of parameters is $\alpha=1, \beta=0.5907$. Note that the capital gain for stochastic mixing of game is along the line $\alpha=1-\beta$.

Let's now consider the special case of $\alpha=\beta$. This is to say that the player, although endowed with one-step memory, does not know much about the nature of the game C and D and their association with game A and B, so that he simply switch with one parameter $\alpha=\beta$ in the conditional probability in Eq.(3). In this case the matrix Π_s can be separate into two matrices and be written as $\Pi_s = \alpha\mathbf{X} + (1-\alpha)\mathbf{Y}$, where \mathbf{X} can be viewed as a new game which plays game C and game D alternatively, \mathbf{Y} can be thought as a new game that always following the previous games. If the player plays game \mathbf{X} alone, the game sequence will be ...CDCD...; if the player plays game \mathbf{Y} alone, the game sequence will be either ...CCC... or ...DDD..., the interesting point is that both game \mathbf{X} and game \mathbf{Y} are losing game, and stochastic combination of \mathbf{X} and \mathbf{Y} can win. This type of game works because the new switching game is also formed by a convex linear combination. The solution for the optimal value α for highest expected gain can be found analytically

$$\alpha = \frac{(p^2 - p + 1)(2p_g - 1)}{4p^2p_g - 2p^2 - 4pp_g + 3p + 3p_g - 2} \quad (4)$$

for $p_g > 1/2$. Note that this optimal α is independent of p_b . For fair game C, $p=1/2$, and α in Eq.(4) becomes 0.75. Thus, switching with probability 0.75 is an optimal way if the player cannot distinguish the game A and B.

IV. DISCUSSION

For the game with one-steps memory, the optimization question can be interpreted as finding the frequency of switching that generates the highest capital gain. For particular sets of winning probabilities illustrated in Fig. 2, it suggests that $\alpha=1, \beta=0.5907$ is the optimal values, which means that in optimal sequence the game A should not appear continuously since now $P(B_i|A_{i-1})=1; P(A_i|A_{i-1})=0$. In this case, the optimal periodic sequence ABABB^{9, 11} meets the requirement set by this choice of $\alpha=1, \beta=0.5907$. We should point out that this gives higher gain than the gain obtained by $\alpha=\beta$, as now we have some additional knowledge of the A and B game so that we bias towards the switching from A to B for $\alpha=1, \beta=0.5907$. Without this additional knowledge, the yield obtained by setting $\alpha=\beta=0.75$ is optimal. Our switching scheme can be generalized to player with n-steps memory by setting the conditional probability $P(G_i|G_{i-1}^{(n)})$ for different history condition, where $G_{i-1}^{(n)} = G_{i-1}G_{i-2}\dots G_{i-n}$ is the game history with length n . For example in two-step memory, there are four kinds of combination, $\{A_{i-1}A_{i-2}, A_{i-1}B_{i-2}, B_{i-1}A_{i-2}, B_{i-1}B_{i-2}\}$, the matrix's dimension is $4 \times 3 = 12$. In general, the dimension for n steps memory requires a $(3 \cdot 2^n) \times (3 \cdot 2^n)$ transition matrix. Extension to extended Parrondo games¹⁴ with two types of B games can also be treated in a similar way. In the context of flashing ratchet, the question of switching protocol can be viewed as the ON/OFF timing of the saw-tooth asymmetric potential so as to provide a highest particle transport velocity. In conclusion, we have extended the random switching scheme in Parrondo Game to one time step memory switching and found the optimal value of switching is different from random switching. For some special case where two switching probabilities are the same, the optimal value of switching probability is independent of the winning probability of the bad coin of game B. Game involving n-steps memory can also be generalized.

ACKNOWLEDGEMENTS

K.Y. Szeto acknowledges the support of grant FSGRF13SC25 and FSGRF14SC28

- ¹ M. V. Smoluchowski, Phys. Zeitschrift **XIII**, 1069 (1912)
- ² R.P. Feynmann, R.B. Leighton, M. Sands, *The Feynman Lectures on Physics* (1963)
- ³ J.M.R. Parrondo and B.J.D. Cisneros, Appl.Phys. A **75**, 179 (2002)
- ⁴ A. Ajdari and J. Prost, C. R. Acad. Sci., Ser. 2 **315**, 1635 (1992)
- ⁵ R. D. Astumian and M. Bier, Phys. Rev. Lett. **72**, 1766 (1994)
- ⁶ P. Ha'nggi, R. Bartussek, in *Nonlinear Physics of Complex Systems Current Status and Future Trends* (1996) J. Parisi, S.C. Mu'ller, W. Zimmermann (Eds.)
- ⁷ P. Reimann, Phys. Rep. **361**, 57 (2002)
- ⁸ J. M. R. Parrondo, in *Proceeding of EEC HC&M Network on Complexity and Chaos* (1996).
- ⁹ L. Dinis, Phys. Rev. E **77**, 021124 (2008)
- ¹⁰ T.W. Tang, A.Allison, D.Abbott, Fluct.Noise Lett. **04**, L585 (2004)
- ¹¹ D.Wu and K.Y. Szeto, International Conference on Evolutionary Computation theory and Application. ECTA: Rome, Italy Oct 22-24 2014, pp.30-37.
- ¹² P. Flitney, D. Abbott, Phys. Rev. A **314**, 35 (2002)
- ¹³ J. M. R. Parrondo, G. P. Harmer, D. Abobott, Phys. Rev. Lett. **85**, 5226 (2000)
- ¹⁴ D.Wu and K.Y. Szeto, Phys. Rev.E **89**, 022142 (2014)

Asymmetry in Genetic Code and the Role of Parrondo's Paradox in Nature

Lee Kee Jin¹ and Shu Jian Jun^{2*}

¹*Nanyang Technological University,
School of Mechanical and Aerospace Engineering,
50 Nanyang Avenue, Singapore 639798
e-mail address: LEEK0097@e.ntu.edu.sg*
²*Nanyang Technological University,
School of Mechanical and Aerospace Engineering,
50 Nanyang Avenue, Singapore 639798
e-mail address: MJJSHU@NTU.EDU.SG*

I. INTRODUCTION

Genetic code table summarizes how the basic unit of protein – amino acid is encoded from sequences of three nucleotide triplet known as codon. Based on a set of simple rules, codons can be translated into amino acids and thus protein.

Standard genetic code table, as shown in Fig. (1), is arranged in a way that provides insight into physicochemical and biological properties of amino acid that are generated from the DNA/RNA codons. However, the standard genetic code table is oriented in such a manner that overlook the big picture that nature wish to convey to us – symmetry and asymmetry of life and the potential implication of asymmetry. Standard genetic code table can be put under mapping to result in a reconstructed genetic code table that show more clearly the symmetry and asymmetry of life code.

The reconstructed genetic code table, as shown in Fig. (2), shows slight asymmetry embedded in general symmetry, a pattern happens too many a time in nature. Human is a good example – mirror symmetry outside but internally, some of the organs are arranged in an asymmetrical manner. Total symmetry signifies stability, stagnant and eventual death while asymmetry means instability, constant movement and eventual breakthrough to life.

The reconstructed genetic code table shows mirror symmetry except for the small highlighted region in the center. The asymmetrical region is highlighted in Fig. (3). The reconstructed genetic code table is symmetrical around U – C and A – G of the third letter of codon except the above mentioned region, with U and A at the left column while G and C at the right column. Left and right column are symmetrical except for the highlighted region, giving a binary outcome – “left” versus “right”.

Codons in the asymmetrical region encode for three amino acids – Tryptophan, Isoleucine, Methionine and one termination codon. The focus here is Methionine. Several studies have found out that restricting Methionine consumption extends lifespans of some animals and affect their fecundity^{1,2}.

It is believed that asymmetry in genetic code table might have something to do with 3rd order path-dependent Parrondo's paradox. Parrondo's paradox is a counter-intuitive phenomenon whereby two individually losing games – game A and game B, can be mixed to produce a winning combine game.

In this case, noise can be seen as game A – a random process, while protein translation process can be seen as game B. Wobble base pair or the surrounding environment can serve to provide the noise component. The translation process can be biased into depressing methionine codon expression or promoting methionine codon expression. Parrondo's paradox will get in depending on whether noise is present or not.

In the scenario where the translation process is designed to promote the expression of methionine, introduction of noise has the paradoxical effect of decreasing the expression of methionine. Perhaps this is the design of nature, that in stable time, when there is no noise or less noise, the normal process of promoting expression of methionine take place, where individual reduce their life span in exchange for reproducing more rapidly.

On the other hand, in turbulent period where the situation is unsuitable for raising offspring, it would be better to increase individual survivability at the expense of reproduction capability. During unstable period, there will be an increase in the amount of noise and as a result of noise introduction, Parrondo effect will come in. The normal translation process (game B) will couple with noise (game A) and result in the outcome of suppressing the expression of methionine (Combine game), thus increasing the lifespan and survivability of individual while restricting reproduction.

In conclusion, 3rd order path dependent Parrondo's paradox and asymmetry in life code have both been independently developed. The study proposes a possible linkage between Parrondo's paradox and life code but the exact mechanism has yet to be firmly established. Evidence has been pointing towards that direction but the mystery remains determined not to be unraveled.

II. RESULT

3rd order path-dependent Parrondo's paradox can be seen as an extension of history dependent Parrondo's paradox³. Game A and game B both has binary outcome – “Win” and “loss”. Game A has winning probability of p and losing probability of $(1 - p)$ while game B has winning probability p_k and losing probability of $(1 - p_k)$ depending on the result of previous three games.

The winning probabilities of game B can be summarized in the table below.

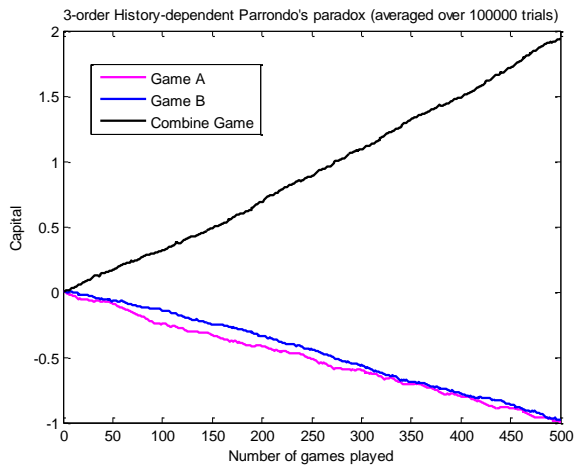
State k	Result of game at (t - 3)	Result of game at (t - 2)	Result of game at (t - 1)	Winning Probability, p_k , at time t
1	Loss	Loss	Loss	p_1
2	Loss	Loss	Win	p_2
3	Loss	Win	Loss	p_3
4	Loss	Win	Win	p_4
5	Win	Loss	Loss	p_5
6	Win	Loss	Win	p_6
7	Win	Win	Loss	p_7
8	Win	Win	Win	p_8

One of the many possible sets of winning probabilities used in game A and game B are as shown:

Game A	Winning Probability	Game B	Winning Probability
p	0.499	p_1	0.899
		p_2	0.499
		p_3	0.499
		p_4	0.249
		p_5	0.249
		p_6	0.499
		p_7	0.499
		p_8	0.699

*Note: Losing probability = 1 - winning probability

The result of two individually losing game A and game B with a winning combine game, using the set of probabilities above, is as shown below:



III. FIGURES

Phenylalanine	Serine	Tyrosine	Cysteine
Phenylalanine	Serine	Tyrosine	Cysteine
Leucine	Serine	Stop	Stop
Leucine	Serine	Stop	Tryptophan
Leucine	Proline	Histidine	Arginine
Leucine	Proline	Histidine	Arginine
Leucine	Proline	Glutamine	Arginine
Leucine	Proline	Glutamine	Arginine
Isoleucine	Threonine	Asparagine	Serine
Isoleucine	Threonine	Asparagine	Serine
Isoleucine	Threonine	Lysine	Arginine
Methionine/Start	Threonine	Lysine	Arginine
Valine	Alanine	Aspartic acid	Glycine
Valine	Alanine	Aspartic acid	Glycine
Valine	Alanine	Glutamic acid	Glycine
Valine	Alanine	Glutamic acid	Glycine

Nonpolar
 polar
 basic
 acidic
 Stop

FIG. 1. Standard Genetic Code Table.

Phenylalanine	Leucine	Leucine	Phenylalanine
Tyrosine	Stop	Stop	Tyrosine
Cysteine	Stop	Tryptophan	Cysteine
Serine	Serine	Serine	Serine
Isoleucine	Isoleucine	Methionine/start	Isoleucine
Asparagine	Lysine	Lysine	Asparagine
Serine	Arginine	Arginine	Serine
Threonine	Threonine	Threonine	Threonine
Valine	Valine	Valine	Valine
Aspartic acid	Glutamic acid	Glutamic acid	Aspartic acid
Glycine	Glycine	Glycine	Glycine
Alanine	Alanine	Alanine	Alanine
Leucine	Leucine	Leucine	Leucine
Histidine	Glutamine	Glutamine	Histidine
Arginine	Arginine	Arginine	Arginine
Proline	Proline	Proline	Proline

FIG. 2. Reconstructed Genetic Code Table

Stop	Stop
Stop	Tryptophan
Serine	Serine
Isoleucine	Methionine/start

FIG. 3. Asymmetrical region in genetic code table

¹ Grandison. R.C., Piper. M.D.W. and Partridge. L., Nature **462**, pp. 1061-1064 (2009).
² Miller. R.A., Buehner. G., Chang. Y., Harper. J.M., Sigler. R., and Smith-Wheelock. M., Aging cell **4**, pp. 119-125 (2005).

³ Parrondo. J.M.R., Harmer. G.P. and Abbott. D., Physical Review Letters **85**, pp. 5226-5229 (2000).

Percolation noise at the metal–insulator transition of nanostructured VO₂ films^{a)}

Zareh Topalian¹, Shu-Yi Li¹, Gunnar A. Niklasson¹, Claes G. Granqvist¹ and Laszlo B. Kish^{1,2}

¹Department of Engineering Sciences, The Ångström Laboratory, Uppsala University, P. O. Box 534, SE-75121 Uppsala, Sweden
e-mail address: Claes-Goran.Granqvist@angstrom.uu.se

²Department of Electrical and Computer Engineering, Texas A&M University, College Station, TX 77843-3128, USA
e-mail address: Laszlokish@tamu.edu

I. INTRODUCTION

Thermochromism in VO₂ is associated with a first-order metal–insulator transition (MIT) at $T_c \approx 68$ °C,¹ and VO₂ is capable of transforming between a low-temperature (monoclinic, M1) semiconducting state and a high-temperature (rutile, R) metallic-like state. Thin films are of intense current interest for numerous applications such as glazings for energy-efficient buildings and a large number of (opto)electronic, bolometric, and sensing devices.^{2–5}

In single crystals of VO₂, the MIT is characterized by sharp real-space phase boundaries between the R and M1 structures and by the fact that these boundaries can propagate along the crystallographic *c*-axes,⁶ *i.e.*, the transition is non-percolating in nature. Thin films of VO₂ are normally distinctly different, however, and the MIT is gradual with metallic-like regions growing in extent as the sample temperature T_s approaches T_c from below and with semiconducting regions disappearing as T_s becomes increasingly larger than T_c .^{7,8–13} The percolative character of the MIT in VO₂ films has been emphasized several times.^{9,14–17} The percolation is not only of theoretical interest but also relevant for the energy-savings potential for VO₂-type films used in energy-efficient fenestration.¹⁸

Percolation enhances macroscopic resistance fluctuations, as is well known,¹⁹ and such fluctuations have been investigated in some prior studies^{20–23} especially with regard to bolometer performance.

II. EXPERIMENTS

VO₂ films with grain-like features at the 50 nm length scale were prepared by reactive DC magnetron sputtering onto heated sapphire substrates and were used to make 100-nm-thick samples that were 10 μm wide and 100 μm long.

The thermochromic properties of the VO₂ micro-bridge was verified by measurements of electrical resistance R_s during heating and cooling in the $20 < T_s < 80$ °C interval. The temperature recording had to rest at least for 10 minutes at each setting in order to stabilize the T_s and resistance readings. Figure 1 shows that R_s changes by a factor ~2000 in the range between ~50 and ~70 °C and that the transition displays thermal hysteresis amounting to ~7 °C. The origin of the hysteresis may be stress build-up and release and associated effects of super- and sub-cooling. Energetically, this can be represented by a system of microscopic double-potential wells connected with pinning forces via interactions with the substrate.

After installing a home-made temperature control that provided about a million times less temperature fluctuations (in the nano-Kelvin range) than commercial units (in the milli-Kelvin range), we were able to measure power density spectra $S(f)$ of resistance

noise around T_c and to demonstrate unambiguous $1/f$ behavior, thus proving that the measured noise was not due to temperature fluctuations.

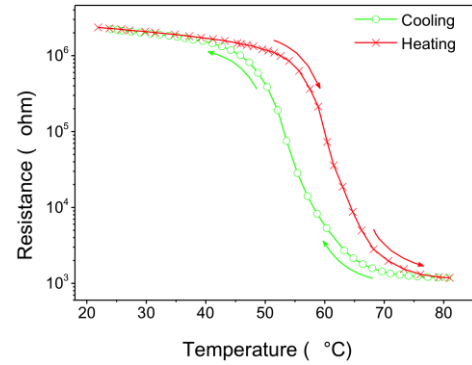


FIG. 1. Resistance hysteresis upon heating and cooling of a VO₂ film.^{a)}

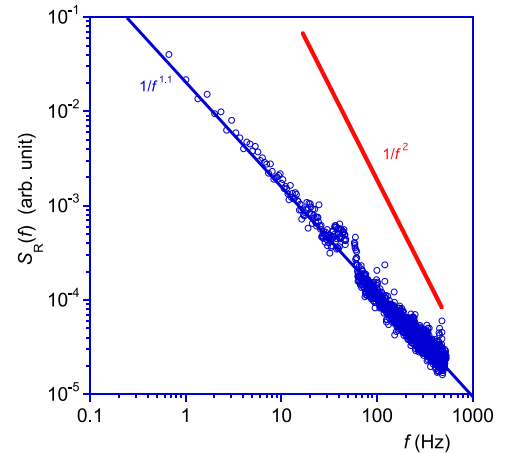


FIG. 2. Resistance noise spectrum of a VO₂ film. The data show $1/f$ -like performance even at the middle of the resistive transition.^{a)}

At 10 Hz, we performed a scaling analysis of the normalized noise *versus* the resistance, where temperature was a hidden parameter. The normalized spectrum scaled as

$$\frac{S_R}{R_s^2} \propto R_s^x, \quad (1)$$

where S_R is the resistance noise spectrum and R_s is the sample

resistance. The noise exponent x was -2.6 for $T_s < T_c$ and $+2.6$ for $T_s > T_c$.

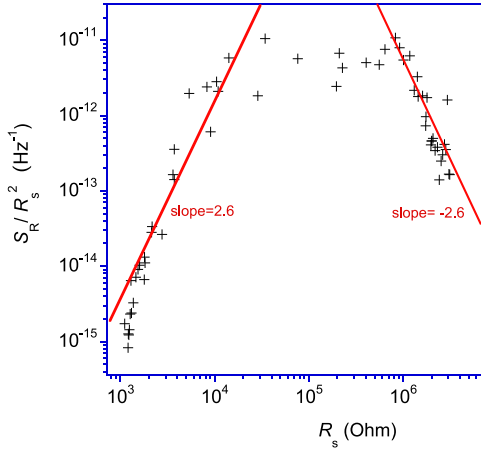


FIG. 3. Scaling plot of the normalized resistance noise spectrum for a VO₂ film.^{a)}

III. UNSOLVED PROBLEMS

Theoretical models and experiments of conductor–insulator and conductor–superconductor transitions fail to produce the empirical noise exponents at both¹⁹ or one side²⁴ of the transition, except for the *Pennetta–Trefán–Reggiani* (PTR) model²⁵ where the positive exponent was empirically obtained by computer simulations²⁵ and

- ^{a)} The *non-UPoN* parts of this extended abstract are based on a recent paper by the same authors, *J. Appl. Phys.* **117**, 025303 (2015). (Authorized by copyright agreement).
- ¹ F. J. Morin, *Phys. Rev. Lett.* **3**, 34 (1959).
 - ² Z. Chen, Y. Gao, L. Kang, C. Cao, S. Chen, and H. Luo, *J. Mater. Chem. A* **2**, 2718 (2014).
 - ³ C. G. Granqvist, *J. Vac. Sci. Technol. B* **32**, 060801 (2014).
 - ⁴ S.-Y. Li, G. A. Niklasson, and C. G. Granqvist, *J. Appl. Phys.* **115**, 053513 (2014).
 - ⁵ M. E. A. Warwick and R. Binions, *J. Mater. Chem. A* **2**, 3275 (2014).
 - ⁶ B. Mun, K. Chen, J. Yoon, C. Dejoie, N. Tamura, M. Kunz, Z. Liu, M. E. Grass, S.-K. Mo, C. Park, Y. Y. Lee, and H. Ju, *Phys. Rev. B* **84**, 113109 (2011).
 - ⁷ See, for example, M. M. Qazilbash, M. Brehm, B.-G. Chae, P.-C. Ho, G. O. Andreev, B.-J. Kim, S. J. Yun, A. V. Balatsky, M. B. Maple, F. Keilmann, H.-T. Kim, and D. N. Basov, *Science* **318**, 1750 (2007).
 - ⁸ P. U. Jepsen, B. M. Fischer, A. Thoman, H. Helm, J. Y. Suh, R. Lopez, and R. F. Haglund, Jr., *Phys. Rev. B* **74**, 205103 (2006).
 - ⁹ Y. J. Chang, J. S. Yang, Y. S. Kim, D. H. Kim, T. W. Noh, D.-W. Kim, E. Oh, B. Kahng, and J.-S. Chung, *Phys. Rev. B* **76**, 075118 (2007).
 - ¹⁰ B.-J. Kim, Y. W. Lee, S. Choi, J.-W. Lim, S. J. Yun, H.-T. Kim, T.-J. Shin, and H.-S. Yun, *Phys. Rev. B* **77**, 235401 (2008).
 - ¹¹ K. L. Holman, T. M. McQueen, A. J. Williams, T. Klimczuk, P. W. Stephens, H. W. Zandbergen, Q. Xu, F. Ronning, and R. J. Cava, *Phys. Rev. B* **79**, 245114 (2009).
 - ¹² J.-G. Ramírez, A. Sharoni, Y. Dubi, M. E. Gómez, and I. K.

the negative exponent follows^a from duality arguments in two dimensions. But there are open questions:

- (i) How is the $1/f$ noise spectrum generated, especially near the percolation threshold, in such small systems?
- (ii) Is there an analytic solution of the PTR model to produce these exponents?
- (iii) Are the noise exponents universal in periodic lattices, or do they depend on the type of resistor lattice?
- (iv) Which assumptions of the healing–recovering dynamics are essential to get these noise exponents?
- (v) Is duality indeed enough to explain the negative exponent in two dimensions or extra assumptions are needed?
- (vi) What are the exponents in three dimensions, *i.e.*, can we expect a dimensional crossover in thicker films?

ACKNOWLEDGEMENTS

We are grateful to Per Nordblad and Peter Svedlindh for their assistance with the ultra-low noise temperature control system. Hans-Olof Blom is thanked for guidance with sample preparation. Financial support was obtained from the European Research Council under the European Community’s Seventh Framework Program (FP7/2007–2013)/ERC Grant Agreement No. 267234 (GRINDOOR). LK’s work in Sweden was partially funded by Texas A&M University.

- Schuller, *Phys. Rev. B* **79**, 235110 (2009).
- ¹³ J. Kim, C. Ko, A. Frenzel, S. Ramanathan, and J. E. Hoffman, *Appl. Phys. Lett.* **96**, 213106 (2010).
 - ¹⁴ J. Rozen, R. Lopez, R. F. Haglund, Jr., and L. C. Feldman, *Appl. Phys. Lett.* **88**, 081902 (2006).
 - ¹⁵ D. Ruzmetov, K. T. Zawilski, S. D. Senanayake, V. Narayanamurti, and S. Ramanathan, *J. Phys.: Condens. Matter* **20**, 465204 (2008).
 - ¹⁶ A. R. Gentle, G. B. Smith, and A. I. Maarouf, *J. Nanophotonics* **3**, 031505 (2009).
 - ¹⁷ V. Sh. Aliev, S. G. Bortnikov, and I. A. Badmaeva, *Appl. Phys. Lett.* **104**, 132906 (2014).
 - ¹⁸ M. E. A. Warwick, I. Ridley, and R. Binions, *Energy Buildings* **77**, 80 (2014).
 - ¹⁹ G. A. Garfunkel and M. B. Weissman, *Phys. Rev. Lett.* **55**, 296 (1985).
 - ²⁰ A. A. Velichko, G. B. Stefanovich, A. L. Pergament, and P. P. Boriskov, *Pis'ma Tekh. Fiz.* **29**(10), 82 (2003) [*Tech. Phys. Lett.* **29**, 435 (2003)].
 - ²¹ N. Chi-Anh and S. Moon, *Infrared Phys. Technol.* **50**, 38 (2007).
 - ²² G. Neto, L. A. L. de Almeida, A. M. N. Lima, C. S. Moreira, H. Neff, I. A. Khrebtov, and V. G. Malyarov, *Opt. Eng.* **47**, 073603 (2008).
 - ²³ H. A. Basantani, S. Kozłowski, M.-Y. Lee, J. Li, E. C. Dickey, T. N. Jackson, S. S. N. Bharadwaja, and M. Horn, *Appl. Phys. Lett.* **100**, 262108 (2012).
 - ²⁴ L. B. Kiss and P. Svedlindh, *Phys. Rev. Lett.* **71**, 2817 (1993).
 - ²⁵ C. Pennetta, G. Trefán, and L. Reggiani, *Phys. Rev. Lett.* **85**, 5238 (2000).

Frequency-dependent shot noise in single-electron devices interpreted by means of waiting time distributions

Vincent Talbo¹, Javier Mateos¹, Sylvie Retailleau², Philippe Dollfus² and Tomás González¹

¹Departamento de Física Aplicada, Universidad de Salamanca, Plaza de la Merced S/N, E-37008 Salamanca, Spain

²Institut d'Electronique Fondamentale, Université Paris-Sud, CNRS UMR 8622, F-91405 Orsay, France
e-mail address: vtalbo@usal.es

I. INTRODUCTION

Silicon quantum dot (QD)-based single-electron devices, in particular single-electron transistors (SETs), can now operate at room-temperature, thanks to the recent progress in nanofabrication techniques, scaling QDs down to 5 nm¹, then paving the way to various applications for logic or memory circuits, or random number generator.

Meanwhile, the detection of single-electron processes is available experimentally thanks to quantum point contacts, giving access to current fluctuations². In particular, interests are focused on the shot noise (SN), consequence of charge granularity, that gives more information about electronic transport, thus has been intensively studied during the past decades³. The SN is often characterized by the ratio of the current spectral density of the device $S(f)$ to the spectral density of a Poissonian process $2qI$ where I is the mean current. At zero-frequency, the ratio $F = S(0)/2qI$ is called Fano factor. Most of the theoretical studies of the SN are performed at zero-frequency, using the full counting-statistics tool (FCS), which calculates current-correlations from probability distributions of number of electrons transferred during a long period of time⁴. For example, it has been shown that in a case of a multi-level QD, the noise can be enhanced up to super-Poissonian noise⁵ ($F > 1$).

The time- and frequency-dependent SN, through autocorrelation functions (AFs) and current spectral density respectively have been less explored. Recently, a new method emerged called waiting time distribution (WTD), focusing on the distributions of times between two single-electron events⁶.

The aim of this work is to present the close link between WTDs and AFs, thus the current spectral densities in a Si-QD-based double-tunnel junction (DTJ), shown in Fig. (1), in order to understand the specific dynamics of the electronic transport in this device. The structure is simulated through the homemade 3D self-consistent code SENS⁷ (Single-Electron Nanodevices Simulation).

II. SENS CODE

To take into account the quantization effects in Si-QD, the first stage of the simulation relies on the calculation of the electronic structure of the QD according to the bias voltage and the number of electrons inside it by solving the Poisson-Schrödinger coupled equations within the Hartree and effective mass approximations.

The resulting wave functions are then used to compute the tunnel transfer rates source-to-dot $\Gamma_{in}(N)$ and dot-to-drain $\Gamma_{out}(N)$ depending on the number of electrons N in the QD by means of the Fermi golden rule and Bardeen formalism.

Finally, the transfer rates are introduced in analytic expressions or a Monte-Carlo algorithm to reach all electrical characteristics, such as current, AFs and current spectral densities. The WTDs are also obtained from tunnel transfer rates.

III. RESULTS AND DISCUSSION

The simulated DTJ consists in an 8-nm-diameter Si-QD; with source and drain tunnel barriers of 1.2 nm and 1.8 nm thicknesses, respectively. The current and Fano factor, F , are shown in Fig. (2). The current shows a positive differential conductance in the first two Coulomb stairs, while a negative differential conductance is observed in subsequent stairs. F decreases on the two first stairs, reaching its minimum just before the third step, and then increases until reaching its maximum value at the beginning of the fourth step. The behavior of the current and F are explained in previous articles^{7,8}.

The current spectral densities for three different regimes (sub-, super- and Poissonian Fano factor) as well as their corresponding autocorrelation functions are plotted in Fig (3) and (4), respectively. In the case of a super- (sub-)Poissonian Fano factor, the spectral density remains higher (lower) than the Poissonian spectral density $2qI$ with frequency, which is the consequence of an always positive (negative) AF with time lag. However, we notice that in the case of a Fano factor slightly higher than 1, the spectral density goes below the Poissonian value in the [10^6 10^7] frequency range, thus indicating specific dynamics. This peculiar behavior is also noticeable on the corresponding AF, the correlation going from negative to positive values before reaching the uncorrelated value.

This specific dynamic occurs in the third step of the Coulomb staircase ($V = 0.95$ V), i.e., when 4 states are available (0, 1, 2 or 3 electrons in the dot). To clarify the understanding of this behavior around Poissonian SN, we have simulated the same device with only 3 states available. In this case, looking at the source junction, only two tunnel events are adding one electron in the QD: the transitions $0 \rightarrow 1$ (01) and $1 \rightarrow 2$ (12). In Fig. (5), the WTDs and auto- and cross-correlations between those two tunnel events are shown. We see that the autocorrelation of (12) events C_{12-12} is responsible of the behavior global autocorrelation C_{II} . At low times, the WTD between two 12 events is zero, due to the fact that another transition (21 – the second electron is exiting the QD through the drain junction) is necessary to reach an other (12) event. Therefore, it is very unlikely to have two (12) events within such low time lag, and C_{12-12} is negative. Then, the AF increases with its corresponding WTD, and eventually reaches positive value around the maximum of WTD. The WTD and AF decrease then accordingly, to finally reach the uncorrelated value.

ACKNOWLEDGEMENTS

This work has been partially supported by the Dirección General de Investigación Científica y Técnica (MINECO) through Project TEC2013-41640-R and by the Junta de Castilla y León through Project SA052U13. V. Talbo wants to thank the European Social Fund (ESF) for financing his postdoctoral contract.

¹ Y. Tanahashi, R. Suzuki, T. Saraya, and T. Hiramoto, Jap. Journ. Appl. Phys. **53**, 04EJ08 (2014)
² N. Ubbelohde, C. Fricke, C. Flindt, F. Hohls, and R. J. Haug, Nature Comm. **3**, 612 (2012).
³ Y. Blanter and M. Büttiker, Phys. Rep. **336**, pp. 1-166 (2000).
⁴ L.S. Levitov, H. Lee, G.B. Lesovik, J. Math. Phys. **37**, pp. 4845 (1996).
⁵ W. Belzig, Phys. Rev. B **71**, 161301 (2005).
⁶ M. Albert, G. Haack, C. Flindt, and M. Büttiker, Phys. Rev. Lett. **108**, 186806 (2012).
⁷ J. Sée, P. Dollfus and S. Galdin, IEEE Trans. Electron. Dev. **53**, pp. 1268 (2006).
⁸ V. Talbo, D. Querlioz, S. Retailleau, and P. Dollfus, Fluct. Noise Lett. **11**, 1242006 (2012).

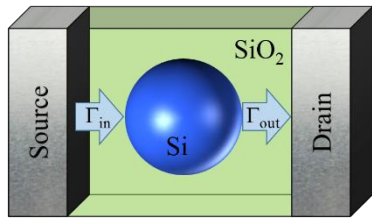


FIG. 1. Schematic view of a DTJ.

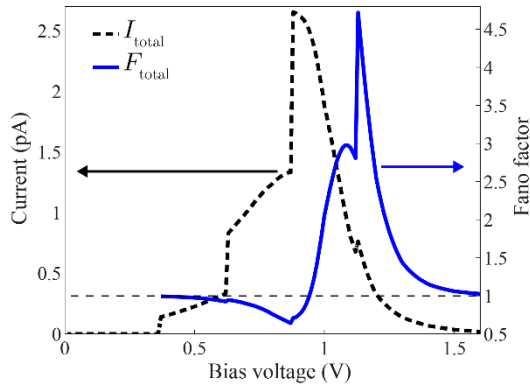


FIG. 2. Current (dashed) and Fano factor (solid) as a function of the applied voltage.

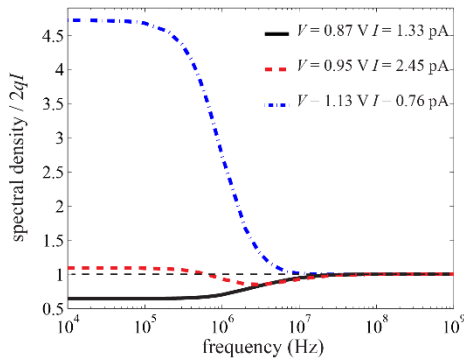


FIG. 3. Current spectral density as a function of frequency for three different biases corresponding to different transport regimes.

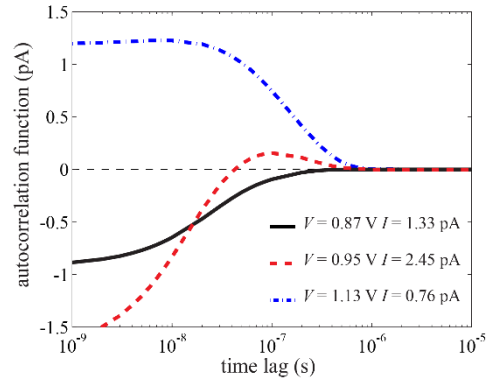


FIG. 4. Current autocorrelation functions as a function of time lag for three different biases corresponding to different transport regimes

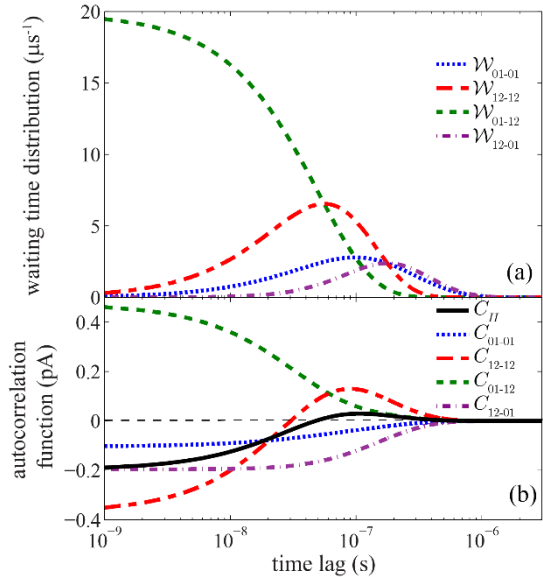


FIG. 5. (a) WTDs and (b) Auto- and cross-correlation functions between (01) and (12) current pulses as a function of time, for a bias corresponding to Poissonian Fano factor $F \sim 1$ in the 3-state case.

Conductance fluctuations in Si nanowires studied from first-principles

Riccardo Rurali¹, F. Iori², and S. Ossicini²

¹*Institut de Ciència de Materials de Barcelona (ICMAB–CSIC), Campus de Bellaterra, 08193 Bellaterra, Barcelona, Spain*

e-mail address: rrurali@icmab.es

²*Università di Modena e Reggio Emilia, via Amendola 2 Pad. Morselli, I-42100 Reggio Emilia, Italy*
e-mail address: federico.iori@unimore.it, stefano.ossicini@unimore.it

I. INTRODUCTION

Silicon nanowires (NWs) are among the most promising building blocks for emerging devices and novel applications in nanoelectronics^{1,2}. Although reconfigurable transistors that explicitly avoid the use of dopants have been demonstrated³, the modulation of the conductivity by impurity doping is still the most common design strategy for Si NW based devices. Dopants in NWs are a very special class of impurities: they are added on purpose to provide free carriers that allow tailoring the conductivity, but at the same time they act as scattering centers, decreasing the mobility. Besides the intrinsic difficulty in obtaining radially⁴ and axially⁵ uniform doping profiles, ultrathin NWs pose a fundamental problem related to the variability of the performances of the resulting devices^{6,7}.

In bulk Si, all lattice sites are equivalent. In a NW, this is true only when moving along the wire axis and lattice sites are radially inequivalent, i.e., substitution of an impurity at a site in the innermost part of the wire results, in principle, in different energetics and properties from substitution at a site close to the surface.

Several studies have already shown that dopant impurities exhibit a mild to strong tendency (depending on surface defects) to surface segregation^{8,9} and that the scattering induced by an impurity depends strongly on its exact (radial) position^{10,11}. Clearly, this is a serious problem from the design viewpoint. Due to their reduced diameter, achieving a doping concentration of 10^{18} cm^{-3} means having one dopant every 50 nm in a NW with a 5 nm diameter, which amounts to 196 impurities in a 10 μm -long NW.

Infinitely long NW tends to some average properties, because in the limit of many dopants all the possible impurity configurations are sampled. However, in many cases, it is desirable to have NW-based devices operating in the ballistic regime, a condition fulfilled by NWs shorter than the phonon mean free path.

II. RESULTS

In this talk I will present the results obtained in our group on the conductance fluctuations in Si nanowires studied from first-principles electronic structure methods.

We combine the ideas of scaling theory and universal conductance fluctuations with density-functional theory to analyze the conductance properties of doped Si nanowires¹². Specifically, we study the crossover from ballistic to diffusive transport in boron or phosphorus doped Si nanowires by computing the mean free path, sample-averaged conductance $\langle G \rangle$, and sample-to-sample variations $\text{std}(G)$ as a function of energy, doping density, wire

length, and the radial dopant profile. Our main findings are (i) the main trends can be predicted quantitatively based on the scattering properties of single dopants, and (ii) the sample-to-sample fluctuations depend on energy but not on doping density, thereby displaying a degree of universality.

We use this approach to calculate the conductance distribution of up to 200 nm long SiNWs with different distributions of impurities, showing that the radial distribution of the dopants influences the conductance properties significantly: surface doped wires have longer mean-free paths and smaller sample-to-sample fluctuations in the cross-over from ballistic to diffusive transport¹⁴.

These findings can be quantitatively predicted in terms of the scattering properties of the single dopant atoms [see Fig.(1)], implying that relatively simple calculations are sufficient in practical device modeling.

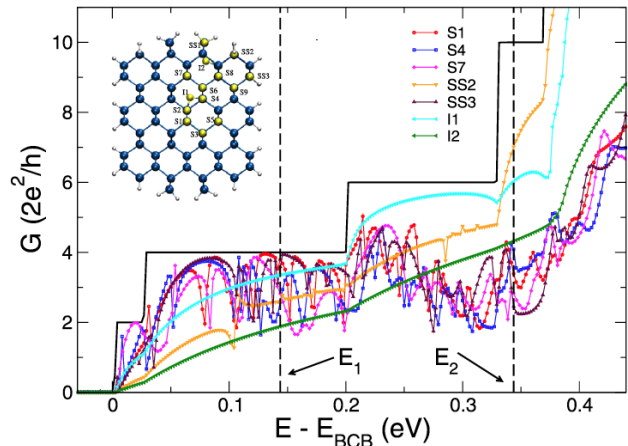


FIG.1. Ballistic conductance of some selected single-dopant configurations. All the point defects studied, nine bulk substitutionals (S1–S9), three subsurface substitutionals (SS1–SS3), and two interstitials (I1–I2), are shown in the inset (from Ref.¹⁵).

We further exploit these ideas to study how the variability of the conductance associated with single-dopant configurations affects the overall conductivity of long, realistic ultrathin Si nanowires (NW)¹⁵. In particular, we quantify the doping dose threshold at which ultrathin nanowires like those investigated here acquire some kind of average properties for lengths $L > 15 \mu\text{m}$, though at lower dopant concentration, variability of the conductivity persists, and is significant, up to 50 μm .

At larger diameters, the fluctuations are expected to decrease, because there will be a much larger fraction of the allowed dopant configurations that yield very similar scattering resistances. For

such thicker wires, it might be possible to suppress the most significant conductance fluctuations and stay within the length limit of ballistic transport, without needing to go to extremely high dopant doses. Yet, variability induced by conductance fluctuations will have to be monitored and is likely to be among the factors that limit the performances of devices based on Si NW with diameters thinner than 10–20 nm. Even a few interstitial defects would significantly degrade the overall conductance, but luckily their expected concentration is negligible and they can be disregarded.

ACKNOWLEDGEMENTS

We acknowledge funding under contract Nos. FEDERFIS2012-37549-C05-05 and CSD2007-00041 of the Ministerio de Economía y Competitividad (MINECO) and grant 2014 SGR 301 of the Generalitat de Catalunya. We thank the Centro de Supercomputación de Galicia (CESGA) for the use of their computational resources.

-
- ¹ R. Rurali, *Rev. Mod. Phys.* **82**, 427 (2010).
 - ² W. Lu and C. M. Lieber, *J. Phys. D: Appl. Phys.* **39**, R387 (2006).
 - ³ A. Heinzig, S. Slesazeck, F. Kreupl, T. Mikolajick, and W. M. Weber, *Nano Lett.* **12**, 119 (2012).
 - ⁴ D. E. Perea, E. R. Hemesath, E. J. Schwalbach, J. L. Lensch-Falk, P. W. Voorhees, and L. J. Lauhon, *Nat. Nanotechnol.* **4**, 315 (2009).
 - ⁵ G. Imamura, T. Kawashima, M. Fujii, C. Nishimura, T. Saitoh, and S. Hayashi, *Nano Lett.* **8**, 2620 (2008).
 - ⁶ M. Bohr, *IEEE Trans. Nanotechnol.* **1**, 56 (2002).
 - ⁷ Y. Li, S.-M. Yu, J.-R. Hwang, and F.-L. Yang, *IEEE Trans. Electron Devices* **55**, 1449 (2008).
 - ⁸ M. V. Fernández-Serra, C. Adessi, and X. Blase, *Phys. Rev. Lett.* **96**, 166805 (2006).
 - ⁹ H. Peelaers, B. Partoens, and F. Peeters, *Nano Lett.* **6**, 2781 (2006).
 - ¹⁰ M.-V. Fernández-Serra, C. Adessi, and X. Blase, *Nano Lett.* **6**, 2674 (2006).
 - ¹¹ N. Seoane, A. Martínez, A. Brown, J. Barker, and A. Asenov, *IEEE Trans. Electron Devices* **56**, 1388 (2009).
 - ¹² T. Markussen, R. Rurali, A.-P. Jauho, and M. Brandbyge, *Phys. Rev. Lett.* **99**, 076803 (2007).
 - ¹³ R. Rurali, T. Markussen, J. Suñé, M. Brandbyge, and A.-P. Jauho, *Nano Lett.* **8**, 2825 (2008).
 - ¹⁴ T. Markussen, R. Rurali, A.-P. Jauho, and M. Brandbyge, *J. Comput. Electron.* **7**, 324 (2008).
 - ¹⁵ F. Iori, S. Ossicini, and R. Rurali, *J. Appl. Phys.* **116**, 074303 (2014).

Chronotaxic dynamics: when the characteristic frequencies fluctuate and the system is stable

Aneta Stefanovska,¹ Philip Clemson,² and Yevhen F. Suprunenko³

¹*Physics Department, Lancaster University, Lancaster, UK
e-mail address: aneta@lancaster.ac.uk*

²*Physics Department, Lancaster University, Lancaster, UK
e-mail address: p.clemson@lancaster.ac.uk*

³*Institute of Integrative Biology, University of Liverpool, Liverpool, UK
e-mail address: yevhen.suprunenko@gmail.com*

I. INTRODUCTION

Complex, fluctuating dynamics abounds in nature. With the fast sensors available today, large numbers of time-series are continuously being measured and analysed. To characterise the underlying dynamics one needs models. Although there are no strict boundaries, two general approaches coexist: stochastic and deterministic, as illustrated in Fig. (1). Of course, the same time series can be characterised either as *stochastic* or as *deterministic*. In the stochastic approach we do not make any assumptions about the properties or values of parameters involved in generating the dynamical behaviour and we analyse the time series using probability theory. But often, in real problems, we need to know the reason for a change in behaviour, for example from a healthy state to a diseased one. In this case we try to generate hypotheses or models and describe the causal relationship using deterministic systems.

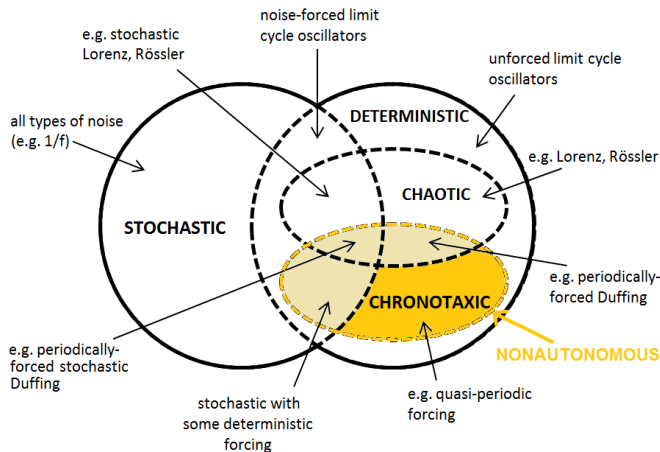


FIG. 1. A simplified representation of dynamical systems with typical examples. Although the chronotaxic systems are fully deterministic, unless influenced by stochastic perturbations, they have been usually treated as stochastic.

Generally, deterministic systems are considered within the theory of autonomous systems. In the last decades, much research has been devoted to chaotic systems, which are a special class of deterministic systems. Of course, as soon as they are perturbed by being coupled to a stochastic system their characteristics change as indicated in Fig. (1).

But many living systems, as well as man-made ones, are thermodynamically open because they exchange energy and matter with the environment. For such systems, the mathematical theory of non-autonomous systems is necessary. Motivated by these needs, recent developments have resulted in advances in non-autonomous dynamical systems theory¹, and in the theory of random dynamical systems².

Furthermore, only when a system is described as non-autonomous, and not transformed into autonomous by adding an extra dimension to account for the time-dependence, can one explain the *stability of its time-dependent dynamics*: such stability does not allow the time-variable dynamics to be changed easily by external *continuous* perturbation, a feature that provides a foundation for the newly-established theory of chronotaxic systems³⁻⁵. The ability of such systems to sustain stability in the amplitude and phase of oscillations under continuous perturbation are key features that were used in naming them chronotaxic (from *chronos* – time and *taxis* – order). Chronotaxic systems possess a *time-dependent point attractor* provided by an external drive system. This allows the frequency of oscillations to be prescribed externally through this driver and response system, giving rise to determinism even when faced with strong perturbations.

It can be shown⁵ that the existence of such stability can cause their non-autonomous dynamics to look stochastic-like, and very complex, perhaps leading to their misidentification as stochastic or chaotic. In fact, because the underlying deterministic dynamics of such systems remains stable, we can decompose the dynamics into a deterministic part and a component due to the external perturbations.

We will now briefly introduce the basic properties of chronotaxic systems and discuss some open questions.

II. CHRONOTAXIC SYSTEMS IN BRIEF

A chronotaxic system³⁻⁵ is a non-autonomous oscillatory dynamical system \mathbf{x} generated by an autonomous system of unidirectionally coupled equations

$$\dot{\mathbf{p}} = \mathbf{f}(\mathbf{p}), \quad \dot{\mathbf{x}} = \mathbf{g}(\mathbf{x}, \mathbf{p}), \quad (1)$$

where $\mathbf{p} \in R^n$, $\mathbf{x} \in R^m$, $\mathbf{f} : R^n \rightarrow R^n$, $\mathbf{g} : R^m \times R^n \rightarrow R^m$; n and m can be any positive integers. The system (1)

may also be called a drive and response system⁶, or a master-slave configuration⁷. Considered in the context of non-autonomous dynamical systems^{1,8}, the system (1) can be viewed as a skew-product flow or as a process.

Importantly, the solution $\mathbf{x}(t, t_0, \mathbf{x}_0)$ of Eqs. (1), depends on the actual time t as well as on the initial conditions (t_0, \mathbf{x}_0) ; whereas the solution $\mathbf{p}(t - t_0, \mathbf{p}_0)$ depends only on initial condition p_0 and on the time of evolution $t - t_0$. The subsystem \mathbf{x} is nonautonomous in the sense that it can be described by an equation which depends on time explicitly, e.g. $\dot{\mathbf{x}} = \mathbf{g}(\mathbf{x}, \mathbf{p}(t))$. A chronotaxic system is described by \mathbf{x} which is assumed to be observable, and \mathbf{p} which may be inaccessible for observation, as often occurs when studying real systems. Rather than assuming or approximating the dynamics of \mathbf{p} ; we focus on the dynamics of \mathbf{x} and use only the following simple assumption: that system \mathbf{p} is such that it creates a time-dependent steady state in the dynamics of \mathbf{x} .

Therefore, the whole external environment with respect to \mathbf{x} is divided into two parts. The first part is given by \mathbf{p} which is the part that makes the system \mathbf{x} chronotaxic. The second part contains the rest of the environment and is therefore considered as external perturbations. The theory for the case where amplitudes and phases are separable have been introduced by Suprunenko *et al*^{3,4}, and it has subsequently been expanded to include the generalized case of chronotaxic systems where such decoupling is not required⁵.

Thus, when perturbations do not destroy the chronotaxic properties of a system, the stable deterministic component of its dynamics can be identified, as shown by Clemson *et al*⁹. This reduces the complexity of the system, enabling us to filter out the stochastic component and focus on the deterministic dynamics and the interactions between system \mathbf{x} and its driver \mathbf{p} , as shown in^{3,9}. For complex and open systems it has the potential to extract properties of the system which were previously neglected.

III. OPEN PROBLEMS

The theory of chronotaxic systems could facilitate more realistic insight into the underlying dynamics of systems whose time-evolution is recorded. As chrono-

taxic systems are inevitably non-autonomous, inverse approach methods, developed for analysis of time-series with time-dependent characteristics¹⁰, can safely be applied to gain initial insights. Specific methods have already been proposed for the detection of chronotaxicity^{9,11}. However, they are applicable to systems in which the amplitude and phase dynamics are separable, as they are applied directly to the extracted phases of the system, while the amplitude information is discarded. Such an approach is valid given that the amplitude dynamics of a chronotaxic system corresponds to the convergence of the system to a limit cycle, influenced only by a negative Lyapunov exponent and external perturbations, while the phase dynamics corresponds to convergence to a time-dependent point attractor^{9,11}. As it is the point attractor in the phase dynamics in which we are primarily interested, the separation into amplitude and phase follows naturally. Using this approach, an example of chronotaxic dynamics has already been demonstrated in a real system, in the case of heart rate variability under paced respiration⁹.

However, in generalized chronotaxic systems⁵, the amplitude and phase are not required to be separable, providing an even greater applicability to real systems, allowing for amplitude-amplitude and amplitude-phase interactions, in addition to the phase-phase dynamics considered hitherto^{3,4}. Therefore, the incorporation of the ability to identify these new possibilities for chronotaxicity will be crucial to the further development of inverse approach methods. These will then provide the means to detect chronotaxicity in systems where the amplitude and phase are not separable, as e.g. is the case of brain dynamics. However, this is an open problem, as yet awaiting a solution.

ACKNOWLEDGMENTS

We are grateful to many collaborators and colleagues for fruitful discussions on various occasions over the years. This work has been supported by the Engineering and Physical Sciences Research Council (UK) (Grant No. EP/I00999X1) and in part by the Slovenian Research Agency (Program No. P20232).

¹ P. E. Kloeden and M. Rasmussen, *Nonautonomous Dynamical Systems* (American Mathematical Society, 2011).

² H. Crauel and F. Flandoli, *Prob. Theory Rel. Fields* **100**: 365–393, 1994.

³ Y. F. Suprunenko, P. T. Clemson and A. Stefanovska, *Phys. Rev. Lett.* **111**: 024101, 2013.

⁴ Y. F. Suprunenko, P. T. Clemson and A. Stefanovska, *Phys. Rev. E* **89**: 012922, 2014.

⁵ Y. F. Suprunenko and A. Stefanovska, *Phys. Rev. E* **90**: 032921, 2014.

⁶ L. Kocarev and U. Parlitz, *Phys. Rev. Lett.* **76**: 1816–1819, 1996.

⁷ H. Haken, *Synergetics: Introduction and Advanced Topics* (Springer-Verlag Berlin Heidelberg, 2004).

⁸ P. E. Kloeden and V. S. Kozyakin, *Dis. Cont. Dyn. Sys.* **7**: 883–893, 2001.

⁹ P. T. Clemson, Y. F. Suprunenko, T. Stankovski and A. Stefanovska, *Phys. Rev. E* **89**: 032904, 2014.

¹⁰ P. T. Clemson and A. Stefanovska, *Phys. Rep.* **542**: 297–368, 2014.

¹¹ G. Lancaster, P. T. Clemson, Y. F. Suprunenko, T. Stankovski and A. Stefanovska, *Entropy*, invited review, to be published.

Fluctuations and effective temperature in an active dumbbell system

Giuseppe Gonnella,¹ Antonio Suma,² and Leticia F. Cugliandolo³

¹*Dipartimento di Fisica, Università di Bari and
INFN, Sezione di Bari, via Amendola 173, Bari, I-70126, Italy**

²*SISSA - Scuola Internazionale Superiore di Studi Avanzati,
Via Bonomea 265, 34136 Trieste Italy†*

³*Sorbonne Universités, Université Pierre et Marie Curie - Paris VI,
Laboratoire de Physique Théorique et Hautes Énergies,
4 Place Jussieu, 75252 Paris Cedex 05, France‡*

I. INTRODUCTION

Active matter refers to systems driven out of equilibrium by internal or external energy sources. They are characterized by many peculiar properties not present in their passive counterparts, like clustering, anomalous diffusion, giant fluctuations, unexpected rheological properties¹⁻³. An open question for these systems is a coherent definition of an effective temperature⁴.

We consider here a two-dimensional system of active dumbbells⁵. Each dumbbell is composed by two colloids kept together by an elastic potential, with an excluded volume interaction modeled through a Weeks-Chandler-Anderson (WCA) potential. They are immersed in an implicit solvent modeled by the Langevin equation. The activity is modeled by a constant force acting along the main axis of the dumbbell. The model can be intended as a coarse-grained description of the behavior of simple bacteria. Hydrodynamic interactions are ignored, being much more demanding computationally.

The two goals of this work are the following. First we want to analyze the diffusion and fluctuation properties of the dumbbell system. At strong enough activity, or small enough temperature, and at sufficient high density, dumbbells segregate into a concentrated and a dilute phase. We focus on the regime without clustering, when the system is globally homogeneous. We find four different regimes for the translational and angular mean square displacement, and show the dependence of the diffusion coefficient of the late-epoch diffusion regime from the temperature, activity and density. We find for example, that for sufficiently high activity, the rotation diffusion is enhanced from increasing density which is different from what usually happens in passive colloidal systems⁶. For what concerns the behavior of the distribution functions of the displacements, at strong activity, we find significant deviations from the gaussian behavior in the superdiffusive regime found before the last usual diffusive regime. At small activity, the initial inertial regime is followed by a subdiffusive regime and also in this case we find slowly decaying codes of the distributions not corresponding to gaussian behavior.

Second, we want to investigate about the definition of the effective temperature in this system, usually defined by a dynamic fluctuation-dissipation relation. For this purpose, we introduce spherical tracers, kinetically coupled with the dumbbells, in order to test the notion of

effective temperature. The effective temperature of the tracers will be compared with that obtained by studying the active dumbbell system by alone. In general, the study of the dynamics of tracers, more accessible experimentally than that of the non-equilibrium system itself, is a convenient way to analyze non-equilibrium systems.

For a single active dumbbell we analytically calculate the diffusion coefficient for its center of mass together with the displacement induced by a pulling force, arriving to a definition of an effective temperature through a fluctuation-dissipation relation. Then we numerically evaluate the above quantities for systems with different densities, temperature and activity. We show how the non trivial non monotonic behavior of diffusion and mobility, at varying activity, is reflected in the behavior of the effective temperature.

On the other hand, we calculate the effective temperature of the active system by analysing the velocity distribution function and a fluctuation dissipation relation for the tracers. The tracer velocity distributions is gaussian and a temperature can be evaluated by the variance of the distribution. We find that the tracer effective temperature, calculated by both methods, for high values of the mass of the tracers, converge to the value of the effective temperature found in the system without tracer.

In the next sections we show selected results for the translation and rotational mean square displacements and for the effective temperature in the system without tracers.

II. MEAN SQUARE DISPLACEMENT

Fig.1 shows the mean square displacement of the center of mass (upper panel) and rotational angle (lower panel) of dumbbells for a high Péclet number and different densities. The Péclet number represents the ratio between active advective contribution to transport rate and diffusive contribution. Different regimes can be observed, depending on the combination of the random noise, the activity and the density of the system.

These regimes correspond to those found analytically in the case of a single dumbbell, where a first ballistic inertial regime is followed by a diffusive regime, then by another ballistic regime due to activity and at the end by the late epoch final diffusive regime. It is interesting to observe that, while the single dumbbell mean square

rotational displacement only exhibits an initial inertial regime followed by the diffusive final regime, at final densities four regime can be observed also for this quantity.

Fig.2 shows the dependence on the density of the rotational diffusion constant, at a fixed value of the Péclet number, varying the temperature T and the active force F_{act} simultaneously⁵. The behavior is independent on the value of T, F_{act} chosen. Clustering effects induce unusual higher rotational diffusion when the density increases, for $\phi < 0.5$.

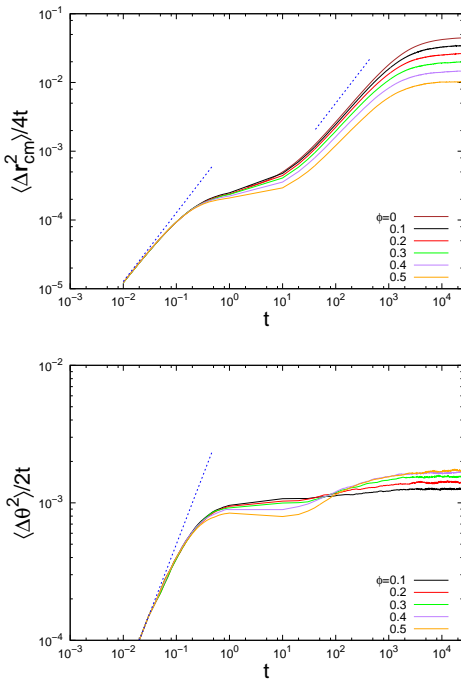


FIG. 1. Translational and rotational mean square displacement of active dumbbells at different densities.

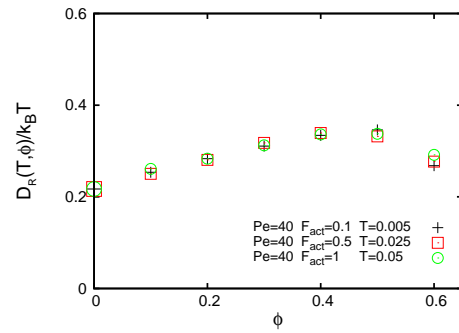


FIG. 2. Rotational diffusion coefficient at same Peclet number and different set of active force and temperature.

III. EFFECTIVE TEMPERATURE

Fig.3 suggests the dependence of the effective temperature on the square of the Péclet number. The theoretical line and the data at different densities are shown. Further analysis would show a non-monotonic behavior as a function of the density. $T_{J_{eff}}$ is calculated by a fluctuation-dissipation relation involving the mean square displacement in the last diffusive regime and the integrated linear response. At the value $F_a = 0.1$ we compared the value of the effective temperature shown above with that coming from the velocity distribution of tracers at different increasing masses. We found that the temperature of the tracer reached the one calculated from the system itself when the ratio between the mass of the tracer and that of the dumbbells is of the order of 10^4 .

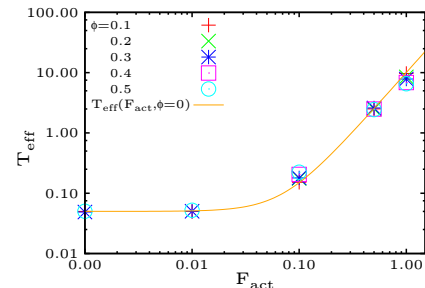


FIG. 3. Effective temperature as a function of the active force.

* gonnella@ba.infn.it

† antonio.suma@gmail.com

‡ leticia@lpthe.jussieu.fr

¹ S. Ramaswamy, The mechanics and statistics of active matter, *Ann. Rev. Cond. Matt. Phys.* **1**, 323 (2010).

² T. Vicsek and A. Zafeiris, Collective motion, *Phys. Rep.* **517**, 71 (2012)

³ G. Gonnella, D. Marenduzzo, A. Suma and A. Tiribocchi, *to appear in* *Compte Rendus de Physique*, 1502.02229 cond-mat arXiv.

⁴ L. F. Cugliandolo, The effective temperature, *Journal of Physics A: Mathematical and Theoretical*, **44**, 483001 (2011).

⁵ A. Suma, G. Gonnella, G. Laghezza, A. Lamura, A. Mossa and L. F. Cugliandolo, Dynamics of a homogeneous active dumbbell system, *Phys. Rev. E* **90**, 052130 (2014).

⁶ G. Gonnella, L. F. Cugliandolo and A. Suma, *submitted to* *Phys. Rev. E*.

Fluctuation Relations applied to characterize heterogeneous molecular ensembles

Alvaro Martinez-Monge,¹ Anna Alemany,¹ and Felix Ritort¹

¹*Small Biosystems Lab, Departament de Física Fonamental,
Universitat de Barcelona, C/ Martí i Franquès 1, 08028 Barcelona, Spain
e-mail address: fritort@gmail.com*

The identification and characterization of heterogeneous populations of biomolecular systems (e.g. cells, proteins, nucleic acids) has aroused a great interest in molecular biology. For instance, the state of the art in cancer research are the targeted and personalized therapies. Such therapies require to identify and characterize with extremely high accuracy the healthy cells and the cancer cells. Thus, it is clear the importance of understanding and characterization of heterogeneous molecular systems.

Thanks to the recent advances in single-molecule experiments¹ we can manipulate with high precision and sensitivity individual molecules, providing us a formidable tool to study and characterize an ensemble of different molecules at the nanoscopic scale.

An essential step in this project is to answer the following question:

Is it possible to discriminate the folding free energies of different structures of a mutational ensemble of DNA hairpins?

To answer this question, we have taken a standard and well-known canonical DNA hairpin, such as CD4², which consists on a stem of 20 base-pairs ending in a tetraloop (see figure 1-A), and we randomized 4 base-pairs (blue circles in figure 1-A) so that several populations of hairpins are obtained. Any of the four nitrogenous bases presents in DNA (adenine, guanine, thymine and cytosine) may be found in each mutated location, so we have $4^8 = 2^{16}$ different populations.

This purpose cannot be done in bulk measurements where only an average behavior of the system is measured. Thus, the context of single-molecule experiments is the perfect scenario to characterize a sample composed by mutated DNA hairpins.

To this end, we carry out pulling experiments using a miniaturized dual-beam laser optical tweezers apparatus³ that allows us to stretch an individual molecular construct (i.e. the DNA hairpin). This device is able to measure the applied force and the end to end distance (distance λ , see figure 1-B). The thermodynamical properties of the molecule under study can be inferred from the resulting force-distance curve. For example, we can extract the free energy difference between the folded and unfolded state of the DNA hairpins using Fluctuation Theorems.

In particular, Crooks Fluctuation Theorem⁴ allows us to extract free energy differences of formation of native molecular structures from bidirectional pulling experiments (that is, combining work measurements along unfolding and refolding paths):

$$\frac{P_F(W)}{P_R(-W)} = e^{\beta(W-\Delta G)} \quad (1)$$

Where W is the work exerted on the system that can be calculated using⁵:

$$W = \int_{\lambda_i}^{\lambda_f} f d\lambda \quad (2)$$

$\Delta G = G(\lambda_f) - G(\lambda_i)$ is the free energy between the folded and unfolded state and $P_F(W)$, $P_R(-W)$ are the work distributions along the forward (F, unfolding) and the reverse (R, refolding) processes, respectively and $\beta = 1/k_B T$.

In consequence, this method allows us to characterize the energy spectrum of the mutant ensemble (see figure 1-C). In consequence, we can say that it is possible to discriminate between the elements of an ensemble using the free energy of formation at zero force.

Besides, we have find out that the global work distributions of the mutational ensemble satisfy the Crooks Fluctuation Relation with an effective temperature higher than the actual temperature (see figure 1-D). In this work we have developed a theoretical model that, combined with the previous result, make possible to quantify and characterize the degree of heterogeneity of a mutant population of nucleic acids.

This work is the previous step that makes clear the fact that we can study evolution at a molecular scale using single-molecule techniques.

Since 1859, when Charles Darwin founded the grounds of evolutionary biology in his work “The Origin of Species”⁶, the study of evolution has aroused a great interest within all scientific disciplines. Darwin explained for the first time how species evolve in time through mutations and selective amplifications of the fittest. In other words, the main features of evolution are variation and selection.

On the other hand, we know that evolution does not only takes place in macroscopic organisms. In fact, evolution can be regarded as a process where environmental information is encoded into the genetic code of organisms⁷. Therefore, variability (i.e. heterogeneity) and selection are also present at molecular scale.

Thus, combining our experimental and theoretical framework with directed evolution methods we can make feasible to study molecular evolution.

Stochastic facilitation in the brain?

Lawrence M. Ward¹ and Priscilla E. Greenwood²

¹*University of British Columbia, Department of Psychology and Brain Research Centre, Vancouver, Canada
e-mail address: lward@psych.ubc.ca*

²*University of British Columbia, Department of Mathematics, Vancouver, Canada
e-mail address: pgreenw@math.ubc.ca*

I. INTRODUCTION

It is well-known that various forms of stochastic resonance occur in neural tissue, both in vitro and in living brains¹. An unsolved macro-problem is to what extent noise facilitates, or is necessary, for the functioning of various computational tasks accomplished by the brain in giving rise to perception, cognition, and behaviour¹. This presentation describes the context for three important problems within this arena: To what extent may the oscillatory behavior of individual neurons, or linked populations of neurons, best be characterized as noise-driven quasicycles or as noisy limit cycles? What role(s) does neural noise play in the synchronization of, and information transmission between, neural populations located far from one another in the brain? To what extent do noise-driven quasipatterns arise in the brain and affect its overall functioning?

II. NOISY LIMIT CYCLES OR NOISE-DRIVEN QUASICYCLES?

An influential model of the interactions between populations of excitatory and inhibitory neurons in brains (Fig. 1) is

$$\tau_E dV_E(t) = \left[-V_E(t) + g \left[a_E \left(S_{EE} V_E(t) - S_{EI} V_I(t) - \theta_E + P_E(t) \right) \right] \right] dt + \sigma_E dW_E(t), \quad (1)$$

$$\tau_I dV_I(t) = \left[-V_I(t) + g \left[a_I \left(-S_{II} V_I(t) + S_{IE} V_E(t) - \theta_I \right) \right] \right] dt + \sigma_I dW_I(t), \quad (2)$$

where $V_E(t), V_I(t)$ are voltages of excitatory and inhibitory neuron populations, respectively, $S_{EE}, S_{II}, S_{EI}, S_{IE}$ are synaptic efficacies, τ_E, τ_I are time constants, g is a threshold function, $a_E, a_I, \theta_E, \theta_I$ are constants, $P_E(t)$ is input current, and $W_E(t), W_I(t)$ are standard Brownian motions. This model is similar to some models of individual neurons, e.g., the Morris-Lecar neuron, where a pair of differential equations models fast and slow processes within the neuron². When $g(x) = (1 + e^{-x})^{-1}$ and $\sigma = 0$, this model yields

deterministic limit cycles with a characteristic frequency, i.e., neural oscillations³. When $\sigma > 0$ the limit cycle is noisy⁴, and for very large σ the noise obscures the limit cycle and there is no oscillation apparent. If we take $g = 1, a_E = a_I = 1, \theta_E = \theta_I = 0$, and $P(t) = 0$, then the system exhibits a damped oscillation that goes to a fixed point with a rate depending on the synaptic efficacies and the time constants. If we take $\sigma > 0$, however, then the system exhibits quasicycles, that is, the noise drives the system away from the fixed point and we see what appear to be noisy oscillations about that point at a mean frequency determined by the various synaptic efficacies and time constants⁵. Thus, in the limit cycle version of the model, noise is a nuisance that obscures the inherent oscillations that may, or may not, play a significant role in information processing in the brain. In the quasicycle version of the model, however, noise is an essential driving force without which neurons or neuron populations would not exhibit oscillations, or any other interesting behaviour, at all. This is a quinessential example of what McDonnell and Ward¹ called ‘stochastic facilitation.’ Although much theoretical work has been done on the limit cycle model, and some is beginning on the quasicycle version (e.g.,⁴⁻⁶), it is unknown which model best captures the characteristics of oscillatory neural activity in the brain, or indeed whether both models capture neural oscillations at particular scales. There are some reasons to believe that quasicycles dominate at intermediate scales in the brain⁵ but much more information is needed. There exist some methods that may differentiate between noisy limit cycles and quasicycles⁷ but these have yet to be applied to a wide range of neural data at many scales.

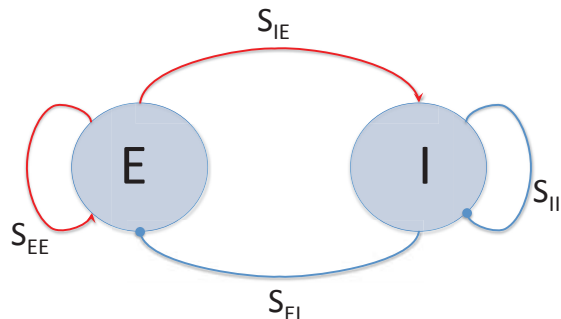


FIG. 1. Typical arrangement of an excitatory (E) and inhibitory (I) neuron pair. $S_{EE}, S_{II}, S_{EI}, S_{IE}$ refer to the synaptic efficacies of the connections; see equations (1), (2).

III. NOISE IN SYNCHRONIZATION AND INFORMATION TRANSMISSION?

Noise is known to facilitate neural synchronization, both through studies of models⁸ and through experiment⁹. Interestingly, even when deterministic versions of the Wilson-Cowan equations are studied, noise is added to the simulation process in order to ‘accelerate’ the process¹⁰. Importantly, both limit cycle¹⁰ and quasicycle¹¹ models of neural interactions exhibit Kuramoto-type synchronization, indicating that for local neural populations at least, noise could be deeply involved in neural synchronization, and thus could play an important role in information transmission in the brain. This is because oscillatory synchronization of neural populations has been seen as an important mechanism for improving information transmission between those populations¹².

There is considerable controversy about the role of neural oscillations in the brain, however. And there have been no direct experiments to our knowledge on the effect of variations in neural noise levels on any information-transmission related neural computational tasks. Moreover, if quasicycles dominate at the scale of interregional information transmission, then there is likely an optimal noise level involved, both for the maintenance of the quasicycles themselves and for the synchronization between sets of quasicycles. It is unknown whether such a noise level would be the same for both functions, or whether different noise sources and levels (synaptic noise for synchronization and ion channel noise for quasicycles?) would be required.

Finally, it is possible that information can be transmitted between brain regions through a multiplexing-demultiplexing process that depends on an oscillatory modulation of noisy firing-rate population codes¹³. It is unknown whether such a scheme requires stochasticity (noise) or whether it would work better without any noise at all.

IV. NOISE-DRIVEN QUASIPATTERNS?

Stochastic differential equation models of neural systems, like the stochastic equations 1 and 2, describe only fluctuating temporal oscillations. But several large scale models of the brain, when simulated, have indicated that spatial patterns of temporal oscillations can occur, e.g.¹⁴. Recently mathematical methods have been developed to derive temporal and spatial patterns (indexed by frequency ω and by wave number k)¹⁵ from a system of stochastic partial differential equations. Power spectra, as in Fig. 2, indicate the existence of temporal-spatial quasipatterns (Turing patterns) occurring on a lattice. Potentially such a system could be extended to describe the types of noise-driven quasipatterns seen in other models and in the brain itself, providing an account of the generation and consequences of such noise-driven quasipatterns. This is yet to be accomplished.

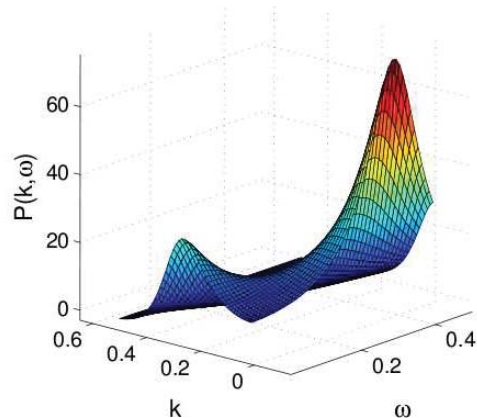


FIG. 2. Power spectrum showing spatial-temporal stochastic patterns. Reprinted with permission from¹⁶.

ACKNOWLEDGMENTS

LMW is supported by a grant from NSERC of Canada.

¹ M.D. McDonnell and L.M. Ward, *Nature Reviews: Neuroscience* **12**, 415 (2011).

² S. Ditlevsen and P.E. Greenwood, *Journal of Mathematical Biology* **67**, 239 (2012).

³ H.R. Wilson and J.D. Cowan, *Biophysical Journal* **12**, 1 (1972).

⁴ E. Wallace, M. Benayoun, W. van Dronglen and J.D. Cowan, *PLOS One* **6**, e14804 (2011).

⁵ P.E. Greenwood, M.D. McDonnell and L.M. Ward, *Neural Computation* **27**, 74 (2015).

⁶ P.C. Bressloff, *Physical Review E* **82**, 051903 (2010).

⁷ M. Pineda-Krch, H.J. Blok, U. Dieckmann and M. Doebeli, *Oikos* **116**, 53 (2007).

⁸ G.B. Ermentrout, R.F. Galan and N.N. Urban, *Trends in Neuroscience* **31**, 428 (2008).

⁹ L.M. Ward, S.E. MacLean and A. Kirschner, *PLOS ONE* **5**, e14371 (2010).

¹⁰ A. Daffertshofer and B.C.M. van Wijk, *Frontiers in Neuroinformatics* **5**, 6-1 (2011).

¹¹ P.E. Greenwood, M.D. McDonnell and L.M. Ward, *Journal of Mathematical Neuroscience* ??, ?? (2015).

¹² G. Deco, A. Buehlmann, T. Masquelier and E. Hugues, *Frontiers in Human Neuroscience* **5**, 4-1 (2011).

¹³ T. Akam and D.M. Kullmann, *Nature Reviews: Neuroscience* **15**, 111 (2014).

¹⁴ P.G. Nunez, *Behavioral and Brain Sciences* **23**, 371 (2000).

¹⁵ A.J. McKane, T. Biancalini and T. Rogers, *Bulletin of Mathematical Biology* **76**, 895 (2014).

¹⁶ T. Butler and N. Goldenfeld, *Physical Review E* **84**, 011112 (2011).

Seeking for a fingerprint: analysis of point processes in actigraphy recording

Ewa Gudowska-Nowak¹

¹*M. Kac Complex Systems Research Center and Malopolska Center of Biotechnology, Jagiellonian University in Kraków, Poland
e-mail address: gudowska@th.if.uj.edu.pl*

I. ABSTRACT

Despite numerous studies indicating anomalous temporal statistics and scaling in spontaneous human activity and interhuman communication, there is much on-going discussion on the origin and universality of observed statistical laws. Behavioral processes are frequently conveniently characterized in terms of stimulus-response approach^{1,2}, by adapting a systematically repeated, the same external sensory protocol which allows to estimate the statistics of subject's responses. In a more general attitude, in which brains are conceived as information processing output-input systems^{3,4}, the observed self-similar temporal patterns of non-stimulated spontaneous neuronal activity can be determined by analyzing spatio-temporal statistics of location and timing of neural signals. Similar to scale-free fluctuations detected in psychophysical time series, also dynamics of collective neuronal activity at various levels of nervous systems exhibit power-law scalings. Remarkable scale-free fluctuations and long-range correlations have been detected on long time scales (minutes and hours) in data recorded with magneto and electroencephalography and have been attributed to the underlying dynamic architecture of spontaneous brain activity discovered with functional MRI (fMRI) and defined by correlated slow fluctuations in blood oxygenation level-dependent signals.

On the other hand, negative deflections in local field potentials recorded at much shorter time scales (milliseconds) have been shown to form spatiotemporal cascades (neuronal avalanches) of activity, whose size (amplitude) and lifetime distributions are again well described by power laws. These power-law scaling behaviors and fractal properties of neuronal long-range temporal correlations and avalanches strongly suggest that the brain operates near a critical, self-organized state³ with neuronal interactions shaping both, temporal correlation spectra and distribution of signal intensities. It seems thus plausible to further investigate timing, location and amplitudes of such cascades to gain information about underlying brain dynamics and to identify characteristics of

stochastic spatial point processes which can serve as reliable models of the ruling dynamics.

Some neurological and psychopathic diseases such as Parkinson disease, vascular dementia, Alzheimer disease, schizophrenia, chronic pain and even sleep disorders and depression are related to abnormal activity symptoms. So far there are many, non-unique evaluative measures used in clinical practice to determine severity of these disorders or the effect of applied drugs. The challenge thus remain to what extent correlations during resting state (spontaneous) activity are altered in disease states and whether a set of characteristic parameters can be classified unambiguously to describe statistics of healthy versus unhealthy mind states and spatiotemporal organization of such disrupted brain dynamics.

Motor activity of humans displays complex temporal fluctuations^{5,6} which can be characterized by scale-invariant statistics, thus documenting that structure and fluctuations of such kinetics remain similar over a broad range of time scales. Former studies on humans regularly deprived from sleep or suffering from sleep disorders predicted change in the invariant scale parameters with respect to those representative for healthy subjects. In these studies we investigate the signal patterns from actigraphy recordings⁵ by means of characteristic measures of fractional point processes. We analyze spontaneous locomotor activity of healthy individuals recorded during a week of regular sleep and a week of chronic partial sleep deprivation. Behavioral symptoms of sleep lack can be evaluated by analyzing statistics of duration times during active and resting states, and alteration of behavioral organization can be assessed by analysis of power laws detected in the event count distribution, distribution of waiting times between consecutive movements and detrended fluctuation analysis (DFA) of recorded time series. We claim that among different measures characterizing complexity of the actigraphy recordings and their variations implied by chronic sleep distress, the exponents characterizing slopes of survival functions in resting states are most effective in determining biomarkers distinguishing between healthy and sleep-deprived groups.

¹ D.R. Bickel, *Estimating the intermittency of point processes with applications to human activity and viral DNA* Physica A **265** 634 (1999).

² A. Proekt, J.R. Banavar, A. Maritan, D. W. Pfaff *Scale invariance in the dynamics of spontaneous behavior* Proc. Natl. Acad. Sci. USA **109** 10564 (2012).

³ E. Tagliazucchi, P. Balenzuela, D. Fraiman, D.R. Chialvo *Criticality in large-scale brain fMRI dynamics unveiled by*

a novel point process analysis Frontiers in Physiology **3** 15 (2012).

⁴ J.M. Palva, A. Zhigalov, J. Hirvonen, O. Korhonen, K. Linkenkaer-Hansen, S. Palva *Neuronal long-range temporal correlations and avalanche dynamics are correlated with behavioral scaling laws* Proc. Natl. Acad. Sci. USA **110t** 3585 (2013).

⁵ J.K. Ochab, J. Tyburczyk, E. Beldzik, D. R. Chialvo, A.

Domagalik, M. Fąfrowicz, E. Gudowska-Nowak, T. Marek, M.A. Nowak, H. Ogińska, J. Szwed *Scale-free fluctuations in behavioral performance: Delineating changes in spontaneous behavior of humans with induced sleep deficiency*

PLoS One **9** e107542 (2014).

⁶ P. M. Holloway, M. Angelova, S. Lombardo, A.S.C. Gibson, D. Lee, and J. Ellis *Complexity analysis of sleep and alterations with insomnia based on non-invasive techniques* J. R. Soc. Interface **93** 20131112 (2014).

Noise in graphene and carbon nanotube devices

B. Plaçais,^{1,*} C. Voisin,¹ G. Fève,¹ and J.M. Berroir¹

¹Laboratoire Pierre Aigrain, Ecole Normale Supérieure-PSL Research University, CNRS, Université Pierre et Marie Curie-Sorbonne Universités, Université Paris Diderot-Sorbonne Paris Cité, 24 rue Lhomond, 75231 Paris Cedex 05, France

I. INTRODUCTION

Carbon nano-materials, specifically carbon nanotubes and graphene, are genuine 1D and 2D systems benefitting from a wide tunability of carrier density by field effect doping. As such they constitute a unique platform for investigating electronic noise in conductors. In increasing sample current I , the current noise spectral density S_I , in reduced units given by the Fano factor $F = S_I/2eI$, is a faithful tracer of the transition from quantum to classic behavior. As depicted in Fig.1, the low bias regime is the realm of quantum scattering where shot noise is ruled by the nature of impurity scatterers; at intermediate bias electron-electron interactions set-in and show up by a hot electron noise characterized by a universal Fano-factor $F = \sqrt{3}/4$; at higher biases electron-phonon relaxation comes into play to cool the hot carriers with a scenario that is very generic in graphene.

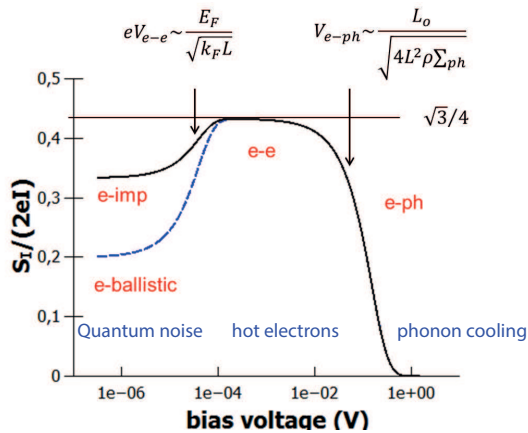


FIG. 1. Crossover from quantum to classical world illustrated by electronic noise.

Due to weak electron phonon coupling, the electronic temperature strongly decouples from phonon temperature in biased graphene (see fig.2). The first mechanism to come are the acoustic (AC) phonons coupling starting by cold-phonons in the Bloch-Grüneisen regime¹, the supercollision hot-phonon regime² and finally the ultimate non degenerate electron regime³. In the biasing process the electronic temperature strongly decouples from lattice temperature, reaching several hundreds of Kelvins. The good understanding of AC-phonon cooling and the recent availability of high mobility graphene, allow to investigate the more exotic case of optical (OP) phonon cooling which sets in above 1000 Kelvin in carbon nano-materials^{4,5}; few issues are yet unsolved like the role of

substrate surface phonons, a very hot electromagnetic environment for electrons in nano-carbon materials.

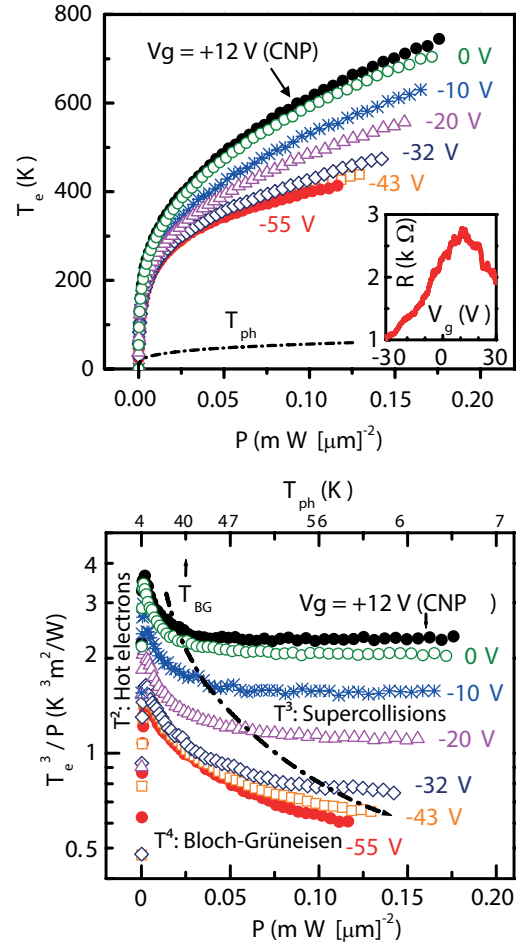


FIG. 2. a) Electronic temperature in graphene measured by high-frequency noise thermometry; b) three regimes of hot electrons in graphene (adapted from Ref.²)

Hot electron thermometry requires high-resolution high-frequency noise measurements. These are needed to overcome the spurious contribution of $1/f$ -noise that scales quadratically with current and invades gradually the thermal white noise spectrum (see Fig.3) which has a sublinear dependence on current (see Fig.3). The $1/f$ -noise itself is a long-standing unsolved problems; it belongs to the family of flicker noises which may have different origins. Thanks to its wide tunability, graphene is a unique and versatile material to revisit the basics or $1/f$ resistance noise and eventually give new clues to the supposed universality of the Hooge constant $\alpha_H \sim 10^{-3}$.

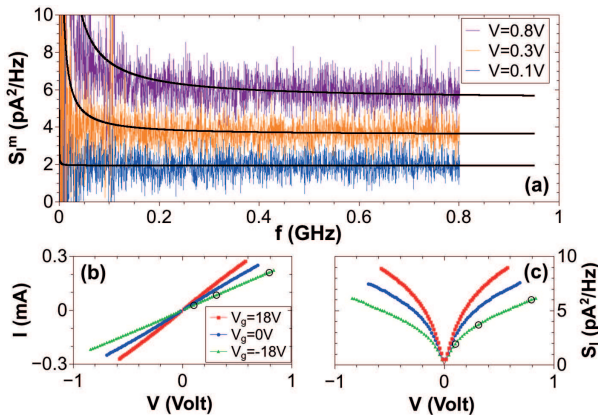


FIG. 3. Principles of hot-carrier noise thermometry (adapted from Ref.¹)

A pillar of noise thermometry is the Johnson noise formula $S_I = 4G_n k_B T_e$ relating the current noise spectrum in a resistor to the electronic temperature via a so-called noise conductance G_n . It is common practice to identify

G_n with the 2-terminal drain-source conductance G_{ds} . However, as pointed out by A. Van der Ziel back in 1962, the noise conductance may eventually deviate from the channel conductance in high-gain field effect transistors (FETs). This question was recently revisited using single carbon nanotube FETs as a ultimate single mode nano-transistor^{7,8}. We could calculate the quantum correction in G_n which is proportional to the transconductance G_m , which is enhanced in CNT-FETs as measured by GHz noise thermometry in Ref.⁸.

In conclusion graphene and carbon nanotubes have proved to be a valuable platform to put to test challenging issues in noise physics. This will probably continue to tackle more Unsolved Problems on Noise in the future.

ACKNOWLEDGMENTS

the research leading to these results have received partial funding from the European union Seventh Framework programme under grant N 604391 Graphene Flagship.

* bernard.placais@lpa.ens.fr

- ¹ Betz, A. C., Vialla, F., Brunel, D., Voisin, C., Picher, M., Cavanna, A., Madouri, A. Fève, G., Berroir, J.-M., Plaçais, B., Pallecchi, E. *Phys. Rev. Lett.* **109**, 056805 (2012). *Hot electron cooling by acoustic phonons in graphene*
- ² A.C. Betz, S.H. Jhang, E. Pallecchi, R. Ferreira, G. Fève, J.-M. Berroir, B. Plaçais, *Nature Physics* **9**, 109 (2013). *Supercollision cooling in undoped graphene*
- ³ A. Laitinen, M. Oksanen, A. Fay, D. Cox, M. Tomi, P. Virtanen, and P. Hakonen, *Nano Lett.* **14**, 3009 (2014). *supercollisions in suspended monolayer graphene*
- ⁴ A. Laitinen, M. Kumar, M. Oksanen, B. Plaçais, P. Virtanen, and P. Hakonen, *Phys. Rev. B* **91**, 121414(R) (2015) *Coupling between electrons and optical phonons in suspended bilayer graphene*
- ⁵ D. Brunel, S. Berthou, R. Parret, F. Vialla, P. Morfin, Q. Wilmart, G. Fève, J.-M. Berroir, P. Roussignol, C. Voisin,

- B. Plaçais, *J. Phys. : Condens. Matter* **27**, 164208 (2015). *Onset of optical phonon cooling in multilayer graphene revealed by RF noise and black-body radiation thermometries*
- ⁶ A. van der Ziel, *Proc. IRE* **50**, 1808 (1962) *Thermal noise in field effect transistors*
- ⁷ J. Chaste, L. Lechner, P. Morfin, G. Fève, T. Kontos, J.-M. Berroir, D. C. Glatli, H. Happy, P. Hakonen, B. Plaçais, *Nano Lett.* **8**, 525 (2008). *Single carbon nanotube transistor at GHz frequency*
- ⁸ J. Chaste, E. Pallecchi, P. Morfin, G. Fève, T. Kontos, J.-M. Berroir, P. Hakonen, B. Plaçais, *Appl. Phys. Lett.* **96**, 192103 (2010). *Thermal shot noise in top-gated single carbon nanotube field effect transistors*

Is the peculiar behavior of $1/f$ noise in graphene the result of the interplay between band-structure and inhomogeneities?

B. Pellegrini, P. Marconcini, M. Macucci, G. Fiori, G. Basso
Dipartimento di Ingegneria dell'Informazione,
via G. Caruso 16, 56122 Pisa, Italy
e-mail address: macucci@mercurio.iet.unipi.it

I. INTRODUCTION

Flicker noise in graphene based devices has attracted significant interest¹ because of the very peculiar features it exhibits, in comparison with what is observed in more traditional materials. In particular, the behavior of the noise power spectral density (PSD) as a function of carrier concentration has turned out to be rather puzzling, especially in bilayer graphene, and several authors²⁻⁶ have made an effort to find an explanation for it. For example, it has been observed that the PSD of flicker noise in bilayer graphene, and sometimes also in monolayer graphene, has a minimum around the Dirac point, where charge concentration also reaches a minimum, while in conductors obeying Hooge's empirical formula⁷ the opposite is expected. Attempts have been made to justify the particular dependence of the flicker PSD on carrier concentration on the basis of the known presence of electron and hole puddles in the graphene sheet², of a supposed variation³ of the Hooge parameter with gate voltage, which would prevail on the effect of the carrier number decrease, of effects linked to mobility fluctuations⁴, of a charge-noise model⁵, or of the bandstructure of single layer and bilayer graphene⁶. Experiments have also shown⁸ that the noise factor in monolayer graphene nanoribbons is independent of the resistance to length ratio, while a clear dependence on such a quantity is observed for bilayer graphene nanoribbons. However, a comprehensive model, capable of explaining all observed features, is still lacking. In the present contribution, we shall try to provide a framework within which a more general understanding of flicker noise in graphene sheets and nanoribbons can be derived.

II. CURRENT FLUCTUATIONS

Our aim is to find an expression for the PSD of flicker current noise in graphene-based devices. We assume that flicker noise is the result of charges moving into and out of traps that have an electrostatic coupling with the channel where the current flows. We also assume that such fluctuations occur on a time scale much longer than that of carrier scattering events (such as phonon scattering). Thus the contribution of each elementary area of the device is due to the fluctuation of the local value of the drift current; this can be related to the current at the terminals via the Ramo-Shockley-Pellegrini⁹⁻¹¹ theorem. In particular, if, for the sake of simplicity, we do not enter into the specific details of the device geometry and as-

sume the electric field E to be somewhat constant across the device, we can write the current at the terminals, as long as we are interested just in the low-frequency fluctuations, in the form

$$I = \frac{1}{L} \int_A \mu n E dx dy, \quad (1)$$

where μ is the mobility, $A = WL$ the area of the device, L being its length and W its width. Let us now move on to the evaluation of the fluctuations of the current. We are interested only in the fluctuations due to charges moving into and out of traps, therefore we can consider just the action of such traps. In principle, trapping and detrapping events have an action not only on the number of carriers available for conduction, but also on the mobility, and on the local electric field. These two latter contributions are in general negligible with respect to the former¹², so that the relative fluctuation for each trap can be written

$$\frac{\Delta i}{I} = \frac{1}{A} \int_A \frac{\Delta n_c}{n_c} dx dy, \quad (2)$$

where $n_c = n_n + n_p$, i.e. the total concentration of carriers, while we also define $n = n_n - n_p$, which, multiplied by the electron charge, gives the total charge density.

Assuming for each trap a random telegraph signal χ for the occupancy (with a value of 1 when the trap is occupied and 0 when it is empty), the relative variation of the current due to a charge moving into the trap can be written¹²

$$\frac{\Delta i}{I} = -\frac{1}{A} \left(\frac{a_c}{an_c} \right) \Delta \chi, \quad (3)$$

where $a_c = \partial n_c / \partial U$ (with U being the electrostatic potential energy), $a = \partial n / \partial U$. The superposition of the Lorentzian spectra associated with the traps leads to a PSD¹³

$$\frac{S}{I^2} = \frac{n_t B}{A} \left(\frac{a_c}{an_c} \right)^2 \frac{1}{f\gamma}, \quad (4)$$

where n_t is the trap density, B is a proper coefficient, and γ is usually 1 (flicker noise). We must consider that the potential is not at all uniform across a graphene sheet, but, rather, it fluctuates, due to the presence of impurities and of defects. Thus the PSD of Eq. (4) has to be weighed with the distribution function $P(U)$ of the potential energy:

$$\frac{\langle S \rangle}{I^2} = \frac{\langle n_t \rangle}{A f \gamma} \int B \left(\frac{a_c}{an_c} \right)^2 P(U) dU, \quad (5)$$

where we assume a Gaussian form for $P(U)$, with a standard deviation σ^* .

III. RESULTS

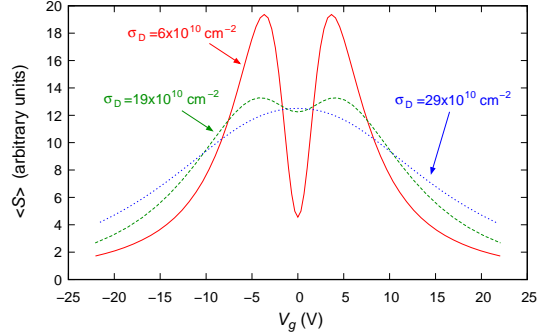


FIG. 1. Behavior of the PSD in monolayer graphene as a function of the applied gate voltage V_g , for three values of the standard deviation σ_D .

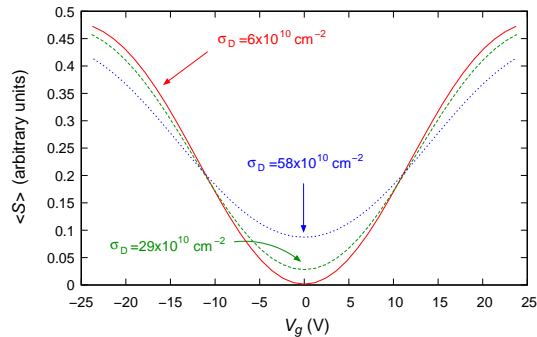


FIG. 2. Behavior of the PSD in bilayer graphene as a function of V_g , for different values of σ_D .

The result for single-layer graphene is shown in Fig. 1 for 3 values of σ_D , where $\sigma_D = \sigma^* \hat{a}$, with $\hat{a} \propto n_0$ the value of a for $U = 0$. The quantity n_0 is the reference density, given by $n_0 = (1/\pi)[k_B T / (\hbar v)]^2 \approx 7 \times 10^{10} \text{ cm}^{-2}$, with

v being the in-plane velocity. For the lowest value of the standard deviation we notice a minimum of the noise around the Dirac point as a result of a suppression of current fluctuations resulting from the presence of an equal concentration of carriers with charges of opposite sign. We see that, for increasing σ_D , the behavior of the noise power spectral density as a function of the applied gate voltage moves from an M shape to a Λ shape, as a result of the increasing smoothing effect of $P(U)$. In Fig. 2 we report instead the behavior of the PSD as a function of the gate voltage for bilayer graphene, for a choice of 3 values of the standard deviation. We notice that now the shape is always of the V type, as a result of the much smoother variation of the energy dispersion relationship around the Dirac point with respect to what happens for

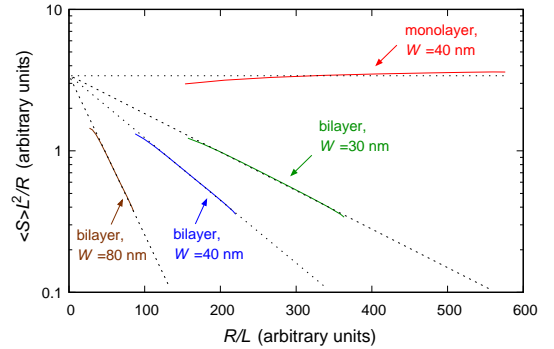


FIG. 3. Noise factor $\psi = \langle S \rangle L^2 / R$ for monolayer (topmost curve) and for bilayer (lower curves) graphene nanoribbons, as a function of R/L .

monolayer graphene. The proposed approach can be applied also to nanoribbons, which are characterized by a peculiar bandstructure. If we consider armchair nanoribbons and compute the quantity $\psi = \langle S \rangle L^2 / R$, where R is the nanoribbon resistance, we get the results reported in Fig. 3, as a function of R/L . We notice that for monolayer graphene nanoribbons there is no significant variation (at least in the considered range of resistances) of the noise factor, while for bilayer graphene, in a semilogarithmic scale, there is a clear linear dependence on the R/L ratio, with a different slope for different nanoribbon widths. This is in agreement with the experimental results by Lin and Avouris⁸.

¹ A. A. Balandin, Nature Nanotechnology **8**, 549 (2013).

² G. Xu, C. M. Torres Jr., Y. Zhang, F. Liu, E. B. Song, M. Wang, Y. Zhou, C. Zeng, and K. L. Wang, Nano Letters **10**, 3312 (2010).

³ Y. Zhang, E. E. Mendez, and X. Du, ACS Nano **5**, 8124 (2011).

⁴ S. Rumyantsev, G. Liu, W. Stillman, M. Shur, and A. A. Balandin, J. Phys.: Condens. Matt. **22**, 395302 (2010).

⁵ I. Heller, S. Chatoor, J. Maennik, M. A. G. Zevenbergen, J. B. Oostinga, A. F. Morpurgo, C. Dekker, and S. G. Lemay,

Nano Letters **10**, 1563 (2010).

⁶ A. N. Pal, S. Ghatk, V. Kochat, E. S. Sneha, A. Sampathkumar, A. Raghavan, and A. Ghosh, ACS Nano **5**, 2075 (2011).

⁷ F. N. Hooge, Physics Letters A **29**, 139 (1969).

⁸ Y. Lin and P. Avouris, Nano Letters **8**, 2119 (2008).

⁹ S. Ramo, Proceedings of the IRE **27**, 584 (1939).

¹⁰ W. Shockley, J. Appl. Phys. **9**, 635 (1938).

¹¹ B. Pellegrini, Phys. Rev. B **34**, 5921 (1986).

¹² B. Pellegrini, Eur. Phys. J. B **86**, 373 (2013).

Monte Carlo study of velocity fluctuations during transient regimes in graphene

José M. Iglesias,^{1,2} R. Rengel,¹ E. Pascual,¹ and María J. Martín¹

¹*Universidad de Salamanca, Applied Physics Dept. Plaza de la Merced, S/N, 37008, Salamanca. SPAIN*

²*e-mail address: josem88@usal.es*

I. INTRODUCTION

Graphene is a two-dimensional carbon allotrope consisting of a single-atom-thick sheet of carbon atoms arranged in a hexagonal lattice. Its remarkable properties have made it become, in the recent years, one of the most fashionable materials among the industry and researchers due to its promising aptitudes for a lot of electronics and optoelectronics applications¹⁻³. The above described crystalline structure gives rise to an unusual gapless conic-shaped dispersion relation in the vicinities of the six K points (i.e. the six points in the Brillouin zone where $E_F = 0$) which is of tremendous interest for being the origin of the massless behaviour that electrons exhibit in this material⁴. The most direct implication of this feature is that electrons in graphene travel with a constant velocity called the Fermi velocity, $v_F \approx 10^6 \text{ cm s}^{-1}$, and therefore carrier velocity along a certain direction depends only on its wavevector orientation: $v_x = v_F \frac{k_x}{|k|}$. As a result, velocity fluctuations in graphene are limited⁵ to a maximum value of $2 v_F$ and velocity relaxation through scattering mechanisms depends only on the momentum orientation, and it is strongly affected by the anisotropy of the scattering mechanisms.

For most of the practical uses, graphene is not used as separated sheets, but attached to a substrate layer. The presence of a substrate affects the graphene performance⁶ by degrading the carrier mobility velocity and diffusion coefficient at low fields but increasing the saturation velocity. In this work, we will assess the influence of h-BN and SiO₂ substrates in the transient regime velocity fluctuations compared to the ideal monolayer suspended graphene.

As a result of the above mentioned interest in this material, several works regarding noise in graphene devices have been carried out⁷⁻¹⁰. With the purpose of offering a microscopic study of the inherent sources of noise in the material, we present a study of instantaneous velocity fluctuations in graphene by means of computational simulation performed with the Ensemble Monte Carlo Method. Our simulator takes into account the massless Dirac Fermions behaviour related to the linear dispersion relation. Pauli exclusion principle is implemented through a rejection technique after each scattering event. The scattering sources taken into account in our simulations are optic, intravalley and intervalley acoustic phonons, and surface polar phonons in case of graphene on a substrate^{11,12}. In addition, we include in this work the effect of elastic

scattering with charged impurities, considering a density $n_{imp} = 5 \times 10^{11} \text{ cm}^{-2}$ in both suspended graphene and graphene on a substrate. Given the importance of all these interactions in the velocity fluctuations, along with the strong dependence of velocity with the wavevector orientation, the anisotropy of all these scattering mechanisms is treated rigorously.

In previous studies we have used Monte Carlo simulations to examine velocity fluctuations in graphene¹³ and diffusion coefficients were calculated from the correlation function of velocity fluctuations^{5,11}. However, when devices work under switching conditions, the carriers are not usually in a steady state, but in a transient situation of change towards the final stationary state associated with the applied electric field. In this work we offer an in-deph study in the transient regime of the velocity fluctuations for suspended graphene and graphene on a substrate. For this, we set transient regimes for low to high electric fields and vice versa. In the case of graphene, due to its high mobility, we chose the low field value so that it is away from the values that produce the saturation velocity. The quantities to be analysed are the transient correlation function and spectral density of velocity fluctuations, which are calculated from the Monte Carlo simulator as follows. The instantaneous velocity fluctuation for a single electron, is $\delta v(t) = v(t) - \langle v(t) \rangle$, where the brackets indicate the ensemble average. The autocorrelation function keeps its traditional definition⁵. On its behalf, since the study of velocity fluctuations is performed over finite times during the transient, the spectral density cannot be obtained as the Fourier transform of the autocorrelation function.¹⁴ Instead, it is calculated at different times with the expression $S_{\delta v}(f, \tau) = \frac{1}{\tau} \left\langle \left| \int_0^\tau \delta v(t) e^{j\omega t} dt \right|^2 \right\rangle$.

II. RESULTS

In Fig. 1 we show the averaged ensemble velocity during the transient from low to high field and vice versa. For the low to high field leap (Fig. 1-a) stationary velocity is reached in a sub-ps time scale. The velocity overshoot is less pronounced in the graphene on a substrate than in suspended samples. It is to highlight the difference in the transient times, that are much longer in high to low field transitions. For the high to low field transient (Fig. 1-b) the trend of the saturation velocity is different if we compare the suspended graphene to graphene lying on a substrate. In the suspended case, the transient velocity experiments an intense drop until

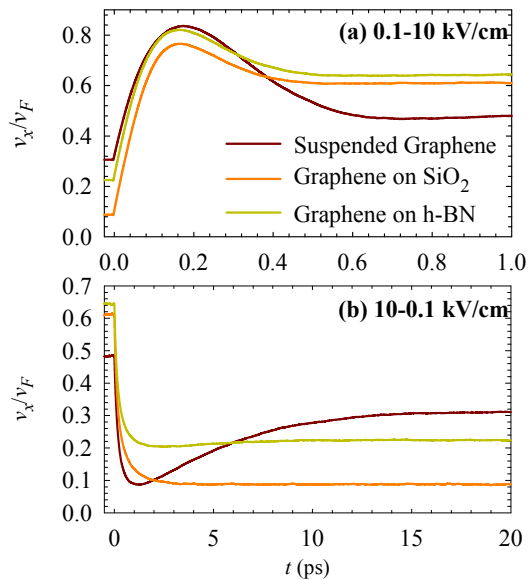


FIG. 1. Time evolution of the averaged ensemble velocity for suspended and supported graphene. The transients are (a) 0.1 to 10 kV cm^{-1} and (b) 10 to 0.1 kV cm^{-1}

reaching a minimum at $t \approx 1 \text{ ps}$ and afterwards there is a progressive increase until reaching the stationary state at around 15 ps. For graphene on a substrate, the steady state velocity for 0.1 kV cm^{-1} is reached in less than 5 ps, being the local minimum totally absent when the substrate is SiO_2 and almost inappreciable if it is h-BN.

Fig. 2 depicts the 0.1 to 10 kV cm^{-1} transient spectral density for various instants for suspended graphene (a) and graphene on SiO_2 (b). The qualitative evolution is quite similar. In the two cases the spectral density starts with similar values. Then, progressively it evolves towards the 10 kV cm^{-1} stationary spectral density, increasing in the frequencies ranging from 500 to 3000 GHz, where there is a maximum, and decreasing less prominently in the rest of the frequency range considered.. In suspended graphene the maximum is

already perceptible at 0.25 ps and shifts towards lower frequencies for the successive intervals. With regard to the SiO_2 sample, the maximum persists around the same frequency for all the intervals considered.

In the conference a deeper study will be offered from the analysis of the microscopic information extracted from the Monte Carlo simulations together with the transient correlation functions and the spectral densities.

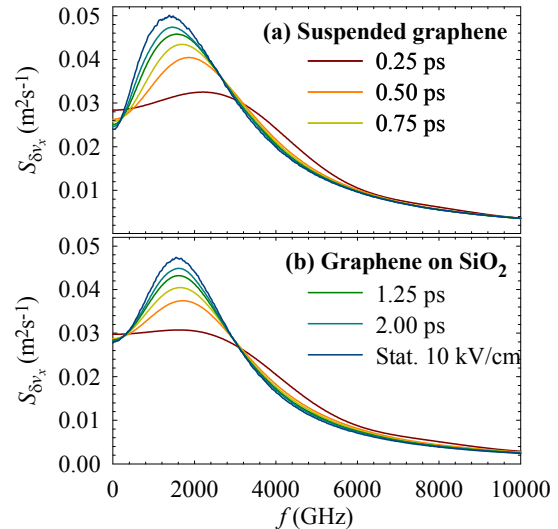


FIG. 2. 0.1 to 10 kV cm^{-1} transient spectral densities for various instants in (a) suspended graphene, and (b) graphene on SiO_2

ACKNOWLEDGMENTS

This work has been supported by the research project TEC2013-42622-R from the Ministerio de Economía y Competitividad

¹ P. Avouris, *Nano Lett.* **10**, 4285 (2010)
² J. Zheng, L. Wang, R. Quhe, Q. Liu, H. Li, D. Yu, W.-N. Mei, J. Shi, Z. Gao and J. Lu, *Sci. Rep.* **3**, 1314 (2013)
³ C.-H. Liu, Y.-C. Chang, T. B. Norris and Zhaohui Zhong, *Nature Nanotechnology* **9**, 273 (2014)
⁴ A. H. Castro, F. Guinea, N. M. R. Peres, K. S. Novoselov, and A. K. Geim, *Rev. Mod. Phys.* **81**, 109 (2009)
⁵ R. Rengel and M. J. Marín, *J. Appl. Phys.* **114**, 143702 (2013)
⁶ A. Konar, T. Fang, and D. Jena, *Phys. Rev. B* textbf82, 115452 (2010)
⁷ S. Rumyantsev, G. Liu, W. Stillman, M. Shur, and A. A. Balandin, *J. Phys.: Condens. Matter* **22**, 395302 (2010)
⁸ J. S. Moon, D. Curtis, D. Zehnder, S. Kim, D. K. Gaskill, G. Jernigan, R. L. Myers-Ward, C. R. Eddy, P. M. Campbell, K.-M. Lee, and P. Asbeck, *IEEE Electron Device Lett.*

32, 270 (2011)
⁹ A. N. Pal, S. Ghatak, V. Kochat, E. S. Sneha, A. Sampathkumar, S. Raghavan, and A. Ghosh, *ACS Nano* **5**, 2075 (2011)
¹⁰ Y. Zhang, E. E. Mendez, and X. Du, *ACS Nano* **5**, 8124 (2011)
¹¹ R. Rengel, E. Pascual, and M. J. Martín, *Appl. Phys. Lett.* **104**, 233107 (2014)
¹² Vasili Perebeinos and Phaedon Avouris, *Phys. Rev. B* **81**, 195442 (2010)
¹³ M. J. Martin, R. Rengel and C. Couso, 22nd International Conference on Noise and Fluctuations, 1-4 (2013)
¹⁴ T. González, J. E. Velázquez, P. M. Gutiérrez and D. Pardo, *J. Appl. Phys.* **72**, 2322 (1992)

Measurements of RF noise in InGaAs/InAlAs recessed diodes: Signatures of shot-noise suppression

Ó. García-Pérez¹, T. González¹, S. Pérez¹, A. Westlund², J. Grahn², and J. Mateos¹

¹ Dept. de Física Aplicada, Univ. de Salamanca, Salamanca, Spain

e-mail address: ogarcia@usal.es, tomasg@usal.es, susana@usal.es, javierm@usal.es

² Dept. of Microtechnology and Nanoscience, Chalmers Univ. of Tech., Gothenburg, Sweden

e-mail address: andreas.westlund@chalmers.se, jan.grahn@chalmers.se

I. INTRODUCTION

Beyond being an obstacle to any electronic communications system, noise can also be an important source of information on the different mechanisms of electron transport in a given device¹. Studies on electronic noise can provide valuable information to better understand the electron transport mechanisms in semiconductor devices. More concretely, the effect of Pauli principle and/or Coulomb interaction on the carrier statistics in ballistic media, and how it may result in suppressed shot-noise levels with respect to the full Poissonian value ($2qI$), is a field of interest for physicists and electronic engineers²⁻³. However, the experimental evidence of such shot-noise suppression mechanisms is rather difficult to obtain.

II. EXPERIMENTAL RESULTS

In this work the measured noise characteristics of a set of recessed planar InGaAs/InAlAs diodes are presented. For the measurement, a PNA-X N5244A with Option 029 from Agilent Technologies has been used, which allows acquiring the output power density from an electronic device with high levels of accuracy and sensitivity⁴. The data in the range between 20 and 30 GHz (in the plateau beyond $1/f$ noise) was averaged in order to improve the precision of the results. The geometry of the diode is depicted in Fig. (1) and basically consists in an ungated HEMT topology with a recess between the drain and source terminals⁵. The recess leads to the presence of a barrier in the potential profile [see Monte Carlo results in the inset of Fig. (1)], which, by modulating the passage of ballistic carriers, is expected to suppress the associated shot-noise by virtue of Coulomb correlations².

In Fig. (2) we present the results of a first experiment with three

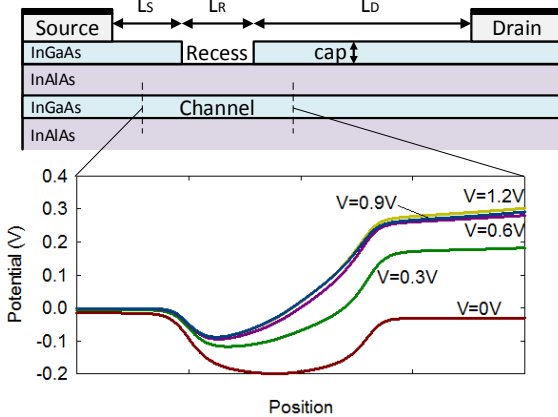


FIG. 1: Sketch of the device and simulated potential profiles in the recess region for several bias voltages.

devices of different recess lengths (L_R), i.e. 200, 500 and 800 nm. The drain/source accesses (L_D and L_S) are 550 nm and 200 nm length in all three cases. For comparison, another device without

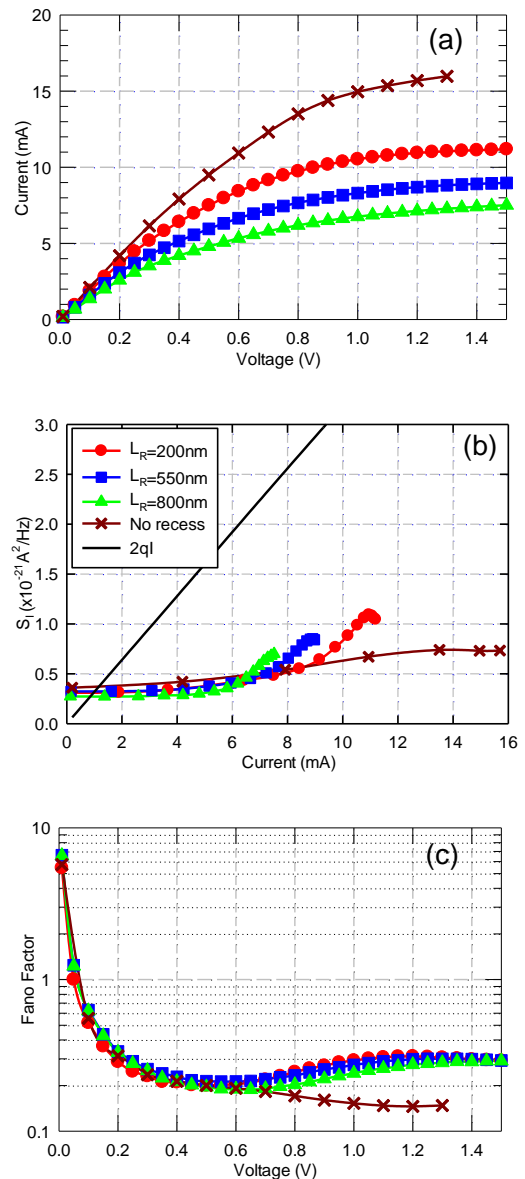


FIG. 2. Measured results of three devices with different recess lengths (L_R): (a) I-V curves, (b) current noise density (S_i) vs. bias current, and (c) Fano factor (F) vs. bias voltage.

recess and 1300 nm total length has also been measured. The I - V curves of all the devices are plotted in Fig. (2a). As expected, longer recess regions make the device more resistive, which in turn provides lower current levels. The current noise density (S_I) and the Fano factor ($F=S_I/2qI$) are shown in Figs. (2b) and (2c), respectively. The current-noise density of the device without recess is nearly constant with bias, which indicates that thermal noise dominates due to the diffusive nature of the transport along the device, leading to a Fano factor continuously decreasing with bias. On the opposite, recessed devices present different response. For low bias, they also show flat current noise density. However, above certain voltage (around 0.6 V, when intervalley mechanisms are activated) the current noise density begins to significantly increase proportionally to current, indicating the presence of shot-noise due to ballistic transport in the recess region, but suppressed with respect to the full shot-noise value. Also, the Fano factor is slightly lower in the device with longer recess due to the presence of a higher barrier in the potential² (counteracting the expected decrease of F due to a lower contribution of the thermal noise of the accesses).

In a second experiment, three devices with different drain access lengths have been characterized. The source (L_S) and recess (L_R) lengths are both 200 nm in all three cases. The I - V curves of the devices are plotted in Fig. (3a). In this case, the three devices present similar characteristics, indicating that the current levels are mainly determined by the recess, which has the same length in this case. The current noise densities are shown in Fig. (3b). Again, noise proportional to current appears, suppressed with respect to the full Poissonian value. Also, it can be observed how for very high bias, the current density decreases in some cases. This effect is more noticeable for longer drain accesses, which in turn present higher resistivity and further attenuate the shot noise generated in the ballistic recess region. As it can be observed in Fig. (3c), F is correspondingly lower in the case of longer drain access, presumably due to the attenuation of the shot noise contribution to the total noise when this region becomes very resistive.

III. CONCLUSIONS

The noise measurements performed in a set of recessed planar InGaAs/InAlAs diodes show evidences of shot noise suppression due to the potential barrier imposed by the recess. An increase of the spectral density at voltages above 0.6 V, in parallel to that of the current, could be understood as a signature of the presence of suppressed shot noise in the recess region where electron transport is quasiballistic and a fluctuating potential barrier is able to regulate the electron flow. The dependence of the total noise and F on the geometrical parameters is consistent with this explanation. However, the thermal noise contribution of the source and drain access regions (together with the one associated to the ohmic contacts) does not allow to precisely extract the value of the noise generated below the recess, and whether it is full or suppressed shot noise.

ACKNOWLEDGEMENTS

This work has been partially supported by the Dirección General de Investigación Científica y Técnica (MINECO) through Project TEC2013-41640-R and by the Junta de Castilla y León through Project SA052U13. O. García wants to thank the European Social Fund (ESF) for financing his postdoctoral contract.

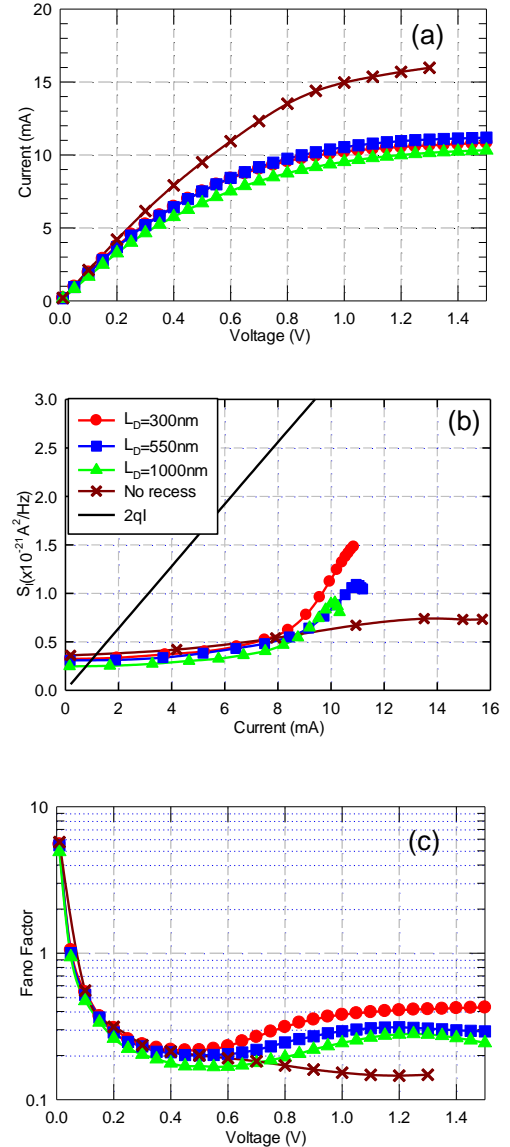


FIG. 3. Measured results of three devices of different drain access lengths (L_D): (a) I - V curves, (b) S_I vs. bias current, and (c) F vs. bias voltage.

¹ R. Landauer, Nature, 392, 658-659 (1998).
² C. Gomila, I. Cantalapiedra, T. González, L. Reggiani, Phys. Rev. B, 66, 075302 (2002).
³ Y. Naveh, A. N. Korotkov, K. K. Likharev, Phys. Rev. B, 60, 2169-2172 (1999).

⁴ Agilent Technologies Inc., *Application Note 1408-20 (5990-5800EN)*, 2013.
⁵ S. Pérez, T. González, D. Pardo, J. Mateos, J. Appl. Phys., 103, 094516 (2008).

1/f noise arising from time-subordinated Langevin equations

Julius Ruseckas and Bronislovas Kaulakys
*Institute of Theoretical Physics and Astronomy,
 Vilnius University, A. Goštauto 12,
 LT-01108 Vilnius, Lithuania
 e-mail address: julius.ruseckas@tfai.vu.lt*

I. INTRODUCTION

Many complex systems exhibit large fluctuations of macroscopic quantities having non-Gaussian power law distributions as well as power law temporal correlations and scaling.¹ The power law distributions, scaling, self-similarity and fractality can be related to the power law behavior of the power spectral density (PSD), which is one of the most important characteristics of a signal. Signals having the PSD at low frequencies f of the form $S(f) \sim 1/f^\beta$ with β close to 1 are commonly referred to as “1/f noise”. Power-law distributions of spectra of signals with $0.5 < \beta < 1.5$, as well as scaling behavior are ubiquitous in physics and in many other fields. For recent reviews see 2–4. Despite the numerous models and theories proposed since its discovery 90 years ago, the subject of 1/f noise remains open for new discoveries. Most models and theories of 1/f noise are not universal due to the usage of assumptions specific to the problem under consideration.

Often 1/f noise is modeled as the superposition of Lorentzian spectra with a wide range distribution of relaxation times.⁵ A class of the models of 1/f noise especially relevant for understanding of complex systems involves the self-organized criticality.⁶ Yet another model of 1/f noise has been proposed by Kaulakys:^{7,8} it has been shown that the origin of 1/f noise in a signal consisting of pulses may be a Brownian motion of the inter-pulse time. The nonlinear stochastic differential equations (SDEs) generating signals with 1/f noise has been obtained starting from this point process model of 1/f noise^{9,10}. Such nonlinear SDEs have been used to describe signals in socio-economical systems^{11,12}.

In this contribution we generalize the mechanism leading to 1/f noise in the signals consisting of a sequence of pulses. Instead of a sequence of pulses we start from an SDE describing a Brownian motion in an external potential. We construct a new equation by interpreting the time in the SDE as an internal parameter and adding an additional equation relating the physical time to the internal time. We show that relation between the internal time and the physical time that depends on the size of the signal can lead to 1/f noise in a wide interval of frequencies.

II. 1/f NOISE AND DIFFUSION IN NON-HOMOGENEOUS MEDIA

Impurities and regular structures in the medium results in a transport of variable speed, the particle may be trapped for some time or accelerated. Non-homogeneous systems are characterized not only by subdiffusion related to traps, but also enhanced diffusion can arise as a result of the disorder.¹³ The dynamics of such a system is described by the continuous time random walk (CTRW) theory. In an equivalent description the dynamics is Markovian and governed by a Langevin equation in an auxiliary, operational time instead of the physical time. This Markovian process is subordinated to the process yielding the physical time.

Since the trap properties should reflect the structure of the medium, a description of the transport should take into account that the waiting time explicitly depends on the position. Here we consider the situation when the small increments of the physical time are deterministic and proportional to the increments of the internal time. The coefficient of proportionality is a function $g(x)$ of a particle position. This function models the position of structures responsible for either trapping or accelerating the particle. Thus, we start from the following set of equations:

$$dx_\tau = F(x_\tau)d\tau + dW_\tau, \quad (1)$$

$$dt_\tau = g(x_\tau)d\tau. \quad (2)$$

Here τ is an internal, operational time and t is the physical time; $F(x)$ is an external force affecting the particle and W_τ is a standard Wiener process.

Writing the Fokker-Planck equation for the two-dimensional density $P(x, t)$ corresponding to (1), (2) and changing the variable t to a variable τ one can reduce the system of equations (1), (2) to a single equation in physical time with a multiplicative noise

$$dx_t = \frac{F(x_t)}{g(x_t)} dt + \frac{1}{\sqrt{g(x_t)}} dW_t. \quad (3)$$

There is a similarity to the signal consisting of pulses, where the internal time is just the pulse number. In order to obtain 1/f noise similarly as in a signal consisting of pulses we choose the function $g(x)$ as a power-law function of x : $g(x) \sim x^{-2\eta}$.

For example, if we start from a simple Brownian motion $dx_\tau = dW_\tau$ restricted to a interval between x_{\min} and x_{\max} and take $g(x) = x^{-2\eta}$ then the resulting equation

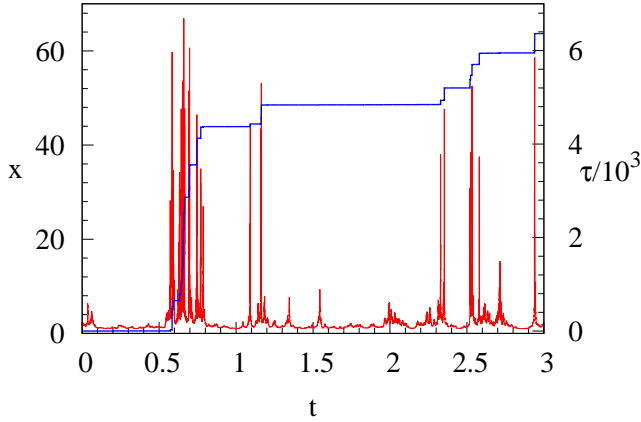


FIG. 1. Signal generated by equation (5) with the parameters $\eta = 5/2$ and $\lambda = 3$ (red line) together with the corresponding internal time (blue line)

in the physical time is $dx_t = x_t^\eta dW_t$. In more general situation the initial equation can have a position-dependent force. If we take the equation describing a Bessel process

$$dx_\tau = \left(\eta - \frac{\lambda}{2} \right) \frac{1}{x_\tau} d\tau + dW_\tau \quad (4)$$

then the resulting equation in the physical time becomes

$$dx_t = \left(\eta - \frac{\lambda}{2} \right) x_t^{2\eta-1} dt + x_t^\eta dW_t \quad (5)$$

This equation is the same as the nonlinear SDE generating signals with $1/f^\beta$ spectrum^{9,10}. As has been shown,¹⁴ the reason for the appearance of $1/f$ spectrum is the scaling properties of the signal: the change of the magnitude of the variable $x \rightarrow ax$ is equivalent to the change of the time scale $t \rightarrow a^{2(\eta-1)}t$.

Equation (4) together with $dt_\tau = x_\tau^{-2\eta} d\tau$ suggest an efficient way of solving the non-linear SDE (5). Discretiz-

ing the internal time τ with the step $\Delta\tau$ and using the Euler-Marujama approximation for the SDE (4) we get

$$x_{k+1} = x_k + \left(\eta - \frac{\nu}{2} \right) \frac{1}{x_k} \Delta\tau + \sqrt{\Delta\tau} \varepsilon_k, \quad (6)$$

$$t_{k+1} = t_k + \frac{\Delta\tau}{x_k^{2\eta}} \quad (7)$$

Here ε_k are normally distributed uncorrelated random variables.

An example of a signal generated by equation (5) together with the internal time is shown in Fig. 1. We see that internal time increases rapidly when the signal acquires large values. The corresponding spectrum is shown in Fig. 2. The numerical solution confirms a presence of a wide region where the spectrum behaves as $1/f$.

In summary, we have demonstrated that the Brownian motion in non-homogeneous medium can result in $1/f$

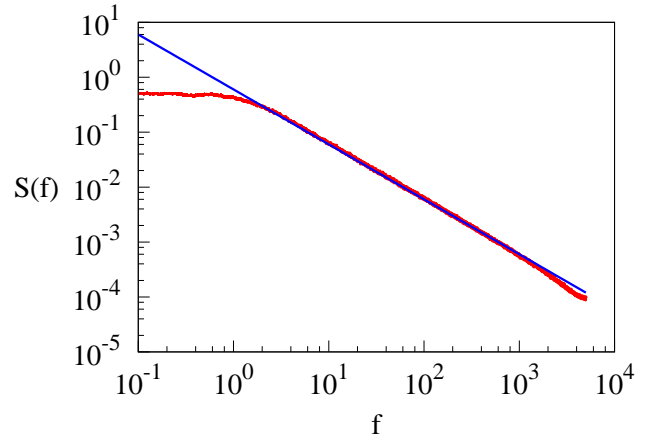


FIG. 2. Spectrum of the signal generated by equation (5) with the parameters $\eta = 5/2$ and $\lambda = 3$ (red curve). Blue line shows the slope $1/f$

noise when the internal time and the physical time are related via power-law function of the position. We expect that the present model can be useful for explaining $1/f$ noise in complex systems.

¹ B. B. Mandelbrot, *Multifractals and 1/f Noise: Wild Self-Affinity in Physics* (Springer-Verlag, New York, 1999).
² C. Castellano, S. Fortunato, V. Loreto, *Rev. Mod. Phys.* **81**, 591 (2009).
³ A. A. Balandin, *Nature Nanotechnology* **8** 549 (2013).
⁴ E. Paladino, Y. M. Galperin, G. Falci, B. L. Altshuler, *Rev. Mod. Phys.* **86**, 361 (2014).
⁵ A. L. McWhorter *Semiconductor Surface Physics* (R. H. Kingston (Ed.), University of Pennsylvania Press, Philadelphia, 1957).
⁶ P. Bak, C. Tang, K. Wiesenfeld, *Phys. Rev. Lett.* **59**, 381 (1987).
⁷ B. Kaulakys, T. Meškauskas, *Phys. Rev. E* **58**, 7013 (1998).
⁸ B. Kaulakys, V. Gontis, M. Alaburda, *Phys. Rev. E* **71**,

051105 (2005).

⁹ B. Kaulakys, J. Ruseckas, *Phys. Rev. E* **70** 020101(R) (2004).
¹⁰ B. Kaulakys, J. Ruseckas, V. Gontis, M. Alaburda, *Physica A* **365**, 217 (2006).
¹¹ V. Gontis, J. Ruseckas, A. Kononovicius, *Physica A* **389**, 100 (2010).
¹² J. Mathiesen, L. Angheluta, P. T. H. Ahlgren, M. H. Jensen, *PNAS* **110**, 17259 (2013).
¹³ E. Ben-Naim and P. L. Krapivsky, *Phys. Rev. Lett.* **102**, 190602 (2009).
¹⁴ J. Ruseckas and B. Kaulakys, *J. Stat. Mech.* **2014**, P06005 (2014).

Plasmonic Noise of Field-Effect Transistors Operating at Terahertz Frequencies

C. Palermo,¹ A. Mahi,¹ H. Marinchio,¹ L. Varani,¹ P. Shiktorov,² E. Starikov,² and V. Gruzinskis²

¹*Univ. of Montpellier, IES, UMR 5214, F-34000, Montpellier, France*
e-mail address: lvarani@um2.fr

²*Semiconductor Physics Institute, Center for Sciences and Technology, LT-01108, Vilnius, Lithuania*

I. INTRODUCTION

The use of nanometer field-effect transistors (FETs) for the development of low-cost THz detectors and emitters working at room temperature is one of the most promising trends in ultrafast modern electronics. Such devices should open the way to a large number of applications and may greatly benefit from the development of integrated systems¹. Mainly, this is associated with the possibility of easy tuning the 2D plasma excitation spectrum inside the transistor channel by changing the external conditions, namely: gate voltage, drain voltage, operation regime, etc.²⁻⁴. Indeed, under special excitation and biasing conditions, stream-plasma instabilities leading to the emission of THz radiation may be created in the transistor channel⁵. On the other hand, it has been proved both by experiments and numerical simulations that the excitation of plasma modes in the transistor channel increases significantly the efficiency of room-temperature direct and heterodyne detection in the THz frequency range^{6,7}.

It is well known that the characteristics of the internal electronic noise of a device reflect the information related to both the eigen-frequency spectrum² and the state of the free carrier system and its changes (for example, in going from equilibrium to nonequilibrium conditions). Such a dependence of the internal noise characteristics on the physical behavior of free carriers can also be used as a precursor of the transition from a first physical state to another one such as, for instance, the transition from a static to a dynamic state, onset of generation processes, etc.. In this contribution we present a critical overview of the main features of electronic noise spectra of FETs operating in the THz frequency range : in particular, we discuss the possible influence of external excitations and the role of the transistor geometry.

II. THEORETICAL MODEL

Carrier transport and related fluctuations are modeled as a one-dimensional (1D) process by using simple hydrodynamic (HD) equations²

$$\frac{\partial n}{\partial t} + \frac{\partial nv}{\partial x} = 0 \quad (1)$$

$$\frac{\partial v}{\partial t} + \frac{\partial}{\partial x} \left[\frac{v^2}{2} + \frac{e}{m^*} \varphi \right] + e\nu D \frac{\partial n}{\partial x} + \nu v = \tilde{f} \quad (2)$$

where n and v are the concentration and velocity of electrons in the channel, respectively, ν is the velocity relaxation rate, m^* the electron mass, D the longitudinal diffusion coefficient, and \tilde{f} the Langevin force which describes the source of thermal fluctuations at the lattice temperature T with the spectral density

$$S_{ff} = \frac{4k_B T \nu}{m^*} \quad (3)$$

The self-consistent potential $\varphi(x)$ inside the channel is described by a 1D approximation of the 2D Poisson equation⁸:

$$\varepsilon_c \frac{\partial^2}{\partial x^2} \varphi + \varepsilon_s \frac{U_g - \varphi}{d(x)\delta} = \frac{e}{\varepsilon_0} [n(x) - N_D(x)] \quad (4)$$

where δ is the channel width, U_g the gate potential, N_D the effective donor concentration in the channel, $d(x)$ the effective gate-to-channel distance. A dependence of $d(x)$ on the coordinate in the channel allows us to describe in the framework of Eq. (3) both gated regions where $d(x)$ has certain finite value and ungated regions where $d(x) \rightarrow \infty$ is supposed to tend to infinity.

III. PLASMA RESONANCES EXCITATED BY THERMAL FLUCTUATIONS

The system of Eqs. (1) to (4) is closed and it allows to calculate numerically the spectral densities of current and voltage fluctuations, $S_{JJ}(\omega)$ and $S_{UU}(\omega)$, respectively at the transistor terminals as:

$$S_{\xi\xi}(\omega) = \int_0^L n(x_0) |G_\xi(\omega, x_0)|^2 S_{ff}(x_0) dx_0 \quad (5)$$

where L is the full length of the channel, $G_\xi(\omega, x_0)$ the spectral representation of the response function ($\xi = J, U$) to a local δ -like excitation at $x = x_0$ induced by the Langevin force $\tilde{f}(x_0)$.

Therefore, it is possible to calculate the spectral density of current fluctuations in source-drain (SD) and source-gate (SG) circuits. A typical result calculated at constant voltage operation, that is for $\Delta U_g = 0$ and $\Delta U_d = 0$, is reported in Fig. 1. We observe that, as expected, oscillations in the noise spectra which are related to the resonant excitation of spatial modes of plasma waves in the dielectric layer separating the channel from the gate.

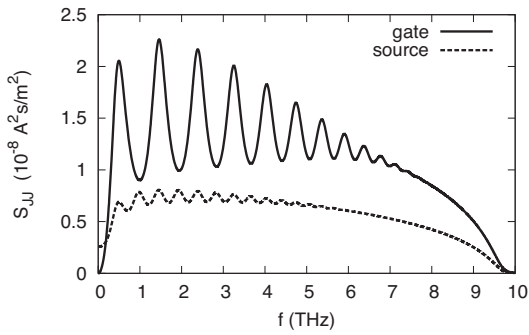


FIG. 1. Calculated spectral density of current fluctuations in source-drain and source-gate circuits calculated with $U_d = 0$ and $U_g = 0$.

IV. CRITICAL ANALYSIS AND OPEN QUESTIONS

Using the previously described model we will present a critical analysis of the main features of noise spectra and a discussion of the following debated questions in the literature:

1. To which extent the widely employed Dyakonov-

Shur model can describe correctly the noise spectra and the associated plasma resonances?

2. What happens if the transistor channel is not a perfect 2D gas, i.e. which is the role of the channel thickness?
3. Which is the effect of a realistic topology, i.e. channel regions whose electrostatic potential is not directly controlled by the gate electrode?
4. Which is the effect of the embedding circuit, i.e. can the plasma resonances be tuned by playing on external discrete elements?
5. Can the noise be suppressed or enhanced by using external electromagnetic excitations ?

ACKNOWLEDGMENTS

This work is partially supported by grant No. MIP - 058/2013 of the Research council of Lithuania. The support of TeraLab-Montpellier is also acknowledged.

- ¹ S. Blin, L. Tohme, S. Hisatake, K. Arakawa, P. Nouvel, D. Coquillat, A. Penarier, J. Torres, L. Varani, W. Knap, T. Nagatsuma, "Plasma-Wave Detectors for Terahertz Wireless Communication", *Electron. Lett.* **33**, pp 1354-1356 (2012).
- ² P. Shiktorov, E. Starikov, V. Gružinskis, L. Varani, G. Sabatini, H. Marinchio and L. Reggiani, "Problems of noise modeling in the presence of total current branching in high electron mobility transistor and field-effect transistor channels," *Journal of Statistical Mechanics: Theory and Experiment* **2009**, iss. 01, p. 01047 (2009)
- ³ M. Dyakonov and M. Shur, "Plasma wave electronics: novel terahertz devices using two dimensional electron fluid", *IEEE Trans. Electron. Devices* **43**, pp. 1640-1645 (1996).
- ⁴ J.-F. Millithaler, L. Reggiani, J. Pousset, L. Varani, C. Palermo, W. Knap, J. Matéos, T. González, S. Pérez and D. Pardo, "Monte Carlo investigation of terahertz plasma oscillations in ultrathin layers of n-type $\text{In}_{0.53}\text{Ga}_{0.47}\text{As}$ ", *Appl. Phys. Lett.* **92**, p. 042113 (2008).
- ⁵ P. Nouvel, J. Torres, S. Blin, H. Marinchio, T. Laurent, C. Palermo, L. Varani, P. Shiktorov, E. Starikov, V.

- Gružinskis, F. Teppe, Y. Roelens, A. Shchepetov, S. Bol-laert, "TeraHertz emission induced by optical beating in nanometer-length field-effect transistors", *J. Appl. Phys.* **111**, p. 103707 (2012).
- ⁶ P. Nouvel, H. Marinchio, J. Torres, C. Palermo, D. Gasquet, L. Chusseau, L. Varani, P. Shiktorov, E. Starikov, V. Gružinskis, "Terahertz spectroscopy of optically excited resonant plasma waves in high electron mobility transistor", *J. Appl. Phys.* **106**, p 013717 (2009).
- ⁷ H. Marinchio, L. Chusseau, J. Torres, P. Nouvel, L. Varani, G. Sabatini, C. Palermo, P. Shiktorov, E. Starikov and V. Gružinskis, "Room-temperature terahertz mixer based on the simultaneous electronic and optical excitations of plasma waves in a field effect transistor", *Appl. Phys. Lett.* **96**, p013502, (2010).
- ⁸ H. Marinchio, C. Palermo, G. Sabatini, L. Varani, P. Shiktorov, E. Starikov and V. Gružinskis, Pseudo-two-dimensional Poisson equation for the modeling of field-effect transistors, *Journal of Computational Electronics* **9**, iss. 3-4, pp. 141-145 (2010).

Fluctuation theorems and stochastic thermodynamics : applications to energy fluctuations in electric circuits and micro devices

Sergio Ciliberto¹

¹*Université de Lyon, Laboratoire de Physique,
École Normale Supérieure de Lyon, CNRS UMR5672,
46, Allée d'Italie, 69364 Lyon Cedex 07, France*

Thermal fluctuations play a very important role and cannot be neglected in small systems, such as electric circuits and micro-devices driven out of equilibrium by external forces. In these systems the work performed by the external forces and the dissipated heat fluctuate and stochastic thermodynamics imposes several constraints on their behavior. In this talk we will recall first the main concepts of stochastic thermodynamics using experimental measurements of work and heat in electric circuits and micro-devices. We will show that the probability distributions of the injected work and dissipated heat satisfy an asymptotic Fluctuation Theorem (FT), which imposes strong constraints on the energy fluctuations. We will introduce the stochastic and total entropies which satisfy an FT for any time. We will apply these concepts to the experimental and theoretical study of the statistical properties of the energy exchanged between two electrical conductors, kept at different temperature by two differ-

ent heat reservoirs, and coupled only by the electric thermal noise. Such a system is ruled by the same equations as two Brownian particles kept at different temperatures and coupled by an elastic force. We measure the heat flowing between the two reservoirs, the thermodynamic work done by one part of the system on the other, and we show that these quantities exhibit a long time fluctuation theorem. Furthermore, we evaluate the fluctuating entropy, which satisfies a conservation law. These experimental results are fully justified by the theoretical analysis. The other important point that we will describe is the case of the fluctuations of the work done by an external Gaussian random force on an atomic force microscopy cantilever. We finally discuss the open problems of the stochastic thermodynamics and useful perspectives, such as the efficiency of energy transformation in small devices and the connections with information.

¹ S. Ciliberto, R. Gomez-Solano, and A. Petrosyan, *Fluctuations, Linear Response, and Currents in Out-of-Equilibrium Systems*, Annual Review of Condensed Matter, **4**, 235 (2013).

² S. Joubaud, N. Garnier, S. Ciliberto, *Fluctuations of the total entropy production in stochastic systems*, Eur. Phys. Lett. **82**, 3, 30007, (2008).

³ S. Ciliberto, A. Imparato, A. Naert, and M. Tanase,

Heat Flux and Entropy Produced by Thermal Fluctuations, Phys. Rev. Lett., **110**, 180601 (2013).

⁴ A. Bérut et al., *Experimental verification of Landauer's principle linking information and thermodynamics*, Nature, **483**, 187189 (2012).

⁵ J. R. Gomez-Solano, L. Bellon, A. Petrosyan and S. Ciliberto, *Steady-state fluctuation relations for systems driven by an external random force*, Europhys. Lett., **89**, 60003 (2010).

Experimental realization of a microscopic Carnot engine

L. Dinis,¹ I.A. Martínez,² E. Roldán,³ J.M.R Parrondo,⁴ and R. A. Rica⁵

¹*GISC and Dpto. Física Atómica Molecular y Nuclear. Universidad Complutense de Madrid
ldinis@ucm.es*

²*Laboratoire de Physique, Ecole Normale Supérieure,
CNRS UMR5672 46 Allée d'Italie, 69364 Lyon, France.*

³*Max Planck Institute for the Physics of Complex Systems, Nöthnitzer Str. 81, 01187 Dresden, Germany.*

⁴*GISC and Dpto. Física Atómica Molecular y Nuclear. Universidad Complutense de Madrid*

⁵*ICFO Institut de Ciències Fotòniques, Mediterranean Technology Park,
Av. Carl Friedrich Gauss, 3, 08860, Castelldefels (Barcelona), Spain*

I. INTRODUCTION

Carnot engine played a crucial role in the development of thermodynamics, setting a fundamental upper limit to the efficiency of a motor operating between two thermal baths. Nowadays, micromanipulation techniques make it possible to explore the thermodynamics of small systems at scales where fluctuations cannot be neglected. In this contribution, I will present an experimental realization of a Carnot engine with a single optically trapped Brownian particle as working substance. We have fully characterized the thermodynamics of the engine when operating both in and out of equilibrium, observing that our device reaches Carnot efficiency for slow driving. I will also discuss the fluctuations of the finite-time stochastic efficiency, showing that Carnot efficiency can be surpassed in individual or ensembles of a few number of non-equilibrium realizations of the engine. Finally I will briefly comment on the stochastic efficiency large deviation behaviour which could provide information about the fundamental characteristics of the engine. A number of open questions arise due to the stochastic nature of the processes realized with a single Brownian particle which will be addressed in the final section.

II. EXPERIMENTAL SETUP

Fig. (1) depicts our experimental setup^{1,2} which consists in a single polystyrene sphere of radius $R = 500\text{nm}$ immersed in water and trapped with an optical tweezer. A pair of aluminium electrodes located in the chamber are used to apply a voltage of controllable amplitude. When a random electric field is applied to the electrodes, the colloidal particle experiences a random force that mimics a higher temperature thermal reservoir². The effective temperature of the particle is related to the intensity of the random force and can be obtained from the enhanced position fluctuations:

$$T_{\text{kin}} = \frac{\kappa \langle x^2 \rangle}{k}. \quad (1)$$

Using our setup, we can realize any thermodynamic process in which the stiffness of the trap and the kinetic temperature of the particle can change with time arbitrarily following a protocol $\{\kappa(t), T_{\text{kin}}(t)\}$.

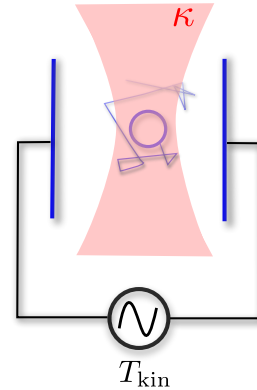


FIG. 1. Schematic of the experimental setup

III. MEASURING KINETIC ENERGY

For the case of microscopic dielectric beads immersed in water, the momentum relaxation time is of the order of nanoseconds. Therefore, in order to accurately measure the instantaneous velocity of a Brownian particle, it would be necessary to sample the position of the particle with sub-nanometer precision and at a sampling rate above MHz.

In our experiment, we do not have direct access to the instantaneous velocity due to our limited sampling frequency which is in the kHz range. However, we have developed a technique that allows to extrapolate the instantaneous velocity from the time averaged velocity (TAV) \bar{v}_f over a time $\Delta t = 1/f$. With this technique, the kinetic energy changes can be measured giving access to the full thermodynamics of the particle. Work, heat, potential and kinetic energy and entropy changes can be measured in this setup³.

IV. MICROADIABATICITY

Until now, the design of microscopic heat engines has been restricted to those cycles formed by isothermal processes or instantaneous temperature changes⁴. Among all the non-isothermal processes, adiabatic processes are of major importance in thermodynamics since they are the building blocks of the Carnot engine.

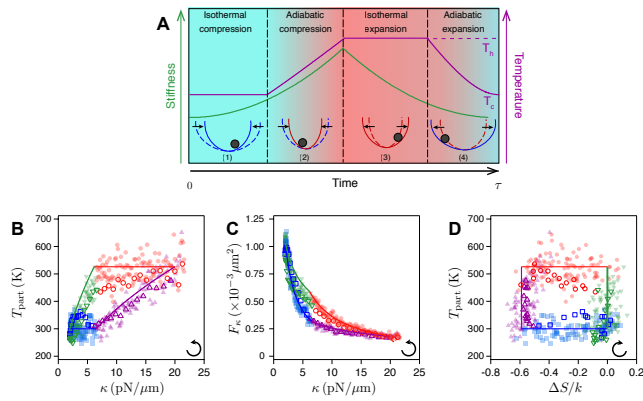


FIG. 2. The Brownian Carnot engine. (A) Time evolution of the experimental protocol. (B-D) Thermodynamic diagrams of the engine: Isoth. compression (blue); Adiab. compression (magenta); Isoth. expansion (red); Adiab. expansion (green). Solid lines are the values in the quasistatic limit. Filled symbols are obtained from ensemble averages over slow cycles while open symbols are obtained fast cycles. (B) $T - \kappa$ diagram. (C) Clapeyron diagram (D) $T - S$ diagram.

Microadiabaticity, i.e. adiabaticity at the microscopic scale, cannot be realized for single-trajectories due to the unavoidable heat flows between microscopic systems and their surroundings. However, a process where no net heat transfer is obtained when averaged over many trajectories could in principle be realized.

We have experimentally realized adiabatic processes⁵ following a theoretical proposal aimed at keeping constant the phase space volume enclosed by the energy surface^{6,7}. In the adiabatic protocol both T and the stiffness κ are modified keeping T^2/κ constant. To achieve this, we have taken advantage of the aforementioned technique to measure kinetic energy changes, as a full underdamped description is mandatory to take into account entropy changes in the velocity degree of freedom.

V. BROWNIAN CARNOT CYCLE

The experimental realization of a Carnot cycle with a single Brownian particle had previously remained elusive due to the difficulties of implementing an adiabatic process. In our setup, the Carnot cycle is implemented by modifying the stiffness κ and the temperature of the particle in a sequence of two isothermal steps joined by two adiabatic steps as in Fig. (2A)⁸.

Taken all together, the thermodynamic diagrams under quasistatic driving (Figs. (2B-D)) are equivalent to those for a single particle ideal gas in a Carnot cycle. We have analyzed both the average power extracted and the efficiency of heat to work conversion. The efficiency is given by the ratio between the extracted work and the input of heat, which is usually considered as the heat flowing from the hot thermal bath to the system. In our experiment, however, there is a non-zero fluctuating heat in the adiabatic steps, which must be taken into account in the definition of the stochastic efficiency of the engine during a finite number of cycles. In the quasistatic limit our engine attains approximately Carnot efficiency. We have also tested a number of theoretical predictions of the stochastic thermodynamics for a Carnot engine in our setup regarding the distribution of the fluctuating efficiency^{9,10}.

VI. OPEN QUESTIONS

A number of questions remain open and are the subject of current and future work. In the contribution I will try to discuss some of them:

- Can adiabatic processes, either at realization or average level, be realized in other microscopic systems in contact with a thermal bath?
- In which cases must the efficiency include the fluctuating heat in the adiabatic steps?
- Are there reversible trajectories with finite power?
- Can we improve the efficiency of the finite time Carnot engine using measurements?

¹ P. Mestres, I.A. Martínez, A. Ortiz-Ambriz, R. A. Rica, E. Roldán, Phys. Rev. E **90**, 032116 (2014)
² I. A. Martínez, E. Roldán, J. M. R. Parrondo, and D. Petrov, Phys. Rev. E **87**, 032159 (2013).
³ É. Roldán, I. A. Martínez, L. Dinis and R. A. Rica. Appl. Phys. Lett. **104**, 234103 (2014)
⁴ V. Blickle and C. Bechinger, Nature Phys. **8**, 143 (2011).
⁵ I. A. Martínez, E. Roldán, L. Dinis, D. Petrov, R. A. Rica. arXiv:1409.7578, Accepted in Phys. Rev. Lett.

⁶ K. Sekimoto, F. Takagi, and T. Hondou, Phys. Rev. E **62**, 7759 (2000).
⁷ T. Schmiedl and U. Seifert, EPL **81**, 20003 (2008).
⁸ I. A. Martínez, E. Roldán, L. Dinis, D. Petrov, J.M.R. Parrondo, R. A. Rica. arXiv:1412.1282 (2015)
⁹ M. Polettini, G. Verley, M. Esposito, arXiv:1409.4716 (2014).
¹⁰ K. Proesmans, B. Cleuren and C. Van den Broeck, Europhys. Lett. **109** 20004 (2015)

Equilibrium and non-equilibrium fluctuations at the single molecule level: from free-energy measurements to inference

M. Ribezzi-Crivellari¹ and F. Ritort²

¹*Departament de Física Fonamental, Universitat de Barcelona, Diagonal 647, Barcelona
e-mail address: marco.ribezzi@gmail.com*

²*Departament de Física Fonamental, Universitat de Barcelona, Diagonal 647, Barcelona
e-mail address: fritort@gmail.com*

Optical tweezers allow the measurement of fluctuations at the nano-scale, in particular fluctuations in the end-to-end distance of single bio-molecules. This kind of experiments, at the interface between biology, chemistry and physics offer the possibility of testing recent results in non-equilibrium statistical physics and applying them in high-resolution measurement of intra and inter-molecular interactions. Thermal fluctuations play a prominent role in these experiments and fluctuation spectra yield valuable information. However fluctuation spectra can be easily distorted by unavoidable instrumental effects¹. I will show how, once instrumental effects are correctly taken into account, equilibrium fluctuations in the end-to-end distance of a single molecule allow for a precise measurement of its entropic elastic response and of its folding kinetics. I will then describe non-equilibrium experiments in which optical tweezers perform work on a tethered molecule, forcing its unfolding. The statistics of the work necessary to unfold the molecule, collected in

repeated cycles, allow us to measure the equilibrium folding free energy from non-equilibrium pulling experiments via the so-called fluctuation relations² (FR). In the last part of the talk I will move the discussion to a more general level and will present a tentative but general strategy to use FRs in measurements, which we call an *inference* via the FR, inspired by our recent work on FRs in dual-trap setups³. Our starting point will be the following: the violation of FRs is itself an important information since it hints that we are probably missing some contribution to the entropy production. Can the extent of this violation tell us something about the missing entropy? Can we extract meaningful quantitative information from such violation? These questions are particularly interesting if a “hidden” entropy source is not directly measurable. This situation is found in many experiments, e.g. in systems with hidden degrees of freedom⁴, systems with incomplete detection⁵ and systems with more than one configurational variables³.

¹ Marco Ribezzi-Crivellari, Anna Alemany, and Felix Ritort. Recent progress in fluctuation theorems and free energy recovery. *Opt. Lett.* 40(5), pp. 800-803 (2015)

² Anna Alemany, Marco Ribezzi-Crivellari, and Felix Ritort. Recent progress in fluctuation theorems and free energy recovery. *Nonequilibrium Statistical Physics of Small Systems: Fluctuation Relations and Beyond*, pp. 155-179 (2011)

³ Marco Ribezzi-Crivellari and Felix Ritort. Free-energy inference from partial work measurements in small systems. *Proceedings of the National Academy of Sciences*,

111(33):E3386–E3394, (2014).

⁴ J. Mehl, B. Lander, C. Bechinger, V. Blickle, and U. Seifert. Role of hidden slow degrees of freedom in the fluctuation theorem. *Phys. Rev. Lett.*, 108:220601 (2012).

⁵ Klaara L Viisanen, Samu Suomela, Simone Gasparinetti, Olli-Pentti Saira, Joachim Ankerhold, and Jukka P Pekola. Incomplete measurement of work in a dissipative two level system. *arXiv preprint arXiv:1412.7322*(2014).

Fluctuations of intensive variables and non-equivalence of thermodynamic ensembles

A.Ya. Shul'man¹

¹ V.A. Kotel'nikov Institute of Radio Engineering and Electronics of the RAS, 125009 Moscow, Russia
e-mail address: ash@cplire.ru

The concept of incomplete thermodynamic equilibrium Einstein initiated¹ allows us to define the distribution function of fluctuations for the extensive variables without the addressing to a space of microstates. Further elaboration of this approach led to the Landau-Lifshitz (L-L) formula for the fluctuation probability incorporating also the fluctuations of intensive variables like temperature T and pressure P .² The L-L distribution is widely employed and it now has the direct experimental verification³.

However, there is still a belief that use of the concept of fluctuations of intensive variables contradicts the principles of statistical physics, as these variables are parameters, not arguments for the probability distribution in the space of microstates. The discrepancy between the results of calculations such as $\langle(\Delta T)^2\rangle$ and $\langle(\Delta P)^2\rangle$ using the distribution of either Gibbs or L-L continues to be one of the arguments in favor of this opinion, see⁴⁻⁶ and more.

This report aims to show that obtained contradictions have been spawned by discrepancy of the set of independent state variables when calculating the fluctuations with each of the probability distributions. Therefore, the

equivalence theorem of thermodynamic ensembles is violated in the case of fluctuations.

This violation appears as a mathematical consequence of using the second differential in the theory of thermodynamic fluctuations, which is non-invariant with respect to the choice of independent variables in its usually adopted form. It is shown that the L-L distribution allows to take this fact into account and does not give rise results contradicting Gibbs distribution if used appropriately.

The principal unavoidability of the fluctuations of the intensive thermodynamic variables is discussed as a consequence of the inevitable chaotic nature of microscopic motion. The unsolved problem which particularly nanophysics dictated is to generalize the Landau-Lifshitz approach for the quantum region.

ACKNOWLEDGMENTS

The partial financial support by grants ##10-02-00869 and 13-02-1238 of the Russian Foundation for Basic Researches is gratefully acknowledged.

¹ A. Einstein, Ann. Phys. **22**, 569 (1907); **33**, 1275 (1910).

² L.D. Landau and E.M. Lifshitz, *Statistical Physics, Part.1, Ch. 12. 4th ed.* (Nauka-FM, Moscow 1995).

³ T.C.P. Chui, D.R. Swanson, M.J. Adriaans et al, Phys. Rev. Lett. **69**, 3005 (1992).

⁴ A. Münster, Nuovo Cimento Suppl. **13** (1960).

⁵ K.W. Kratky, Phys. Rev. A **31**, 945 (1985).

⁶ Yu.G. Rudoï and A.D. Sukhanov, Phys. Usp. **43**, 1169 (2000); [Uspekhi Fiz. Nauk, **170**, 1265 (2000)].

How can the fluctuations in the motion of kayak-paddlers be used to estimate performance?

Gergely Vadai¹ and Zoltán Gingl¹

¹Department of Technical Informatics, University of Szeged, Szeged-6720, Hungary
e-mail address: vadaig@inf.u-szeged.hu ; gingl@inf.u-szeged.hu

I. INTRODUCTION

In several cases periodic signals shape, period have some fluctuations that can be informative. From periodically working machines to heart movements the variability can be used to know more about proper behavior¹. Nowadays several devices – like smart watches, wrist-bands, smart phones, actigraphs – can measure movements, motion patterns by inertial sensors for several applications including monitoring daily activity cycles for health analysis.

Similar inertial sensors are used in coaching devices developed for professional kayak paddlers and trainers, where classical parameters, quantities and their shape in one stroke cycle are used to classify the athletes performance²⁻⁴. In a previous work we have shown that because the optimal motion of a kayak is clearly periodic, therefore the fluctuations of its period could be an indicator of athletes' performance⁵. We have calculated a signal-to-noise ratio using the raw signals' spectra and it seemed to be a good indicator too and it does not require the detection of strokes.

As we show hereinafter, more detailed analysis needed to examine the relationship between these fluctuations and paddlers performance, many questions are still open about how one should define and calculate the temporal and spectral indicators, how these fluctuation based indicators can be used to classify similar periodic processes.

II. KAYAK MOTION DATA

The examined motion signals of the kayaks were measured by a special portable instrument developed in our laboratory. The device recorded the 3-axis acceleration and 3-axis angular velocities of the kayak with a sample rate of 1000 Hz^{5,6}.

Our goal was to find the best indicators of athletes' performance based on a classification done by the trainer. In order to compare the typical performance of paddlers in the same circumstances (as much as possible), we have analysed the first 10 minutes of long range (>5 km) training paddling of 14 athletes with different age and technical skills.

The fluctuation-based indicators (time or frequency domain based both) were calculated for shorter window lengths (30 seconds in figures), and the averages for the examined 10 minutes long part were compared.

III. TEMPORAL INDICATORS

The classical parameters of stroke cycles (stroke time, stroke impulse etc.) were calculated by peak and level crossing detection algorithms, using the forward axis acceleration signal⁶.

As we have pointed out in previous works^{5,6}, not only the mean values of these parameters, but their fluctuations can also give information about athletes' performance. As it is shown on Fig. (1), the relative standard deviation (SD) of the stroke impulse and the period decreases with better class significantly.

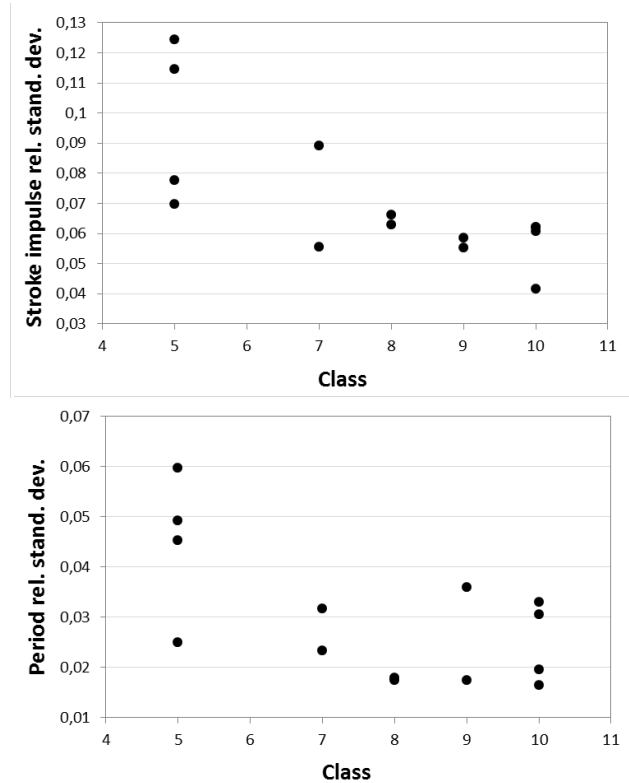


FIG. 1. Relative standard deviation of the detrended stroke impulse and period in the function of technical skills' classification (higher number is better). The parameters were calculated for whole periods (total duration of a left and a right hands stroke).

On the other hand, there are some open questions about how we should calculate these SDs. Changing stroke rate and effects of tiredness can be observed in every paddling, so the length of the processed data and using detrending algorithms could have impact on the indicators' values and the their observed relationship with technical skills. Furthermore, calculating absolute or relative SDs, defining the motions period as one stroke cycle or the sum of a left and a right hands stroke could affect this relationship, too.

IV. SPECTRAL INDICATORS

Precisely detecting the strokes using the complex signals with additional irregularities and noise could be rather complicated and inaccurate in most cases. Therefore calculating indicators based on the spectra of raw signals has many advantages concerning the signal processing. Note that it can be even extended to joint time-frequency analysis. Following this we have used a certain kind of

signal-to-noise ratio (SNR) as another possible indicator for performance estimation⁵.

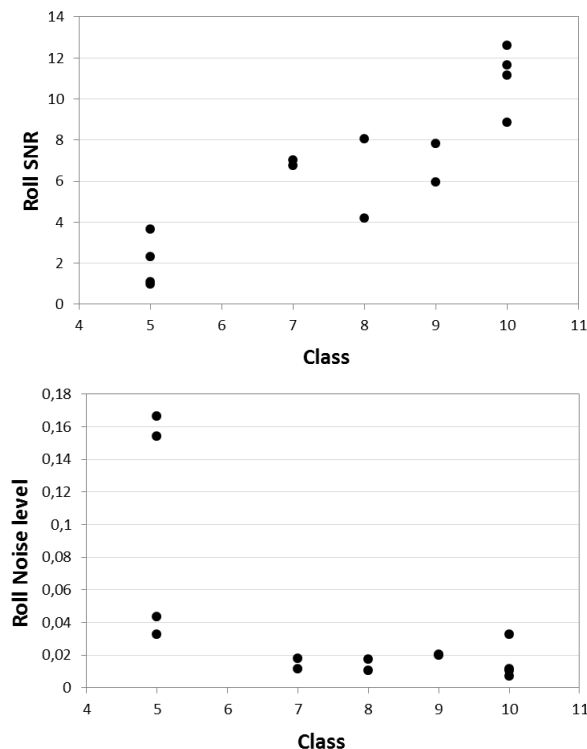


FIG. 2. Signal to noise ratio (SNR) and noise level of roll axis angular velocity as a function of technical skills' classification. Signal level of the spectrum were defined as the power of 0.2 Hz width peaks on fundamental frequency and first 5 harmonic frequencies, while the noise level was the power of the rest of the spectrum.

One of the most important question is how one can separate the "signal" and the "noise" in the power density spectra. In case of one acceleration and two gyroscope signals, the dominant frequency is the first harmonic (belongs to one stroke cycle), but the in the case of the other three signals, the fundamental frequency is more significant (belongs to the period of both hands strokes). Consequently there are several ways to calculate SNRs. Also, beyond the ratio, the signal and noise levels could be indicators as well.

Detecting the peaks precisely is not simple at all. We have designed numerical methods for finding the signal power in the spectra based on fixed peak or estimated half-width, and we have used them in different signal and noise definitions. We have

- ¹ U. Rajendra Acharya, K. Paul Joseph, N. Kannathal, C. Lim and J. S. Suri, „Heart rate variability: a review,” *Medical and Biological Engineering and Computing*, **44**, 1031-1051 (2006).
- ² J. S. Michael, R. Smith and K. B. Rooney, “Determinants of kayak paddling performance”, *Sports Biomech* **8**, 167-179 (2009).
- ³ M. G. Robinson, L. E. Holt, T. W. Pelham and K. Furneaux, “Accelerometry Measurements of Sprint Kayaks: The Coaches' New Tool”, *Int. J. Coaching Sci.* **5**, 45-56, (2011).
- ⁴ Z. Ma, J. Zhang, Y. Sun and T. Mei, “Sports Biomechanical

compared all of these results for different window length and types.

We found that estimating the signal level precisely is rather difficult, however the noise level alone seems to be a usable indicator of the technical skills as well. As depicted on Fig. (2) a certain type of SNR (details can be found in the caption) and noise level both show strong relationship with the technical quality.

V. OPEN PROBLEMS

As we have already pointed out, there are many questions about how we should calculate the temporal and spectral indicators. We present several different definitions for SNR, signal and noise level and simple algorithms to calculate them using six inertial sensors' signals.

The fact that the spectral indicators worked only for the signals whose dominant frequency is the fundamental frequency, and the temporal indicators also were better when the period was the sum of a left and a right hands stroke implies that the steadiness of the motion has a primary role in the paddling quality.

There can be other temporal parameters or spectral methods that can indicate the performance even better, so more detailed analysis is worth to be performed.

The indicators discussed above were tested using classification of technical skills, however the actual performance of the athlete depends on many factors. This is exceptionally important in order to determine how reliably the indicators can be used for certain cases, to determine what kind of data processing is needed.

Furthermore, it is an exciting question what are the sources of the noise can be detected in the paddling periodicity and strength. It can depend on mechanical effects – movement of the kayak and of the human body, dissipation –, learned technical skills and even mental condition, can be correlated to other processes.

Another interesting question is how this analysis can be related to other periodic motions, other sport fields, performance and reliability estimation, actigraphy or even more.

ACKNOWLEDGEMENTS

The authors thank Gergely Makan, Róbert Mingesz and athletes, trainers for their help and valuable discussions.

The publication/presentation is supported by the European Union and co-funded by the European Social Fund. Project title: “Telemedicine-focused research activities on the field of Mathematics, Informatics and Medical sciences” Project number: TÁMOP-4.2.2.A-11/1/KONV-2012-0073.

- Information Acquisition and Evaluation for Kayaking Events”, *Int.J. Inf. Acquisition* **6**, 213-223 (2009).
- ⁵ G. Vadai, Z. Gingl, R. Mingesz and G. Makan, “Performance estimation of kayak paddlers based on fluctuation analysis of movement signals”, in *Proc. of 22nd International Conference on Noise and Fluctuations*, Montpellier, France, (2013).
- ⁶ G. Vadai, G. Makan, Z. Gingl, R. Mingesz, J. Mellár, T. Szépe and A. Csamangó, “On-water measurement and analysis system for estimating kayak paddlers' performance”, in *Proc. of 36th Int. Conv., Microelectronics, Electronics and Electronic Technology*, Opatija, pp. 144-149. (2013).

Is There an Optimal Search Strategy?

Michael F. Shlesinger¹
¹Office of Naval Research
 Arlington VA 22203 USA
Mike.Shlesinger@navy.mil

I. INTRODUCTION

Bayesian analysis changes probability estimates as information is acquired. If you are searching for something and after some time you do not find it, that information can be used to estimate if the object of the search is present or not. Assume a searcher has finite resources and finite time to carry out a search and the searcher can search different areas and can use a variety of search methods. The unsolved question is when is it optimal to give up searching an area with a single method and switch methods or switch areas of search. Examples could be as simple as looking for a piece of paper between two cluttered desks, an animal foraging for food, or looking for a lost person, ship, or aircraft. Noise will cause fluctuations in the model parameters.

II. NET GAIN EQUATION

Let's start with the equation for searching two separate areas, 1 and 2, or the same area with two different methods also denoted by 1 and 2,

$$N(T, \tau) = G_1 p_1 \Phi_1(T - \tau) + G_2 p_2 \Phi_2(\tau) - C_1(T - \tau) - C_2 \tau \quad (1)$$

where N is the net gain or reward, T is the allotted search time, τ is the time spend in region 2 or with search method 2, G is the gain, p is the probability that the target is present, $\Phi(t)$ is the probability, if the target is present, that it will be found by time t, and C is the cost of the search, per unit time.

III. GENERALIZATIONS: THIN OR FAT TAILS

Several possibilities can be explored, e.g. exponential or algebraic probability distributions,

$$\Phi(t) = 1 - \exp(-\lambda t) \quad (2)$$

or

$$\Phi(t) = \frac{\tau_0}{\tau_0^2 + t^2/n}$$

where larger n corresponds to a fatter tail.

IV. BROWNIAN OR BALLISTIC

In the exponential case, λ can be studied for Brownian motion as

$$\lambda \propto \frac{D}{\langle d \rangle^2} \quad (3)$$

where D is the diffusion constant and $\langle d \rangle$ is the mean distance between targets.

For ballistic motion with velocity v, the success rate λ can be,

$$\lambda \propto \frac{vR}{\langle d \rangle^2} \quad (2D)$$

$$\lambda \propto \frac{vR^2}{\langle d \rangle^3} \quad (3D) \quad (4)$$

where R is the range at which a target can be sighted. If the targets are on a fractal set of dimension α , then d is replaced by $d^{1/\alpha}$. In the second case, larger n values mean fatter tails with successful search relegated probabilistically to longer times.

V. SPLITTING RESOURCES

With finite resources available, the success rate might need to be split between search of type 1 and type 2, i.e. there is a maximum Λ and it gets split between 1 and 2, $\Lambda = (\Lambda - \lambda) + \lambda$ where the term $\Lambda - \lambda$ is the success rate allotted to search of type 1 and λ is for the type 2 search.

VI. THE TARGET FLEES

Another generalization is that the target moves away to avoid detection, say in the manner,

$$p \Rightarrow p \exp(-\beta t) \tag{5}$$

VII. CHASE OR AMBUSH

The cost, over a time t , of a constant velocity search might be related to kinetic energy expended so $C \propto mv^2 t$, but then the success rate might increase proportional to v . One can contrast a predator practicing ambushing prey so the cost is $C=0$ while waiting, against chasing prey with a velocity v .

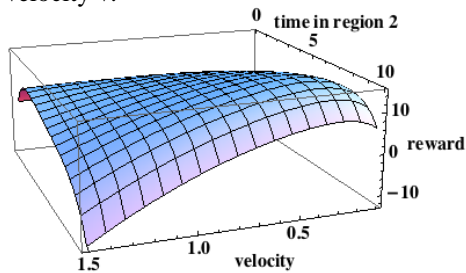


FIG. 1 A representative example of maximizing the gain as a reward (measured in the z direction) as a function of time spent in region 2 (along the y axis) and velocity of the searcher in region 2 whose success rate λ is proportional to

velocity, but the cost of searching is proportional to kinetic energy expended, i.e. v^2 .

VIII. DO NOT PICK LOW HANGING FRUIT

Or perhaps the gain $G = G(\lambda)$ is proportional to $1/\lambda$, so easier to find targets will typically have less value.

IX. CONCLUSIONS

The factors for a net gain can be generalized in several directions, and each type of search will have its own trade space of variables.

1. P. M. Morse, and G. E. Kimball, *Methods of Operations Research*, Technology Press of MIT (1951).
2. L. D. Stone, *The Theory of Optimal Search*, Operations Research Society of America, (1975).
3. S. J. Benkoski, M. G. Monticino, and J. R. Weisinger, A Survey of the Search Literature, *Naval Research Logistics*, **38**, Issue 4, (1991).
4. *The Physics of Foraging: An Introduction to Random Searches and Biological Encounters*, G. M. Viswanathan, M. G. E. da Luz, E. P. Raposo, and H. E. Stanley, Cambridge U. Press (2011).
5. *J. Phys. A*: **42** No 43 (2009) Special Issue on *The Random Search Problem*

A stochastic model for phytoplankton dynamics in the Tyrrhenian Sea

Davide Valenti,¹ Giovanni Denaro,¹ Bernardo Spagnolo,^{1,2,3} Fabio Conversano,⁴ and Christophe Brunet⁴

¹*Dipartimento di Fisica e Chimica, Università di Palermo,
Interdisciplinary Theoretical Physics Group, Università di Palermo and CNISM,
Unità di Palermo, Viale delle Scienze, Edificio 18, 90128 Palermo, Italy*

²*Radiophysics Department, Lobachevsky State University,
23 Gagarin Avenue, 603950 Nizhniy Novgorod, Russia*

³*Istituto Nazionale di Fisica Nucleare, Sezione di Catania, Via S. Sofia 64, I-90123 Catania, Italy*

⁴*Stazione Zoologica Anton Dohrn, Villa Comunale, 80121 Napoli, Italy*

I. INTRODUCTION

In this work we try to answer the question how relevant the random fluctuations are in the dynamics of a natural system. Specifically we ask which role the external fluctuations play in a real ecosystem, which is a typical example of complex system, since it is governed by nonlinear dynamics and subject to deterministic and random perturbations coming from the environment. For this purpose we study the spatio-temporal dynamics of phytoplankton abundances in a marine ecosystem, comparing results from the model with experimental findings. The study is based on a stochastic reaction-diffusion-taxis model, which is used to analyze the spatio-temporal dynamics of five phytoplankton groups in the middle of the Tyrrhenian Sea, inside the Modified Atlantic Water (MAW), that is the upper layer of the water column of the Mediterranean Sea (from the surface down to 200 m). The study is performed by considering the intraspecific competition of the phytoplanktonic groups for limiting factors^{1,2,3}, i.e. light intensity and nutrient concentration, and the seasonal changes of environmental variables⁴.

Moreover, we take into account the effects of the random fluctuations of the temperature and the velocity field on the phytoplankton populations by inserting terms of multiplicative noise in the differential equations of the model. In order to compare theoretical results with experimental findings, the picophytoplankton abundances obtained by the stochastic model are converted in *chlorophyll a* concentrations^{5,6}. The statistical analysis, based on the chi-square test, shows that the vertical distributions of total chlorophyll concentration are in a good agreement with experimental data acquired in the marine site investigated during four different sampling periods (seasons) of the year.

II. THE MODEL

Our stochastic model, which describes the spatio-temporal dynamics of five populations ($i=1,\dots,5$) distributed along a one-dimensional spatial domain (z -direction), is defined by the following equations

$$\begin{aligned} \frac{\partial b_i(z,t)}{\partial t} &= b_i G_i(z,t) + \frac{\partial}{\partial z} \left[D(z,t) \frac{\partial b_i(z,t)}{\partial z} \right] \\ &\quad - v_i \left(\frac{\partial G_i(z,t)}{\partial z} \right) \frac{\partial b_i(z,t)}{\partial z} + b_i \xi_{b_i}(z,t), \end{aligned}$$

$$\begin{aligned} \frac{\partial R(z,t)}{\partial t} &= - \sum \frac{b_i(z,t)}{Y_i} \cdot \min(f_{I_i}(I), f_{R_i}(R)) \\ &\quad + \frac{\partial}{\partial z} \left[D(z,t) \frac{\partial R(z,t)}{\partial z} \right] + \sum \varepsilon_i m_i \frac{b_i(z,t)}{Y_i}, \\ &\quad + R \xi_R(z,t) \end{aligned}$$

$$I(z,t) = I_{in}(t) \exp \left\{ - \int_0^z \left[\sum a_i \cdot chl a_i(Z,t) + a_{bg} \right] dZ \right\},$$

where $b_1(z,t)$, $b_2(z,t)$, $b_3(z,t)$, $b_4(z,t)$, and $b_5(z,t)$ indicate the cell concentrations of the five populations considered, i.e. Synechococcus, Haptophytes, Prochlorococcus HL, Pelagophytes and Prochlorococcus LL, respectively. Here $R(z,t)$ represents the phosphorus (nutrient) concentration, and $I(z,t)$ is the light intensity which is assumed to decrease exponentially with the depth z , according to the Lambert-Beer's law^{4,7,8,9}.

Moreover ε_i , m_i , and $1/Y_i$ are phosphorus recycling coefficient, specific loss rate, and nutrient content of the i -th picophytoplankton population, respectively; $G_i(z,t)$ are the net per capita growth rates, which depend on $f_{I_i}(I)$ and $f_{R_i}(R)$ given by the Michaelis-Menten formulas, and the specific loss rate of the i -th picophytoplankton group^{1,4}; v_i is the swimming velocity of each picophytoplankton population as a function of the corresponding gradient of the net growth rate; a_i are the *chl a*-normalized average absorption coefficients of the i -th picophytoplankton population, and a_{bg} is the background turbidity; $I_{in}(t)$ is the incident light intensity at the water surface, varying with the time due to daily changes; $D(z,t)$ is the vertical turbulent diffusivity, which changes as a function of the time and depth.

The spatio-temporal behaviour of the picophytoplankton abundance is modeled considering three processes¹: net growth (reaction term), active movement (taxis term) and passive movement (diffusion term). Moreover, the environmental random fluctuations are considered by inserting terms of multiplicative Gaussian noise in the differential equations. Specifically we use the noise sources $\xi_{b_i}(z,t)$ and $\xi_R(z,t)$ with the following statistical properties: $\langle \xi_{b_i}(z,t) \rangle = 0$, $\langle \xi_R(z,t) \rangle = 0$, $\langle \xi_{b_i}(z,t) \xi_{b_i}(z',t') \rangle = \sigma_{b_i} \delta(z-z') \delta(t-t')$, $\langle \xi_R(z,t) \xi_R(z',t') \rangle = \sigma_R \delta(z-z') \delta(t-t')$, with $i = 1, \dots, 5$. Here, σ_{b_i} and σ_R are the intensities of the noise sources which act on the i -th population and nutrient, respectively.

The boundary conditions for cell concentration of the i -th picophytoplankton population have to describe the absence of biomass flux through both the surface layer $z = 0$

and the deepest layer of the MAW $z = z_b$:

$$\left[D(z, t) \frac{\partial b_i}{\partial z} - v_i b_i \right] \Big|_{z=0} = \left[D(z, t) \frac{\partial b_i}{\partial z} - v_i b_i \right] \Big|_{z=z_b} = 0,$$

Moreover, the boundary conditions for the nutrient have to describe the absence of nutrient flux from the water surface, and fix the phosphorus concentration at the bottom of the MAW ($z = z_b$) equal to the average value measured R_{in} :

$$\frac{\partial R}{\partial z} \Big|_{z=0} = 0, \quad R(z_b) = R_{in}.$$

The theoretical distributions of cell concentration for the five picophytoplankton groups are obtained by integrating the system of stochastic differential equations and averaging over 1000 realizations.

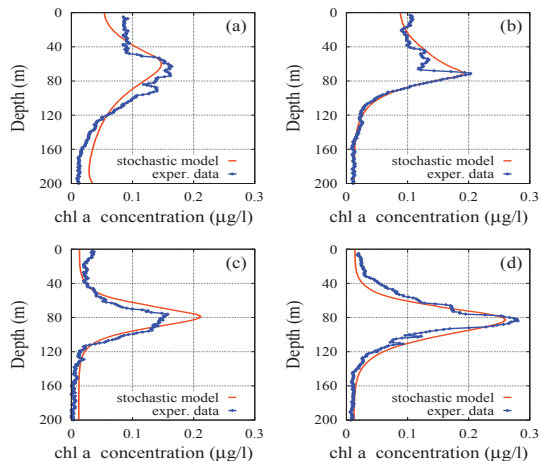


FIG. 1. Theoretical distributions (orange line) and experimental profiles (blue line) of the total *chlorophyll a* concentration. The numerical results, obtained by the stochastic model for $\sigma_R = 0.0005$ and $\sigma_{b_i} = 0$, are compared with the experimental data collected in the sampling site ($39^\circ 30'.00N$, $13^\circ 30'.00E$), in different period of the year: 24 November 2006 (panel a); 3 February 2007 (panel b); 22 April 2007 (panel c); 9 June 2007 (panel d).

Afterwards, the theoretical abundances of the five populations are converted into *chlorophyll a* concentrations by using the experimental cellular content measured by Morel and the conversion curves obtained by Brunet et al.^{5,6}. The numerical results are shown in Fig. 1, where the distributions of total *chlorophyll a* concentration obtained by the stochastic model are compared with the corresponding experimental profiles.

Results (here not reported) of the goodness-of-fit test χ^2 indicate the presence of a quite good agreement between experimental and theoretical findings in all four seasons analyzed, even if the best value of reduced chi-square in each season is reached for a different noise intensity. Specifically, in accordance with previous studies¹⁰, the χ^2 test shows that the stochastic model reproduces the experimental data better than the deterministic one in three sampling periods over four. In fact, in the fourth period (corresponding to the late spring) the best reduced chi-square is obtained by the deterministic model. This can be explained considering that in late spring the random fluctuations of environmental parameters are strongly reduced along the whole water column^{4,11,12}. The results obtained emphasize therefore the lack of information on the noisy behaviour of relevant physical and biological variables, suggesting that a better modeling needs a deeper knowledge of: i) velocity components subject to random fluctuations during the year; ii) nutrient half-saturation constants, which are significantly influenced by seasonal changes; iii) properties of the environmental noise which directly affects the phytoplankton populations.

ACKNOWLEDGMENTS

Authors acknowledge the financial support by Ministry of University, Research and Education of Italian Government, Project PON02_00451.3362121 "PESCATEC – Sviluppo di una Pesca Siciliana Sostenibile e Competitiva attraverso l'Innovazione Tecnologica", and Project PON02_00451.3361909 "SHELF-LIFE – Utilizzo integrato di approcci tecnologici innovativi per migliorare la shelf-life e preservare le proprieta' nutrizionali di prodotti agroalimentari".

-
- [1] C. A. Klausmeier and E. Litchman, *Limnol. Oceanogr.* **46**, 1998-2007 (2001).
 - [2] J. Huisman, N. N. Pham Thi, D. M. Karl and B. Sommeijer, *Nature* **439**, 322-325 (2006).
 - [3] A. B. Ryabov, L. Rudolf and B. Blasius, *J. Theor. Biol.* **263**, 120-133 (2010).
 - [4] D. Valenti, G. Denaro, B. Spagnolo, F. Conversano and C. Brunet, *PLoS ONE* **10**(1), e0115468 (2015).
 - [5] A. Morel, *Limnol. Oceanogr.* **42**(8), 1746-1754 (1997).
 - [6] C. Brunet, R. Casotti, V. Vantrepotte and F. Conversano, *Mar. Ecol. Prog. Ser.* **346**, 15-26 (2007).
 - [7] N. Shigesada and A. Okubo, *J. Math. Biol.* **12**, 311-326 (1981).
 - [8] A.E. Hickman, S. Dutkiewicz, R.G. Williams and M.J. Follows, *Mar. Ecol. Prog. Ser.* **406**, 1-17 (2010).
 - [9] J. T. O. Kirk, *Light and Photosynthesis in Aquatic Ecosystems (2nd edition)* (Cambridge University Press, 1994).
 - [10] G. Denaro, D. Valenti, A. La Cognata, B. Spagnolo, A. Bonanno, G. Basilone, S. Mazzola, S. Zgozi, S. Aronica, C. Brunet, *Ecol. Complex.* **13**, 21-34 (2013).
 - [11] M. Ribera d'Alcalá, M., C. Brunet, F. Conversano, F. Corato, R. Lavezza, *Deep-Sea Res. PT II* **56**, 676-686 (2009).
 - [12] M. Denis, M. Thyssen, V. Martin, B. Manca, F. Vidussi, *Biogeosciences* **7**, 2227-2244 (2010).

All that glitters is not gold: Zero-point energy in the Johnson noise of resistors

Laszlo B. Kish

Department of Electrical and Computer Engineering, Texas A&M University, College Station, TX 77843-3128, USA
e-mail address: Laszlokish@tamu.edu

The thermal noise (Johnson noise) in resistors was discovered¹ by Johnson and explained² by Nyquist in 1927, a year later than the foundations of quantum physics were completed. The Johnson-Nyquist formula states that

$$S_u(f) = 4RhfN(f,T) \quad (1)$$

where $S_u(f)$ is the power density spectrum of the voltage noise on the open-ended resistor of resistance R (replaced by the real part of the impedance if impedance is used); and h is the Planck constant. The Planck number $N(f,T)$ is the mean number of hf energy quanta in a linear harmonic oscillator with resonance frequency f , at temperature T

$$N(f,T) = [\exp(hf/kT) - 1]^{-1}, \quad (2)$$

which is $N(f,T) = kT/(hf)$ for the classical physical range $kT \gg hf$. Eq. 2 results in an exponential cut-off of the Johnson noise in the quantum range $f > f_p = kT/h$, in accordance with Planck's thermal radiation formula. In the deeply classical (low-frequency) limit, $f \ll f_p = kT/h$, Eqs. 1-2 yield the familiar form used in electrical engineering

$$S_u(f) = 4kTR \quad (3)$$

where the Planck cut-off frequency f_p is about 6000 GHz at room temperature, well-beyond the reach of today's electronics.

The quantum theoretical, generalized treatment of thermal noise was given only 24 years later by Callen and Welton³ (often called Fluctuation-Dissipation Theorem (FDT)). The quantum version³ of the Johnson-Nyquist formula has an additive 0.5 to the Planck number, corresponding to the zero-point energy of linear harmonic oscillators:

$$S_u(f) = 4Rhf[N(f,T) + 0.5]. \quad (4)$$

Thus the quantum correction of Eq. 1 is a temperature-independent additive term in Eq. 2:

$$S_{u,zp}(f) = 2hfR, \quad (5)$$

which linearly depends on the frequency and it exists for any $f > 0$ frequency, even in the deeply classical, $f \ll f_p = kT/h$, frequency regime, and even at zero temperature. The zero-point term described by Eq. 5 has acquired a wide theoretical support during the years, e.g.⁴⁻⁶.

However, there have also been contra-arguments and debates. MacDonald⁸ and Harris⁹ argued that extracting energy/power from the zero-point energy is impossible thus Eq. 5 should not

exist.

Grau and Kleen¹⁰ (similarly to the original treatment of Nyquist²), argued that the Johnson noise of a resistor connected to an antenna, see Figure 1, must satisfy Planck's thermal radiation formula thus the noise must be zero at zero temperature, which would imply that Eq. 5 is invalid. It should be emphasized that it is a hard experimental fact that the zero-point term does not exist in the thermal radiation. This is obvious even by naked-eye observations: at 6000 K temperature, at 600 nm (orange color), the Planck number $N = 0.0164$. Thus the zero-point term (0.5) is 30 times greater, implying that, if it would be present in the radiation, looking into a dark room instead of the sun, the light intensity at this wavelength would decrease only about a negligible 3%.

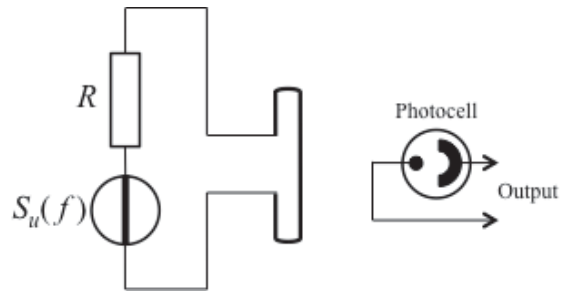


Figure 1. Measurement scheme based on an antenna and a photon counter, which does not show the zero-point term (Eq. 5) at its output.

Kish¹¹ showed that the existence of the zero-point term, which has and "f"-noise implies a 1/f noise and related logarithmic divergence of the energy of a shunt capacitor in the high-frequency limit. While this does not disprove the existence of the term, it may indicate that the problem is a renormalization problem, a mathematical artifact, which is not actually present at measurements.

Recently, Reggiani, et al.¹² objected the derivation³⁻⁶ of Eq. 4 but did not show what the results avoiding their criticism should be.

Yet, on the contrary of all the criticisms above, the experimental test by Koch, van Harlingen and Clarke¹³ fully confirmed the theoretical result Eq. 4 by measurements on resistively shunted Josephson-junctions.

However, Haus¹⁴ and Kleen¹⁵ stated that the zero-point term (Eq. 5) in Eq. 4 is the consequence of the uncertainty principle at phase-sensitive amplitude measurements, see Figure 2, which the linear voltage amplifiers measuring Johnson noise represent. Nevertheless, the uncertainty principle argument cannot disprove Eqs. 4,5. The claimed zero-point term in the noise voltage may still exist and satisfy the uncertainty principle instead of being solely an experimental artifact.

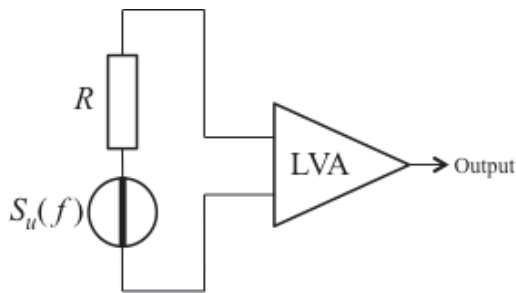


Figure 2. Measurement scheme based on a linear amplifier (LVA) system indicating the existence of the zero-point term or its uncertainty relation based artifact.

To claim the existence or non-existence of the debated zero-point noise term in the voltage is a serious matter because of its implications of the related current and energy flow.

Thus we devote our talk to the following question:

Is the zero-point voltage noise term (Eq. 5) and the power/energy flow it implies actually present in the wire connected to a

resistor?

Abbott, et al.,¹⁶ write in their education-article on thermal noise: "Until further evidence, the quantum zero- field should be regarded as a conservative field as far as the extraction of energy is concerned."

In this talk, we address this comment and close this issue by serving evidence¹⁷ that the zero-point voltage component cannot exist in the wire otherwise at least two different types of perpetual motion machines can be built and both the energy conservation law and the second law of thermodynamics are violated¹⁷.

The remaining *unsolved problem of noise* after our treatment is:

What is the proper general formula or formulas of Johnson noise in the voltage of resistors? The formula(s) that can reflect on the type of measurement that we use to characterize the Johnson noise of a resistor?

- 1 J.B. Johnson, Nature **119**, 50 (1927).
- 2 H. Nyquist, Phys. Rev. **29**, 614 (1927).
- 3 H. B. Callen and T. A. Welton, Phys. Rev. **83**, 34 (1951)
- 4 L. Landau and E. Lifshitz, Statistical Physics (Addison Wesley Reading, Mass., 1974).
- 5 R. Kubo, M. Toda and N. Hashitsume, Statistical Physics II (Springer-Verlag, Berlin, 1985).
- 6 V. L. Ginzburg and L. P. Pitaevskii, Quantum Nyquist formula and the applicability ranges of the Callen-Welton formula, Sov. Phys. Usp. **30**, 168 (1987).
- 8 D.K.C. MacDonald, Physica **28**, 409 (1962).
- 9 I.A. Harris, Electron. Lett. **7**, 148 (1971).
- 10 G. Grau and W. Kleen, Solid-State Electron. **25**, 749 (1982).
- 11 L.B. Kiss, Solid State Comm. **67**, 749 (1988).
- 12 L. Reggiani, P. Shiktorov, E. Starikov and V. Gruz'inskis, Fluct. Noise Lett. **11**, 1242002 (2012)
- 13 H. Koch, D. J. van Harlingen and J. Clarke, Phys. Rev. Lett. **47**, 1216 (1981).
- 14 H.A. Haus and J.A. Mullen, Phys. Rev. **128**, 2407 (1962).
- 15 W. Kleen, Solid-State Electron. **30**, 1303-1304, (1987).
- 16 D. Abbott, B.R. Davis, N.J. Phillips, K. Eshraghian, IEEE Trans. Education **39**, 1 (1996).
- 17 L.B. Kish, "Zero-point energy in the Johnson noise of resistors: Is it there?", <http://vixra.org/abs/1504.0183> , <http://arxiv.org/abs/1504.08229>,

The spectral characteristics of steady-state Lévy flights in an infinitely deep rectangular potential well

A.A. Kharcheva,¹ A.A. Dubkov,¹ B. Spagnolo,^{2,3} and D. Valenti³

¹*Radiophysical Department, Lobachevsky State University,
Gagarin ave.23, 603950 Nizhni Novgorod, Russia
e-mail address: anya-kharcheva@yandex.ru
e-mail address: dubkov@rf.unn.ru*

²*Istituto Nazionale di Fisica Nucleare, Sezione di Catania, Via Santa Sofia 64, I-95123 Catania, Italy
e-mail address: bernardo.spagnolo@unipa.it*

³*Dipartimento di Fisica e Chimica, Università di Palermo and CNISM,
Unità di Palermo, Group of Interdisciplinary Physics,
Viale delle Scienze, Edificio 18, I-90128 Palermo, Italy
e-mail address: davide.valenti@unipa.it*

The anomalous diffusion in the form of Lévy flights is of permanent interest due to wide application in different areas of science¹⁻³. At the same time, to explore this phenomenon, unlike the standard Brownian motion, one requests to apply the complex apparatus of fractional derivatives and state non-trivial boundary conditions. As a result, the steady-state probability density function of the particle coordinate can be found only for some simple potential profiles⁴⁻⁶.

Investigation of the spectral properties of the steady-state Lévy flights in potentials with sufficiently steepness remains an unsolved problem. Here one can mention the exact result for the correlation time of Lévy flights in the symmetric quartic potential recently obtained in the article⁷.

Our main goal is to find the spectral power density of the coordinates of the particles by diffusion in the form of the steady-state Lévy flights in an infinitely rectangular deep potential well

$$U(x) = \begin{cases} 0, & |x| < L, \\ \infty, & |x| > L. \end{cases} \quad (1)$$

It should be emphasized that the exact formula for the spectral density of the coordinate of Brownian particle moving in the potential (1) is given by⁸

$$S(\omega) = \frac{2D}{\omega^2} \left(1 - \frac{1}{L} \sqrt{\frac{D}{2\omega}} \cdot \frac{\sinh L\sqrt{2\omega/D} + \sin L\sqrt{2\omega/D}}{\cosh L\sqrt{2\omega/D} + \cos L\sqrt{2\omega/D}} \right), \quad (2)$$

where D is the diffusion coefficient.

We start from the following general operator formula for the correlation function $K[\tau]$ of a stationary Markovian process $x(t)$ previously obtained in the paper⁹

$$K[\tau] = \left\langle x e^{\hat{L}^+(x)\tau} x \right\rangle_{st}, \quad (3)$$

where $\hat{L}^+(x)$ is the adjoint kinetic operator and $\langle \dots \rangle_{st}$ denotes averaging on the steady-state probability density function.

According to the Wiener-Khinchin theorem the spectral power density reads

$$S(\omega) = \int_{-\infty}^{\infty} K[\tau] \cos \omega\tau d\tau = 2\text{Re} \left\{ \tilde{K}[i\omega] \right\}, \quad (4)$$

where $\tilde{K}[p]$ is the Laplace transform of $K[\tau]$. From equation (4) we arrive at

$$\tilde{K}[p] = \left\langle x \frac{1}{p - \hat{L}^+(x)} x \right\rangle_{st}. \quad (5)$$

According to equation (5), one has to solve the following differential equation for the auxiliary function $\varphi(x)$

$$\hat{L}^+(x)\varphi(x) - p\varphi(x) = -x \quad (6)$$

and to find the average $\tilde{K}[p] = \langle x\varphi(x) \rangle_{st}$.

In particular, from equation (4) the correlation time can be calculated as

$$\tau_k = \frac{1}{\langle x, x \rangle} \int_0^{\infty} K[\tau] d\tau = \frac{S(0)}{2\langle x, x \rangle}, \quad (7)$$

where $\langle x, x \rangle$ is the variance of the particle coordinate.

Further we consider the anomalous diffusion in the form of Lévy flights in a potential $U(x)$ which is governed by the following Langevin equation for the particle coordinate $x(t)$

$$\frac{dx}{dt} = -\frac{dU(x)}{dx} + \xi_{\alpha}(t), \quad (8)$$

where α is the Lévy index ($0 < \alpha < 2$) and $\xi_{\alpha}(t)$ is the symmetric α -stable Lévy noise.

The corresponding fractional Fokker-Planck equation for the probability density function takes the form³

$$\frac{\partial P}{\partial t} = \frac{\partial}{\partial x} \left(\frac{dU}{dx} P \right) + D_{\alpha} \frac{\partial^{\alpha} P}{\partial |x|^{\alpha}}. \quad (9)$$

For potential (1) the boundaries at $x = \pm L$ are impermeable for particles, i.e. $P(x, t) = 0$ at $|x| > L$. In the stationary case, according to the definition of the spatial fractional derivative, equation (9) transforms to

$$\int_{-L}^L \frac{P_{st}(z) - P_{st}(x)}{|x - z|^{1+\alpha}} dz = 0. \quad (10)$$

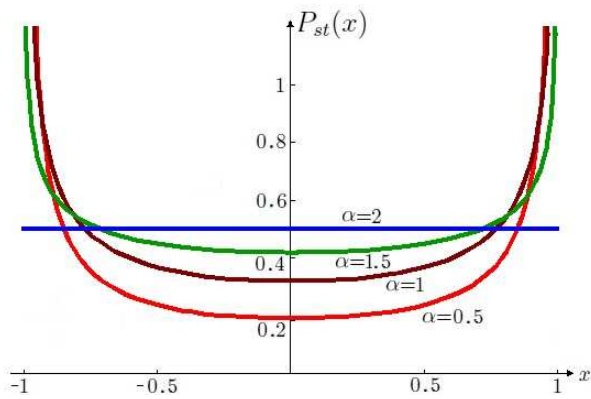


FIG. 1. Plots of stationary probability density for different values of the Lévy index α . The value of the parameter $L = 1$. The case $\alpha = 2$ corresponds to usual Brownian motion.

The solution of the integral equation (10) has been found

in the article¹⁰ and has the following form

$$P_{st}(x) = \frac{(2L)^{1-\alpha} \Gamma(\alpha)}{\Gamma^2(\alpha/2)(L^2 - x^2)^{1-\alpha/2}}, \quad (11)$$

where $\Gamma(x)$ is the Gamma function.

The stationary probability density function (11) for different Lévy index α is shown in Fig. 1. It should be noted that the result (11) in the case $\alpha = 1$ can be derived from the steady-state probability distribution for smooth potential $U(x) = \frac{\gamma}{2m} \left(\frac{x}{L}\right)^{2m}$, previously obtained in article⁶, in the limit $m \rightarrow \infty$.

Substituting the operator $\hat{L}^+(x)$ in equation (6), we need to solve the following integral equation for the function $\varphi(x)$

$$\int_{-L}^L \frac{\varphi(z) - \varphi(x)}{|x - z|^{1+\alpha}} dz - p\varphi(x) = -x. \quad (12)$$

The spectral characteristics in the steady state for asymmetric Lévy flights in potential profile considered still remain an open problem. Moreover, the role of Lévy index α to get steady-state characteristics in general potential profiles is still unknown.

¹ R. Metzler and J. Klafter, Phys. Rep. **339**, 1 (2000).

² A.V. Chechkin, et al., Adv. Chem. Phys. **133**, 439 (2006).

³ A.A. Dubkov, B. Spagnolo, and V.V. Uchaikin, Int. J. Bifurc. Chaos **18**, 2649 (2008).

⁴ A.V. Chechkin et al, Chem. Phys., **284**, 233 (2002).

⁵ A.V. Chechkin et al, J. Stat. Phys., **115**, 1505 (2004).

⁶ A.A. Dubkov and B. Spagnolo, Acta Phys. Pol. B **38**, 1745 (2007).

⁷ A.A. Dubkov, and B. Spagnolo Eur. Phys. J. Special Topics **216**, 31 (2013).

⁸ A.A. Dubkov, V.N. Ganin, and B. Spagnolo, Acta Phys. Pol. B **35**, 1447 (2004).

⁹ S.Yu. Medvedev, Radiophys. Quant. Electr. **20**, 863 (1977).

¹⁰ S.I. Denisov, W. Horsthemke, and P. Hänggi, Phys. Rev. E **77**, 061112 (2008).

Stationary states in 2D systems driven by Lévy noises

Bartłomiej Dybiec^{1*} and Krzysztof Szczepaniec^{†1}

¹*Institute of Physics, Jagiellonian University, Lojasiewicza 11, 30-348 Krakow, Poland*
*e-mail addresses: *bartek@th.if.uj.edu.pl, †kszczepaniec@th.if.uj.edu.pl*

I. INTRODUCTION

The description of complex interactions with surrounding can be provided by the Langevin equation, which in the overdamped limit takes the common form

$$\dot{x}(t) = f(x) + \zeta(t), \quad (1)$$

where $f(x)$ is a deterministic force, while $\zeta(t)$ represents complex interactions of a test “particle” with its environment. Usually it is assumed that the noise is white and Gaussian. Here, however we use the more general type of noise: i.e. Lévy noise, which is still of the white type but it naturally leads to heavy-tailed power-law fluctuations.

Heavy tailed fluctuation have been observed in versatilities of models including physics, chemistry or biology^{1,2}, paleoclimatology³ or economics⁴ and epidemiology⁵ to name a few. Observations of the so-called Lévy flights boosted the theory of random walks and noise induced phenomena into new directions^{6,7} which involve examination of space fractional diffusion equation (Smoluchowski-Fokker-Planck equation) and stimulated development of more general theory^{8,9}.

The present work¹⁰ addresses properties of stationary states in 2D systems driven by Lévy flights. The research performed here extends earlier studies of 1D systems¹¹⁻¹⁶ where analysis of symmetric and asymmetric Lévy flights in harmonic, superharmonic and subharmonic potentials have been presented.

II. MODEL

In 1D, a motion of an overdamped particle subject to the α -stable Lévy type noise is described by the Langevin equation

$$\frac{dx}{dt} = -V'(x) + \sigma\zeta_{\alpha,0}(t), \quad (2)$$

which can be rewritten as $dx = -V'(x)dt + \sigma dL_{\alpha,0}(t)$, where $L_{\alpha,0}(t)$ is a symmetric α -stable motion⁸, which is the generalization of the Brownian motion (Wiener process) to the situation when increments of the process are distributed according to α -stable densities, i.e. densities with power law asymptotics $p(x) \propto |x|^{-(\alpha+1)}$ with $0 < \alpha < 2$. $\zeta_{\alpha,0}(t)$ represents a white α -stable noise which is a formal time derivative of the symmetric α -stable motion $L_{\alpha,0}(t)$. Eq. (2) is associated with the fractional Smoluchowski-Fokker-Planck equation^{17,18}

$$\frac{\partial p(x,t)}{\partial t} = \frac{\partial}{\partial x} [V'(x)p(x,t)] + \sigma^\alpha \frac{\partial^\alpha p(x,t)}{\partial |x|^\alpha} \quad (3)$$

where $\frac{\partial^\alpha}{\partial |x|^\alpha} = -(-\Delta)^{\alpha/2}$ is the fractional Riesz-Weil derivative (laplacian) defined via its Fourier transform

$\mathcal{F} [-(-\Delta)^{\alpha/2} p(x,t)] = -|k|^\alpha \mathcal{F} [p(x,t)]$. Contrary to systems driven by white Gaussian noise, for $\alpha < 2$, the stationary solutions for Eq. (3) are not of the Boltzmann-Gibbs type and exist for potential wells which are steep enough¹⁵. The exponent c characterizing a potential well $V(x) = |x|^c$ needs to be larger than $2 - \alpha$, i.e. $c > 2 - \alpha$. Otherwise, the potential well is not steep enough in order to produce a stationary state. The stationary states (if exist) have power-law asymptotics

$$p_{\text{st}}(x) \propto |x|^{-(c+\alpha-1)} \quad (4)$$

determined by the stability index α and the exponent c characterizing steepness of the potential well^{13,15,16}. For $c = 2$ when the stationary density is of the same type (except the scale parameter) as the α -stable distribution associated with the underlying noise¹³, see Eq. (2).

Analytical formulas for stationary states for systems driven by α -stable noises with $\alpha < 2$ are known only in a very limited number of cases. For the quartic 1D Cauchy oscillator, i.e. $V(x) = \frac{1}{4}x^4$ with $\alpha = 1$, the stationary state of the fractional diffusion equation (3) is given by¹³ $p_{\text{st}}(x) = \sigma / [\pi(\sigma^{4/3} - \sigma^{2/3}x^2 + x^4)]$.

By analogy to 1D system^{17,18}, the bi-variate system is described by the following Langevin equation driven by the bi-variate α -stable Lévy type noise

$$\frac{d\mathbf{r}}{dt} = -\nabla V(\mathbf{r}) + \sigma\boldsymbol{\zeta}_\alpha(t). \quad (5)$$

Eq. (5) can be rewritten as $d\mathbf{r} = -\nabla V(\mathbf{r})dt + \sigma d\mathbf{L}_\alpha(t)$, where $\mathbf{L}_\alpha(t)$ is a bi-variate α -stable motion and $V(\mathbf{r})$ is an external potential.

Equation (5) is associated with the Smoluchowski-Fokker-Planck equation which has the general form

$$\frac{\partial p(\mathbf{r},t)}{\partial t} = \nabla \cdot [\nabla V(\mathbf{r})p(\mathbf{r},t)] + \sigma^\alpha \boldsymbol{\Xi} p(\mathbf{r},t), \quad (6)$$

where $\boldsymbol{\Xi}$ is the fractional operator due to bi-variate α -stable noise $\boldsymbol{\zeta}$, see Eq. (5). The diffusive term in Eq. (6) depends on the noise type.⁹ For the bi-variate α -stable noise with the uniform spectral measure the fractional operator $\boldsymbol{\Xi} = -(-\Delta)^{\alpha/2}$, i.e. it is the fractional laplacian defined via the Fourier transform $\mathcal{F} [-(-\Delta)^{\alpha/2} p(\mathbf{r},t)] = -|\mathbf{k}|^\alpha \mathcal{F} [p(\mathbf{r},t)]$.

The main scope of current research is to check if stationary states for harmonic and quartic potentials subject to bi-variate α -stable noises exist and what are their shapes depending on a noise type and noise parameters.

For the harmonic potential $V(x,y) = \frac{1}{2}(x^2 + y^2)$ and the uniform spectral measure the fractional diffusion equation (6) takes the form

$$\frac{\partial p}{\partial t} = \frac{\partial}{\partial x} (xp) + \frac{\partial}{\partial y} (yp) - (-\Delta)^{\alpha/2} p, \quad (7)$$

where $p = p(x, y, t)$. In the Fourier space Eq. (7) is equivalent to

$$\frac{\partial \hat{p}}{\partial t} = -k \frac{\partial \hat{p}}{\partial k} - l \frac{\partial \hat{p}}{\partial l} - (k^2 + l^2)^{\alpha/2} \hat{p}. \quad (8)$$

The characteristic function of the stationary density is

$$\hat{p} = \exp \left[-\frac{(k^2 + l^2)^{\alpha/2}}{\alpha} \right], \quad (9)$$

which is the characteristic function of the bi-variate α -stable density with the uniform spectral measure. Therefore, in 2D like in 1D, the stationary state of the harmonic 2D oscillator is the bi-variate α -stable density like the one of the underlying noise. In particular, for $\alpha = 2$, the stationary density is the bi-variate Gaussian distribution, while for $\alpha = 1$ it is the bi-variate Cauchy distribution.

For the quartic potential $V(x, y) = \frac{1}{4}(x^2 + y^2)^2$ and the uniform spectral measure the fractional diffusion equation (6) takes the form

$$\frac{\partial p}{\partial t} = \frac{\partial}{\partial x} [(x^2 + y^2)xp] + \frac{\partial}{\partial y} [(x^2 + y^2)yp] - (-\Delta)^{\alpha/2} p. \quad (10)$$

In the Fourier space Eq. (10) takes the form

$$\frac{\partial \hat{p}}{\partial t} = k \frac{\partial^3 \hat{p}}{\partial k^3} + k \frac{\partial^3 \hat{p}}{\partial k \partial l^2} + l \frac{\partial^3 \hat{p}}{\partial k^2 \partial l} + l \frac{\partial^3 \hat{p}}{\partial l^3} - (k^2 + l^2)^{\alpha/2} \hat{p}. \quad (11)$$

The stationary density fulfills

$$-\frac{\hat{p}'}{z} + [\hat{p}'' - z^\alpha \hat{p}] + z\hat{p}''' = 0, \quad (12)$$

where $z = \sqrt{k^2 + l^2}$. Exact solutions can be constructed by numerical methods only, e.g. Langevin dynamics see Fig. 1.

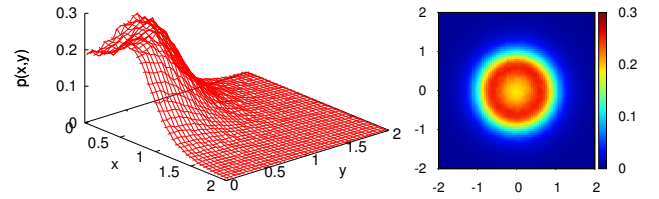


FIG. 1. Stationary states for the quartic potential $V(x, y) = \frac{1}{4}(x^2 + y^2)^2$ and α -stable noise with $\alpha = 1.0$, i.e. the Cauchy noise.

III. SUMMARY AND CONCLUSIONS

For the 2D harmonic potential stationary states reconstruct (up to rescaling) the noise distribution. In the limit of $\alpha = 2$ bi-variate α -stable densities converge to the bi-variate Gaussian distribution. Therefore, both types of bi-variate α -stable noises produces the same stationary state.

For the quartic potential stationary states are spherically symmetric and have local minima at the origin. With increasing value of the stability index α minima become shallower. Finally, in the limit of $\alpha = 2$ the Boltzmann-Gibbs distribution is reconstructed.

In general for single well potentials of $(x^2 + y^2)^{c/2}$ type (with $c \geq 2$) subject to action of bi-variate α -stable noises with uniform spectral measures stationary densities have power-law $(x^2 + y^2)^{-(c+\alpha)/2}$ asymptotics. Consequently, marginal densities have also power-law asymptotics with the exponent $-(c + \alpha - 1)$.

ACKNOWLEDGMENTS

This project has been supported in part by the grant from National Science Center (2014/13/B/ST2/020140). Computer simulations have been performed at the Academic Computer Center Cyfronet, Akademia Górniczo-Hutnicza (Kraków, Poland)

¹ *Lévy flights and related topics in physics*, edited by M. F. Shlesinger, G. M. Zaslavsky, and J. Frisch (Springer Verlag, Berlin, 1995).

² *Lévy processes: Theory and applications*, edited by O. E. Barndorff-Nielsen, T. Mikosch, and S. I. Resnick (Birkhäuser, Boston, 2001).

³ P. D. Ditlevsen, *Geophys. Res. Lett.* **26**, 1441 (1999).

⁴ R. N. Mantegna and H. E. Stanley, *An introduction to econophysics. Correlations and complexity in finance* (Cambridge University Press, Cambridge, 2000).

⁵ D. Brockmann, L. Hufnagel, and T. Geisel, *Nature (London)* **439**, 462 (2006).

⁶ A. A. Dubkov, B. Spagnolo, and V. V. Uchaikin, *Int. J. Bifurcation Chaos. Appl. Sci. Eng.* **18**, 2649 (2008).

⁷ T. Srokowski, *Phys. Rev. E* **79**, 040104 (2009).

⁸ A. Janicki and A. Weron, *Simulation and chaotic behavior of α -stable stochastic processes* (Marcel Dekker, New York, 1994).

⁹ G. Samorodnitsky and M. S. Taqqu, *Stable non-Gaussian random processes: Stochastic models with infinite variance* (Chapman and Hall, New York, 1994).

¹⁰ K. Szczepaniec and B. Dybiec, *Phys. Rev. E* **90**, 032128 (2014).

¹¹ S. Jespersen, R. Metzler, and H. C. Fogedby, *Phys. Rev. E* **59**, 2736 (1999).

¹² A. V. Chechkin *et al.*, *Chem. Phys.* **284**, 233 (2002).

¹³ A. V. Chechkin *et al.*, *Phys. Rev. E* **67**, 010102(R) (2003).

¹⁴ A. A. Dubkov and B. Spagnolo, *Acta Phys. Pol. B* **38**, 1745 (2007).

¹⁵ B. Dybiec, A. V. Chechkin, and I. M. Sokolov, *J. Stat. Mech.* P07008 (2010).

¹⁶ T. Srokowski, *Phys. Rev. E* **81**, 051110 (2010).

¹⁷ V. V. Yanovsky, A. V. Chechkin, D. Schertzer, and A. V. Tur, *Physica A* **282**, 13 (2000).

¹⁸ D. Schertzer *et al.*, *J. Math. Phys.* **42**, 200 (2001).

Typical pure states and rare events for quantum many-body systems

Takaaki Monnai¹

¹*Department of Materials and Life Sciences, Seikei University 180-8633, Tokyo, Japan
e-mail address: monnai@st.seikei.ac.jp*

I. INTRODUCTION

Recently, considerable attentions have been paid to the fluctuation of the entropy production for mesoscopic transports. In particular, the tails of the probability distribution represent rare but important phenomena for the stochastic thermodynamics. Experimentally, however, it is difficult to sample sufficient number of rare events. The rare events have been explored for a dragged Brownian particle in water, RNA stretching, the electron transport thorough quantum dots, to name only a few. This issue suggests an unsolved problem: How should we sample the rare events? Several numerical methods were developed for the efficient sampling.

In this presentation, we discuss on an alternative way to calculate the probability distribution on the basis of a single sample for quantum many-body systems. Our results treat whole the range of the probability distributions equally well. With the use of the single sample, we can accurately reproduce the full statistics of the ensemble, which is an assembly of many pure states. Hence, the difficulty of sampling the rare events is partially solved.

II. TYPICAL PURE NONEQUILIBRIUM STATES AND PROBABILITY DISTRIBUTION

We use the intrinsic thermal nature of a typical pure state $|\phi\rangle$ on the energy shell \mathcal{H}_E . Let us randomly sample a pure state $|\phi\rangle$ from \mathcal{H}_E according to the Haar measure. Then, for an arbitrary observable \hat{A} , the expectation value $\langle\phi|\hat{A}|\phi\rangle$ well agrees with the microcanonical average $\langle\hat{A}\rangle_{mc}$ with a probability almost unity^{1,2}. For large system size, the equivalence of ensembles claims that the canonical and microcanonical averages for the total system are quantitatively similar. And, we simply denote the microcanonical average as $\langle\hat{A}\rangle_{eq}$.

It is a challenging problem to explore the nonequilibrium processes on the basis of the pure state. We extend the availability of the thermal nature of typical states to the nonequilibrium processes which start from an equilibrium state³. We can also construct a class of typical pure nonequilibrium stationary states based on the scattering approach⁴, and calculate the stationary current.

The important point is that \hat{A} can be arbitrary higher order polynomials of local operators. For example, \hat{A} can be the exponential of a local operator. One might think that we can distinguish the pure and microcanonical states from the expectation values of higher correlations. However, this is not the case. Hence, we can calculate the characteristic function of, for example, the en-

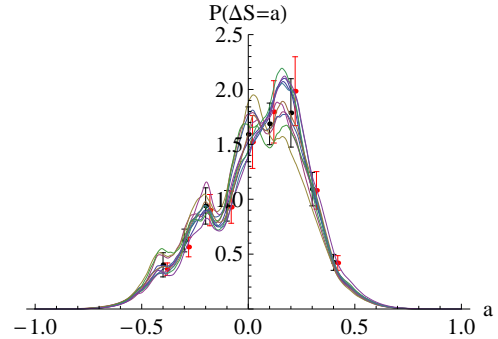


FIG. 1. The probability distribution $P_{eq}(\Delta S = a)$ for the microcanonical ensemble and $P_\phi(\Delta S = a)$ for pure states. The error bars show $P_{eq}(\Delta S = a)/\sqrt{d}$ (red) and fluctuation of 10 randomly sampled pure states (black).

ropy production $\langle U(t)^\dagger e^{i\xi\beta\hat{H}(t)} U(t) e^{-i\xi\beta\hat{H}(0)} \rangle_{eq}$ on the basis of the pure state $|\phi\rangle$. Here, $\hat{H}(t)$ is the Hamiltonian at time t , and $U(t)$ is the unitary evolution operator. By the Fourier transformation, we can calculate the probability distribution $P(\beta W = a)$ only from a fixed pure state $|\phi\rangle$ ³. The deviation roughly satisfies

$$P_{eq}(\beta W = a) = P_\phi(\beta W = a) \left(1 + \mathcal{O}\left(\frac{1}{\sqrt{d}}\right)\right), \quad (1)$$

where $P_{eq}(\cdot)$ and $P_\phi(\cdot)$ are the probability distributions calculated by the initial microcanonical ensemble and the pure state $|\phi\rangle$. Here, $d = \dim\mathcal{H}_E$ is the dimension of the initial energy shell at an energy scale E . Since d exponentially grows with the system size N , the error is negligible also for relatively small systems. The error estimation (1) is considered as model-independent, and determined only by the absolute value of the probability and the dimension.

In Fig. 1, we numerically calculate the probability distribution of the entropy production for $N = 10$ sites quantum spin chain which is externally perturbed by a time dependent magnetic field. Here, we ignore the boson or fermion statistics, however, the same argument essentially holds for these cases by constraining both the total energy and the number of particles. This issue is important to explore the energy and particle currents for quantum junctions in nonequilibrium steady states⁴. The Hamiltonian is

$$\hat{H}(t) = -J \sum_{j=1}^{N-1} \sigma_j^z \sigma_{j+1}^z + \sum_{j=1}^N \sigma_x + h(t) \sum_{j=1}^{N_s} \sigma_j^z + \gamma \sum_{j=1}^N \sigma_j^z. \quad (2)$$

Here, we use the ferromagnetic exchange energy $J = 1$, and the z component of the magnetic field is $\gamma = 0.5$.

The time-dependent magnetic field $h(t) = \sin 2\pi\omega t$ is acting on the subsystem $0 \leq j \leq N_s$ with $N_s = 2$ and $\omega = 0.4$. The parameter γ controls the integrability. We randomly sample 10 pure states from an energy shell \mathcal{H}_E , and calculate the probability distributions. The error bars show the theoretically predicted deviation from the microcanonical case, and the numerical fluctuation. The deviation is in agreement with the theoretical estimation.

The distribution function $P(\beta W = a)$ contains a continuous parameter a , and the error estimation above

holds for most of a as verified in Fig. 1. In particular, we can accurately reproduce the tails or large deviations.

ACKNOWLEDGMENTS

This work is partially supported by JSPS Grants-in-Aid for Young Scientists (B) (No. 26800206) from Japan.

¹ A. Sugita, Nonlinear Phenom. Complex Syst. **10** 192 (2007); cond-mat/0602625 [cond-mat.stat-mech] (2006)

² P. Reimann, Phys. Rev. Lett. **99** 160404 (2007)

³ T. Monnai, and A. Sugita, J. Phys. Soc. Jpn. **83** 094001 (2014)

⁴ T. Monnai, and K. Yuasa, Europhysics Letters, **107** 40006

Degradation Stochastic Resonance Concept: Benefits of Controlled Noise Injection in Adaptive Averaging cell-based Architecture

Nivard Aymerich¹, Sorin Cotofana² and Antonio Rubio³

¹Broadcom Networks Spain, S.L.

e-mail address: nivard@broadcom.com

²Delft University

e-mail address: S.D.Cotofana@tudelft.nl

³UPC, BarcelonaTech

e-mail address: antonio.rubio@upc.edu

I. INTRODUCTION

Future nano-scale technologies will exhibit high defect ratios, large parameter variability and reduced noise margins. Special architectures are needed to build reliable mid/large nanocircuits. Several architectures at different system levels have been proposed to build circuits based on nanoscale devices^{1,2}. Among them the architectures based on active redundant circuits, such as R-modular redundancy (RMR) or NAND multiplexing are designed to tolerate malfunctioning elements by combining the information of redundant circuits performing the same function. Such techniques are capable of protecting the system against transient and permanent errors without testing and reconfiguring but have a reduced capacity to tolerate static errors or defects in its original organization. These techniques distribute the information processing, storage, and communication along N identical elements. The redundant elements combined with some form of signal restitution—which recover the signal levels before the information is lost—permit the design of reliable circuits using unreliable elements. These structures are promising for nanotechnology. Of them the alternative named Averaging Cell (AVGc) has recently shown a very high efficiency as the decision element uses an analog computing principle. In a recent work³ authors have introduced the principle of adaptive-averaging cell (AD-AVG), architecture that is able to deal not only with permanent and dynamic but also with the independent time-varying variability of the elements caused by the degradation of components. In this abstract we present how AD-AVG-based computer design can benefit of the appearance of a counterintuitive degradation stochastic resonance effect.

II. THE AD-AVG ARCHITECTURE

The AD-AVG architecture, graphically depicted in Fig (1), is a fault-tolerant technique based on hardware redundancy. It calculates the most probable value of a binary variable from a set of error-prone physical replicas. The AD-AVG is demonstrated to tolerate high amounts of heterogeneous variability and accumulated degradation in the physical replicas.

The AD-AVG operation is based on a weighted average of R input replicas y_i of a binary variable y .

$$y' = \sum_{i=1}^R c_i y_i \quad \hat{y} = \begin{cases} V_{cc} & \text{if } y' > V_{cc}/2 \\ 0 & \text{if } y' < V_{cc}/2. \end{cases}$$

where c_i is the weight corresponding to replica i . The AD-AVG calculates the respective weights following a variability monitor and weight driver (Fig. 1)

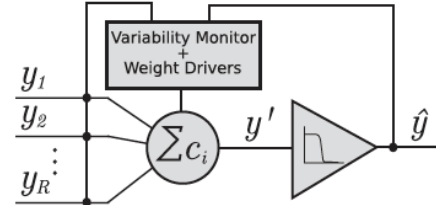


Fig. 1. AD-AVG architecture. Different weights are applied to inputs determined with the use of the monitor.

III. DEGRADATION STOCHASTIC RESONANCE (DSR)

We analyze (by analytical and simulating methods) what happens in an R-input AD-AVG when the variability of the input replicas increases independently as a consequence of degradation. A complete analysis can be found in a recent paper³. Fig. (2) depicts the resulting function yield of the AD-AVG cell against degradation, we assume noise in the variability monitor (σ_s).

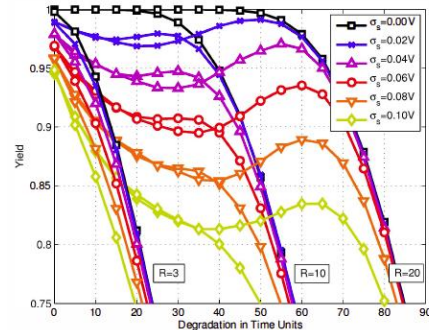


Fig. 2. Yield analysis of different size AD-AVGs against degradation. We consider different levels of noise in the variability monitor σ_s .

In the figure we clearly observe how the yield characteristic of the cell changes over time due to degradation stochastic resonance effect. Thanks to this effect it is possible to obtain higher factors of AD-AVG yield after specific amounts of degradation. Regarding this experiment on the DSR effect we can extract the following ideas:

- The DSR effect becomes more relevant in AD-AVGs with larger number of inputs.
- Given an AD-AVG in a particular situation of degradation in time and noise level it is not always the best option to use all the available replicas. There are situations in which less input replicas provide higher yield with the same degradation in time and noise in the variability monitor.

IV. CONTROLLED DEGRADATION STOCHASTIC RESONANCE IN AD-AVG CELLS

The main idea behind extending the DSR effect occurrence to get benefit of the resonance peak is to add virtual degradation to the system in order to force DSR peak degradation conditions regardless of its actual degradation level. Degradation affects the hardware and causes a variability increase in the input signals. Therefore, one way to achieve this virtual degradation is to increase the input variability levels to make the system behave like it would have been in a higher degradation status. It may be considered the option of adding a controllable noise generator to each of the input replicas to virtually increase the instantaneous amount of degradation in time up to the resonance point. This operation is feasible as long as the level of degradation in time is below the resonance point. Fig.3 shows the modification of the AD-AVG to inject independent controlled-level noise at the cell inputs. Fig. 4 shows the effect of behavior of a 20-input AD-AVG when we inject different levels of noise at the inputs σ_x .

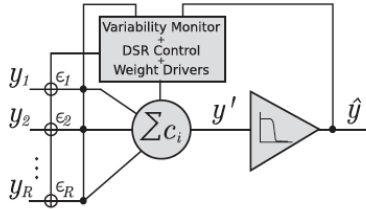


Fig. 3. Adaptive averaging cell with independent noise generators added to the inputs ϵ_i .

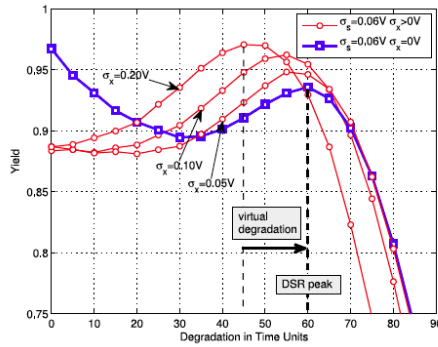


Fig. 4. Yield against degradation with different levels of noise. Thick blue line corresponds to the AD-AVG cell a noise $\sigma_x=0.06V$.

Given that we demonstrated that we can control the DSR peak position by means of input variation levels, we can make a step forward and define a strategy that allows us to get the maximum yield during all the circuit lifetime, by enabling DSR peak relocation as a consequence of degradation evolution. The basic principle of the DSR control is to check at runtime the instantaneous amount of degradation in terms of the input

variability estimators and update the input noise magnitude accordingly.

The target is to keep the reliability characteristic at the highest value regardless of the particular degradation level. In order to observe which is the input noise magnitude that we have to inject into the circuit in order to accomplish our goal, we present in Fig. (5) simulation results for a 20-input AD-AVG with noise in the Variability Monitor of magnitude $\sigma_s = 0.06 V$ sweeping over different input noise levels from $\sigma_x = 0 V$ to $\sigma_x = 0.9 V$.

Fig. 5 depicts in thick blue line the curve associated to the null input noise case, thin colored lines are the curves associated to the sweeping values of σ_x from 0 to 0.9 V. We also highlight in the figure in thick black line the curve that the yield follows when we apply the proper input noise magnitude at each degradation level. If we apply the proper noise magnitude, we can move along the involute of the thin colored curves obtaining a yield even higher than that provided by the resonance peak.

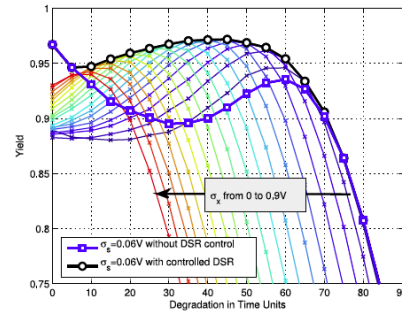


Fig. 5. Impact of adding noise to the input of the cell. The thick black line corresponds to the obtained yield when the noise is plied to maximize reliability.

V. CONCLUSIONS

In this paper, we present the DSR effect in the context of AD-AVG architectures. This counterintuitive effect implies an enhancement in the system reliability against hardware degradation for specific noise conditions. For example, the yield of a 20-input AD-AVG, with a noise level of 0.06 V in the Variability Monitor, decreases from 1 to 0.89 as the system degradation is increasing, then it grows up to 0.94 at the DSR peak, and finally decreases to zero when the system reaches its end of life. Moreover, in order to take the full advantage of the DSR effect, we propose to add controllable noise injectors to the AD-AVG inputs to virtually increase the amount of hardware degradation and create the DSR conditions regardless of the degradation level. By this method, we shift the characteristic yield to the DSR peak, regardless of the degradation level, and significantly enhance the system yield. Simulation results indicate that by applying the proper noise magnitude we can provide an optimum and nearly flat reliability level at any time before the DSR peak degradation level

ACKNOWLEDGEMENTS

This work has been funded by the Spanish MINECO and ERDF project TEC2013-45638-C3-2.

- ² M. Stanisavljevic et al., Nanotechnology, vol. 19, no. 46, pp.1-9, (2008)
- ³ N. Aymerich et al., IEEE Tr. on Nanotechnology, vol. 12, no.6, pp. 888-896, (2013).

¹ M. Mishra and S. Goldsein, Proc. Workshop Nonsilicon Computation (NSC) Conference, pp. 78-85, (2002).

Noise on resistive switching: a Fokker-Planck approach

G. A. Patterson,^{1,*} D. F. Grosz,^{2,3} and P. I. Fierens^{1,2,†}

¹*Instituto Tecnológico de Buenos Aires, Ciudad de Buenos Aires, Argentina*

²*Consejo Nacional de Investigaciones Científicas y Técnicas, Argentina*

³*Instituto Balseiro, San Carlos de Bariloche, Argentina*

Stotland and Di Ventra¹ were the first to present an analysis of the influence of noise on memristors. The interplay between noise and resistive switching has been further characterized, both experimentally and through simulations, in several papers²⁻⁴.

In this work we go back to their seminal paper, where they analyzed the influence of additive white Gaussian noise on a simple model of a memristor put forth by Strukov *et al.*⁵. By means of numerical simulations, they showed that the contrast between low- and high-resistive states is enhanced by the addition of internal noise in the presence of a weak harmonic driving signal, and provided an explanation in terms of a stochastic resonance phenomenon.

In this contribution, we aim at extending the work of Stotland and Di Ventra. Motivated by the potential application of resistive switching in the area of non-volatile data storage, we consider the case of non-harmonic driving signals. Noise is also shown to enhance the contrast between resistive states, and we provide an alternative explanation of the observed behavior in terms of the associated Fokker-Planck equation.

According to the model by Strukov *et al.*⁵, resistance in a memristor can be written as

$$R(x) = \alpha(1 - \delta R x), \quad (1)$$

where $\alpha, \delta R \in \mathbb{R}^+$ are adequate constants and $x \in [0, 1]$ is a state variable governed by the equation

$$\frac{dx}{d\tau} = \frac{4x(1-x)}{1-\delta R x} v(\tau), \quad (2)$$

where τ is a suitably normalized time variable and $v(\tau)$ is the (normalized) external voltage drive. It is easy to verify that $x(\tau)$ can be found as a solution to the equation

$$x^\beta(\tau) + g^\beta(\tau)x(\tau) - g^\beta(\tau) = 0, \quad (3)$$

where $\beta = (1 - \delta R)^{-1}$ and

$$g(\tau) = \frac{x(0)}{(1-x(0))^{\frac{1}{\beta}}} \exp \left\{ 4 \int_0^\tau v(t) dt \right\}. \quad (4)$$

In this section, we consider the case in which equation (2) is modified by additive white Gaussian noise $\eta(\tau)$ such that $\langle \eta(\tau) \rangle = 0$ and $\langle \eta(\tau)\eta(\tau') \rangle = \Gamma\delta(\tau - \tau')$. We emulate an alternating 0-1 writing-pattern of a memory device by considering a non-harmonic drive $v(\tau)$ which consists of a sequence $+1 \rightarrow -1 \rightarrow +1 \rightarrow \dots$ of pulses of width τ_b .

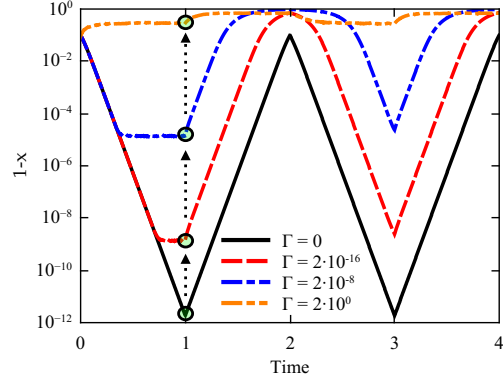


FIG. 1. Temporal evolution of the state variable x for several noise intensities. Results are the average of 1000 realizations.

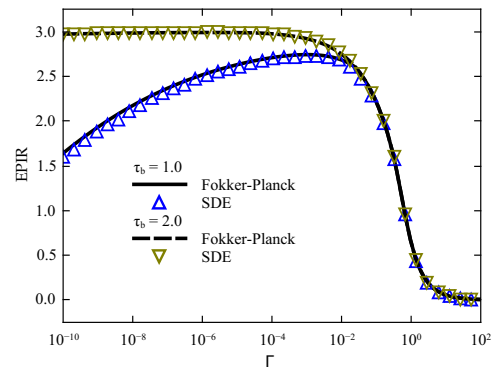


FIG. 2. EPIR ratio as a function of internal noise intensity. Solid and dashed lines correspond to quasi-analytic predictions developed in the text. Results corresponding to the average of 1000 realizations of the stochastic differential equation are represented by triangles.

Fig. 1 shows the temporal evolution of x for several noise intensities and $\tau_b = 1$. Observe that the maximum value that the state variable of x reaches after a $+1$ pulse is applied decreases as the noise intensity increases, as noted by circles and arrows. A usual way of quantifying the contrast between low (R_l) and high (R_h) resistance states is through the Electric Pulse Induced Resistance (EPIR) ratio given by $\frac{R_h - R_l}{R_l}$. As it can be observed in Fig. 2, the EPIR ratio is maximized for a certain optimal noise intensity and pulsewidth.

Results in Fig. 1 can be understood by resorting to the associated Fokker-Planck equation. Assuming that τ_b is

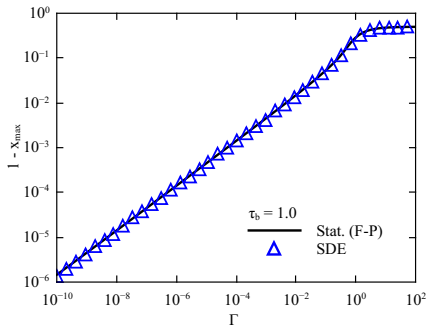


FIG. 3. Maximum value of x vs. noise intensity: approximation given by the stationary distribution (solid line) and by integration of the SDE (blue triangles).

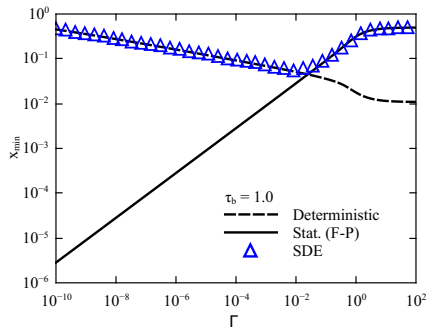


FIG. 4. Minimum value of x vs. noise intensity: approximation given by the stationary distribution (solid line), approximation given by the deterministic solution (dashed), and result of integrating the SDE (blue triangles).

large enough, we can work with its stationary solution

$$P(x, \tau_b) \approx P_s(x) \propto \exp \left\{ \frac{2}{\Gamma} \int_0^x v(\tau_b) \frac{4y(1-y)}{1-\delta Ry} dy \right\}, \quad (5)$$

and $\langle x(\tau_b) \rangle$ can be computed by numerical integration. Fig. 3 shows a good agreement between simulations of the stochastic differential equation (SDE) and results obtained through the stationarity hypothesis. As it is readily seen from equations (3)-(4), the deterministic evolution of $x(\tau)$ is highly dependent on the initial condition. One of the effects of noise is to erase the memory of the initial condition. Indeed, as expected, the stationary probability distribution in equation (5) does not depend

on the initial condition. However, the time of convergence to stationarity does depend on the initial condition. In general, the convergence time decreases as the noise intensity increases, *i.e.*, a higher noise intensity erases the memory of the initial condition faster.

We can try to use the stationarity hypothesis to compute the minimum value attained by x after a -1 pulse is applied, *i.e.*, $x(2\tau_b)$. Fig. 4 shows $\langle x(2\tau_b) \rangle$ as a function of the noise intensity (the stationary probability is similar to that in equation (5)). The behavior for low noise intensities deviates from that predicted by the stationary distribution. Indeed, for the given initial condition ($\langle x(\tau_b) \rangle$ in Fig. 3, the x value at the end of the previous $+1$ pulse), the pulsewidth τ_b is not large enough to allow for the convergence to stationarity and higher noise intensities are needed to erase the memory of the initial condition. Moreover, when the noise intensity is low, the value of $x(2\tau_b)$ can be approximated by the deterministic solution in equations (3)-(4).

Using the predictions based on the stationary probability distribution and the deterministic solution (for low noise intensities) in Figs. 3-4, we can estimate the EPIR ratio. The result is shown in Fig. 2 and agrees very well with simulations. Intuitively, the main effect of the added noise is to lower the value of x at the end of the first $+1$ pulse in such a way that $\langle x(\tau_b) \rangle$ is smaller than expected from the deterministic solution. For low noise intensities, this ‘new’ initial condition for the differential equation for $\tau > \tau_b$ results in a mean value of $x(2\tau_b)$ smaller than that in the noiseless case and, thus, leads to an enhanced EPIR ratio. For high noise intensities, values of the state variable x attained at the end of each pulse are independent of the initial conditions and determined by the stationary solution of the corresponding Fokker-Planck equation. Furthermore, as Γ increases, the distribution in equation (5) broadens, $\langle x_s \rangle$ tends to $1/2$ and the EPIR ratio goes to zero.

In summary, we introduced a Fokker-Planck approach to tackle the effect of internal noise on resistive switching, and used it to explain the resistive-contrast enhancement found in numerical simulations. It remains an open question whether such an approach can be applied to account for the beneficial role of external noise in resistive switching as it was reported in a previous work².

ACKNOWLEDGMENTS

We gratefully acknowledge financial support from AN-PCyT under project PICT-2010 # 121.

* Now at Center for Genomic Regulation, Barcelona Biomedical Research Park, Barcelona, Spain.

† Corresponding author: pfierens@itba.edu.ar

¹ A. Stotland and M. Di Ventra, Phys. Rev. **85** 011116 (2012).

² G. A. Patterson, P. I. Fierens, A. A. Garcia and D. F. Grosz, Phys. Rev. E **87**, 012128 (2013).

³ G. A. Patterson, P. I. Fierens and D. F. Grosz, Applied Physics Letters **103**, 074102 (2013).

⁴ G. A. Patterson, F. Sangiuliano Jimka, P. I. Fierens and D. F. Grosz, Physica Status Solidi (C) **12**, 187 (2015).

⁵ D. B. Strukov, G. S. Snider, D. R. Stewart and R. S. Williams, Nature **453**, 80 (2008).

Stochastic enhancement of absolute negative mobility

Lukasz Machura,¹ Jakub Spiechowicz,¹ and Jerzy Luczka¹

¹*Institute of Physics, Department of Theoretical Physics,
University of Silesia, Bankowa 12, 40-007 Katowice, Poland
e-mail address: lukasz.machura@us.edu.pl*

I. INTRODUCTION

Classical, dynamical systems have been analysed for ages. And they still are intensively studied in all contexts of nowadays science. They are the core part of applied maths, biology, chemistry, financial markets, physics (still!) and all the possible mixtures like econophysics, biophysics, biochemistry to name but a few. In general, one can write down short equation that creates endless possibilities for defining and later investigation of system in question

$$\ddot{x}(t) = F(x, \dot{x}, t). \quad (1)$$

Here x and t is the position and time respectively. Dot means the differentiation with respect to time. The F on the r.h.s. stands for any force that can act in the system like classical, non-classical, constant, time-dependent, deterministic or stochastic.

One of the global understanding of the Newton's Second Law of Motion is that the particle described by the eq. (1) follows the force it feels. If we push the coffee-cup lying on the table to the left it will move to the left. We cannot imagine other picture than that. It all happens because the forces are linear and we all drink coffee in the macro-world. In the micro-world, however, the linearities happen rarely. For finite temperatures noise effects appear, not just contributing to the loss of the system's dynamical abilities, but many times enhancing it¹. On the other hand, for very low temperatures chaos seems to be inevitable. This all ingredients makes the equation (1) alive and well, still attracting strong attention.

So, what is typical? If the linear systems are in minority, noise doesn't destroy the dynamics, chaos seems to be everywhere, and even positive mobility is not so distinctly common².

The absolute mobility can be defined as the ratio of the velocity of the particle to the force $\mu = \dot{x}/F$. This ratio is commonly positive. There are situations, however, where it can become negative and the system shows counter-intuitive dynamics. This phenomenon is called the abso-

lute negative mobility. It has been reported for the classical, non-linear system with periodic potential driven by the periodic time-dependent force, constant force f in the presence of the equilibrium thermal noise, typically modelled by the δ -correlated Gaussian white noise ξ of zero mean³

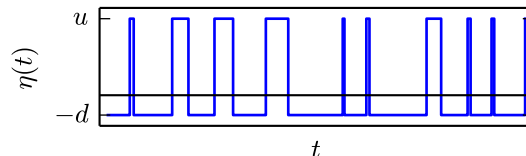
$$\ddot{x} = \sin(x) + a \cos(\omega t) + f + \xi(t). \quad (2)$$

For a certain conditions the absolute mobility can be negatively valued. The original numerical findings has been later confirmed experimentally⁴.

What if one would test the system not against constant bias force f , but instead apply stochastic force, with the same *average* value as the constant force above? The dynamics would change drastically, but surprisingly the effect stays if one would consider biased Poissonian white shot noise⁵. The question if the effect would be similar for other type of non-equilibrium random forces appears naturally. Maybe even the *enhancement* of the ANM effect can be possible for random noise? One of the natural candidates to test the idea seem to be the two-state noise also known as a random telegraph noise

$$\eta(t) = \{-d, u\}, \quad d, u > 0, \quad (3)$$

The probabilities of transition per unit time from state $-d$ to u and back is given by μ_d and μ_u respectively.



Over the talk we'll try to address those questions, formulate the problem and discuss the dynamics of the classical system (2) where the constant bias will be replaced by the mean value of the dichotomous noise

$$f = \langle \eta(t) \rangle = \frac{u\mu_d - d\mu_u}{\mu_d + \mu_u}. \quad (4)$$

¹ L. Gammaitoni, P. Hänggi, P. Jung, and F. Marchesoni, Rev. Mod. Phys. **70** 223 (1998)

² M. Kostur, L. Machura, P. Talkner, P. Hänggi, and J. Luczka, Phys. Rev. B **77** 104509 (2008)

³ L. Machura, M. Kostur, P. Talkner, J. Luczka, and P. Hänggi, Phys. Rev. Lett. **98** 040601 (2007)

⁴ J. Nagel, D. Speer, T. Gaber, A. Sterck, R. Eichhorn, P. Reimann, K. Ilin, M. Siegel, D. Koelle, and R. Kleiner, Phys. Rev. Lett. **100**, 217001 (2008)

⁵ J. Spiechowicz, J. Luczka and P. Hänggi, J. Stat. Mech. **P02044** (2013)

Cascade Amplification of Fluctuations

Michael Wilkinson, Marc Pradas¹ and Robin Guichardaz, Alain Pumir²

¹*Department of Mathematics and Statistics, The Open University,
Walton Hall, Milton Keynes, MK7 6AA, England,
e-mail address: m.wilkinson@open.ac.uk*

²*Laboratoire de Physique, Ecole Normale Supérieure de Lyon,
CNRS, Université de Lyon, F-69007, Lyon, France,*

I. INTRODUCTION

We consider a dynamical system which has a stable attractor and which is perturbed by an additive noise. Under some quite typical conditions, the fluctuations from the attractor are intermittent and have a probability distribution with power-law tails. We show that this results from a cascade of amplification of fluctuations due to transient periods of instability.

II. POWER-LAW FLUCTUATIONS

In a one-dimensional example the equation of motion might be

$$\dot{x} = v(x, t) + \sqrt{2D}\eta(t) \quad (1)$$

where $\eta(t)$ is a white noise signal (defined by (2) below) and D is the diffusion coefficient of the corresponding Brownian motion. We shall be primarily concerned with the case where D is small. The underlying system (without the noise term) is taken to be stable in the sense that its Lyapunov exponent λ is negative, implying that nearby trajectories converge. When a small noise term is added to the equation of motion, the trajectories do not reach the attractor of the underlying deterministic system. The separation of two trajectories, Δx , can be characterised by its probability density $P_{\Delta x}$. (Several stochastic variables are introduced here: we use P_X to denote the probability density function for a quantity X , and $\langle X \rangle$ to denote its expectation value). It might be expected that $P_{\Delta x}$ would be well-approximated by a Gaussian distribution, and for a generic class of models this expectation is correct. An example is the case where the underlying dynamical system is $\dot{x} = \lambda x$ (with $\lambda < 0$), which approaches the attractor $x = 0$. If this equation of motion is replaced by $\dot{x} = \lambda x + \sqrt{2D}\eta(t)$, where $\eta(t)$ is white noise, with statistics

$$\langle \eta(t) \rangle = 0, \quad \langle \eta(t)\eta(t') \rangle = \delta(t - t') \quad (2)$$

these equations describe an Ornstein-Uhlenbeck¹ process. The deviations from the fixed point have a Gaussian distribution in the limit as $t \rightarrow \infty$:

$$P_x = \sqrt{\frac{\lambda}{2\pi D}} \exp\left[-\frac{|\lambda|x^2}{2D}\right]. \quad (3)$$

provided $\lambda < 0$. The deviation Δx of two trajectories from each other is also Gaussian distributed, with

double the variance. We argue, however, that there is also a generic class of models for which the distribution $P_{\Delta x}(\Delta x)$ of separations of trajectories has power-law tails:

$$P_{\Delta x} \sim |\Delta x|^{-1+\alpha} \quad (4)$$

when Δ is large compared to $\sqrt{D/|\lambda|}$, (and we must have $\alpha > 0$ if this distribution is to be normalisable). The large excursions of $\Delta x(t)$ which are the origin of the power-law tails are a form of intermittency. The intermittency of $\Delta x(t)$ is illustrated in figure 1 for a model of colloidal particles in a turbulent flow. Figure 2 shows evidence that Δx has a power-law distribution in the same model, with an exponent which is independent of D . The power-law distribution has both an upper and a lower cutoff scale, and the lower cutoff scale decreases as $D \rightarrow 0$.

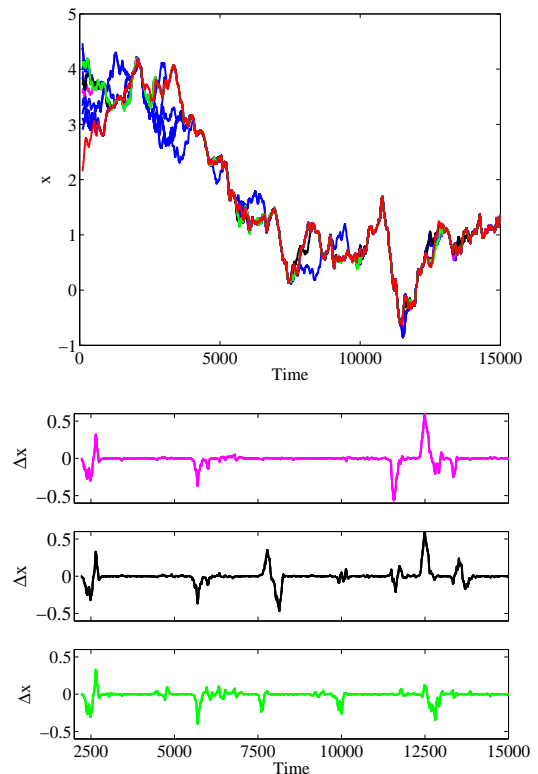


FIG. 1. **a** Set of trajectories of a model of colloidal particles in suspension. Different trajectories separate and recombine. **b** Intermittent separation of pairs of trajectories $\Delta x(t)$.

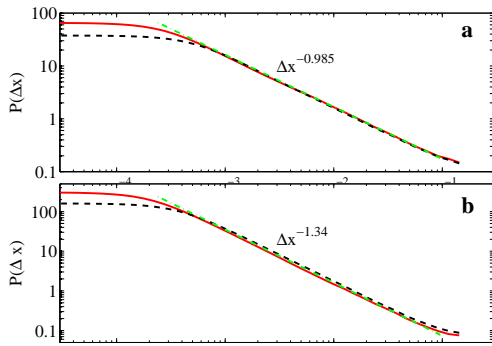


FIG. 2. The probability distribution $P_{\Delta x}$ for a model system, for two values of D ($D = 3 \times 10^{-10}$, full curve, and $D = 10^{-9}$, dashed curves), showing fits by a power law $|\Delta x|^{-(\alpha+1)}$.

In this talk we explain the origin of this intermittency and show how it can be quantified by making an analytical theory of the exponent α . The intermittency which is considered here is different from that which is discussed in most studies²⁻⁵, where intermittency arises because a system is just above a threshold of instability. The systems considered in this work are driven by external noise, and we are concerned with what might be termed *subcritical intermittency*, which is observed when the underlying system converges to an attractor. The intermittency effect discussed in this paper is only observed in non-autonomous systems, where the linearised dynamics in the vicinity of the attractor is fluctuating.

Beyond the point at which the underlying system becomes unstable, that is, when the Lyapunov exponent λ is greater than zero. The system ceases to have a point attractor, and instead it has a strange attractor, where phase points cluster on a fractal measure⁵. We argue that as λ approaches zero from below, the exponent α in (4) approaches zero from above. When $\lambda > 0$, the two-point correlation function of the strange attractor, $g(\Delta x)$, has a power-law dependence: $g(\Delta x) \sim |\Delta x|^{D_2-1}$ where D_2 is

the correlation dimension of the strange attractor⁶. The analogy with (4) suggests that the exponents are related by

$$\alpha = -D_2 \quad (5)$$

so that normalisable distributions of fluctuations correspond to negative values of D_2 . Equation (4) therefore gives a clear physical meaning to a negative fractal dimension.

III. EXPLANATION

The talk will present an explanation of the effect, expanding upon the summary below.

Consider the linearisation of Eq. (1) to give the separation between two nearby trajectories:

$$\delta \dot{x} = Z(t)\delta x + 2\sqrt{D}\eta(t), \quad Z(t) = \frac{\partial v}{\partial x}(x(t), t). \quad (6)$$

Note that when $D = 0$, $Z(t)$ is the logarithmic derivative of the separation $\delta x(t)$, and we can think of $Z(t)$ as being an *instantaneous Lyapunov exponent*. In the case of autonomous systems with an attractor, the attractor must be a fixed point in phase space, and $Z(t)$ approaches a constant $\lambda < 0$ as $t \rightarrow \infty$. In this case the fluctuations are described by an OU process and the distribution $P_{\Delta x}$ is Gaussian. In cases where the dynamical system is non-autonomous, $Z(t)$ need not approach a constant value. If the external driving is a stationary stochastic process, $Z(t)$ is a fluctuating quantity with stationary statistics. The origin of the power-law tails described by (4) is that the fluctuations are amplified during periods when $Z(t) > 0$. This noise amplification is independent of the initial amplitude, because the fluctuating quantity $Z(t)$ acts multiplicatively in Eq. (6). This leads to a stochastic cascade amplification process, whereby large amplitude fluctuations are built up by a succession of periods where $Z(t) > 0$. The power-law tail in the fluctuation distribution arises whenever $Z(t)$ is positive for some intervals of time, however short.

¹ G. E. Uhlenbeck and L. S. Ornstein, *Phys. Rev.*, **36**, 823-41, (1930).

² Y. Pomeau and P. Manneville, *Commun. Math. Phys.*, **74**, 189-97, (1980).

³ E. Ott and J.C. Sommerer, *Physics Letters A*, **188**, 39-47, (1994).

⁴ S. C. Venkataramani, T. M. Antonsen Jr., E. Ott and J. C.

Sommerer, *Physica D*, **96**, 66-99, (1996).

⁵ E. Ott, *Chaos in Dynamical Systems*, 2nd edition, University Press, Cambridge, (2002).

⁶ P. Grassberger and I. Procaccia, *Physica D*, **13**, 34-54, (1984).

⁷ M. Wilkinson, K. Gustavsson and B. Mehlig, *Europhys. Lett.* **89**, 5002 (2010).

Conversion of mechanical noise into useful electrical energy using piezoelectric 2D materials

Gabriel Abadal¹, Miquel López-Suárez², Warner Venstra³, Francesc Torres¹, Luca Gammaitoni² and Riccardo Rurali⁴
¹*Departament d'Enginyeria Electrònica, Universitat Autònoma de Barcelona, 08193 Bellaterra, Barcelona, Spain.*

E-mail address: gabriel.abadal@uab.cat

²*Department of Physics, University of Perugia, via A. Pascoli, 1, 06100 Perugia, Italy*

³*Kavli Institute of Nanoscience, Delft University of Technology, Delft 2628CJ, The Netherlands*

⁴*Institut de Ciència de Materials de Barcelona (ICMAB-CSIC) Campus de Bellaterra, 08193 Bellaterra, Barcelona, Spain*

I. INTRODUCTION

Understanding energy conversion processes at the nanoscale has become crucial for the future development of energy aware ICT technologies¹. In a new scenario where computing energy consumption is pushed to the fundamental limit², proposals oriented to power such a future *zeropower* ICT devices using the energy harvested from ambient sources have started to make sense. Vibration energy harvesting (VEH) technology has demonstrated to be a real alternative to standard electrochemical battery technology for powering portable devices from ambient mechanical energy in the form of vibrations, but only few large scale examples have shown to be useful in real applications³. Among all the challenging topics identified in VEH technology, enhancement of the harvested energy density and widening of the frequency response are two of the most intensively investigated. In previous works^{4,5,6}, we have demonstrated that both challenges can be simultaneously addressed by miniaturizing at the nanoscale the VEH transducers and engineering the non-linearity of their mechanical properties. Nanoelectromechanical structures (NEMS) based on piezoelectric 2D materials have been proposed for this aim. In particular, it has been theoretically demonstrated that tuning the bistable non-linearities of suspended h-BN monoatomic ribbons by a compressive strain induced buckling allows, from one hand, maximizing the energy harvested from wide band Gaussian vibration noise and, from the other, getting power density levels above the state of the art⁷. However, the problem of converting the energy of ambient mechanical noise into useful electrical energy by means of NEMS based on piezoelectric 2D materials is still open. To solve this problem it will be necessary to provide experimental evidence, currently lacking, but previously, a good model for the electromechanical processes involved in the conversion mechanism has to be developed. In this contribution we will present our last theoretical results of the dynamics of one atom thick h-BN suspended nanoribbons. Two computational procedures have been followed: (i) From one hand, we have obtained the deformation potential energy by first performing ab-initio calculations and then we have calculated the dynamics by solving numerically a Langevin type equation. (ii) Alternatively, we have treated also the dynamic part of the problem at the atomistic level by means of molecular dynamics calculations.

II. STATIC CALCULATIONS

Suspended h-BN nanoribbons along the x direction in a clamped-clamped configuration are brought under a compressive strain ε by bringing closer the two clamped ends as depicted in Fig. (1). Eventually, the structure is buckled and, consequently, two symmetric stable states are induced around the plane defined by the uncompressed configuration.

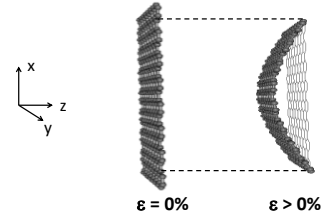


FIG. 1. Schematic representation of 1-atom thick h-BN clamped-clamped suspended nanoribbon in a non-compressed state, $\varepsilon=0\%$ (left) and a compressed $\varepsilon>0\%$ state (right).

The elastic potential energy, E , and the 2D longitudinal polarization P_{2D} , have been calculated using DFT as implemented within the SIESTA package⁸ in order to have a purely atomistic description and an electronic structure obtained from first-principles. Fig. (2) shows the change in the elastic energy, ΔE , with respect to the ground state energy defined as the energy of the flat and non-compressed ribbon, i.e. $E_{0,0}=E(z=0,\varepsilon=0)$, as a function of the deformation amplitude, z , corresponding to a h-BN nanoribbons 17 nm long and 1 nm wide.

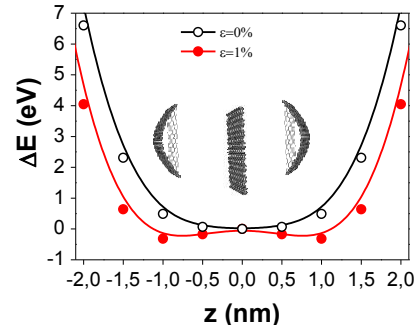


FIG. 2. Elastic energy change, ΔE , with respect to the ground state, $E_{0,0}$ (as defined by the energy of the flat, $z=0$, non-compressed, $\varepsilon=0$, ribbon) as a function of the vertical static displacement, z , of the central atoms of the h-BN ribbons. Dimensions are in all cases 17 nm long and 1 nm wide.

At a certain compression between 0% and 1%, h-BN ribbons relax the compression energy by buckling their structure and a bistable non-linearity is induced, which is characterized by two energy wells (around $z=\pm 1\text{nm}$) and an energy barrier which separation and height grow with compression^{5,6}.

III. DYNAMIC CALCULATIONS

The h-BN structures have been excited by an external force with a WGN (white Gaussian noise) spectrum of $F_{\text{rms}}=5\text{pN}$ of intensity. In these particular conditions, a Langevin equation coupled to a piezoelectric transduction equation have been solved for different compression values from 0% up to 1%. For $\epsilon=0\%$ and low compression values, the structure randomly vibrates around $z=0$ by the action of the noisy external force, since bistability is still not well defined. When compression increases (for $\epsilon>0\%$), the two energy wells start to influence the dynamics of the system and the structure start to eventually jump from one energy well to the opposite one. Such inter-well excursions grow in amplitude when compression increases, since inter-well distance also increases. However, energy barrier height also grows as compression increases and, consequently, when the compression reaches a certain value the barrier is too high and the structure gets stuck into one of the wells, where it vibrates in a similar random way as in the low compression regime.

Those three regimes can be identified in the z_{rms} curve of Fig. (3) (black open circles) and the corresponding P_{rms} curve (red filled circles): the z_{rms} value is larger in the inter-well jumping regime (around $\epsilon=0.3\%$) than in the low and high compression states, where no inter-well excursions are produced.

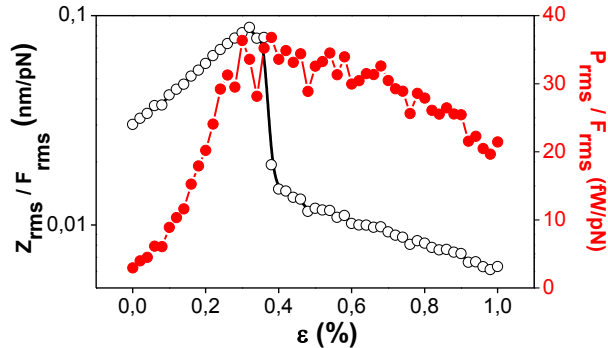


FIG. 3. Response normalized to the excitation force versus compression ϵ of the rms vertical position of central atoms, z_{rms} (black curves, left axis), and of the rms power delivered to the optimal load* (red curve, right axis). Quality factor is supposed to be $Q=100$. *The h-BN nanoribbon is electrically loaded by a $R_l=240\text{ k}\Omega$ resistor, which maximizes the electrical power transferred from the 2D piezoelectric transducer.

Similar results as those obtained by solving the Langevin equation (see Fig. (3)) can be derived by means of molecular dynamics (MD) simulations performed with the LAMMPS code⁹. Thermal excitation is considered in this case as the external vibrational source of noise and temperature is used as the control magnitude of the noise intensity. However, MD gives additional information about the modes of vibration of the nanoribbons and, more specifically, about the dynamics of the transitions between the two fundamental buckled states. In Fig. (4), three representative snapshots of the dynamics of a $100.8\text{ nm} \times 7.5\text{ nm}$ nanoribbon with a compression of 1.5 % are shown. An excited mode (snapshot b) with a node in the middle of the nanoribbon usually shows up between two fundamental modes (snapshots a and c) associated to the buckled states.

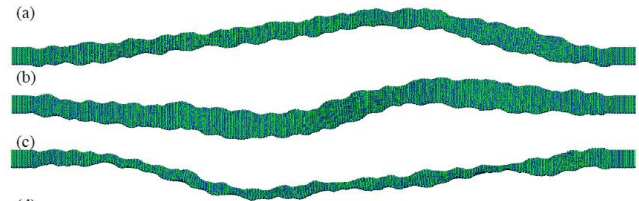


FIG. 4. Snapshots sequence of the dynamics of a $100.8\text{ nm} \times 7.5\text{ nm}$ h-BN nanoribbon subjected to a compression of $\epsilon=1.5\%$ and thermally excited at $T=300\text{K}$.

With the aim of improving the accuracy of the dynamic model of the compressed piezoelectric h-BN nanoribbons, we are currently introducing the effect of the non-linear damping terms associated to the ripples of the structure. Such instabilities have been previously attributed to the quality factor dependence on the compressive strain level, which has been experimentally observed in suspended nanoribbon structures made of other 2D materials. Additional relevant information derived from this non-linear damping effect is expected to provide new insights to advance on solving the problem of converting the energy of ambient mechanical noise into useful electrical energy.

ACKNOWLEDGEMENTS

Funding from the MINECO under contract No. TEC2013-41767-R (PISCES) and FIS2012-37549-C05-05 is greatly acknowledged.

¹ G. Fagas, L. Gammaitoni, D. Paul and G. Abadal, *ICT-Energy - Nanoscale Energy Management Concepts Towards Zero-Power Information and Communication Technology* (Intech Open Science, Croatia, 2013).
² <http://www.ict-energy.eu/>
³ <http://www.perpetuum.com/>
⁴ F. Cottone, H. Vocca, and L. Gammaitoni, *Phys. Rev. Lett.* **102**, 080601 (2009).

⁵ M. López-Suárez, R. Rurali, L. Gammaitoni and G. Abadal, *Phys. Rev. B* **84**(16) 161401 (2011).
⁶ M. López-Suárez, M. Pruneda, G. Abadal, R. Rurali. *Nanotechnology*, **25**, 175401 (2014).
⁷ M. López-Suárez, M. Pruneda, R. Rurali, G. Abadal, *MRS Proceedings* **1701**, mrs14-1701-nn03-29 (2014).
⁸ J.M. Soler, E. Artacho, J.D. Gale, A. Garcia, J. Junquera, P. Ordejon, D. Sanchez-Portal, *Journal of Physics: Condensed Matter*, **14**, 2745 (2002).
⁹ S. Plimpton, *J. Comp. Phys.* **117** (1), 1-19 (1995).

Classical and quantum non-linear dynamics in optomechanical systems

Yaroslav M. Blanter¹

¹*Kavli Institute of Nanoscience, Delft University of Technology, Lorentzweg 1, 2628CJ, the Netherlands
e-mail address: y.m.blanter@tudelft.nl*

I. INTRODUCTION

Light-matter interaction is one of the most complex phenomena in natural sciences. It has been studied for 400 years as classical optics and for 50 years as quantum optics, and it still remains an active research field. The simplest device which demonstrates light-matter interaction is an optomechanical cavity, regarded as a single mode of electromagnetic radiation confined between two mirrors. One of the mirrors is static, and another one is attached to a spring and can mechanically move. Light and mechanical motion are coupled by the radiation pressure¹. Massive effort in cavity optomechanics resulted in the recent years in a number of ground-breaking experiments, for example, demonstration of cooling of mechanical resonators to their quantum mechanical ground state, optomechanical squeezing of light, and observation of radiation pressure shot noise.

In optomechanical experiments, both cavities and mechanical resonators are perfectly linear.

An important development of the last few years was circuit (microwave) optomechanics — a technology in which mechanical elements are embedded into (superconducting) microwave cavities. Whereas microwaves and light are both electromagnetic waves, and the physical principles of cavity optomechanics and microwave optomechanics are similar, the setups and the operation regimes are very different. An important aspect we address here is that microwave cavities can be made intrinsically non-linear by adding Josephson junctions and can be integrated with non-linear mechanical elements, for example based on multi-layer graphene. This opens a whole new field of non-linear optomechanical systems.

The optomechanical system is described by a compact Hamiltonian, written in the second-quantized form as follows,

$$\hat{H} = \hbar\omega_c\hat{a}^\dagger\hat{a} + \hbar\omega_m\hat{b}^\dagger\hat{b} + \hbar g_0\hat{a}^\dagger\hat{a}(\hat{b}^\dagger + \hat{b}) . \quad (1)$$

Here, \hat{a} and \hat{b} are creation operators for photons and mechanical vibrations, respectively, the first term describes the optical or the microwave cavity with the frequency ω_c , the second one — the mechanical resonator with the frequency ω_m , and the last term corresponds to the radiation pressure coupling, with g_0 being the (single-photon) coupling constant. In optomechanical cavities, ω_c is the frequency of visible light (THz range), and therefore the mechanical frequency ω_m , which can range between kHz and GHz, is always several orders of magnitude less than ω_c . In microwave cavities, the cavity frequency is in the hundreds of GHz range, still much greater than ω_m .

A very common step in treating the Hamiltonian (1)

is to assume that the number of photons in the cavity is large. Then the coupling term can be linearized, and the Hamiltonian becomes

$$\hat{H} = \hbar\omega_c\hat{a}^\dagger\hat{a} + \hbar\omega_m\hat{b}^\dagger\hat{b} + \hbar g(\hat{a}^\dagger + \hat{a})(\hat{b}^\dagger + \hat{b}) , \quad (2)$$

where g is the so-called multi-photon coupling. It is related to the single-photon coupling by $g = g_0\sqrt{N}$, where N is the average number of photons in the cavity. In the experiments, this number can be made very big, and therefore g is much stronger than g_0 , sometimes by several orders of magnitude. In contrast to the non-linear Hamiltonian (1), (2) is linear and thus represents a significant simplification.

II. CLASSICAL SQUID GEOMETRY

A simple example of a non-linear microwave cavity of a superconducting quantum interference device (dc SQUID), a superconducting loop with two junctions. dc SQUID is a very sensitive detector of magnetic field. If one of the arms of the SQUID is suspended and vibrates, the sensitivity is sufficient to detect these mechanical vibrations via the variation of the flux. This mechanism of detection of mechanical oscillations was proposed theoretically^{2,3} and demonstrated experimentally⁴.

Subsequent experiments demonstrated strong backaction at low voltages in a partially suspended SQUID (the mechanical frequency and the quality factor of the mechanical resonator were affected by the biasing conditions of the SQUID, such as the current bias and the magnetic flux)⁵ and even self-sustained oscillations in a fully suspended (torsional) SQUID⁶.

This is a purely classical problem, which has been solved theoretically by considering classical equations of motion. The two Josephson junctions were modeled in the framework of the resistively and capacitively shunted junction model, when a current-biased junction is represented as a combination of three circuit elements connected in parallel — a Josephson junction proper, a resistor, and a capacitor. The coupling between superconducting phases and the mechanical motion was provided by the position dependence of the magnetic flux and by the Lorentz force acting on the mechanical resonator. Rather than giving here the details of the calculation^{5,6}, we present here an argument which facilitates the understanding of the origin of the self-sustained oscillations. The equation of motion for the resonator reads

$$m\ddot{x} + m\omega_m Q^{-1}\dot{x} + m\omega_m^2 x = F \cos \omega t + \alpha \tilde{I} , \quad (3)$$

where m , Q , and x are the mass, the quality factor, and the coordinate of the (single-mode) mechanical oscillator,

the first term on the right hand side stands for the driving force, and the second term represents the Lorentz force and is proportional to the current through the suspended arm of the SQUID.

In practice, the dynamics of the mechanical resonator is several orders of magnitude slower than the dynamics of the phases of Josephson junctions. Furthermore, in the experiments the junctions were overdamped. In this situation, the current \bar{I} can be approximated by the time-averaged (with respect to the plasma frequency of the SQUID) value, $\bar{I} \approx C\dot{V} + V/R$, where $V/R = (I^2 - I_c^2)$, I is the bias current, and I_c is the flux-dependent critical current through the SQUID. The flux dependence of I_c provides the dependence of \bar{I} on x and \dot{x} , thus renormalizing the frequency and the quality factor in the oscillator. In particular, the renormalization of the quality factor originates from the term \dot{V} . Its sign depends on the magnetic field, and its value diverges at $I \rightarrow I_c$, thus providing a possibility for the negative effective quality factor — a necessary condition for self-sustained oscillations, observed in the experiment.

III. OPTOMECHANICALLY INDUCED ABSORPTION

One of the signatures of the quantum nature of electromagnetic radiation in optomechanical systems is electromechanically induced transmission / absorption (OMIT/OMIA), which is a sharp peak/dip in the transmission/reflection spectrum of the cavity exactly at the cavity frequency ω_c if the cavity is driven at the red-shifted frequency $\omega_c - \omega_m$. For a linear cavity, the peak is harmonic. It has been observed in several experiments, including a recent measurements in the microwave cavity with graphene membrane serving as one of the mirrors⁷.

The same device⁷ showed clear signs of non-linear behavior as the power of the probe increased. This behavior was due to mechanical non-linearities of the graphene membrane. We performed systematic theoretical studies of non-linear response of the microwave cavity coupled to a Duffing oscillator — the simplest model of a non-linear oscillator⁸. The main conclusions are as follows,

- The shape of the peak does not necessarily correspond to the response profile of a driven Duffing oscillator. Instead, the response develops a sharp peak without an inflection point.
- The depth of the OMIA dip is almost independent on the probe power, however, the position depends on it.
- At low probe powers, there is hysteretic behavior, which disappears at higher probe powers.

These theoretical conclusions are in a good agreement with experimental results.

IV. UNSOLVED PROBLEMS

Despite a great success of microwave optomechanics, there are currently more questions than answers in the field. The most interesting issue is how one can reliably manipulate with the mechanical resonator in the quantum regime, and, in particular, whether one can create non-classical states (defined as states with negative Wigner function). A superposition of two lowest mechanical Fock states has been previously achieved but not in the cavity geometry.

For a linear cavity, one can only transfer a Gaussian state of the cavity into a Gaussian state of the mechanical resonator. Thus, to create non-classical states, one needs non-linearity. To access the quantum regime, one needs strong coupling, and thus strongly coupled non-linear cavities become of interest.

Lifetime of quantum states of a mechanical resonator is not really well understood, and the mechanisms of decoherence are not understood at all. The decoherence in quantum non-linear mechanical systems will certainly be one of the most important issues in the coming research.

ACKNOWLEDGMENTS

This work was supported by the Netherlands Foundation for Fundamental Research on Matter (FOM).

¹ M. Aspelmeyer, T. J. Kippenberg, F. Marquardt, arXiv:1303.0733.

² X. Zhou, A. Mielzner, Phys. Rev. Lett. **97**, 267201 (2006).

³ M. P. Blencowe, E. Buks, Phys. Rev. B **76**, 014511 (2007).

⁴ S. Etaki, M. Poot, I. Mahboob, K. Onomitsu, H. Yamaguchi, H. S. J. van der Zant, Nature Physics **4**, 785 (2008).

⁵ M. Poot, S. Etaki, I. Mahboob, K. Onomitsu, H. Yamaguchi, Ya. M. Blanter, H. S. J. van der Zant, Phys. Rev. Lett. **105**, 207203 (2010).

⁶ S. Etaki, F. Kopschelle, Ya. M. Blanter, H. Yamaguchi, H. S. J. van der Zant, Nature Communications **4**, 1803 (2013).

⁷ V. Singh, S. J. Bosman, B. H. Schneider, Ya. M. Blanter, A. Castellanos-Gomez, G. A. Steele, Nature Nanotechnology **9**, 820 (2014).

⁸ O. Shevchuk, V. Singh, G. A. Steele, Ya. M. Blanter, in preparation.

Pauli-Heisenberg Oscillations in Electron Quantum Transport

Karl Thibault,^{1,*} Julien Gabelli,^{2,†} Christian Lupien,^{1,‡} and Bertrand Reulet^{1,§}

¹Département de physique, Université de Sherbrooke, Sherbrooke, Québec, J1K 2R1, Canada

²Laboratoire de Physique des Solides, Univ. Paris-Sud,

CNRS, UMR 8502, F-91405 Orsay Cedex, France

I. INTRODUCTION

Conduction of electrons in matter is ultimately described by quantum mechanics. Yet at low frequency or long time scales, low temperature quantum transport is perfectly described by this very simple idea: electrons are emitted by the contacts into the sample which they may cross with a finite probability^{1,2}. Combined with Fermi statistics, this partition of the electron flow accounts for the full statistics of electron transport³. When it comes to short time scales, a key question must be clarified: are there correlations between successive attempts of the electrons to cross the sample? While there are theoretical predictions¹ and several experimental indications for the existence of such correlations⁴⁻⁶, no direct experimental evidence has ever been provided.

In order to probe temporal correlations between electrons, we have studied the correlator between current fluctuations $i(t)$ measured at two times separated by τ , $C(\tau) = \langle i(t)i(t+\tau) \rangle$, where $\langle \cdot \rangle$ denotes statistical averaging. We calculate this correlator by Fourier transform of the detected frequency-dependent power spectrum of current fluctuations generated by a tunnel junction placed at very low temperature. The very short time resolution required to access time scales relevant to electron transport is achieved thanks to the ultra-wide bandwidth, 0.3-13 GHz, of our detection setup.

We report the measurement of the frequency-dependent noise spectral density of both thermal noise (no dc bias, various temperatures) and shot noise (low-est temperature, various voltage biases), from which we determine the current-current correlator in time domain $C(\tau)$. In complex quantum systems, the method we have developed might offer direct access to other relevant time scales related, for example, to internal dynamics, coupling to other degrees of freedom, or correlations between electrons.

In the following, the noise spectral density is expressed in terms of noise temperature : $T_N(f) = S(f)/(2k_B G)$.

II. RESULTS

Thermal noise spectroscopy. On Fig. 1, we show measurements of the noise temperature T_N vs. frequency for various electron temperatures T between 35 and 200 mK, when the sample is at equilibrium, *i.e.* with no bias ($V = 0$). We observe that at low frequency one has $T_N(0) = T$ which is the classical Johnson-Nyquist noise. At high frequency $hf \gg k_B T$, all experimental curves approach the zero temperature curve (theoretical dotted

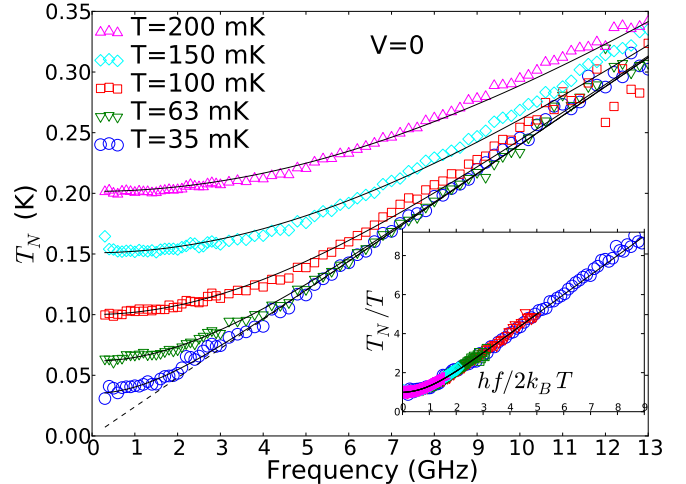


FIG. 1. **Equilibrium noise temperature vs. frequency for various electron temperatures T .** Symbols are experimental data and solid lines are theoretical expectations of Eq. (1).

Inset : Experimental rescaled noise temperature T_N/T vs. rescaled frequency $hf/(2k_B T)$.

black line) which corresponds to the so-called vacuum fluctuations $S_{vac}(f) = Ghf$. Our data are in very good agreement with the theoretical predictions given by⁷ :

$$S_{eq}(f, T) = Ghf \coth\left(\frac{hf}{2k_B T}\right). \quad (1)$$

Shot noise spectroscopy. Fig. 2 shows the measurements of T_N vs. frequency for various bias voltages V . The data are taken at the lowest electron temperature $T = 35$ mK. At low frequencies, *i.e.* $hf < eV$, one observes a plateau corresponding to classical shot noise $S = eI$. When $hf \gg eV$, the vacuum fluctuations take over and $S = S_{vac}(f)$. Black lines on Fig. 2 are the theoretical predictions of the out of equilibrium noise spectral density⁸

$$S(f, V, T) = \frac{1}{2} \left[S_{eq}\left(f + \frac{eV}{h}, T\right) + S_{eq}\left(f - \frac{eV}{h}, T\right) \right]. \quad (2)$$

Current-current correlator in time domain. The current-current correlator in the time domain is given by the Fourier Transform of Eq. (2) :

$$C(t, T, V) = C_{eq}(t, T) \cos\left(\frac{eVt}{\hbar}\right). \quad (3)$$

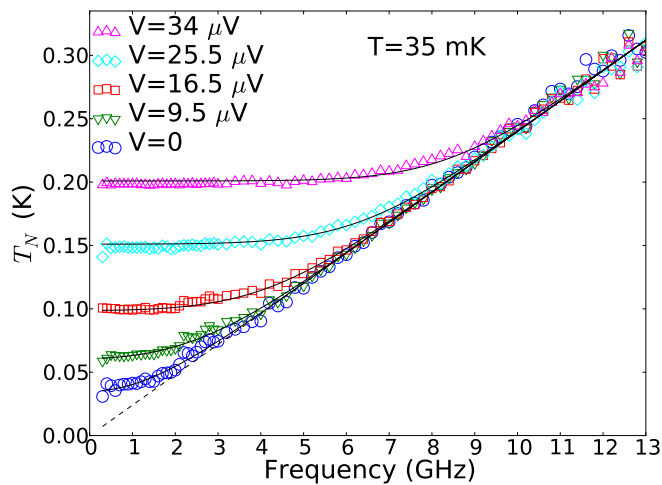


FIG. 2. **Out of equilibrium noise temperature vs. frequency for different dc voltage biases V at $T = 35$ mK.** Symbols are experimental data and solid lines are theoretical expectations.

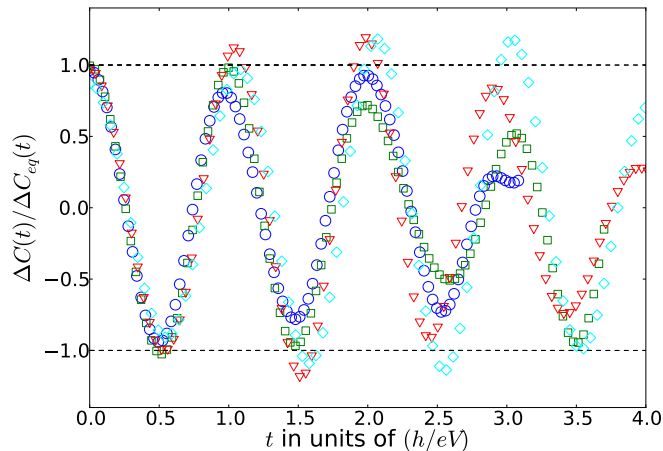


FIG. 3. **Rescaled current-current correlator in time domain vs. reduced time eVt/h for various bias voltages $V = 25.5, 30.6, 35.7$ and 40.8 μV .**

However, $S_{eq}(f)$ diverges as $|f| \rightarrow \infty$, so $C_{eq}(t, T)$ diverges at all times. To circumvent this problem, we define the *thermal excess noise* and its corresponding time domain correlator :

$$\begin{aligned} \Delta S(f, T, V) &= S(f, T, V) - S(f, T = 0, V) \\ \Delta C(t, T, V) &= \Delta C_{eq}(t, T) \cos\left(\frac{eVt}{\hbar}\right), \end{aligned} \quad (4)$$

We show experimental data for $\Delta C(t, V)/\Delta C_{eq}(t, T)$ as a function of the rescaled time h/eV on Fig. 3. This rescaling clearly demonstrates the oscillation period being h/eV , in agreement with Eq. (4).

III. INTERPRETATION

These oscillations are the result of both the Pauli principle and Heisenberg uncertainty relation. To see this, let us consider a single channel conductor crossed at $t = 0$ by two electrons of energy E and E' . According to Pauli principle, the energies must be different, $E \neq E'$. But how close can E and E' be? According to Heisenberg uncertainty relation, it takes a time $t_H \simeq \hbar/(|E - E'|)$ to resolve the two energies, so E and E' cannot be considered different for times shorter than t_H . This means that if one electron crosses at time $t = 0$, the second one must wait. Since $|E - E'| < eV$, one has $t_H > \hbar/eV$: there is a minimum time lag \hbar/eV between successive electrons. The regular oscillations we observe on ΔC are a direct consequence of this blockade and reflect the fact that electrons try to cross the sample regularly at a pace of one electron per channel per spin direction every \hbar/eV . The decay of $\Delta C(\tau)$ we observe at long time reflects the existence of a jitter which is of pure thermal origin.

At high bias voltage, $eV \gg k_B T, \hbar f$, the oscillation period \hbar/eV becomes so small that the electrons no longer have to wait before tunneling. This high energy regime is the classical limit where the current flowing through the junction is characterized by a Poisson distribution. The noise spectral density is thus given by the Schottky limit $S = eI$. At low bias voltage, there are correlations between successive tunneling electrons and the resulting current distribution is no longer Poissonian.

* Karl.Thibault@USherbrooke.ca

† Julien.Gabelli@U-PSud.fr

‡ Christian.Lupien@USherbrooke.ca

§ Bertrand.Reulet@USherbrooke.ca

¹ T. Martin and R. Landauer, Phys. Rev. B **45**, 1742 (1992).

² M. Büttiker, Phys. Rev. B **46**, 12485 (1992).

³ G. B. Lesovik and L. S. Levitov, Phys. Rev. Lett. **46**, 538 (1994).

⁴ M. Reznikov, M. Heiblum, H. Shtrikman, and D. Mahalu, Phys. Rev. Lett. **75**, 3340 (1995).

⁵ A. Kumar, L. Saminadayar, D. C. Glatli, Y. Jin, and B. Etienne, Phys. Rev. Lett. **76**, 2778 (1996).

⁶ N. Ubbelohde, K. Roszak, F. Hohls, N. Maire, R. J. Haug, and T. Novotný, Scientific Reports **2**, 538 (2012).

⁷ H. B. Callen and T. A. Welton, Phys. Rev. B **83**, 34 (1951).

⁸ A. J. Dahm, A. Denenstien, D. N. Langenberg, W. H. Parker, D. Rogovin, and D. J. Scalapino, Phys. Rev. Lett. **22**, 1416 (1969).

Effects of non-Gaussian α -stable noise sources on the transient dynamics of long Josephson junctions

Claudio Guarcello,^{1,2,*} Davide Valenti,¹ and Bernardo Spagnolo^{1,2,3}

¹*Dipartimento di Fisica e Chimica, Università di Palermo,
Interdisciplinary Theoretical Physics Group, Università di Palermo and CNISM,
Unità di Palermo, Viale delle Scienze, Edificio 18, 90128 Palermo, Italy*

²*Radiophysics Department, Lobachevsky State University,
23 Gagarin Avenue, 603950 Nizhniy Novgorod, Russia*

³*Istituto Nazionale di Fisica Nucleare, Sezione di Catania, Via S. Sofia 64, I-90123 Catania, Italy*

I. INTRODUCTION

The transient dynamics of noisy *Josephson junctions* (JJ) is studied by a theoretical analysis. A JJ is a mesoscopic system in which macroscopic quantities, as voltage and current, are directly dependent on the *order parameter* φ through the well-known Josephson relations. The parameter φ is the phase difference between the macroscopic wave functions describing the superconducting condensate in the two electrodes forming the device.

The behavior of Josephson junctions is strongly influenced by environmental perturbations, and specifically by the presence of noise source responsible for decoherence phenomena. The role played by random fluctuations in the dynamics of these devices has recently solicited a large amount of work and investigation on the effects both of thermal and non-thermal noise sources on their transient dynamics¹⁻⁴. In the last decade, theoretical progress allowed one to calculate the entire probability distribution of the noise signal and its cumulants, performing a *full counting statistics* of the current fluctuations². Moreover, the presence of non-Gaussian noise signals has been found experimentally in many systems^{1,3}. Non-equilibrated heat reservoir is an example of non-Gaussian noise source. Within this context, experimental investigations have been performed, studying the effect of sources of non-Gaussian fluctuations on the average escape time from the superconducting metastable state of a current biased JJ^{1,3}.

Recently, the characterization of JJs as detectors, based on the statistics of the escape times, has been proposed⁵⁻¹⁰. Specifically, the statistical analysis of the switching from the metastable superconducting state to the resistive running state of the JJ has been exploited to detect weak periodic signals embedded in a noisy environment^{6,7}. Moreover, the escape rate from one of the metastable wells of the tilted washboard potential of a JJ has been used to encode information on the non-Gaussian noise present in the input signal^{5,8-10}. After the seminal paper of Tobiska and Nazarov⁴, JJs used as threshold detectors allow to study non-Gaussian features of the current noise^{8,9}. Specifically, when a JJ leaves the metastable zero voltage state, it switches to a running resistive state and a voltage appears across the junction. Therefore, it is possible to measure directly in experiments the escape times or switching times and obtain their probability distribution¹¹⁻¹⁴.

Motivated by these studies, in view of a deeper understanding of the transient dynamics of a JJ interacting with a noisy environment, we carry out an analysis on the role of non-Gaussian noise sources in the switching times of a long JJ. The dynamics of this system is ruled by a nonlinear PDE, the perturbed *sine-Gordon* (SG) equation, which includes in this work a stochastic term. The noise signal is modeled by using different α -stable (or *Lévy*) distributions $S_\alpha(\sigma, \beta, \mu)$, where $\alpha \in]0, 2]$ is the *stability index* (or characteristic exponent) which determines how the distribution tails go to zero, β ($|\beta| \leq 1$) is an *asymmetry parameter*, and $\sigma > 0$ and μ are two real numbers which define the profile of the distribution and are called, for this reason, *shape parameters*. Specifically $\beta = 0$ ($\beta \neq 0$) gives a symmetric (asymmetric) distribution. These statistics allows to describe real situations, in which some variables of the studied system show abrupt jumps and very rapid variations called *Lévy flights*¹⁵. The behavior of short and long JJs in the presence of non-Gaussian noise sources was previously studied^{16,17} considering only few Lévy distributions, namely those with a probability density function for which an explicit form is known, that is Gaussian ($\alpha = 2$, $\beta = 0$), Cauchy-Lorentz ($\alpha = 1$, $\beta = 0$) and Lévy-Smirnov ($\alpha = 0.5$, $\beta = \pm 1$) distributions. In particular, the mean switching times (MST) and the mechanisms ruling the escape events from the metastable superconducting state were explored, considering also the effect of an external sinusoidal driving. Furthermore, the noise induced generation of nonlinear SG excitations along the junction, i.e. solitons and breathers, was taken into account. Fig. 1 shows the phase dynamics of junctions of different lengths ($L = 2$ and $L = 15$)¹⁷. Considering lengths larger than a certain threshold value, the junction switches to the resistive state by soliton creation (left panel of Fig. 1), that is by formation of 2π steps in φ . Otherwise, the junctions elements move between the metastable states as a whole (right panel of Fig. 1). Solitons are the pillars of the transient dynamics in long JJ, so the noise induced effects in the MST behavior has to strongly depend on the solitons originated by random fluctuations. The soliton solutions are strongly stable, appearing clearly in the I-V characteristic of the junction, and maintaining their shape after collisions or reflections at the boundaries. Instead a breather is a travelling SG solution formed by a soliton-antisoliton bounded couple, oscillating with a proper internal frequency. Many practical difficulties to

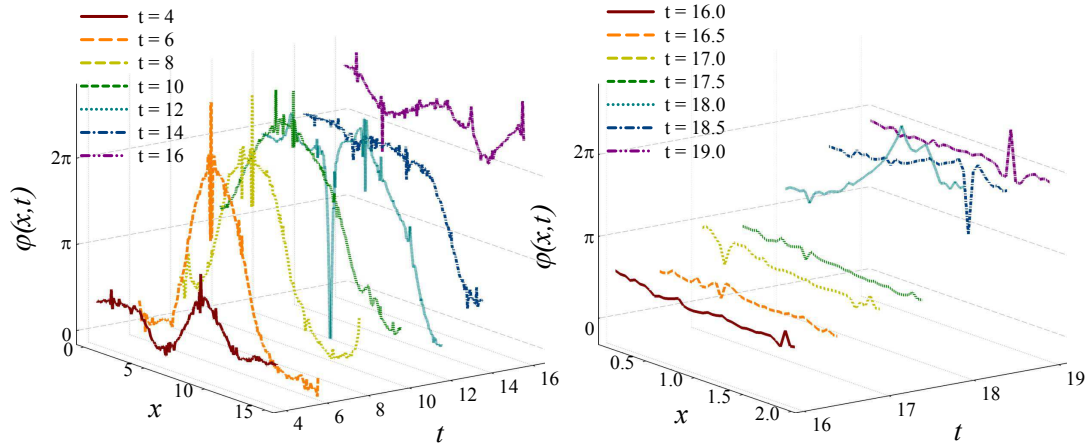


FIG. 1. LJJ phase dynamics during the switching to the resistive state using a Cauchy-Lorentz noise source. The length of junction is $L = 2$ (right panel) and $L = 15$ (left panel). The curves show the characteristic Lévy flights of the CL statistics inducing nonlinear excitations along the junction. Figure adapted from 17.

experimentally evidence breathers in long JJ exist. Indeed, breathers are unstable and rapidly decay in time, moreover the magnetic flux associated with a breather is zero, as well as the voltage difference across the junction. Therefore, an actual challenge in this field, both from experimental and theoretical point of view, is the capacity to generate, observe and sustain breathers in long JJ.

The mechanisms ruling the nonlinear modes excited in a SG system in the presence of non-Gaussian noise sources is a research field not completely explored. The focus of this work is therefore a deeper investigation of the transient dynamics of the phase difference φ in a long JJ, subject to noise sources with different α -stable distributions $S_\alpha(1, \beta, 0)$. In particular, the MST as a function of the noise intensity, the frequency of the driving force and the junction length is studied, exploring the complete spectrum of α and β values within the intervals $]0, 2]$ and $[-1, +1]$, respectively. Interesting nonmonotonic behaviors are expected to characterize the MST

data, namely *noise enhanced stability* (NES) and *resonant activation* (RA) effects. From a theoretical point of view, the appearance of breathers, induced by Lévy flights, was highlighted by Valenti *et al*¹⁷, modeling the noise source *only* by the CL statistics (see the narrow peaks in the curves of Fig. 1). When α -stable statistics different from Gaussian, Cauchy-Lorentz and Lévy-Smirnov are used, a lack of knowledge exists about the characteristics (rate of appearance, oscillation frequency, intensity) of nonlinear SG excitations induced by the noise. In particular, in view of a deeper comprehension of the role of the noise in the transient dynamics of long JJs, it has to be further studied how the features of different Lévy-distributed noises (fat tails, mode and limited space displacement around it) affect the SG nonlinear modes. Finally, another interesting open problem is the role of the breathers in the out of equilibrium dynamics of long JJs.

* claudio.guarcello@unipa.it

¹ B. Huard, H. Pothier, N. O. Birge, D. Esteve, X. Waintal, and J. Ankerhold, *Ann. Phys.* 16, 736 (2007).

² T. Novotný, *J. Stat. Mech.: Theory Exp.* P01050, (2009).

³ J. T. Peltonen, A. V. Timofeev, M. Meschke, T. T. Heikkil, and J. P. Pekola, *Physica E* 40, 111 (2007).

⁴ J. Tobiska, and Yu. V. Nazarov, *Phys. Rev. Lett.* 93, 106801 (2004).

⁵ H. Grabert, *Phys. Rev. B* 77, 205315 (2008).

⁶ G. Filatrella, and V. Pierro, *Phys. Rev. E* 82, 046712 (2010).

⁷ P. Adesso, G. Filatrella, and V. Pierro, *Phys. Rev. E* 85, 016708 (2012).

⁸ J. Ankerhold, *Phys. Rev. Lett.* 98, 036601 (2007).

⁹ E. V. Sukhorukov, and A. N. Jordan, *Phys. Rev. Lett.* 98, 136803 (2007).

¹⁰ M. Köpke, and J. Ankerhold, *New J. Phys.* 15, 043013 (2013).

¹¹ G. Sun, N. Dong, G. Mao, J. Chen, W. Xu, Z. Ji, L. Kang, P. Wu, Y. Yu, and D. Xing, *Phys. Rev. E* 75, 021107 (2007).

¹² C. Pan, X. Tan, Y. Yu, G. Sun, L. Kang, W. Xu, J. Chen, and P. Wu, *Phys. Rev. E* 79, R030104 (2009).

¹³ M. H. Devoret, J. M. Martinis, D. Esteve, and J. Clarke, *Phys. Rev. Lett.* 53, 1260 (1984).

¹⁴ M. H. Devoret, J. M. Martinis, and J. Clarke, *Phys. Rev. Lett.* 55, 1908 (1985).

¹⁵ A. A. Dubkov, B. Spagnolo, and V. V. Uchaikin, *Int. J. Bif. Chaos* 18, 2649 (2008).

¹⁶ G. Augello, D. Valenti, and B. Spagnolo, *Eur. Phys. J. B* 78, 225 (2010).

¹⁷ D. Valenti, C. Guarcello, and B. Spagnolo, *Phys. Rev. B* 89, 214510 (2014).

On the weak measurement of the electrical THz current: a new source of noise ?

D. Marian,¹ N. Zanghì,² and X. Oriols¹

¹*Departament d'Enginyeria Electrònica, Universitat Autònoma de Barcelona, Bellaterra 08193, Spain*
e-mail address: damiano.marian@uab.es

²*Dipartimento di Fisica dell'Università di Genova and INFN sezione di Genova, Italy*

I. INTRODUCTION

What does it mean measuring the electrical current at Tera Hertz (THz) frequency? Answering this questions is not easy neither from an experimental nor theoretical point of view. At such frequencies, the displacement current (time-dependent variations of the electric field) becomes even more important than the conduction (particle) current. For semi-classical electron device simulations, it is assumed that the interaction with an external measuring apparatus does not alter the properties of the system itself. On the contrary, for rigorous quantum device simulations, one must take into account the effect of the measuring apparatus on the measured system (the quantum device evolves differently if the system is measured or not!).

The traditional procedure to describe the interaction between a quantum system and a measuring apparatus is by *encapsulating* through a non-unitary operator. However, *which is the operator that determines the (non-unitary) evolution of the wave function when measuring the electrical THz current? Is it “continuous” or “instantaneous”?* with a “weak” or “strong” perturbation of the wave function?¹ To the best of our knowledge, no such THz-total-current operator has been presented.

In this conference we will discuss a present an original and accurate modelization for the quantum measurement of the total (conduction plus displacement) current at THz frequency. We will consider the interaction between the electrons in a metal surface, working as a sensing electrode, and the electrons in the device active region. We will show that the measurement of the THz current is weak (in the sense of Aharonov *et al.*²), implying a small perturbation of the quantum system and a new source of noise³.

II. A NOVEL QUANTUM APPROACH TO INCLUDE THE THZ MEASURING APPARATUS

The interaction between the quantum system and the measuring apparatus is studied here through quantum (Bohmian) trajectories, without the need of postulating an operator. In principle, we need to consider all the particles of Fig. 1 a). However, because of the large distance between the system and the ammeter, we consider only the interaction between the particle x_1 belonging to the quantum system, and the near electrons, $\mathbf{x}_2, \dots, \mathbf{x}_N$, in the metal surface S_m (see Fig. 1 b)). Therefore, we compute the total current on the surface S_L , while the rest of not simulated particles, which do not have a direct effect on the back-action suffered by the particle x_1 , are the responsible of translating the value of the to-

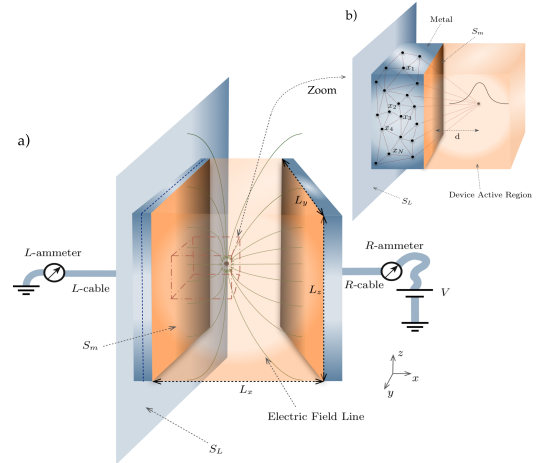


FIG. 1. a) Schematic representation of a two terminal device. The ideal surface S_L collects all the electric field lines. b) Zoom of the red region in Fig. 1 a). It is schematically depicted the coulomb interaction (red dashed lines) and the conditional wave function (black solid line) defined in Eq. (1).

tal current on S_L until the ammeter. The conditional (Bohmian) wave function⁴ of the system (i.e. the wave function of the quantum subsystem in the active region of the device) provides an excellent tool to numerically computing the interaction between the particles plotted in Fig. 1 b). Under the approximation reported in Ref. [5], the conditional (Bohmian) wave function evolves as

$$i\hbar \frac{\partial \psi(x_1, t)}{\partial t} = [H_0 + V] \psi(x_1, t), \quad (1)$$

where $V = V(x_1, \mathbf{X}_2(t), \dots, \mathbf{X}_N(t))$ is the conditional Coulomb potential felt by the system and H_0 is its free Hamiltonian. With capital letter, we denote the actual positions of the (Bohmian) particles. The total current, $I_T(t) = I_p(t) + I_d(t)$, is composed by the displacement component $I_d(t)$ plus the particle component, $I_p(t)$, defined as the net number of electron crossing a surface S_L . For simplicity, we shall focus only on the displacement component of the total current (no electrons crossing the surface where the current is measured). So, $I_d(t)$ can be computed as the time derivative of the flux F of the electric field $\mathbf{E}(\mathbf{r}, t)$ produced by all N electrons (system *plus* metal) on the large ideal surface S_L using the relation:

$$I_T(t) = \int_{S_L} \epsilon(\mathbf{r}) \frac{d\mathbf{E}}{dt} \cdot d\mathbf{s} = \sum_{i=1}^N \nabla F(\mathbf{X}_i(t)) \cdot \mathbf{v}_i(t), \quad (2)$$

where the flux F depends on each electron position and \mathbf{v}_i is the Bohmian velocity.^{3,6} From the numerical simula-

tion, we see that the quantum system is only slightly affected by the interaction with the electrons in the metal.³ On the other hand, in Fig. 2, we show that the instantaneous current measured in the surface S_L when considering the contribution of all the electrons in the metal or when considering only the electron in the device active region, i.e. without including the apparatus, differs considerably. The large fluctuations in the current reported in Fig. 2 means an additional source of noise due to the interaction of the electrons in the metal with the particle x_1 in the active region of the device (it can be seen as the unavoidable effect of plasmons in the sensing electrodes).

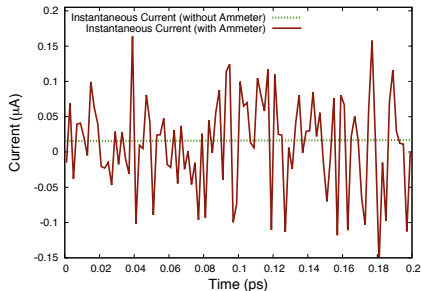


FIG. 2. Value of the total current. With solid line is reported the instantaneous value of the total current calculated from Eq. (2) (with ammeter) and with dashed lines obtained from a mean field simulation for particle x_1 alone (without ammeter).

III. WEAK MEASUREMENT

The measurement scheme present in Sec. II, implies that when the information of the measured total current is very noisy, the quantum system is only slightly perturbed, and vice versa.³ This fact is completely in agreement with the fundamental rules of quantum weak² measurement: if one looks for precise information, one has to pay the price of perturbing the system significantly (the so-called collapse of the wave function). On the other hand if one does not require such a precise information (for example, the instantaneous value of the total current seen in Fig. 2) one can leave the wave function of the system almost unaltered²). Repeating many times the same (numerical) experiment the mean value of the (weak) measured total current computed from Eq. (2) is equal to the value obtained without considering the ammeter. See Fig. 3. Thus, we show that the measurement of the high-frequency current is weak in the sense

of Aharonov *et al.*².

IV. CONCLUSIONS AND DISCUSSIONS

In this work, we have studied the quantum backaction associated to the quantum measurement of the THz electrical current of electronic devices. According to our analysis, when a large fluctuation in the current appears, the measurement of the THz current implies a slightly

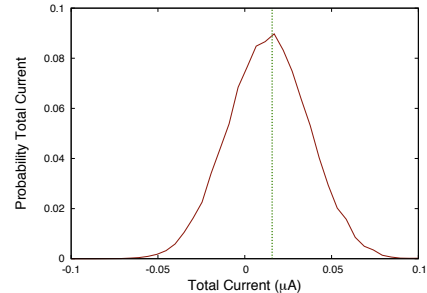


FIG. 3. Red solid line probability distribution of the measured total current from Eq. (2) in a time interval $T = 0.2$ ps of the simulation from 39000 experiments. Green dashed line mean value obtained from a mean field simulation.

perturbation of the quantum system, and vice versa. Additionally, we have also shown that the mean value obtained from repeating many times the same experiment provides the strong value of the measurement. Therefore, we conclude:

- The measurement of the total current in a quantum device at THz regime is a *weak measurement*.²
- The weak measurement implies that another source of noise needs to be considered when predicting high frequencies quantum transport.

Finally, it should also be mentioned that the weak measurement of the total current at high frequency opens a new path for envisioning experiments for reconstructing (Bohmian) trajectories and wave function in solid state systems, similar to those already performed for photons.⁷

ACKNOWLEDGMENTS

Work supported by the “Ministerio de Ciencia e Innovación” through the Spanish Project TEC2012-31330 and by the Grant agreement no: 604391 of the Flagship initiative “Graphene-Based Revolutions in ICT and Beyond”. N. Z. is supported in part by INFN.

¹ F. L. Traversa, G. Albareda, M. Di Ventra, and X. Oriols, Phys. Rev. A **87**, 052124 (2013).

² Y. Aharonov, D. Z. Albert, and L. Vaidman, Phys. Rev. Lett. **60**, 1351 (1988).

³ D. Marian, N. Zanghì, and X. Oriols, Proc. of IWCE, IEEE, 117 (2014).

⁴ D. Dürr, S. Goldstein, and N. Zanghì, J. Stat. Phys. **67**, 843-907 (1992).

⁵ X. Oriols, Phys. Rev. Lett. **98**, 066803 (2007).

⁶ G. Albareda, D. Marian, A. Benali, S. Yaro, N. Zanghì and X. Oriols, J. Comp. Electr. **12**(3), 405-419 (2013).

⁷ S. Kocis, *et al.*, Science **332**, 1170 (2011). J. S. Lundeen, *et al.*, Nature **474**, 188 (2011).

Elementary events and probabilities in time-dependent quantum transport

Wolfgang Belzig¹ and Mihajlo Vanevic²

¹*Department of Physics, University of Konstanz, D-78457 Konstanz
e-mail address: Wolfgang.Belzig@uni-konstanz.de*

²*Department of Physics, University of Belgrade, Studentski trg 12, 11158 Belgrade, Serbia
e-mail address: mihajlo.vanevic@gmx.com*

I. INTRODUCTION

A central problem of quantum transport is to find the statistics of electron transfer in a coherent quantum point contact (QPC) driven by an arbitrary time-dependent voltage. For the dc-case this question has been first addressed and theoretically answered by Levitov and Lesovik¹, who calculated the cumulant generating function (CGF) of probability distribution of the transferred charge $S_{t_0}(\chi) = \ln \sum_N P_{t_0}(N) e^{i\chi N}$. The astonishingly simple result in the zero-temperature limit was that the statistics is just binomial

$$S(\chi) = \frac{2eVt_0}{h} \sum_n \ln [1 + T_n (e^{i\chi} - 1)] , \quad (1)$$

where V is the applied bias voltage, t_0 is the observation time, and T_n are the transmission coefficients of the individual quantum channels. It should be emphasized that the result is nontrivial in that the Fermi sea of both contacts enters into the calculation.

The question of time-dependent driving has been addressed only recently. The CGF of a quantum contact can be expressed by the extended Keldysh action²

$$S(\chi) = \text{Tr} \ln [1 + T_n (\{\check{G}_L(\chi), \check{G}_R\} - 2) / 4] , \quad (2)$$

where now $\check{G}_{L/R}$ are the Keldysh Green's functions of the two leads. The counting field χ is introduced in Keldysh space via $\check{G}(\chi) = \exp(-i\chi\check{\tau}_K/2)\check{G}\exp(i\chi\check{\tau}_K/2)$, where $\check{\tau}_K$ is the current operator matrix. This formulation is valid for all possible quantum contacts comprising superconducting leads or time-dependent driving fields.

II. TIME-DEPENDENT VOLTAGE DRIVE

In time-dependent problems the Green's functions have to be considered as operators in a two-time (or two-energy) space, however the general formulation remains valid. Based on this observation it was shown that the electric current due to a voltage drive $V(t)$ with period T is composed of elementary events of two kinds³: unidirectional one-electron transfers determining the average current and bidirectional two-electron processes contributing to the noise only. These events are sketched in Fig. 1. As consequence the CGF takes the form

$$S(\chi) = S_{1p}(\chi) + S_{2p}(\chi) . \quad (3)$$

Here the first term describes so-called uni-directional one-particle processes, shown in Fig. 1(c) and is essentially

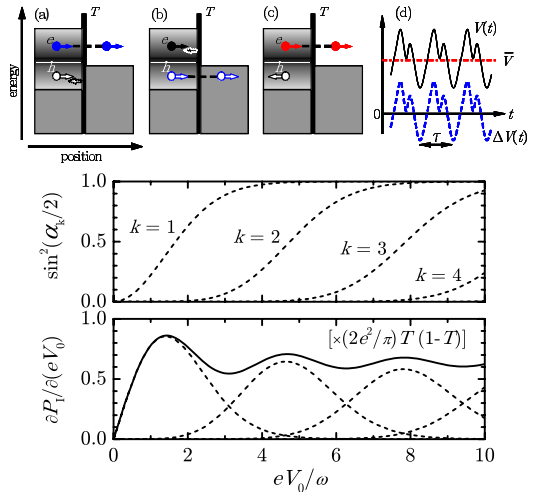


FIG. 1. Elementary events of a quantum point contact driven by a time-dependent voltage $V(t)$ with average \bar{V} shown in (d). (a) and (b) depict the two-particle events in which an electron-hole pair is created and either the electron or the hole is transmitted (and the other is reflected). (c) are the unidirectional events in which simply one electron is transferred. The lower two plots show the elementary event analysis for a harmonic voltage drive (see text for an explanation).

given by Eq. (1), in which V is the average voltage \bar{V} . The two particle events contribute as

$$S_{2p}(\chi) = \omega t_0 \sum_k \ln [1 + 2p_k TR (\cos(\chi) - 1)] . \quad (4)$$

Here $p_k = \sin^2(\alpha_k/2)$ is the probability of an elementary event. The above formulation allows to decompose the transport statistics of a voltage-driven QPC into its elementary constituents. An example is shown in Fig. 1 for a harmonic voltage drive $V_0 \cos(\omega t)$. The dependence of the probabilities on the amplitude of the drive are shown in the upper plot and the corresponding shot noise $P = -\partial^2 S(\chi) / \partial \chi^2 |_{\chi=0} / t_0$, which shows characteristic oscillations as function of the oscillation amplitude.

III. CONTROLLING ELEMENTARY EVENTS

One question emerging is how the elementary events can be controlled. A very interesting possibility was explored in⁶, where the authors have applied a biharmonic time dependent drive at the contact. The experimental result was that by adding an in-phase second harmonic of

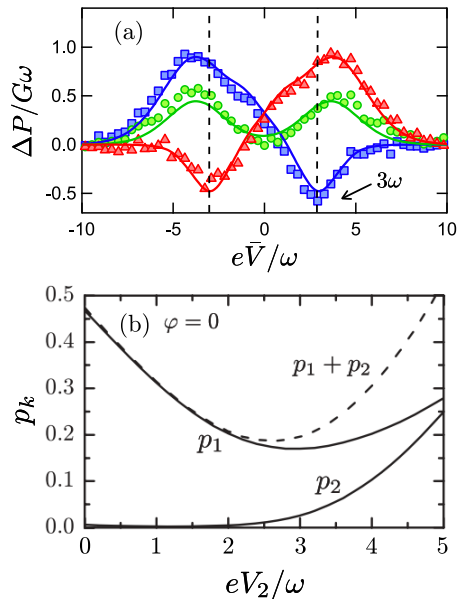


FIG. 2. (a) Difference ΔP between the noise generated by biharmonic drive $V(t) = \bar{V} + V_1 \cos(\omega t) + V_2 \cos(2\omega t + \varphi)$ and the noise generated by the first harmonic only. Parameters are $eV_1/\omega = 5.4$, $eV_2/\omega = 2.7$ and $\varphi = 0$ (blue), $\pi/2$ (green), and π (red curve). (b) Probabilities p_k of the electron-hole pair creations as a function of the amplitude V_2 for the biharmonic voltage drive with $e\bar{V}/\omega = 3$, $eV_1/\omega = 5.4$, and $\varphi = 0$.

a certain amplitude, it is possible to minimize the overall noise in the junction below the noise level produced by the first harmonic only, see Fig. 2 (a). This is because of a complex response of the Fermi sea upon time-dependent perturbation: the time-dependent drive mixes the electronic states of different energies which, in combination with the Pauli principle, gives a non-trivial charge transfer statistics. The explanation in terms of electron-hole pairs created in the system has been put forward in⁵. For a simple harmonic drive there is only one electron-hole pair generated per period with probability p_1 . When the second harmonic is in phase with the first one, the probability p_1 of the pair generation decreases as the amplitude V_2 of the second harmonic is increased, see Fig. 2 (b). As V_2 is increased further, the second electron-hole pair is generated with an increasing probability p_2 per period. For the amplitude $eV_2/\omega \approx 2.6$, the total probability $p_1 + p_2$ of the electron-hole pair creation exhibits a minimum. This gives the minimal excess noise which

has been observed in⁶. More fundamentally, it means the elementary excitations are controlled dynamically by shaping the time dependence of the driving voltage.

Another approach to control the excitations is to shape the voltage pulses as a Lorentzian, which should lead to special excitation states in which an exact integer number of charges is excited - so-called levitons⁷. As shown in Eq. 3, however this holds only for pulses of integer flux $\int dt V(t) = nh/e$ with the Planck quantum h , because otherwise additional electron-hole pairs are excited. Due to the finite temperature in the experiment⁸, however, the minimal excitations are not found exactly for integer flux. A full analysis in terms of elementary events in this case is still missing.

IV. UNSOLVED PROBLEMS

So far the analysis of the current fluctuations is restricted to the zero-frequency current correlators. This quantity only contains information on the probabilities of the charge transfer, viz. contained in \bar{V} and p_k . However the open problem is how to access the temporal shape of the excited wave function. On the theoretical side, the unsolved problem is how to approach these correlations in a quantum point contact between two many-body Fermi systems. The problem is complicated by the fact that a time-dependent voltage severely disturbs the Fermi sea even at zero temperature. Hence, it is in general not possible to resort to a simple single-particle picture. One way to attack this problem theoretically is to make use of the extended Keldysh-Greens function formalism² summarized in Eq. (2) and reformulate the methods developed for the time-dependent voltage-driven full counting statistics³ for time-resolved detection schemes. In this contribution we will formulate this unsolved problem of the theory of quantum transport and present first steps towards a solution.

ACKNOWLEDGMENTS

We thank J. Gabelli for useful discussion. WB acknowledges financial support by DFG through SFB 767 and the German Excellence Initiative through CAP. MV acknowledges MES project No. 171027.

¹ L. S. Levitov and G. B. Lesovik, Pis'ma Zh. Eksp. Teor. Fiz. **58**, 225 (1993) [JETP Lett. **58**, 230 (1993)].

² W. Belzig and Yu. V. Nazarov, Phys. Rev. Lett. **87**, 197006 (2001).

³ M. Vanevic, Y. V. Nazarov, and W. Belzig, Phys. Rev. Lett. **99**, 076601 (2007).

⁴ M. Vanevic, Y. V. Nazarov, and W. Belzig, Phys. Rev. B **78**, 245308 (2008).

⁵ M. Vanevic and W. Belzig, Phys. Rev. B **86**, 241306(R) (2012).

⁶ J. Gabelli and B. Reulet, Phys. Rev. B **87**, 075403 (2013)

⁷ L. S. Levitov, H.-W. Lee, and G. B. Lesovik, J. Math. Phys. **37**, 4845 (1996).

⁸ J. Dubois, T. Jullien, F. Portier, P. Roche, A. Cavanna, Y. Jin, W. Wegscheider, P. Roulleau, and D. C. Glattli, Nature **502**, 659 (2013).

Electron interferometry in quantum Hall edge channels

Jérôme Rech,¹ Claire Wahl,¹ Thibaut Jonckheere,¹ and Thierry Martin¹

¹*Aix Marseille Université, Université de Toulon,
CNRS, CPT, UMR 7332, 13288 Marseille, France
e-mail address: jerome.rech@cpt.univ-mrs.fr*

I. ELECTRON QUANTUM OPTICS

Electron quantum optics aims at transposing quantum optics experiments, allowing for the controlled preparation, manipulation and measurement of single electronic excitations in ballistic quantum conductors.

High-mobility 2D electron gases are a perfect testbed for conducting this task as several building blocks of quantum optics can readily be recreated in this context. First, the phase-coherent ballistic propagation of electrons is ensured by chiral edge states of the integer quantum Hall effect (IQHE). After propagation, these electrons collide at a quantum point contact (QPC), a tunable tunnel barrier mimicking a beamsplitter. The only missing ingredient finally appeared recently in the form of an on-demand single electron source (SES), opening the way to all sorts of interference experiments.¹

II. THE HONG-OU-MANDEL SETUP

The Hong-Ou-Mandel² (HOM) interferometer is a celebrated tool of quantum optics. It allows to probe the degree of indistinguishability of two photons. When they collide on a beamsplitter at the same time, they exit in the same outgoing channel, showing a sudden vanishing of the output coincidence rate. This bunching phenomenon is a direct consequence of the bosonic statistics.

In a recent work,³ we studied, from a theoretical standpoint, the outcome of this experiment at the single electron level, where two independently emitted electrons travel along counter-propagating opposite edge states and meet at a QPC, in the integer quantum Hall regime at filling factor $\nu = 1$. This goes beyond the simple transposition of an optics setup as several major differences exist between photons and electrons. In particular, electrons differ because of their statistics, the presence of the Fermi sea, and the possibility of holes.

We showed that valuable physics is encoded in the noise properties of the system, in particular the zero-frequency current correlations measured at the output of the QPC (R/L being right- and left-movers)

$$S_{\text{HOM}} = \int dt dt' [\langle I_R^{\text{out}}(t) I_L^{\text{out}}(t') \rangle - \langle I_R^{\text{out}}(t) \rangle \langle I_L^{\text{out}}(t') \rangle]. \quad (1)$$

We predicted that the current correlation exhibits a dip as a function of the time delay δT between injections, whose shape is in direct correspondence with the one of the injected wavepackets. When δT vanishes, this HOM

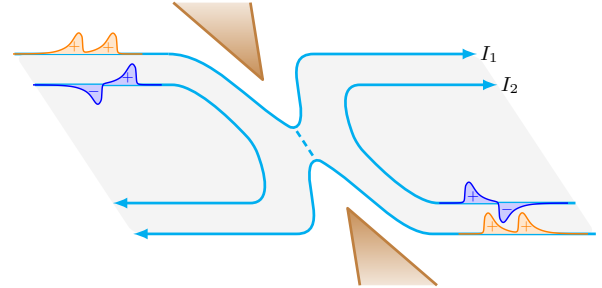


FIG. 1. The setup: two opposite edge states, each made out of two interacting co-propagating channels, meet at a QPC, and an electronic wavepacket is injected on both incoming outer channels.

dip extends down to zero signaling the existence of a unique outcome for the collision (a single electron in each output channel), a signature which we could tie back to the Pauli principle. Our work also suggests the possibility of asymmetric dips when different wavepackets collide, or even an HOM peak in the case of electron-hole collision.

The experimental realization of an electronic HOM interferometer in the IQHE soon followed,⁴ albeit performed in the slightly different regime of filling factor $\nu > 1$, due to technical constraints. The puzzle with these results is that although the HOM dip clearly appears on top of a flat background contribution, it does not vanish as predicted for $\nu = 1$, therefore signaling interesting effects happening beyond this simple picture. Indeed, another important difference between photons and electrons is the presence of interactions, and electron quantum optics offers a fascinating playground to explore the emergence of many-body physics. In a subsequent work,⁵ we proposed an interaction-based decoherence scenario which explains these striking experimental results.

III. NOISE AS A PROBE FOR FRACTIONALIZATION AND DECOHERENCE

We consider a quantum Hall bar at $\nu = 2$, in the strong coupling regime and at finite temperature. There, each edge state is made out of two co-propagating channels coupled via Coulomb interaction, as shown in Fig. (1). This is expected to lead to energy exchange between channels, and to charge fractionalization.

Our noise calculations rely on an accurate model of the injection of electrons, their propagation along the edges, and their scattering at the QPC. We introduce a prepared state consisting in a single exponential wavepacket

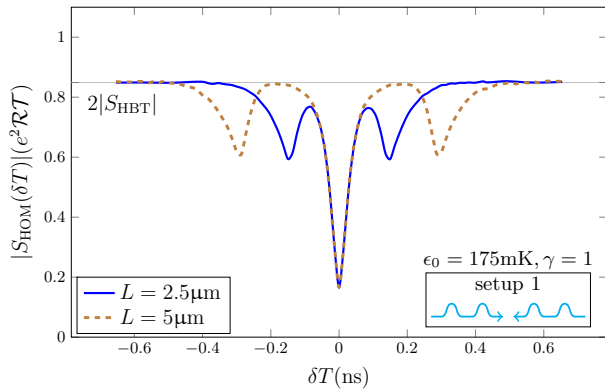


FIG. 2. Modulus of S_{HOM} as a function of the time delay for wide packets in energy (injection energy $\epsilon_0 = 175\text{mK}$ and energy resolution $\gamma = 1$) and two propagation lengths.

deposited on the outer channel, thus mimicking the SES in its optimal regime of operation. Each edge is then modeled as a chiral Luttinger liquid with both intra- and inter-channel interactions, which upon diagonalization naturally brings about two freely propagating collective modes: a fast charged mode and a slow neutral one. We compute the correlations of output current in the HOM setup as a function of the time delay between right- and left-moving injected electrons, and reveal three characteristic signatures in the noise. The interference pattern is provided in Fig. (2) for a given set of parameters.

First, a central dip appears for zero time delay, corresponding to the interference of both fast and slow-right-moving excitations with their left-moving counterparts. As observed in the experiment, this dip never quite reaches zero in our calculations, and its depth strongly correlates with the energy resolution of the injected wavepackets. This is actually a probing tool of the degree of indistinguishability of the excitations colliding at the QPC. Because of the strong inter-channel interaction, some coherence of the injected object is lost in the co-propagating channels which do not scatter, and this Coulomb-induced decoherence is responsible for the dramatic reduction of contrast of the HOM dip.

Interestingly, smaller satellite dips appear in the noise at finite δT and seem to vanish for well-resolved wavepackets in energy. These correspond to interference between excitations traveling at different velocities, and provide an interesting noise signature of the interference of charged modes with neutral ones.

A more quantitative comparison between experimental and theoretical results is currently under way,⁶ and

already shows a remarkable agreement with no adjustable parameters. However, a major challenge still remains unsolved: the HOM dip bears a striking independence on the injection energy from the SES. This is in stark contrast with the $\nu = 1$ case, where the shape of the dip is directly related to the overlap of the injected wavepackets and thus depends crucially on the injection energy. This naturally brings about the question of the content in energy of the excitations colliding at the QPC. What does the new many-body state resulting from interactions over the propagation length truly look like? Could the noise be used as a way to reconstruct the decohered state which tunnels at the QPC?

IV. THE FRACTIONAL CASE

Interactions dramatically change the nature of the excitations, and the HOM interferometry offers the possibility to probe the incoherent mixture of fractionalized electronic excitations induced by Coulomb interactions. A natural extension of this work consists in studying a system where the ground state itself is a strongly correlated state of matter: the fractional quantum Hall effect (FQHE). There, one would be dealing not with electrons, but with single quasiparticles with fractional charge and statistics which should lead to dramatically new physics.

This constitutes a challenge at various levels, as a lot of open questions remain, from the nature of the quasiparticle injector to the results of an interferometry setup in the spirit of the HOM one. Indeed, the single electron source is clearly not the best candidate to generate on-demand single quasiparticles in the FQHE. Can single quasiparticles be dynamically emitted? What setup would guarantee the emission of on-demand single quasiparticles with little to no charge fluctuations?

The link between the measurement of low frequency noise correlations and the statistics of the carriers is well known. HOM interferometry with photons or electrons allows to probe the statistics through second order coherence, whether this is also enough to access the fractional statistics of quasiparticles is still under debate and deserves to be explored.

ACKNOWLEDGMENTS

We are grateful to D. Ferraro, G. Fève, B. Plaças and P. Degiovanni for useful discussions.

¹ G. Fève et al., *Science* **316**, 1169 (2007).

² C.K. Hong, Z.Y. Ou and L. Mandel, *Phys. Rev. Lett.* **59**, 2044 (1987).

³ T. Jonckheere, J. Rech, C. Wahl and T. Martin, *Phys. Rev. B* **86**, 125425 (2012).

⁴ E. Bocquillon et al., *Science* **339**, 1054 (2013).

⁵ C. Wahl, J. Rech, T. Jonckheere and T. Martin, *Phys. Rev. Lett.* **112**, 046802 (2014).

⁶ V. Freulon et al., in preparation (2015).

Functional approach to heat-exchange, application to the spin boson model: from Markov to quantum noise regime.

Matteo Carrega,¹ Paolo Solinas,² Alessandro Braggio,³ Maura Sassetti,⁴ and Ulrich Weiss⁵

¹*SPIN-CNR, Via Dodecaneso 33, 16146 Genova, Italy*
e-mail : matteo.carrega@spin.cnr.it

²*SPIN-CNR, Via Dodecaneso 33, 16146 Genova, Italy*

³*SPIN-CNR, Via Dodecaneso 33, 16146 Genova, Italy*

⁴*Dipartimento di Fisica, Università di Genova, Via Dodecaneso 33, 16146 Genova, Italy*

⁵*II. Institut für Theoretische Physik, Universität Stuttgart, D-70550 Stuttgart, Germany*

I. INTRODUCTION

The emerging field of quantum thermodynamics aims to extend basic concepts of thermodynamics at the nanoscale. Indeed lowering the dimension of a system, fluctuations and quantum effects become crucial and classical thermodynamics cannot be simply applied. The question of how a small system exchanges heat and energy with a bigger one is very important both from technological and fundamental point of view. A deep understanding of heat exchange at the nanoscale is necessary in view of the realization of quantum devices such as quantum heat engines which could have great technological impact. Despite much recent efforts, the thermodynamics of quantum systems is still poorly understood, at least when compared to its classical counterpart. Here we aim to go a step forward towards a microscopic and rigorous description of heat exchange in quantum system.

II. PATH-INTEGRAL APPROACH

We consider a quantum system coupled to a thermal reservoir and the energy flows between them. Starting from very few and plausible assumptions, we approach the problem with the path integral technique. In this framework we can write a general heat influence functional which embodies all the dissipative mechanisms and allows us to study heat processes.

We present the exact formal solution for the moment generating functional which carries all statistical features of the heat exchange process for general linear dissipation. We derive an exact formal expression for the transferred heat and applied this formalism to the dissipative two level system. We show that the difference between the dynamics of the heat transfer and the dynamics of the reduced density matrix (RDM) is an additional time-nonlocal correlation function which correlates intermediate states of the RDM with the final state.

III. APPLICATION TO THE TWO LEVEL SYSTEM

As an application, we concentrate on a two level system, described by the Hamiltonian

$$H_S = -\frac{\Delta}{2}\sigma_x - \frac{\epsilon(t)}{2}\sigma_z \quad (1)$$

where Δ is the tunneling amplitude and $\epsilon(t)$ describe a generic time-dependent external bias. The two level system is coupled to a thermal bath and we calculate, by means of the heat influence functional, the average heat and the heat power exchanged between them.

To investigate the potential of the present method, we calculate the dynamics of the average heat power and average heat in analytic form for weak Ohmic dissipation both in the Markovian regime relevant at high temperatures and in the non-Markovian quantum noise regime holding when temperature is of the order of the level splitting Ω or lower. In the latter regime, the heat is represented by a convolution integral which involves the population and coherence correlation functions of the dissipative two level system and the polarization correlation function of the reservoir. In particular we arrive to the compact form:

$$\begin{aligned} \langle P(t) \rangle &= \frac{\pi K}{2} \delta^2 - \frac{\Delta}{2} \int_0^t d\tau L'(\tau) \\ &\left(\langle \sigma_x(t-\tau) \rangle_s \langle \sigma_z(\tau) \rangle_s - \langle \sigma_z(t-\tau) \rangle_a \langle \sigma_x(\tau) \rangle_a \right. \\ &\left. - p_0 \left[\langle \sigma_x(t-\tau) \rangle_a \langle \sigma_z(\tau) \rangle_s - \langle \sigma_z(t-\tau) \rangle_s \langle \sigma_x(\tau) \rangle_a \right] \right) \\ &+ \frac{\tan(\pi K)}{2} \int_0^t d\tau L'(\tau) \frac{d\langle \sigma_z(\tau) \rangle_s}{d\tau}. \end{aligned} \quad (2)$$

We find that the heat transfer receives contributions both from singularities related to the system dynamics and from Matsubara singularities resulting from the system-reservoir correlations. The latter yield significant contributions in the quantum noise regime while they are absent in the Markovian regime. Representative example for the average heat power are given in Fig. (1).

Altogether we have achieved a complete description of the dynamics of the heat transfer for weak damping ranging from the classical regime down to zero temperature.

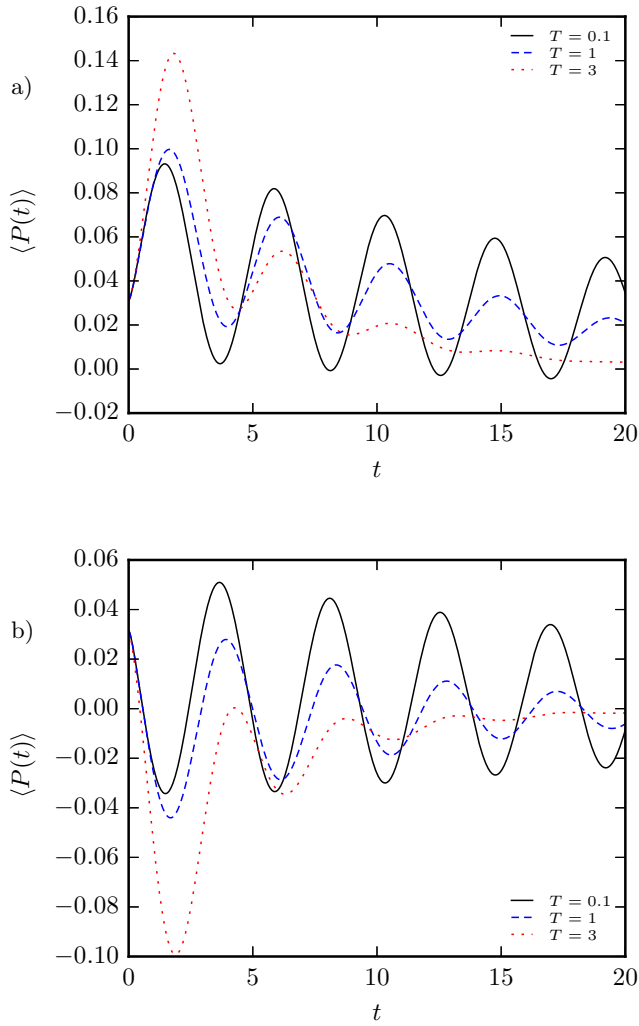


FIG. 1. Time evolution of the average heat power for the two level system. Here we show that at low temperatures quantum noise effects play a significant role in the system dynamics.

¹ M. Esposito, U. Harbola, and S. Mukamel *Rev. Mod. Phys.* **81** 1665 (2009).
² M. Campisi, P. Hänggi, and P. Talkner *Rev. Mod. Phys.* **83** 771 (2011).
³ R. Dorner, S. Clark, L. Heaney, R. Fazio, J. Goold, and V. Vedral *Phys. Rev. Lett.* **110** 230601 (2013).

⁴ P. Solinas, D. V. Averin, and J. P. Pekola *Phys. Rev. B* **87** 060508(2013).
⁵ U. Weiss *Quantum dissipative systems*, 4th edition, (World Scientific, Singapore) (2012).
⁶ M. Carrega, P. Solinas, A. Braggio, M. Sassetti, and U. Weiss *Arxiv/cond-mat:1412.6991* (2014).

Heat and charge current fluctuations in a thermoelectric quantum dot

Adeline Crépieux¹ and Fabienne Michelini²

¹Aix Marseille Université, Université de Toulon, CNRS, CPT UMR 7332, 13288 Marseille, France

e-mail address: adeline.crepieux@cpt.univ-mrs.fr

²Aix Marseille Université, CNRS, IM2NP, UMR 7334, 13288 Marseille, France

e-mail address: fabienne.michelini@univ-amu.fr

I. INTRODUCTION

The adage “*The noise is the signal*”¹ has been proved many times. In the domain of quantum electric transport for example, the zero-frequency noise gives the conductance in the linear regime via the fluctuation-dissipation theorem, or gives the charge in the weak transmission regime via the Schottky relation. One of the beautiful illustrations of this latter fact was the measurement of the fractional charge of a two dimensional electron gas in the fractional quantum Hall regime^{2,3}.

In the recent wave of quantum heat transport studies, some works are devoted to heat noise^{4,5,6,7,8,9} but very few to the fluctuations between the charge and heat currents^{10,11} that we call the *mixed noise*¹². In addition to the characterization of such a “new” quantity, our objective was to find which kind of information can be extracted from it. For this, we have calculated the correlator between the charge current and the heat current for a two terminal quantum dot system using the scattering theory and we have studied its possible relation with quantities such as the thermoelectric efficiency and the figure of merit.

II. SYSTEM AND DEFINITION

We considered a single level quantum dot connected to two reservoirs with distinct chemical potentials $\mu_{L,R}$ and temperatures $T_{L,R}$ as depicted on Fig. 1.

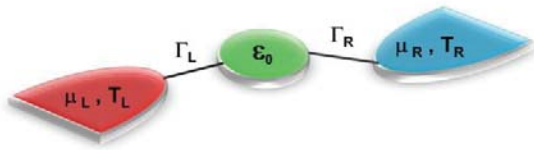


FIG. 1. Schematic picture of a single level quantum dot connected to two reservoirs with distinct chemical potentials and temperatures.

In a similar way to the standard definitions of the charge current noise, S_{pq}^{II} , and heat current noise, S_{pq}^{JJ} , we define the mixed noise as the zero-frequency Fourier transform of the correlator mixing the charge and the heat currents:

$$S_{pq}^{IJ} = \int_{-\infty}^{\infty} \langle \delta \hat{I}_p(0) \delta \hat{J}_q(t) \rangle dt \quad (1)$$

where $\delta \hat{I}_p$ refers to the charge current and $\delta \hat{J}_p$ refers to the heat current. The indices p and q designate the left (L) or the right (R) reservoirs.

III. MIXED NOISE

Using the Landauer-Büttiker scattering theory, which applies in the absence of interactions, we obtain the expression of the mixed noise in terms of the transmission coefficient \mathcal{T} and Fermi-Dirac distribution functions f_p :

$$S_{pq}^{IJ} = \pm \frac{1}{h} \int_{-\infty}^{\infty} (\varepsilon - \mu_q) F(\varepsilon) d\varepsilon \quad (2)$$

with

$$F(\varepsilon) = \mathcal{T}(\varepsilon) [f_L(\varepsilon)(1-f_L(\varepsilon)) + f_R(\varepsilon)(1-f_R(\varepsilon))] + \mathcal{T}(\varepsilon) [1-\mathcal{T}(\varepsilon)] [f_L(\varepsilon) - f_R(\varepsilon)]^2 \quad (3)$$

In the linear response regime, the fluctuation-dissipation theorem holds and leads to the following relation between the noises and the electrical conductance G , the Seebeck coefficient S and the thermal conductance $\kappa = \tilde{\kappa} - S^2 T_0 G$:

$$\begin{aligned} S^{II} &= 2k_B T_0 G \\ S^{JJ} &= 2k_B T_0^2 \tilde{\kappa} \\ S^{IJ} &= S^{JI} = -2k_B T_0^2 S G \end{aligned} \quad (4)$$

where T_0 is the average temperature of the sample. The p and q indices have been removed in Eq. (4) since the noises are identical in amplitude in both reservoirs in the linear response regime. From these results, one shows that the thermoelectric figure of merit, defined as $ZT_0 = S^2 T_0 G / \kappa$, can be expressed fully in terms of noises such as:

$$ZT_0 = \frac{(S^{IJ})^2}{S^{II} S^{JJ} - (S^{IJ})^2} \quad (5)$$

When one leaves the linear response regime, the figure of merit is not more the relevant parameter to quantify thermoelectric conversion and one has rather to consider directly the efficiency which is defined as the ratio between the output and input powers. According to the thermoelectric engine that one wants to build, the powers are given either by the product between charge current and voltage or directly by the heat current. In general, it is not possible to connect these quantities to the noises. However, in the Schottky regime, i.e., in the weak transmission regime, with the help of the proportionality relations between the noises and the currents, we have shown that¹²:

$$\eta = \frac{(S_{LR}^{IJ})^2}{(S_{LR}^{II})^2 - S_{LR}^{II} S_{LR}^{JJ}} \quad (6)$$

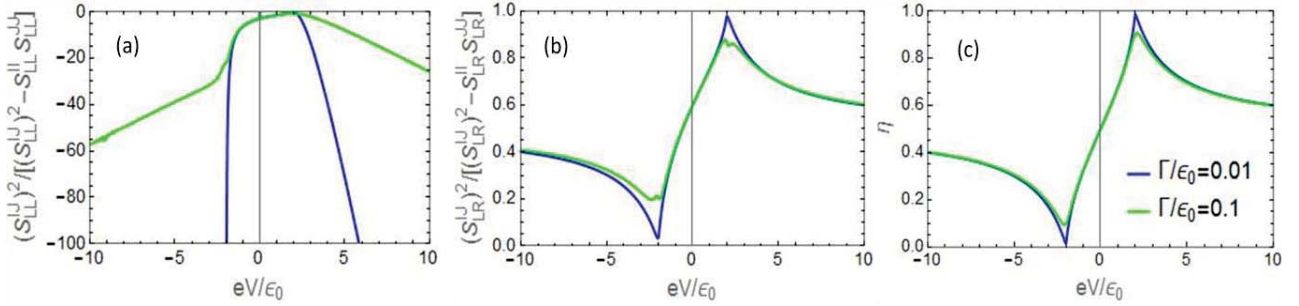


FIG. 2. (a) Auto-ratio of noises, (b) cross-ratio of noises, and (c) thermoelectric efficiency as a function of voltage.

A crucial point in Eq. (6) is the fact that it is needed to consider the ratio of cross-noises, i.e., the correlators between distinct reservoirs; otherwise the value that we get does not correspond to the efficiency. As a graphical proof, three quantities are shown on Fig. 2: the auto-ratio of noises, the cross-ratio of noises and the efficiency. As stated in Eq. (6), the cross-ratio of noises and the efficiency coincide at low transmission Γ , i.e., in the Schottky regime, whereas the profile of the auto-ratio of noises has nothing to do with these two first quantities. From this result, one can conclude that the mixed cross-noise is a measure of the efficiency. From Eq. (6) we also see that a vanishing mixed cross-noise cancels the thermoelectric efficiency.

Outside the linear response regime or the Schottky regime, i.e., in the intermediate regime, one needs to perform numerical calculations in order to characterize the behavior of the mixed noise. In Fig. 3 are shown the absolute values of the noises as a function of voltage and dot energy level at $\Gamma = T_{L,R}$, taken in the same reservoir ($p = q$) or in distinct reservoirs ($p \neq q$). Whereas the charge and heat noises present some symmetry, the mixed noise is fully asymmetrical. One knows that the asymmetry in noise gives information on the system, such as for example the asymmetry in the frequency noise spectrum which is directly related to the ac conductance through a generalized Kubo formula¹³. Thus, the identification of the information that may be contained in the asymmetry of the mixed noise and their possible relations to the thermoelectric conversion is a problem which remains to be addressed.

IV. CONCLUSION

The mixed noise has fulfilled much of its promises since we showed that it is related to the thermoelectric figure of merit in the linear response regime or directly to the thermoelectric efficiency in the Schottky regime. We think that this quantity deserves to be

studied on the same level than the charge and heat noises, both theoretically and experimentally. At the experimental side, the challenge is to find a way to measure such a quantity, whereas at the theoretical side, it is needed to calculate it using more realistic approaches that include, among others, interactions and many terminals.

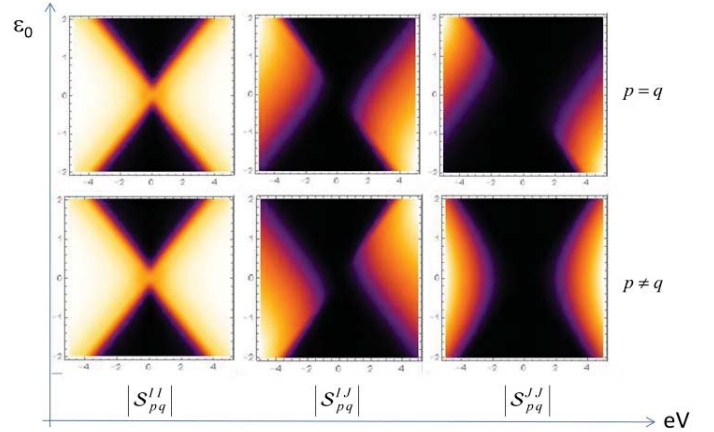


FIG. 3. Absolute value of the charge noise (left column), mixed noise (central column) and heat noise (right column) as a function of voltage and dot energy level. The black regions correspond to the lowest values (close to zero) and the bright regions to the highest values of the noises.

ACKNOWLEDGEMENTS

A.C. thanks T. Martin and R. Whitney for discussions on noise and thermoelectricity.

¹ R. Landauer, Nature **392**, 658 (1998).
² L. Saminadayar, D.C. Glattli, Y. Jin, and B. Etienne, Phys. Rev. Lett. **79**, 2526 (1997).
³ R. de Picciotto, M. Reznikov, M. Heiblum, V. Umansky, G. Bunin, and D. Mahalu, Nature London **389**, 162 (1997).
⁴ M. Kindermann and S. Pilgram, Phys. Rev. B **69**, 155334 (2004).
⁵ D. Sergi, Phys. Rev. B **83**, 033401 (2011).
⁶ F. Battista, M. Moskalets, M. Albert, and P. Samuelsson, Phys. Rev. Lett. **110**, 126602 (2013).

⁷ F. Battista, F. Haupt, and J. Splettstoesser, Phys. Rev. B **90**, 085418 (2014).
⁸ M. Moskalets, Phys. Rev. Lett. **112**, 206801 (2014).
⁹ M. Moskalets, Phys. Rev. Lett. **113**, 069902 (2014).
¹⁰ F. Giazotto, T.T. Heikkilä, A. Luukanen, A.M. Savin, and J.P. Pekola, Rev. Mod. Phys. **78**, 217 (2006).
¹¹ R. Sánchez, B. Sothmann, A.N. Jordan, and M. Büttiker, New J. Phys. **15**, 125001 (2013).
¹² A. Crépeux and F. Michelini, J. Phys.: Condens. Matter **27**, 015302 (2015).
¹³ R. Zamoum, A. Crépeux, and I. Safi, Phys. Rev. B **85**, 125421 (2012).

Non-Gaussian Stochastic Diffusion: Accounting Fourth Cumulant

Boris Grafov¹

¹ A.N. Frumkin Institute of Physical Chemistry and Electrochemistry of Russian Academy of Sciences, 31 Leninskii prospect, Bld.4, Moscow 119071, Russia
e-mail address: boris.grafov@yandex.ru

I. RESUME

In this report I discuss the non-Gaussian stochastic diffusion in electrochemical circuit of alternating current. I found the Fokker-Planck equation with the spatial derivative of second order that takes into account the excess function of the Poissonian electrochemical noise. The open question is formulated.

II. EQUATIONS

Let us consider the electrochemical circuit of alternating current showed on Fig. (1).

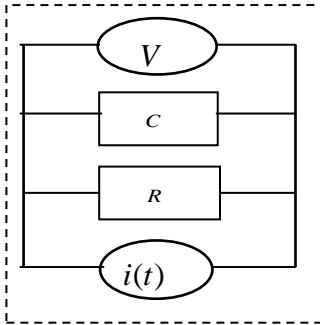


FIG. 1. Non-Gaussian Markov's electrochemical noise circuit

The circuit on Fig. (1) contains the double layer capacity C , the resistance of electrochemical discharge R , and the non-Gaussian current noise source $i(t)$ (t is time). The noise $i(t)$ describes the random character of electrochemical discharge. The voltmeter V measures the random voltage $e(t)$ on capacity C .

Let us introduce the random quantity Ψ as the electrochemical analog of the random displacement of free Brownian particle:

$$\Psi = \int_{-\theta}^0 dt \varepsilon(t) \quad (1)$$

In Eq. (1) the symbol θ stands for observation time. At large observation time ($\theta \gg RC$) we have for the symmetric (Poissonian) electrochemical discharge ¹:

$$\Psi^{(2)} = 2D\theta \quad (2)$$

$$\Psi^{(3)} = 0 \quad (3)$$

$$\Psi^{(4)} = 4!D_4\theta \quad (4)$$

Left-hand side of Eqs. (2), (3), and (4) equals the second, third and fourth cumulant of quantity Ψ correspondingly. The symbols D and D_4 stand for the coefficients.

Eqs. (2) - (3) are the corollaries of the Einstein stochastic diffusion equation (5) for the probability density function $W(\Psi, \theta)$:

$$\left[\frac{\partial}{\partial \theta} - D \frac{\partial^2}{\partial \Psi^2} \right] W(\Psi, \theta) = 0 \quad (5)$$

But Eq. (4) is not a corollary of Eq. (5).

Our main result is the Fokker—Planck equation (6):

$$\left[\frac{\partial}{\partial \theta} - \left(D + \frac{D_4}{D} \frac{\partial}{\partial \theta} \right) \frac{\partial^2}{\partial \Psi^2} \right] W(\Psi, \theta) = 0 \quad (6)$$

Eqs. (2), (3), and (4) are the corollaries of Eq. (6).

III. OPEN QUESTION

In general case of the any duration of the observation time, the Einstein stochastic diffusion equation (5) must be replaced by the Cattaneo equation (7) (telegrapher's equation type) ^{2,3}:

$$\left[\left(1 + RC \frac{\partial}{\partial \theta} \right) \frac{\partial}{\partial \theta} - D \frac{\partial^2}{\partial \Psi^2} \right] W(\Psi, \theta) = 0 \quad (7)$$

My open question is:

How I can find the analog of Cattaneo equation (7) for Eq. (6)?

ACKNOWLEDGEMENTS

The idea discussed in this report was born during the 27 Marian Smoluchowski Symposium on Statistical Physics (Zakopane, Poland, September 22-26, 2014). I am grateful to Professors I.M. Sokolov, E. Gudowska-Nowak, and A.A. Dubkov for useful discussion of the Cattaneo equation.

This report is financially supported by the Russian Foundation for Basic Research, grant no. 14-03-00332-a.

¹ B.M. Grafov, Russian Journal of Electrochemistry **48**, 144 (2012).

² C. Cattaneo, Atti Sem. Mat. Fis. Univ. Modena **3**, 83 (1948).

³ A.K. Das, J. Appl. Phys. **70**, 1355 (1991).

Quasi-stable PDF of velocities of accelerated metal clusters on graphite before joining an island

Ekaterina I. Anashkina,¹ Aleksey V. Kargovsky,² Olga A. Chichigina,³ and Alexandra K. Krasnova⁴

¹*Faculty of Physics, Lomonosov Moscow State University, Leninskie Gory, 119992 Moscow, Russia
Group of Interdisciplinary Theoretical Physics, Università di Palermo and CNISM,
Unità di Palermo, Viale delle Scienze, Edificio 18, 90128 Palermo, Italy
e-mail address: anashkina@physics.msu.ru*

²*Faculty of Physics and International Laser Center,
Lomonosov Moscow State University, Leninskie Gory, 119992 Moscow, Russia
e-mail address: kargovsky@yumnr.phys.msu.ru*

³*Faculty of Physics and International Laser Center,
Lomonosov Moscow State University, Leninskie Gory, 119992 Moscow, Russia
e-mail address: chichigina@ilc.edu.ru*

⁴*Faculty of Physics, Lomonosov Moscow State University, Leninskie Gory, 119992 Moscow, Russia
Schmidt Institute of Physics of the Earth of the Russian Academy of Sciences — 10-1,
Bolshaya Gruzinskaya Str., Moscow, Russian Federation, 123995
e-mail address: krasnova@physics.msu.ru*

Neutral mass-selected clusters are deposited with low initial energy on the graphite substrate. The flux of clusters is uniform and constant during the experiment. After deposition the clusters start to diffuse on the surface. Moving clusters meet each other and stick together thereby forming islands. The islands grow by capturing new clusters. This process is shown in the Fig. (1).

The anomalously high diffusion coefficients for different metallic clusters have been discovered in experiments^{1,2}. The hypothesis that each cluster is accelerated arises from the fact that the initial velocity is low and the diffusion is fast. It has been shown that the properties of the graphite substrate are most probably responsible for the effect, since fast diffusion has been observed for different metallic clusters. This fact is explained using the model of Fermi acceleration and is supposed to be the result of the interaction of clusters with a part of graphite layer called 'flake', that is involved in thermal motion as a whole³. A thermodynamic interpretation of Fermi acceleration in billiards was presented in⁴.

The effect of the motion of flakes on cluster dynamics can be described as a noise. This equilibrium noise depends on temperature. On the contrary, the motion of a cluster is far from equilibrium. The energy of the chaotic motion of a cluster is increasing in time. Time-dependent probability distribution of the cluster velocity is calculated in work⁵ using Langevin equation, and the corresponding PDF is not Maxwell. The accelerated motion of the cluster is terminated at a boundary of an island. The contradictory character of the problem of cluster dynamics under influence of flake fluctuations is as follows. Fermi mechanism results in the superdiffusion. The diffusion constant should increase with measurement time. However, experiments yield time-independent diffusivity. Therefore, either the experimental results are incorrect or the theory is not relevant. To solve the contradiction we introduce an ensemble of moving clusters. This ensemble consists of a constant (on average) number of clusters in the approximation of slow growth of islands.

Such an ensemble is an open system: new slow clusters arrive in the system due to deposition and fast clusters depart from the system being captured by islands. The motion of ensemble of clusters is stable and characterized by the stationary probability distribution. Thereafter, we can estimate an mean velocity and effective temperature of the cluster ensemble. The long lifetime of the quasi-equilibrium state makes it possible to assume that a local equilibrium principle is satisfied and that an effective temperature characterizing this state can be introduced.

We analyse factors that influence the effective temperature. A decrease in this temperature results from cluster capturing by islands. The higher the velocity of a cluster, the higher the probability that this cluster will arrive to the island boundary and join the island. We consider conditional probability distribution of velocities under condition that the cluster has not reached the boundary yet and is still moving. Thus, we come to such a quasistable state of a system in which the velocities of the particles are limited.

An increase in the effective temperature is caused by Fermi acceleration. We introduce the age of each cluster, which is a time interval from the cluster deposition to the moment of observation. To obtain stationary PDF of velocities of clusters in ensemble, we average the time-dependent PDF of one Fermi-accelerated cluster using probability distribution of ages of clusters.

We describe a nonequilibrium state in conventional terms of equilibrium thermodynamics, which are convenient for application of the results in the production of the thin films.

ACKNOWLEDGMENTS

We are very grateful to Dr. Andrey Chikishev for fruitful discussion.

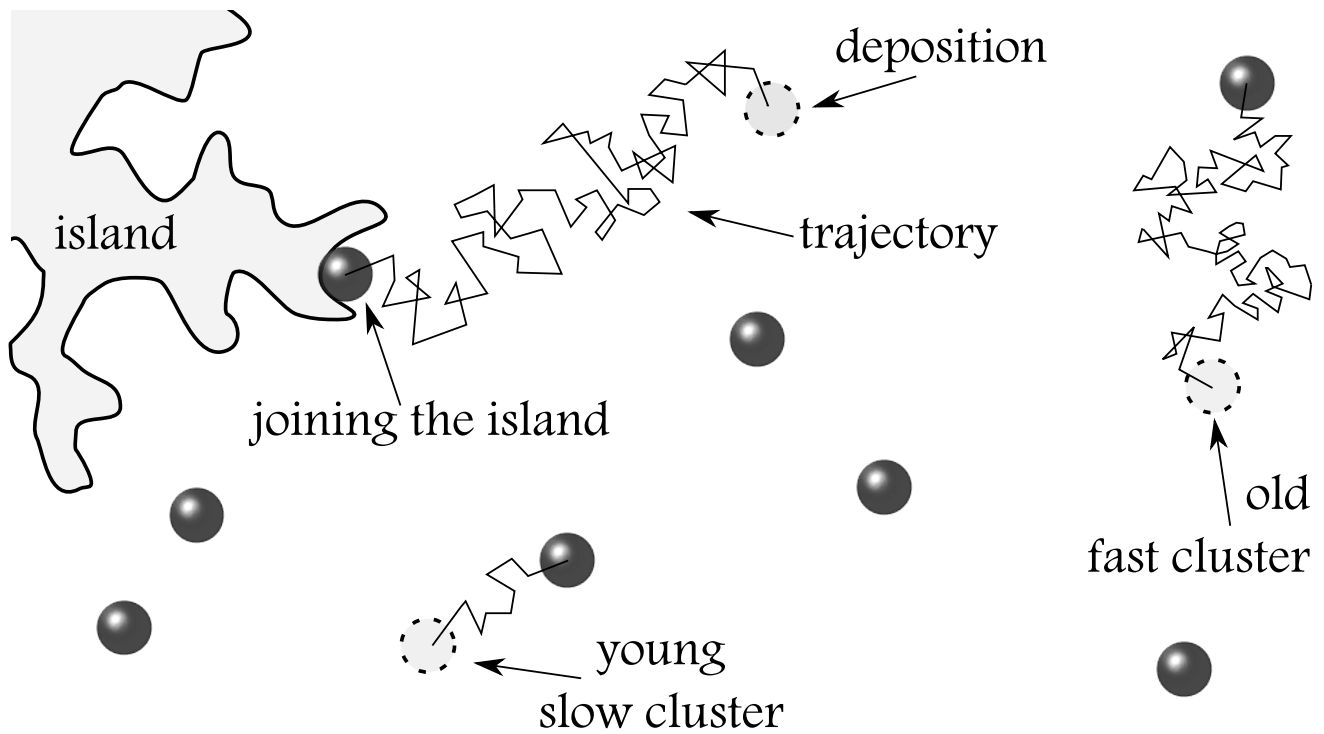


FIG. 1. The process of deposition, diffusion and aggregation of clusters that results in the formation of islands.

¹ P. Jensen, *Rev. Mod. Phys.* **71**, page 1695 (1999).

² A. Perez, P. Melinon, V. Dupuis, et al., *Int. J. Nanotechnol.* **7**, page 523 (2010).

³ A.K. Krasnova and O.A. Chichigina, Moscow University

Physics Bulletin **67**, page 48 (2012).

⁴ A. Loskutov, O. Chichigina, and A. Rjabov, *Int. J. Bifurcation Chaos* **18**, page 2863 (2008).

⁵ A.V. Kargovsky, E.I. Anashkina, O.A. Chichigina, A.K. Krasnova, *Phys. Rev. E* **87**, page 042133 (2013).

Random walks in random stochastic environments

Miguel Ángel García-March,^{1,*} Gerald J. Lapeyre Jr.,² Pietro Massignan,¹ and Maciej Lewenstein^{1,3}

¹*ICFO – Institut de Ciències Fotòniques, Castelldefels (Barcelona) 08860, Spain*

²*IDAEA – Institute of Environmental Assessment and Water Research,
c/ Jordi Girona, 18-26, Barcelona 08034, Spain*

³*ICREA – Institució Catalana de Recerca i Estudis Avançats,
Passeig Lluís Companys, 23 Barcelona 08010, Spain*

I. INTRODUCTION

Recently, there has been considerable interest in random walk models in disordered media characterized by random diffusivity (cf.^{1,2} and references therein). Such models lead in a natural way to the appearance of anomalous subdiffusive behavior, lack of ergodicity, aging and similar effects. For these reasons they are suitable to model various complex phenomena, such as diffusion of enzymes or receptors on a cell surface, observed using single particle imaging in *in vivo*², or an impurity strongly interacting with a condensed matter system.

The main aim of the present project is to formulate and investigate a family of “microscopic” models of a random walk in a random stochastic medium. The dynamics of the medium will be described by a kinetic process that depends on the location of the walker (or, in more general cases, on the walker’s history). At every moment, the dynamics of the walker will depend on the configuration of the environment. Both dependences will be assumed to be local, i.e. they involve only the vicinity of the walker’s locations. By appropriately modeling these couplings we expect to formulate new families of many-body stochastic models with a moving impurity, capable of reproducing results for random walks in quenched disorder (if the environment dynamics is ultra slow), and much more. As an example we discuss here a paradigm model of a random walker in the environment described by Glauber’s famous kinetic Ising model³.

II. EXAMPLE

Let us consider systems described by classical Hamiltonians $H(\sigma)$. We are interested in Hamiltonians following Markovian dynamics towards equilibrium. For concreteness, we consider σ to be the N -dimensional Ising vectors $\sigma = (\sigma_1, \dots, \sigma_N)$, with Ising variables $\sigma_i = \pm 1$. Let us denote the conditional probability of reaching state σ at time t when the system is initially in the state σ_0 as $P(\sigma, t | \sigma_0, 0)$ (of course $P(\sigma, 0 | \sigma_0, 0) = \delta_{\sigma, \sigma_0}$). We use the shorthand notation $P(\sigma, t)$. Then, the dynamical evolution is given by

$$\dot{P}(\sigma, t) = \sum_{\sigma'} [w(\sigma' \rightarrow \sigma)P(\sigma', t) - w(\sigma \rightarrow \sigma')P(\sigma, t)], \quad (1)$$

where the transition rates $w(\sigma' \rightarrow \sigma)$ are the probability per unit time for the transition from configuration σ' to σ . It is natural to assume the detailed balance condition

(DBC), that is, to impose that

$$w(\sigma' \rightarrow \sigma)P_{\text{eq}}(\sigma') = w(\sigma \rightarrow \sigma')P_{\text{eq}}(\sigma) \quad (2)$$

with $P_{\text{eq}}(\sigma) = P(\sigma, t \rightarrow \infty)$.

Let us consider the ferromagnetic Ising model, $H(\sigma) = -J \sum_i^{N-1} \sigma_i \sigma_{i+1}$, $J > 0$. The probability distribution at equilibrium is

$$P_{\text{eq}}(\sigma) = \frac{1}{Z_N} e^{-\beta H(\sigma)}, \quad (3)$$

with partition function $Z_N = 2^N (\cosh^N \beta J + \sinh^N \beta J)$. We restrict the dynamics to single spin flips, $\sigma' = D_i \sigma$. That is, a configuration σ is only connected to other configurations by this process and the transition rates are of the form $w(D_i \sigma \rightarrow \sigma)$. With these assumptions Eq. (1) becomes

$$\dot{P}(\sigma, t) = \sum_{i=1}^N [w(D_i \sigma \rightarrow \sigma)P(D_i \sigma, t) - w(\sigma \rightarrow D_i \sigma)P(\sigma, t)].$$

Under these conditions a conventional form for the transition rates is³

$$w(D_i \sigma \rightarrow \sigma) = \Gamma \left[1 - \frac{1}{2} \tanh [2\beta J] \sigma_i (\sigma_{i-1} + \sigma_{i+1}) \right], \quad (4)$$

where the parameter Γ is the time scale at which the transitions occur.

Let us make the Ansatz $P(\sigma, t) = \sqrt{P_{\text{eq}}(\sigma)} \phi(\sigma, t)$, with $\phi(\sigma, t)$ to be determined. For our model Hamiltonian this reads $P(\sigma, t) = \exp [\beta J \sum_i \sigma_i \sigma_{i+1} / 2] \phi(\sigma, t)$. Then, from Eq. (1) we have

$$\begin{aligned} \dot{\phi}(\sigma, t) = \sum_{\sigma'} \left\{ P_{\text{eq}}^{-1/2}(\sigma) w(\sigma' \rightarrow \sigma) P_{\text{eq}}^{1/2}(\sigma') \right. \\ \left. - P_{\text{eq}}^{-1/2}(\sigma') \sum_{\sigma''} w(\sigma' \rightarrow \sigma'') P_{\text{eq}}^{1/2}(\sigma') \delta_{\sigma \sigma''} \right\} \phi(\sigma', t), \end{aligned}$$

which can be written as a Schrödinger equation $\dot{\phi}(\sigma, t) = H\phi(\sigma, t)$. For Glauber’s case [transition rates given by Eq. (4)] one has

$$\begin{aligned} H(\gamma) = -\Gamma \sum_i \{ [A(\gamma) - B(\gamma) \sigma_{i-1}^z \sigma_{i+1}^z] \sigma_i^x \\ - [1 - \frac{\gamma}{2} \sigma_i^z (\sigma_{i-1}^z + \sigma_{i+1}^z)] \}, \end{aligned}$$

with $\gamma = \tanh 2\beta J$, σ^z and σ^x the Pauli matrices, $A(\gamma) = \gamma^2 / [2(1 - \sqrt{1 - \gamma^2})]$ and $B(\gamma) = 1 - A(\gamma)$. Hamiltonian (5) can be diagonalized by a Jordan-Wigner transformation.

III. CURRENT PROJECT

Our aim is to analyze systems derived from this model in the presence of an impurity. In these models, when the impurity occupies site m , the system's coefficients are changed in some way. The following models show this behavior:

- The energy is increased locally by \bar{h} at the position of the impurity. That is

$$H = -J \sum_{i=1}^{N-1} \sigma_i \sigma_{i+1} + H_{\text{I-bath}} \quad (5)$$

with $H_{\text{I-bath}} = \sum_i^N h_i^m$ with $h_i^m = \bar{h} \delta_{im} \sigma_i$ (site impurity) or $h_i^m = \bar{h} (\delta_{i,m} \sigma_i + \delta_{i-1,m} \sigma_{i-1})$ (link impurity). In the first case, when the impurity is at site m , if the spin at that site is $+1$, energy is increased by \bar{h} , and is decreased by \bar{h} if it is -1 .

- The interaction energy depends on the position of the impurity. Then,

$$H = - \sum_{i=1}^{N-1} J_i^m \sigma_i \sigma_{i+1} \quad (6)$$

with $J_i^m = J + \chi (\delta_{i,m} + \delta_{i+1,m})$.

- Spread the effect of the impurity over a range of sites. For example, Hamiltonian (6) with $J_i^m = J + \sum_{j,(j,m)} \chi \delta_{im}$.

Additionally, one can consider that the impurity may be subject to an external potential $V(m)$. This potential can be parabolic or a random potential, that is, something which forces the impurity to be localized in equilibrium. The configuration of the system of spins plus impurity is (σ, m) , with Ising variables $\sigma_i = \pm 1$, $i = 1, \dots, N$ and $m \in 1, \dots, N$ being the position of the impurity. One can write a Master equation for this system as

$$\begin{aligned} \dot{P}(\sigma, m, t) = & \sum_i [w(D_i \sigma, \sigma) P(D_i \sigma, t) - w(\sigma, D_i \sigma) P(\sigma, t)] \\ & + [W(m+1, m) P(m+1, t) + W(m-1, m) P(m-1, t) \\ & - W(m, m+1) P(m, t) - W(m, m-1) P(m, t)], \end{aligned}$$

where the transition rates $w(D_i \sigma, \sigma)$ do not change the position of the impurity and the transition rates $W(m', m)$ stand for the probability per unit time that the impurity changes position from m' to m . It should conserve probability, be local, and obey DBC. The probabilities at equilibrium are in general

$$P_{\text{eq}} = \frac{1}{Z} \exp[-\beta H(\sigma, m)]. \quad (7)$$

However, in equilibrium the impurity may be fully delocalized for those Hamiltonians which do not break translational symmetry for the impurity.

For Hamiltonian (6) one can go a bit further. The transition rates can be generalized from Glauber's to $1 - \tanh[2\beta J_i^m] \sigma_i (\sigma_{i-1} + \sigma_{i+1})$ and the Master equation can be written as

$$\begin{aligned} \dot{P}(\sigma, m, t) = & \Gamma \sum_i \left[[D_i - 1] \left(1 - \frac{1}{2} \tanh 2\beta J_i^m h_i P(\sigma, m, t) \right) \right. \\ & + \alpha \exp[\chi \sigma_{m+1} (\sigma_m + \sigma_{m+2}) P(\sigma, m+1, t)] \\ & + \alpha \exp[\chi \sigma_{m-1} (\sigma_m + \sigma_{m-2}) P(\sigma, m-1, t)] \\ & \left. - 2\alpha \exp[-\chi \sigma_m (\sigma_{m-1} + \sigma_{m+1}) P(\sigma, m, t)] \right] \quad (8) \end{aligned}$$

with $h_i = \sigma_i (\sigma_{i-1} + \sigma_{i+1})$ and where α and Γ allow for different time scales in both types of transitions. Our goals are: i) find models such as those described above that are exactly solvable in 1D; ii) Perform numerical studies of these kind of models with Monte Carlo and Tensor Network States methods; iii) Apply them to various realistic scenarios, as the aforementioned biological systems or to exotic applications like a classical model for gravity.

ACKNOWLEDGMENTS

We acknowledge support from ERC AdG OSYRIS, MINCIN Project FOQUS, EU IP SIQS, EU FET-Proactive QUIC.

* miguel.garcia-march@icfo.es

¹ P. Massignan, C. Manzo, J.A. Torreno-Pina, M.F. García-Parajo, M. Lewenstein, and G. J. Lapeyre Jr, *Non-ergodic subdiffusion from Brownian motion in an inhomogeneous medium*, arXiv:1401.6110, Phys. Rev. Lett. **112**, 150603 (2014).

² Carlo Manzo, Juan A. Torreno-Pina, Pietro Massignan, Gerald J. Lapeyre Jr., Maciej Lewenstein, and Maria F. García Parajo, *Weak ergodicity breaking of receptor motion in living cells stemming from random diffusivity*, arXiv:1407.2552, Phys. Rev. X *in press* (2015).

³ R.J. Glauber, J. Math. Phys. **4**, 294 (1963).

Independence of superdiffusion in random low-density Lorentz gas on geometrical properties of moving scatterers

Alexandra K. Krasnova,^{1,2} Olga A. Chichigina,³ and Ekaterina I. Anashkina⁴

¹*Physics Faculty, Moscow State University - GSP-1,
1-2 Leninskiye Gory, Moscow, Russian Federation, 119899
e-mail address: krasnova@physics.msu.ru*

²*Schmidt Institute of Physics of the Earth of the Russian Academy of Sciences - 10-1,
Bolshaya Gruzinskaya Str., Moscow, Russian Federation, 123995*

³*Physics Faculty, Moscow State University - GSP-1,
1-2 Leninskiye Gory, Moscow, Russian Federation, 119899
e-mail address: chichigina@ilc.edu.ru*

⁴*Physics Faculty, Moscow State University - GSP-1,
1-2 Leninskiye Gory, Moscow, Russian Federation, 119899
e-mail address: ahashkina@physics.msu.ru*

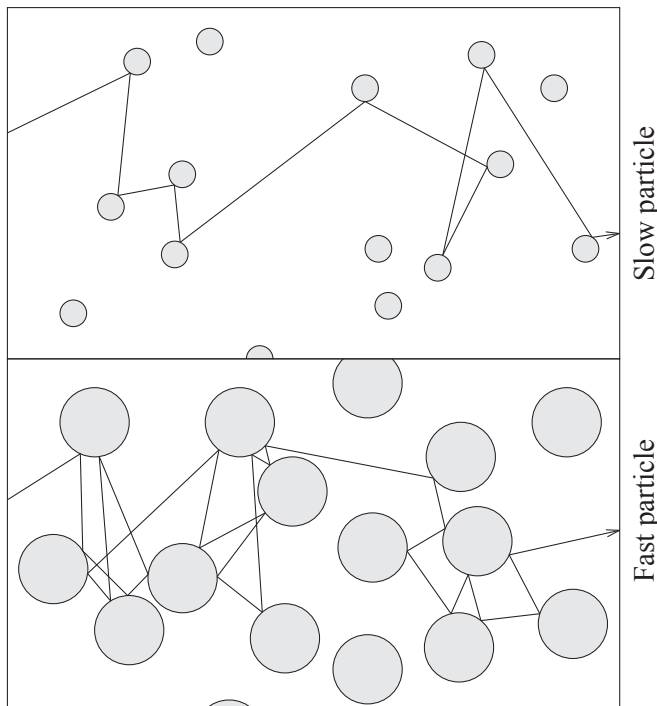


FIG. 1. Random Lorentz gas with different size of scatterers.

A random Lorentz gas with time-dependent boundaries is a two-dimensional system containing a set of heavy discs (scatterers) distributed randomly. Particles move freely among these discs. The boundaries of the scatterers oscillate. The unlimited linear growth of particle velocity in these systems is called the Fermi acceleration phenomenon². Even for periodical and correlated motion of boundaries the influence of this motion on particle can be considered as noise, because the moments of particle collisions with the scatterers are random. Langeving equation can be used to calculate particle dynamics¹.

Fermi acceleration leads to anomalous transport². Dependence of mean square displacement on time is linear $\sqrt{x^2} = kt$. The constant of proportionality k increases

with the increase of amplitude of boundary velocity and can be called the coefficient of superdiffusion. This parameter has a dimension of velocity.

The great number of investigations in billiards-like systems proved strong dependence of their transport properties on geometry of Lorentz gas. At the same time thermodynamics interpretation and analogy with ideal gas suppose independence on the size and concentration of the scatterers. These parameters define the mean free path. The only parameters of the model are amplitude of boundary velocity and the mean free path. There are no parameters with time dimension. Therefore, we cannot construct coefficient of superdiffusion using parameters of length.

The unsolved problem was: does the coefficient of superdiffusion k depend on geometrical properties of random low-density Lorentz gas. To solve the problem we have calculated the coefficient of superdiffusion analytically, taking into account Fermi acceleration. We have also performed computer simulation of particle motion. The theoretical and numerical results are in good agreement. The coefficient of superdiffusion k is defined only by amplitude of boundary velocity and dimensionless coefficient describing the kind of scatterers motion, which can be random or periodical. The explanation of this independence on the mean free path comes from the fact that the usual diffusion coefficient linearly increase with this path. At the same time Fermi acceleration, on the contrary, decreases. Fig. 1 illustrate this fact. On the top picture the mean free path is relatively large, but Fermi acceleration is relatively small due to the low rate of the collisions. On the bottom picture, on the contrary, the mean free path is relatively small and Fermi acceleration is relatively large. Therefore, the two factors that influence the diffusion of particle compensate each other, and the coefficient of superdiffusion does not depend on geometrical properties of random low-density Lorentz gas.

ACKNOWLEDGMENTS

We are very grateful to Dr. Andrey Chikishev for fruitful discussion.

¹ A. Kargovsky, E. Anashkina, A. Krasnova, O. Chichigina, Phys. Rev. E **87**, 042133 (2013).

² A. Loskutov, O. Chichigina, A. Krasnova, I. Sokolov, EPL **98**, 10006 (2012).

Finite-frequency noise in a non-interacting quantum dot

Redouane Zamoum,¹ Mireille Lavagna,² and Adeline Crépieux³

¹*Faculté des sciences et des sciences appliquées, Université de Bouira, rue Drissi Yahia, Bouira 10000, Algeria e-mail address: zamoum.redouane@gmail.com*

²*Commissariat à l'Energie Atomique de Grenoble INAC/SPSMS, 17 rue des Martyrs, 38054 Grenoble Cedex 9, France e-mail address: mireille.lavagna@cea.fr*

³*Aix Marseille Université, Université de Toulon, CNRS, CPT UMR 7332, 13288 Marseille, France e-mail address: adeline.crepieux@cpt.univ-mrs.fr*

I. INTRODUCTION

In this work we study a one channel quantum dot connected to two reservoirs. We calculate the non-symmetrized finite frequency noise in the framework of the Keldysh Green's function formalism. The transmission processes are introduced using a transmission amplitude defined with the help of the hopping parameter and the Green's functions of the dot. The expression of the non-symmetrized finite frequency noise is obtained. When we symmetrize our result, it coincides with the expression of the Büttiker formula of the finite frequency noise.

II. MODEL

We consider a one channel quantum dot as depicted in Fig. (1). The Hamiltonian reads as $H = H_L + H_R + H_T + H_{cen}$, where:

$$H_{\alpha=L,R} = \sum_{k \in \alpha} \varepsilon_k c_k^\dagger c_k \quad (1)$$

$$H_T = \sum_{\alpha=L,R} \sum_{k \in \alpha} V_k c_k^\dagger d + h.c. \quad (2)$$

$$H_{dot} = \varepsilon_0 d^\dagger d \quad (3)$$

The $c_{k,p,\sigma}^\dagger$ and $c_{k,p,\sigma}$ are respectively the creation and annihilation operators in the reservoirs. The d_σ^\dagger and d_σ are respectively the creation and annihilation operators in the dot. V_k is the hopping parameter. In our work, we focus on the spinless case.

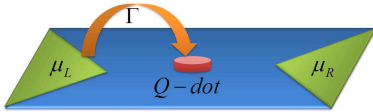


FIG. 1. Schematic representation of the quantum dot and the leads. The tunneling process occurs with a strength Γ . $\mu_{L,R}$ are the chemical potential of the left and right reservoirs. In the following, we take $\mu_{L,R} = \pm eV/2$.

Next, we define the non-symmetrized finite frequency noise in the left reservoir:

$$S(\omega) = \int_{-\infty}^{\infty} \langle \delta \hat{I}_L(0) \delta \hat{I}_L(t) \rangle e^{i\omega t} dt \quad (4)$$

where $\delta \hat{I}_L(t) = \hat{I}_L(t) - \langle I_L \rangle$, where $\langle I_L \rangle$ is the average left current and \hat{I}_L the current operator in the left reservoir, which is given by¹:

$$I_L(t) = \frac{ei}{\hbar} \sum_k \left(V_k c_{k,L}^\dagger d - V_k^* d^\dagger c_{k,L} \right) \quad (5)$$

The next step is the evaluation of the current-current correlator $\langle \delta \hat{I}_L(0) \delta \hat{I}_L(t) \rangle$. For this we need first to rewrite the Hamiltonian in the interaction representation. Then, using an \mathcal{S} -matrix expansion one can rewrite the current-current correlator in the interaction representation. The resulting expression is a function of four-points Green's functions of the dot $G_1^{dd}(\tau, \tau', \tau_1, \tau_2) = i^2 \langle T_C d(\tau) d(\tau') d^\dagger(\tau_1) d^\dagger(\tau_2) \rangle$, where τ is time variable in this representation.

Now we use a Wick theorem in order to factorize the four-points Green's functions in a product of two points Green's functions²:

$$G_1^{dd}(\tau, \tau', \tau_1, \tau_2) = G(\tau, \tau_2) G(\tau', \tau_1) - G(\tau, \tau_1) G(\tau', \tau_2) \quad (6)$$

The results contains two parts, a disconnected part which is equal to the square of the average current, and a connected part which contains fifteen contributions. To rewrite the correlator as a function of the time variable t , we use the Keldysh formalism³. Applying a Fourier transform to the result and after some algebras, one finds the non-symmetrized finite frequency noise expression.

III. RESULTS

In the case of symmetric barriers, the non-symmetrized finite frequency noise reads as:

$$S(\omega) = \frac{e^2}{\hbar} \int d\varepsilon \left[\left[\mathbb{T}(\varepsilon - \omega) \mathbb{T}(\varepsilon) + |t(\varepsilon) - t(\varepsilon - \omega)|^2 \right] f_{LL} + \mathbb{T}(\varepsilon - \omega) \mathbb{T}(\varepsilon) f_{RR} + \mathbb{T}(\varepsilon) \left[1 - \mathbb{T}(\varepsilon - \omega) \right] f_{RL} + \mathbb{T}(\varepsilon - \omega) \left[1 - \mathbb{T}(\varepsilon) \right] f_{LR} \right] \quad (7)$$

where $f_{\alpha\beta} = n_\alpha(\varepsilon)[1 - n_\beta(\varepsilon - \omega)]$ with n the Fermi-Dirac distribution function and $\alpha, \beta = L, R$. The transmission amplitude and the transmission coefficient are re-

spectively given by:

$$t(\varepsilon) = \frac{i\Gamma}{\varepsilon - \varepsilon_0 + i\Gamma} \quad (8)$$

$$\mathsf{T}(\varepsilon) = \frac{\Gamma^2}{(\varepsilon - \varepsilon_0)^2 + \Gamma^2} \quad (9)$$

where ε_0 is the dot energy level, $\Gamma = (2\pi)^{-1}\rho(\varepsilon)|V_k|^2$ is the barriers strength and ρ the density of states of the reservoirs which are considered as identical. The symmetrized noise is obtained from the expression $S_{sym}(\omega) = [S(\omega) + S(-\omega)]/2$. Doing this, we get the Büttiker formula of the symmetrized finite frequency noise^{4,5}:

$$S_{sym}(\omega) = \frac{e^2}{h} \int d\varepsilon \left[\mathsf{T}(\varepsilon - \omega)\mathsf{T}(\varepsilon) + |t(\varepsilon) - t(\varepsilon - \omega)|^2 \right] F_{LL} \\ + \mathsf{T}(\varepsilon - \omega)\mathsf{T}(\varepsilon)F_{RR} + \mathsf{T}(\varepsilon - \omega) \left[1 - \mathsf{T}(\varepsilon) \right] F_{LR} \\ + \mathsf{T}(\varepsilon) \left[1 - \mathsf{T}(\varepsilon - \omega) \right] F_{RL} \quad (10)$$

To see the evolution of the non-symmetrized finite frequency noise, we plot the non-symmetrized excess noise $\Delta S(\omega, V) = S(\omega, V) - S(\omega, 0)$ as a function of frequency for different values of the temperature and for different impurity strengths. In Fig. (2), we plot the non-

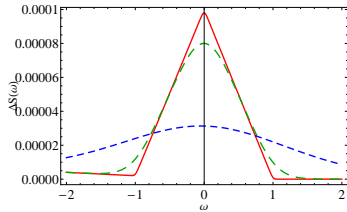


FIG. 2. Non-symmetrized excess noise in units of e^3V/h as a function of frequency in units of eV/h for $\varepsilon_0/eV = 100$, and for fixed $\Gamma/eV = 1$. Solid red line corresponds to $k_B T/eV = 0.01$, dashed green line to $k_B T/eV = 0.1$ and dotted blue line to $k_B T/eV = 0.5$.

symmetrized excess noise as a function of frequency for fixed impurity strength at different values of temperature. What we see first is the fact that the spectrum is symmetric in frequency whatever the temperature is, then the intensity of the excess noise decreases with the temperature. At low temperature, the noise presents a singularity in the vicinity of $\pm eV/h$. Then the cancellation occurs beyond $\pm eV/h$ because of the cancellation of the thermal noise contribution. In Fig. (3), we plot the

non-symmetrized excess noise as a function of frequency for fixed temperature and different values of the impurity strength in the weak impurity regime. The noise here becomes anti-symmetric with a singularity in the vicinity of $\pm eV/2h$. In Fig. (4) we plot the non-symmetrized excess noise as function of the frequency for fixed temperature in an intermediate impurity regime. What we see here is that the noise becomes asymmetric.

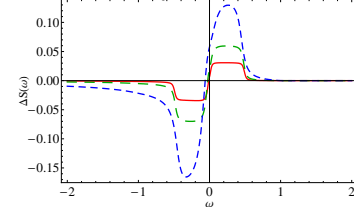


FIG. 3. Non-symmetrized excess noise in units of e^3V/h as a function of frequency in units of eV/h for $\varepsilon_0/eV = 0.01$, and for fixed $k_B T/eV = 0.01$. Solid red line corresponds to $\Gamma/eV = 0.01$, dashed green line to $\Gamma/eV = 0.02$ and dotted blue line to $\Gamma/eV = 0.05$.

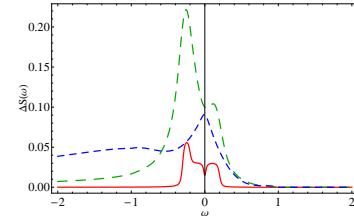


FIG. 4. Non-symmetrized excess noise in units of e^3V/h as a function of frequency in units of eV/h for $\varepsilon_0/eV = 0.3$, and for fixed $k_B T/eV = 0.01$. Solid red line corresponds to $\Gamma/eV = 0.01$, dashed green line to $\Gamma/eV = 0.1$ and dotted blue line to $\Gamma/eV = 1$.

IV. CONCLUSION

In this work we calculated the non-symmetrized finite frequency noise for a single level quantum dot. We used the Keldysh formalism to evaluate the current-current correlator and then we performed a Fourier transform to get the expression of the finite frequency noise. Our result is consistent with the Büttiker formula of the symmetrized finite frequency noise obtained using the scattering theory since the symmetrization of our expression give the formula obtained by Büttiker. Varying the temperature, the dot energy and the barrier strength, the profile of the noise spectrum changes from symmetric behavior, to asymmetric or to anti-symmetric behaviors.

¹ A. P. Jauho, N. S. Wingreen, and Y. Meir, Phys. Rev. B **50**, 5528 (1994).

² H. J. W. Haug and A. P. Jauho, in *Quantum kinetics in transport and optics of semiconductors*, Springer series

(2007).

³ L. V. Keldysh, Sov. Phys. JETP **20**, 1018 (1965).

⁴ M. Büttiker, Phys. Rev. B **45**, 3807 (1992).

⁵ Y.M. Blanter, M. Büttiker, Phys. Rep. **336**, 2 (2000).

Features of Noise in Ultrathin Gold Nanowire Structures

Volodymyr Handziuk¹, Sergii Pud¹, Alexandre Kisner² and Svetlana Vitusevich^{1*}

¹ Forschungszentrum Jülich, Peter Grünberg Institute (PGI 8), Leo-Brandtstr. 1, 52425 Jülich, Germany

e-mail address: v.handziuk@fz-juelich.de; s.pud@fz-juelich.de; *s.vitusevich@fz-juelich.de

² Rutgers University, Dept. Cell Biology and Neuroscience, 604 Allison road Piscataway, NJ, USA

e-mail address: kisner.alexandre169@gmail.com

I. INTRODUCTION

The investigation of ultrathin metal nanowires (NWs) has been widely discussed from the point of view of theoretical and experimental studies due to their unique transport properties. In most technologies, the ultrathin NWs can be produced with a short length and usually they are not stable^{1,2}. They maintain functionality only for a short period of time and require sophisticated conditions like ultrahigh vacuum for storage. Recently, a new approach was reported for the fabrication of ultrathin gold NWs. It enables synthesis of chemically stable NWs with a width of 2 nm and a length of several microns³. They are promising candidates for investigating electrical properties of 1D metal conductors and for usage in nanoscale electronics as contacts between functional elements. However, the development of high-quality nanoscale electronic devices is still challenging. High signal-to-noise ratio and structural performance are the main requirements for many applications, including biosensors and molecular electronics.

Since nanowires are usually produced by wet chemical synthesis, organic molecules on the interfaces between NWs and contacts can strongly influence their electrical properties⁴. This allows investigation of the junction properties of molecular layers. Studies of electron transport in such nanowires have already been performed at room^{5,6} and low⁴ temperatures. At the same time, noise spectroscopy provides useful information, complementing electrical characterization. So far, determining the transport properties in ultrathin gold nanowire structures has not been reported.

Here, we present the results obtained for bundles of Au NWs using the noise spectroscopy technique and we consider the influence of molecular interfaces on the transport properties of NWs. An analysis of different noise components in different systems provides insights into the processes of charge transport in fabricated device structures. Therefore, the properties of molecular interfaces between Au NWs and contacts can also be studied by analyzing the peculiarities of noise behavior in such systems.

II. MATERIALS AND METHODS

The samples studied were bundles of ultrathin gold nanowires (Au NWs) obtained by wet chemical synthesis⁴. The SEM image of the studied structures is shown in FIG. (1). After fabrication of the gold contacts, the ultrathin Au NWs were assembled over these electrodes to investigate the transport and noise properties of the structures. The NWs usually had diameters of about 2 nm and were several micrometers in length.

The schematic of the measurement setup is shown in FIG. (2).

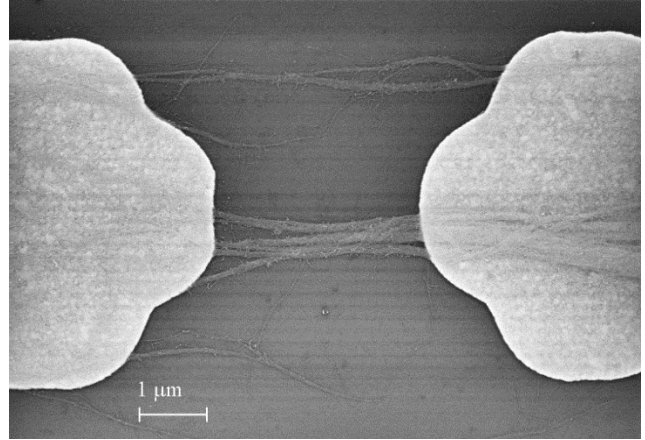


FIG. 1 SEM image of investigated Au NW structure.

This setup was used for both I-V characterization and noise spectra measurement. The voltage applied to the sample from a rechargeable battery was tuned by an adjustable resistor of 2 kOhm. The sample was connected in series with a high-precision variable resistor R_{Load} . The latter was used to evaluate current flowing through the sample.

The drain current of the Au NWs can be calculated using the difference between the voltages, measured by two voltmeters by the formula $I_d = (V_m - V_s) / R_{Load}$. Here V_m is the total voltage on sample plus load, V_s is the voltage on the sample. The noise spectra were measured at several working points of the I-V curve.

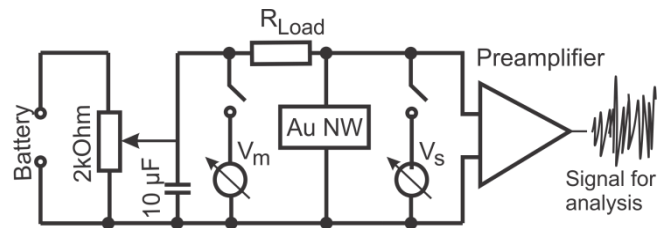


FIG. 2 Schematic of the noise measurement setup.

For the noise measurements, voltage fluctuations in Au NW structures were amplified by a low-noise amplifier developed in-house (24 dB, input noise $2.2 \text{ nV}^2/\text{Hz}$ at 100 Hz) and then amplified by a Stanford low-noise voltage amplifier SR560. The noise signal was registered by a HP35670 dynamic parameter analyzer and then transferred via GPIB interface to a PC. The measurements were performed at room temperature in a shielded environment.

III. RESULTS AND DISCUSSION

The current-voltage characteristic of the investigated sample is shown in FIG. (3).

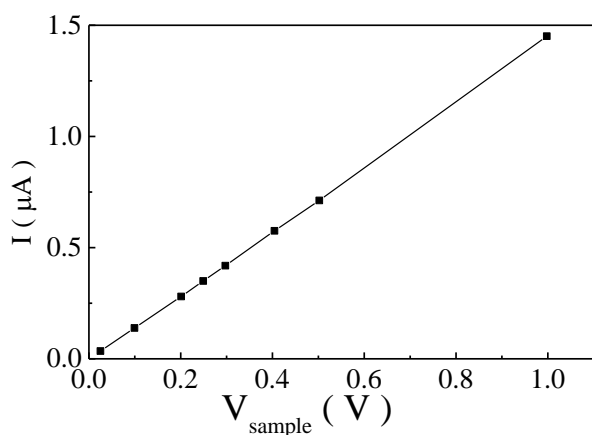


FIG. 3. Typical I-V characteristic of Au NW structure.

I-V characteristic demonstrates quasi-linear behavior, which can be explained by a significant increase in the role of thermally activated processes in charge transport at room temperature⁴.

The noise spectra have several components: thermal, flicker and generation-recombination (GR). These components were extracted by fitting and then analyzed. Flicker noise spectral density multiplied by frequency is proportional to current squared (shown in FIG. (4)). This dependence reflects that transport in the NW structure demonstrates ohmic behavior and an absence of nonlinear processes in the system.

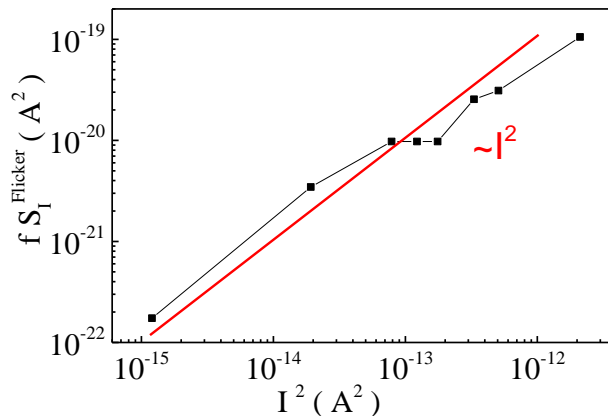


FIG. 4 The dependence of current spectral density of flicker noise multiplied by frequency vs current squared.

An analysis of noise spectra demonstrated several (about four) GR components, which is not typical for pure gold nanowires^{7,8}. Therefore the Lorentzian-shaped components are the result of processes at the interface between gold nanowires and contacts. The frequencies of the Lorentzian-shaped components are mostly independent of the drain bias, which excludes self-heating of the NWs. The GR noise components may be explained by taking into account the molecular layers covering the Au NWs. Indeed, the synthesis of nanowires was performed in oleylamine solution, a lipidic molecule, which assists the growth of nanowires and due to its nature can form a channeled micellar structure. However, at the same time, these molecules are self-assembled on the surface of the grown structures. The presence of such a layer influences the electrical properties⁴ of the structures and also leads to the appearance of GR components in the noise spectra. The physical origin of registered GR noise components is discussed.

IV. CONCLUSIONS

We studied the specific noise properties of bundles of ultrathin gold nanowires obtained by wet chemical synthesis and contacted with gold electrodes. The peculiarities of noise behavior were explained by the presence of an interface layer between NWs and contacts. It was shown that the noise components as well as electronic properties were strongly affected by the organic monolayers assembled on the surface of the nanowires. This new approach can be used to study properties of the molecular thin layer by analyzing the peculiarities of electronic transport and noise in such systems.

¹ Y. Kondo, K. Takayanagi, *Science* **289**, 606 (2000)
² P. Z. Coura, S. B. Legoas, A. S. Moreira, F. Sato, V. Rodrigues and D. S. Galvao, *Nano Lett.* **4**, 1187 (2004)
³ A. Halder, N. Ravishankar, *Adv. Mater.* **19**, 1854 (2007)
⁴ S. Pud, A. Kisner, M. Heggen, D. Belaineh, R. Temirov, U. Simon, A. Offenhäusser, Y. Mourzina and S. Vitusevich *Small* **9**, 846-852 (2013).

⁵ C. Wang, Y. Hu, C.M. Lieber and S. Sun *J. Am. Chem. Soc.* **130**, 8902 (2008).
⁶ Y. Lu, J. Huang, C. Wang, S. Sun and J. Lou, *Nature Nanotechnology* **5**, 218 (2010)
⁷ A. Bid, A. Bora and A.K. Raychaudhuri, *Nanotechnology* **17**, 152 (2006)
⁸ F. Gasparyan, *American Journal of Physics* **3**, 312 (2010)

High Frequency Cutoff in $1/f$ Spectra of Hole Doped $\text{La}_x\text{Ca}_{1-x}\text{MnO}_3$ Manganite Single Crystals

Jacek Przybytek,¹ Jan Fink-Finowicki,² Roman Puźniak,² and Grzegorz Jung^{2,3}

¹*Institute of Experimental Physics, Faculty of Physics, University of Warsaw, 02-093 Warsaw, Poland
e-mail address: jacek.przybytek@fuw.edu.pl*

²*Institute of Physics PAS, 02-668 Warsaw, Poland*

³*Department of Physics, Ben Gurion University of the Negev, 84105 Beer Sheva, Israel
e-mail address: jung@bgu.ac.il*

Electronic transport in phase separated manganites has been a topic of intensive investigations in the last decades. Nevertheless, recent investigations of low temperature properties of hole doped manganites brought new surprising discoveries. Among them, experimental evidence for appearance of the electronic glass state at low hole doping level at low temperatures, associated with ferromagnetic insulating phase, contradicting the conventional double exchange magnetic coupling model is a subject of continuous interest.¹

Hole-doped $\text{La}_{1-x}\text{Ca}_x\text{MnO}_3$ (LCMO) manganites at Ca-doping levels $0.125 < x < 0.225$ are ferromagnetic insulators (FMI) at low temperatures, unlike the ones with x above 0.225, which are ferromagnetic but also metallic, or with x below 0.125, which are insulating antiferromagnets in the ground state. Long range interactions in the ferromagnetic insulating phase lead to the opening of the Coulomb gap in the density of states and to hopping conduction in the presence of such gap.^{1,2} Slow relaxations of charge carriers arising from a large number of low-lying states separated by barriers lead to enhanced low-frequency non-Gaussian $1/f$ resistance noise.^{3,4}

Until now, experimental investigations of $1/f$ noise in Coulomb glass state were limited to the doped semiconductors with electron density close to the critical concentration for the metal-insulator transition and to two-dimensional electron glass in MOSFET-like structures. Observations of $1/f$ non-Gaussian electronic glass in doped manganites in which, in a marked difference to disordered semiconductors, electronic glass arises for the polarized polaronic carriers, significantly widens the class of materials exhibiting such properties.

One of the main topics of discussion in the subject literature was the issue of the low frequency cutoff in the $1/f$ spectra which appears at frequencies much lower than those predicted by the theoretical models.^{2,3} We discuss here the high frequency cutoff of the $1/f$ noise in hole doped manganites in the Coulomb glass state. It is clear that usually the issue of the high frequency $1/f$ noise cutoff is typically experimentally irrelevant because the $1/f$ component simply disappears in the background noise. In our case the cutoff was experimentally observed due to high level of the $1/f$ noise in the investigated crystals and relatively low level of background noise of our electronic set-up.

The experiments were performed using $\text{La}_{0.82}\text{Ca}_{0.18}\text{MnO}_3$ crystals in-house grown by float-

ing zone method with radiative heating. As grown crystal was cut into rectangular bars with the longest dimension being parallel to [100] direction and equipped by vacuum evaporated contacts for transport measurements. The Curie temperature of the crystal, $T_C=182$ K, was determined by measuring dc magnetization as a function of temperature in the field of 10 Oe.

For the noise measurements, voltages developing across dc current biased sample were amplified by a chain of very low noise preamplifiers and the further FFT analysis was processed by a computer. Because of relatively high impedance of the samples, especially at low temperatures, a particular attention was paid to the level of the input signals at the amplifier chain in order not to saturate the amplifiers and not to exceed the allowed common voltage level during the data acquisition. In-

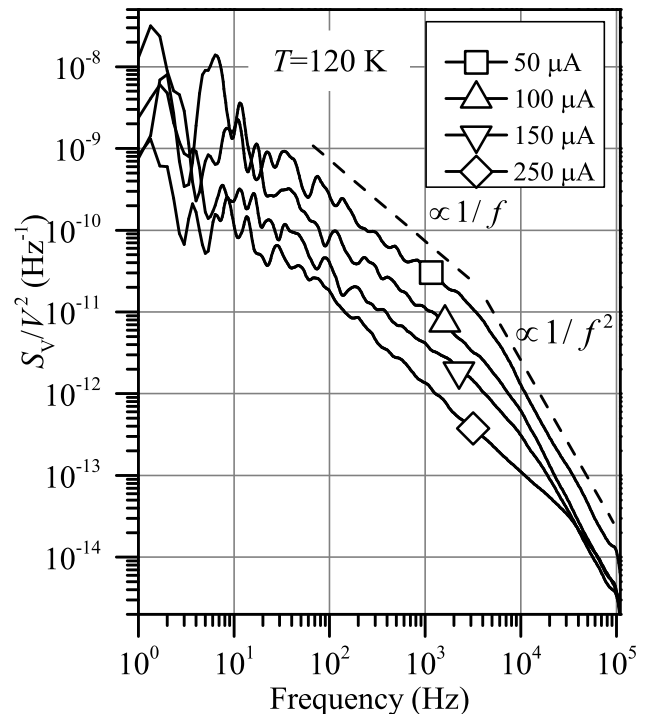


FIG. 1. Normalized noise spectra at temperature $T=120$ K for different currents flowing through the sample. The spectra have been smoothed for better legibility.

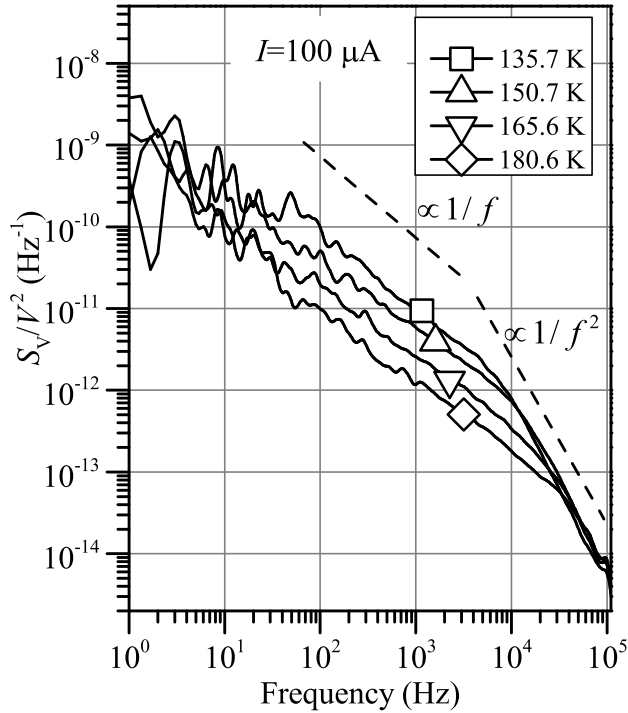


FIG. 2. Normalized noise spectra for different temperatures at current $I=100 \mu\text{A}$ flowing through the sample. The spectra have been smoothed for better legibility.

strumental noise originating from the measuring chain was eliminated by subtracting the reference spectrum, recorded at zero current flow in the LCMO sample, from the spectrum acquired with bias current.

Typically, noise spectra have $1/f$ -like form both below and above the Curie temperature. However, with temperature decreasing below T_C a clear high frequency lorentzian cutoff sets on in the $1/f$ spectra, as illustrated in example shown in Fig. (1) The frequency of the cutoff decreases with decreasing bias current and temperature - see Fig. 1 and Fig. 2.

We tentatively associate the high frequency cutoff of the $1/f$ spectra in the Coulomb glass regime with intrinsic limits of the appearance of $1/f$ noise in the hopping regime. The conclusion of the existence of the glassy state in the investigated material comes from the low temperature dependence of conductivity following the Efros-Shklovskii law and very strong increase of the noise level following approximately the power law with an exponent close to 5.5.

The open questions following our experimental observations and proposed interpretation of the data will be outlined in the presentation.

ACKNOWLEDGMENTS

This work was supported by the Polish NCN grant 2012/05/B/ST3/03157.

¹ R. Laiho, K. G. Lisunov, E. Lahderanta, V. N. Stamov and V. S. Zakhvalinskii, J. Phys.: Condens. Matter **13**, 1233 (2001).

² S. Samanta, A. K. Raychaudhuri and Ya. M. Mukovskii, Phys. Rev. B **85**, 045127 (2012).

³ A. Amir, Y. Oreg, Y. Imry, Ann. Phys. **18**, 836 (2009).

⁴ A. L. Burin, B. I. Shklovskii, V. I. Kozub, Y. M. Galperin and V. Vinokur, Phys. Rev. B **74**, 075205 (2006).

Noise-induced resonance-like phenomena in InP crystals embedded in fluctuating electric fields

D. Persano Adorno,^{1,*} N. Pizzolato,¹ P. Alaimo,¹ and B. Spagnolo^{1,2}

¹*Dipartimento di Fisica e Chimica, Università di Palermo,
Group of Interdisciplinary Theoretical Physics, Università di Palermo and CNISM,
Unità di Palermo, Viale delle Scienze, Edificio 18, 90128 Palermo, Italy*

²*Istituto Nazionale di Fisica Nucleare, Sezione di Catania, Via S. Sofia 64, I-90123 Catania, Italy*

I. INTRODUCTION

The electron velocity fluctuations during the nonlinear transport of hot electrons in semiconductor structures subjected to static or cyclostationary electric fields, have been extensively investigated during last decades¹⁻⁴. In fact, the presence of intrinsic noise both limits the performance of semiconductor based devices and affects their sensitivity. Furthermore, electronic devices are often imbedded into noisy environments that also can affect their performance. In recent years increasing interest has been directed toward the investigation of noise-induced phenomena in nonlinear systems, with a focus on possible positive cooperative effects between the noise and the intrinsic interactions of the system^{5,6}. In particular, theoretical studies have shown that, under specific conditions, the addition of external sources of noise to intrinsically noisy systems may induce an enhancement of the dynamical stability of the system, resulting in a less noisy response⁷. The possibility of suppressing the diffusion noise by the addition of a random fluctuating contribution to the driving periodic electric field, has been previously investigated in GaAs bulks^{8,9}. By superimposing an external noise source to the intrinsic one, it has been possible to tune the dynamic electron response and obtain noise enhanced stability phenomena in the electron transport^{8,9}. In this study, we employ a semi-classical Monte Carlo (MC) approach to simulate the non-linear transport of electrons inside low-doped n-type InP crystals, embedded in sub-THz electric fields, fluctuating for the presence of an external source of noise. The electronic noise features are statistically investigated by computing the correlation function of the velocity fluctuations, its spectral density and the total noise power. Main aim of this work is to deeply explore the occurrence of a noise reduction effect and the appearance of a stochastic resonance-like phenomenon in the noise spectra. Moreover, we will discuss the dependence of these noise-induced positive effects on the relationship among the characteristic times of the external fluctuations and the temporal scales of complex phenomena involved in the electron dynamics.

II. THE MODEL

The transport of electrons in InP bulks is simulated by using a MC algorithm¹⁰. In our model the conduction bands of InP are represented by the Γ - valley,

by four equivalent L -valleys and by three equivalent X -valleys. All possible scattering events of hot electrons in the medium, the main details of the band structure, as well as the heating effects, are taken into account. The scattering probabilities are calculated by using the Fermi Golden Rule and the scattering events are considered instantaneous. Scattering probabilities are assumed to be field-independent. Accordingly, the influence of the external fields is only indirect through the field-modified electron velocities¹⁰. The table of parameters used in the present work is given in Ref¹¹. All results are obtained for a doping concentration of 10^{19} m^{-3} (non-degenerate n-type), at lattice temperature $T = 77 \text{ K}$. The fluctuations of the electron velocity around its average value correspond to the intrinsic noise of the system. Therefore, to characterize the stochastic properties of the electron transport, we statistically analyze the velocity autocorrelation function and the mean spectral density of the velocity fluctuations. Since our sample is driven by a periodic electric field, we calculate a two-time symmetric electron velocity autocorrelation function¹², in order to eliminate any regular contribution and describe only the fluctuating part of $v(t)$. The spectral density of the electron velocity fluctuations is then calculated as the Fourier transform of the correlation function. In our simulations the electrons are driven by a fluctuating periodic electric field $E(t) = E\cos(\omega t) + \eta(t)$, where the deterministic term has amplitude E and frequency $f = \omega/2\pi$. The stochastic component $\eta(t)$ is modelled by an Ornstein-Uhlenbeck (OU) process which obeys the following stochastic differential equation:

$$\frac{d\eta(t)}{dt} = -\frac{\eta(t)}{\tau_c} + \sqrt{\frac{2D}{\tau_c}}\xi(t) \quad (1)$$

where τ_c and D are the correlation time and the intensity of the noise component, respectively⁸.

III. NUMERICAL RESULTS AND DISCUSSION

With the aim to quantify the noise-induced intrinsic noise suppression, we have calculated the Integrated Spectral Density (ISD), i.e. the total noise power, which corresponds to the variance of the electron velocity. In the left panel of Fig. 1, we show the ISD as a function of the noise correlation time τ_c when $E=25 \text{ kV/cm}$, $f=500 \text{ GHz}$, $D^{1/2}=10 \text{ kV/cm}$. In the presence of Gaussian time-correlated fluctuations added to the periodic electric field, it is possible to observe a clear reduction up to

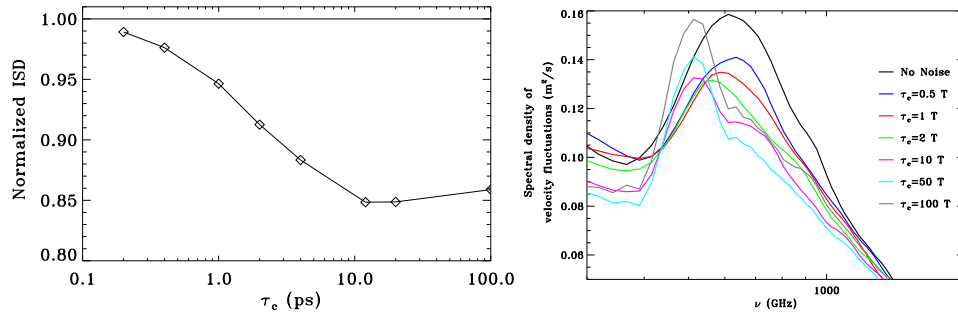


FIG. 1. Left: ISD of the electron velocity fluctuations, normalized to the value obtained in the deterministic case, as a function of the noise correlation time τ_c . Right: Spectral density of the electron velocity fluctuations for different values of the correlation time τ_c . The values of the parameters are $E=25$ kV/cm, $D^{1/2}=10$ kV/cm, $f=500$ GHz, $T=77$ K.

15% of the ISD, i.e. a less noisy response. The suppression enhances with the increase of the correlation time of the external fluctuations up to $\tau_c \approx 10$ ps and then stabilizes. Further studies are needed to deeply investigate why under this regime, the external fluctuations constructively contribute to force the electrons to performing a more ordered dynamics (confirmed by a lower total noise power). In the right panel of fig. 1 we show how the shape of the spectral density of the electron velocity fluctuations modifies around the frequency of the oscillating field in the presence of Gaussian time-correlated fluctuations. The "effective" electric field experienced by the electrons changes. This implies a modification in the number of intervalley transfers with respect to the case in which the external noise is negligible. This fact could be responsible of the changes in the height of the peak in the spectral density. The most interesting effect arises for noise correlation times greater than $10 T$ (2 ps). In fact, in such cases, the presence of time-correlated fluctuations makes the peak strictly resonant at the frequency of the driving periodic field. This resonance-like phenomenon could be an evidence that electrons transfer among the different energy valleys exactly at the same frequency of the applied field, reaching a new more stable equilibrium state.

IV. CONCLUSION

We report the results from a many-valley MC study on the electron non-linear dynamics in low-doped n-type InP crystals operating under a fluctuating sub-Thz electric field. A less noisy response is found, being the correlation time of the electric field fluctuations a crucial quantity for the reduction effect. This noise-induced phenomenon seems to indicate that, under specific time scales, the complex dynamics of electrons in the crystal benefits from the cooperative interplay between the fluctuating electric field and the intrinsic fluctuations of the system itself. Therefore, time-correlated fluctuations on a driving electric field could play a relevant role on controlling and tuning the electronic noise in InP based electronic devices. For noise correlation times greater than $10 T$, a resonance-like phenomenon in the noise spectra is found. This response critically depends on the relationship among the characteristic time of the external noise and the time scales characterizing the complex electron dynamics. However, these preliminary findings leave several open problems on the intrinsic physical mechanism beyond this effect, which will be further investigated mainly in terms of (i) different frequencies of the driving field, (ii) different intensities and typologies of the external fluctuations, (iii) different semiconductor materials.

* dominique.persanoadorno@unipa.it

¹ Sh. Kogan, *Electronic noise and Fluctuations in Solids* (Cambridge University Press, 1996), Chapter 3.
² D. Persano Adorno, M.C. Capizzo, M. Zarcone, *Fluct. Noise Lett.* **8**, L11 (2008).
³ J.F. Millithaler et al, *J. Stat. Mech. Theor. Exp.* **P02030**, (2009).
⁴ S. Amontas, R. Raguotis, S. Bumeliene, *Solid State Sciences* **38**, 156 (2014).
⁵ P. Ghosh, S. Chattopadhyay, J.R. Chaudhuri, *Chemical Phys.* **4022**, 48 (2012).

⁶ D. Valenti et al, *Cent. Eur. J. Phys.* **10**, 560 (2012).
⁷ J.M.G. Vilar, J.M.Rubi, *Phys. Rev. Lett.* **86**, 950 (2001).
⁸ D. Persano Adorno, N. Pizzolato, B. Spagnolo, *J. Stat. Mech. Theor. Exp.* **P01039**, (2009).
⁹ D. Persano Adorno et al, *Rep.Math. Phys.* **70**, 171 (2012).
¹⁰ D. Persano Adorno, M. Zarcone, G. Ferrante, *Laser Phys.* **10**, 310 (2000).
¹¹ D. Persano Adorno, M. Zarcone, G. Ferrante, *Laser Part. Beams* **19**, 81 (2001).
¹² T. Gonzalez et al, *Proc. SPIE* **5113**, 252 (2003).

Study on the origin of 1/f noise in bulk acoustic wave resonators

F. Sthal¹ M. Devel¹, J. Imbaud¹, R. Bourquin¹, S. Ghosh¹ and G. Cibiel²

¹ FEMTO-ST Institute, Besançon, France

e-mail address: fsthal@ens2m.fr

² CNES, Microwave and Time-Frequency, Toulouse, France

I. INTRODUCTION

The Centre National d'Etudes Spatiales (CNES), Toulouse, France and the FEMTO-ST Institute, Besançon, France, investigate the origins of 1/f noise in bulk acoustic wave resonators. Several European manufacturers of high quality resonators and oscillators are involved in this partnership. The goals are first to improve the yield of excellent resonators and second to assess the intrinsic lower limit for the resonator noise.

In this contribution, we first give some relevant information about the realization of the 5 MHz SC-cut resonators used in this study. Then, we report the resulting short term stability of the resonators as a function of the position of the resonators inside the crystal block. Concerning the second goal, a theoretical approach, based on the fluctuation-dissipation theorem, is used in order to put numerical constraints on a model of 1/f noise caused by an internal (or structural) dissipation proportional to the amplitude and not to the speed. The order of magnitude of the noise is then discussed using a candidate physical process. Finally, we conclude on the work that could be done to solve the remaining open problems.

II. RESONATOR REALIZATION

For this investigation, quartz crystal resonators have been cut from a quartz crystal block supplied specifically for this study on 1/f noise (cf. Fig. 1). This crystal block is obtained from a seed cut in a previous synthetic crystal which was grown using a natural seed.



Figure 1 : Quartz crystal resonators according to their positions in the mother block.

Its dimensions were approximately 220 mm along the Y-axis, 36 mm along the Z-axis and 110 mm along the X-axis. Two Y-cut slices have been cut before and after an oriented block used to achieve ten quartz bars. The Y-cut slices are used to obtain dislocations evaluation by X-ray topographies. The red marks show how the crystal is cut in order to get SC-cut blanks from 14 initial bars. First, Fourteen quartz bars pre-oriented on the first rotation angle have been achieved. The length of the bars was

about 70 mm. Taking into account the width of the cutting saw, about 24 blanks could be obtained in each bar. They were distributed to the various manufacturers part of the project, so that they could make 5 MHz SC-cut resonators out of them and give them back for analysis to FEMTO-ST and CNES.

III. EXPERIMENTAL RESULTS

The passive technique using carrier suppression is used to characterize the inherent phase stability of the ultra-stable resonators.

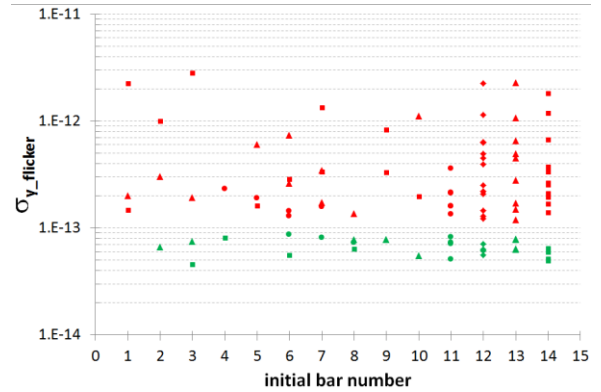


Figure 2 : Short-term stability of quartz crystal resonators according to the position in the mother block.

The short-term stabilities of a large portion of these resonators have been measured to be lower than $8 \cdot 10^{-14}$. However, rest of them shows much worse results around few 10^{-12} , though they have been fabricated with exactly the same process alike the best ones. Although the positions of the blanks are known, no clear correlation between the noise results and the blanks positions (e.g. center or edges) can be found for these bars. We are consequently carrying investigations on the origin of these differences.

IV. THEORETICAL APPROACH

The fluctuation-dissipation theorem^{1,2} (FDT) is used to estimate the power spectral density of thermal noise coming from fluctuations in the thickness ($2h$) of quartz resonators (cf. Fig. 3).

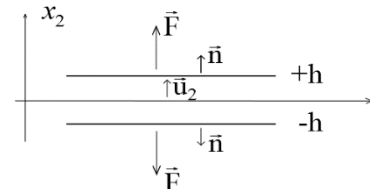


Figure 3 : Resonator design.

An internal friction term, ϕ , is added in the formulation, in order to obtain a 1/f spectrum at low frequencies. Indeed, for this

mode (characterized by the mechanical displacement inside the resonator $u_2(x_2, t)$), the fundamental principle of dynamics for continuum media can be written as:

$$\rho \frac{\partial^2 u_2}{\partial t^2} = c_{22}(1 + j\varphi) \frac{\partial^2 u_2}{\partial x_2^2} + \eta_{22} \frac{\partial^3 u_2}{\partial x_2^2 \partial t} \quad (1)$$

with c_{22} the elastic constant and η_{22} the viscoelastic damping constant of quartz crystal. φ is an internal friction coefficient^{1,2}, ρ the quartz mass per unit volume. Searching for solutions of the type:

$$u_2(x_2, t) = [a \sin(kx_2) + b \cos(kx_2)]e^{j\omega t} \quad (2)$$

with limit condition given by:

$$T_2(\pm h, t) = F \cdot e^{j\omega t} / S \quad (3)$$

with F the modulus of the harmonic mechanical force applied to the surface S of the electrodes (perpendicular to x_2). The complex mechanical admittance of the system is defined by:

$$\bar{Y}(\omega) \equiv \frac{\frac{\partial u_2(\pm h, t)}{\partial t}}{\pm F \cdot e^{j\omega t}} = \frac{j\omega a \sin(kh)}{F} \quad (4)$$

The FDT then states that the spectral power density of the thickness fluctuations in a bandwidth BW , can be computed by^{1,2}:

$$\frac{u_2^2(\pm h, \omega)}{BW} = \frac{4k_B T}{\omega^2} \text{Re}(\bar{Y}(\omega)) \quad (5)$$

with T the absolute temperature (in K) and k_B the Boltzmann constant (in J/K).

The assumptions $\varphi \ll 1$ and $\omega \ll c_{22}/\eta_{22}$ lead to:

$$\frac{u_2^2(\pm h, \omega)}{BW} \approx \frac{4k_B T h}{5\omega c_{22}^2} (\eta_{22} \omega + c_{22} \varphi) \quad (6)$$

Moreover, we can consider that the circular frequency at resonance $\omega_r \sim 1/h$, thus:

$$S_y(\omega) \equiv \frac{(\delta\omega_r)^2}{\omega_r^2 BW} = \frac{u_2^2(\pm h, \omega)}{(2h)^2 BW} \approx \frac{1}{\omega} \times \frac{2k_B T}{V c_{22}} (\eta_{22} \omega + \varphi) \quad (7)$$

where V is the volume of the resonator. One can then see from the previous expression that for circular frequencies lower than $\varphi c_{22}/\eta_{22}$, the internal friction becomes dominant and gives a $1/f$ spectrum, with an Allan standard deviation given by:

$$\sigma_{y_flicker} = \sqrt{2 \ln(2) \frac{2k_B T}{V c_{22}} \varphi} \quad (8)$$

We note that φ could depend upon the temperature and that no assumption where made about this possible dependence. We consider here numerical values typical for a 5 MHz oscillator equipped with an SC-cut quartz crystal resonator. Due to the rotation of the axis, the 2 axis is not the usual one, so that the constants must be evaluated in the rotated basis: $c_{22} = 115$ GPa, $\eta_{22} = 1.36 \cdot 10^{-3}$ Pa·s, $T = 350$ K and $V = 0.104$ cm³. This gives:

$$\sigma_{y_flicker} \approx 1.06 \cdot 10^{-12} \sqrt{\varphi} \quad (9)$$

In order to recover measured values of $\sigma_{y_flicker}$ with this expression, we would need to have φ between 10^{-2} and 10^{-4} , which would mean that even at resonance the internal damping would be dominant over viscoelastic damping. We therefore conclude that internal damping of thickness fluctuations by any force proportional to strain and independent of frequency, may not be the dominant noise mechanism for the best SC-cut quartz resonators. However, other modes may be noisier...

Nonetheless, we try to evaluate this coefficient by the modified Granato-Lücke theory³ of the energy loss due to some

kinds of dislocation motion in the low frequency range. They supposed first that the pinning force F of the impurity atom which arises from elastic interactions depends on the orientation of the dislocation line. Second, they supposed that, once a dislocation has broken away from its pinning points, its motion is not necessarily limited by its line tension, but that the distance it moves may be determined by the stress field of neighboring impurity atoms. With these assumptions, they found an expression of the decrement for the impurity spacing controlled dislocation motion that, in the small stress amplitude limit, is given by:

$$\Delta = \frac{\beta N b L_N}{\pi c^{1/3} \epsilon} \quad (10)$$

Where β is a parameter having approximate value of 1.5. N is the total length of dislocation line in a unit volume of material $\approx 2 \times$ surface dislocation density. This value is of the order of 6 cm/cm³ judging from an X-ray image of the surface of one of the resonator. b is the mean length of a Burger's vector $\approx 3 \times 10^{-8}$ cm. L_N is the network length $= \sqrt{3N}$. c is the atom fraction of impurity which must be lower than 1 ppm to get Q values as high as a few 10^6 . ϵ is the fractional difference between the radius of impurity and host atoms taken to be of the order of 20 %. Finally, we recall that, previously, we saw that $1/Q_{eff} = 1/Q_{viscous} + \varphi$, with $1/Q_{viscous} = \frac{\eta_{22} \omega}{c_{22}}$. Therefore at low frequencies $1/Q_{eff} \approx \varphi$. Hence, we attempt to identify Δ with $\pi\varphi$ at low frequencies, in a first approximation in spite of the fact that we are not in the dominantly viscous regime. This would give $Q_{eff} \approx 10^5$ and $\varphi \approx 10^{-5}$ in the low frequency regime, which would be an interesting order of magnitude to attribute at least some non-negligible part of the $1/f$ noise to the fluctuations of thickness. However, this would also mean that at resonance $\frac{1}{Q_{eff}} = \frac{1}{Q_{viscous}} + \varphi \approx 4 \cdot 10^{-7} + 10^{-5} \approx 10^{-5} = \varphi$, hence that the viscous damping would not be dominant at resonant frequency which is contradictory to experimental facts.

V. CONCLUSION

We have seen that it is possible to find $1/f$ noise through the fluctuation-dissipation theorem, by adding a constant complex part to the elastic constant in the usual differential equation characteristic of a viscously damped harmonic oscillator. This corresponds to a frequency independent energy loss in the limit of small frequencies. The hysteretic motion of the dislocations described by a modified Koehler-Granato-Lücke model could a priori describe such a loss mechanism. Indeed, it could provide an explanation for the experimental observations that the logarithmic decrement generally decreased when the dislocation density decreased when quartz were not as good as now and that sometimes a slightly higher concentration of impurity could improve the quality factor. However, numerical estimations seem to provide values that are at least an order of magnitude too high. Hence the physical origin of $1/f$ noise in quartz crystal ultra-stable oscillators still remains an open question. We therefore plan to study another approach based on thermally activated nucleation and motion of kink-antikink pairs along dislocations, with possibly several different activation energies. This could lead to $1/f$ noise by the mechanism of Lorentzian summation.

¹ H. B. Callen and R. F. Greene, Phys. Rev., 86, 702, (1952).

² P. R. Saulson, Phys. Rev. D, 42, 2437, (1990).

³ J. C. Swartz and J. Weertman, J. Appl. Phys, 32, 1860, (1961).

The electron transit time is not the ultimate responsible for the high-frequency noise: The frontier between electronics and electromagnetism

Z. Zhan,¹ E. Colomés,¹ A. Benali,¹ and X. Oriols¹

¹*Departament d'Enginyeria Electrònica, Universitat Autònoma de Barcelona, 08193, Bellaterra, Spain
e-mail: xavier.oriols@uab.es*

I. INTRODUCTION

It is generally believed (and found in many textbooks¹⁻⁴) that the electron transit time is the ultimate responsible for the high-frequency noise behaviour of the state-of-the-art ballistic electronic devices. In fact, the constant progress in high-frequency applications during the last 50 years has been based mainly on the idea of reducing the electron transit time¹⁻⁴, either by scaling their lengths or introducing materials with higher electron mobility. In this conference, we argue that the ultimate responsible of the high-frequency noise is not the electron transit time, but a new shorter time related to the duration of the current peak detected on a particular surface, say S , while the electron is crossing the device.

It is well-known that the electron movement inside the device generates a time-dependent electric field $\vec{E}(\vec{r}, t)$ on a particular surface S . Such time-dependent electric field implies a displacement current on S . This displacement current, which is present even when the electron is not crossing the device, determines the duration of the current peak⁵⁻⁷. The total current, which includes the particle current density, $\vec{J}(\vec{r}, t)$, gives:

$$i(t) = \int_S \vec{J}(\vec{r}, t) \cdot d\vec{s} + \int_S \epsilon(\vec{r}) \frac{\partial \vec{E}(\vec{r}, t)}{\partial t} \cdot d\vec{s}, \quad (1)$$

where $\epsilon(\vec{r})$ is the inhomogeneous electric permittivity. In the definition of the duration of the current peak due to an electron travelling along the device, there are scenarios where the exact transit time of the electron is not at all a relevant parameter. In addition, we will show that a proper understanding of the relationship between the electron movement and the displacement current opens new unexplored possibilities for the manipulations of the high-frequency performance of electronic devices.

II. DISPLACEMENT CURRENT AND TRANSIT TIME

Ramo⁶ and Shockley⁷, in the 30's, were the pioneers in determining how the high-frequency performance of electronic devices is related to the electron dynamics inside the active region. They showed that an electron moving with velocity $\vec{v} = \{v_x, 0, 0\}$ between two (infinite) metallic plates separated by a distance L_x generates a current peak in one of the plates equal to $i(t) = -q \cdot v_x / L_x$ during $0 < t < \tau$, being q the (unsigned) electron charge. The time-integral of the current during $\tau = L_x / v_x$ gives the expected transmitted charge $-q$. In this particular case,

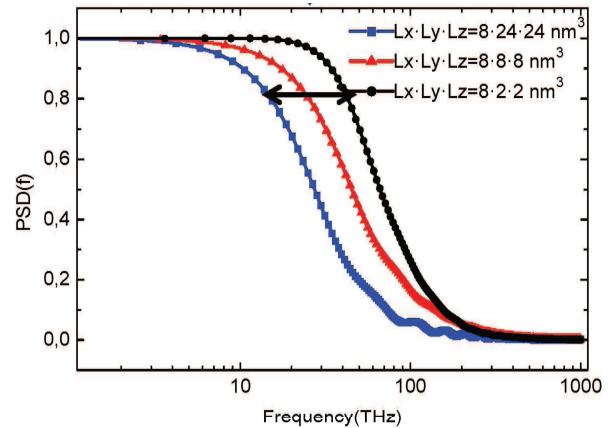


FIG. 1. Power spectral density (PSD) of the current fluctuations (in arbitrary units) as a function of frequency for a GAA FET with different geometries (and identical channel length L_x) operating under DC conditions.

the relevant time for the current is effectively the electron transit time $\tau = L_x / v_x$. Can we envision other scenarios where the displacement current collected on a particular surface is not related to the electron transit time? Below, we answer positively to this question.

To go beyond the previous Ramo-Shockley result is mandatory to deal with, at least, a three terminal device that ensures that the instantaneous current in the source is not equal to that in the drain, while still satisfying the instantaneous current conservation. For this reason, we consider the three terminal Gate-All-Around Field Effect Transistors (GAA FETs). In Fig. 1, we plot the power spectral density (PSD) of the current fluctuations for a particular GAA FETs. Numerical simulations for different geometries (L_x is the transport source-drain direction and L_y and L_z are the lateral directions) of this particular GAA FETs are shown in Fig. 1. We clearly see how the high-frequency cut-off frequency of current fluctuations is independent of the electron transit time $\tau = L_x / v_x$. A variation of an order of magnitude of the noise spectrum range can be achieved without changing the device active region $L_x = 8$ nm nor its (average) velocity v_x . For such particular FETs, the high-frequency performance can be improved without neither length scaling nor using materials with higher electron mobility⁸.

We consider now the same device operating under AC conditions. The conventional small-signal admittance parameter model for the GAA FETs is drawn in Fig. 2. We compute numerical simulations of the gate and drain transients currents $i_1(t) = i_G(t) - i_G^{DC}(t)$

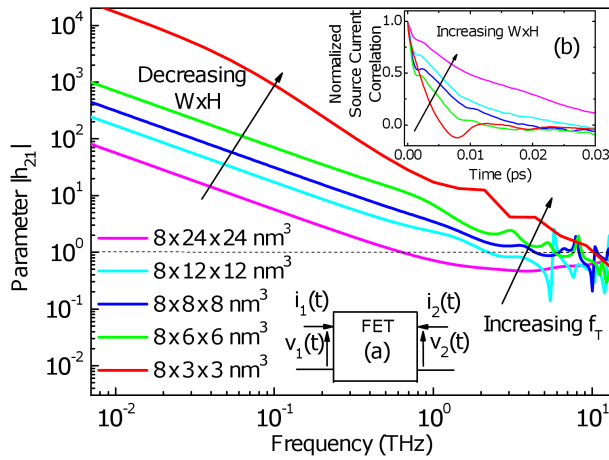


FIG. 2. h_{21} parameters as a function of frequency for the volume $L_x \times L_y(W) \times L_z(H)$. (a) Two-port (admittance) small-signal circuit. (b) Source current autocorrelation with DC bias. The FET with larger lateral area does not satisfy the single band quantum wire requirement, but it is included to show the tendency of the results.

and $i_2(t) = i_D(t) - i_D^{DC}(t)$, being $i_G^{DC}(t)$ and $i_D^{DC}(t)$ the DC value before the voltage step. A Fourier transform of $i_1(t)$ and $i_2(t)$ directly provides the small-signal admittance parameters $Y_{2,1}(f)$ and $Y_{1,1}(f)$. The intrinsic cut-off frequency, f_T , can be computed then as $|h_{2,1}(f_T)| = |Y_{2,1}(f_T)/Y_{1,1}(f_T)| = 1$. To see clearly the effect of the cross section area, we have presented the intrinsic cut-off frequencies in Fig. 2. We notice that for the same longitudinal length L_x , the cut-off frequency increases from $f_T = 0.62 THz$ up to $f_T = 10.20 THz$ when the lateral area is scaled down, as seen in Fig. 2. These results confirm that the geometry of the GAA FETs (for a fixed L_x) has a relevant role in their high-frequency behaviour. In order to confirm the role of the current pulse on the results, we present the correlations of the source current with DC bias for the previous FETs. The results in Fig. 2(b) clearly show that the larger the lateral area is, the wider the current temporal pulse⁹.

III. WHERE IS THE FRONTIER BETWEEN ELECTRONICS AND ELECTROMAGNETISM?

In this conference we present an original strategy to optimize radio-frequency (or digital) performance of GAA FETs by modifying their lateral areas, without L_x scaling or mobility improvement. The ultimate reason of such improvement is that the transit time $\tau = L_x/v_x$ is no longer a limiting high-frequency factor for those GAA FETs where the lateral dimensions L_y, L_z are similar or smaller than their length L_x . A time shorter than $\tau = L_x/v_x$ controls their intrinsic signal and noise high-frequency performance.

The proper understanding of the relationship between the electron movement and the displacement current opens new unexplored possibilities for the influence on high-frequency electronic devices. Traditionally, electronics is based on the manipulation of the particle current (first term in Eq. (1)), while partially neglecting the displacement current (second term of Eq. (1)). On the contrary, electromagnetism is based on the manipulation of the displacement current due to variations of the electric (and magnetic) fields at scenarios where the particle current becomes practically irrelevant. For dimensions shorter than $L_x = 0.1 \mu m$, the electromagnetic vector potential can be reasonably neglected at frequencies lower than around 100 THz. As a consequence, a new type of electronic devices, in the frontier between electronics and electromagnetism, is envisioned by controlling the shape of the displacement current (i.e. electric field) instead of the particle current (i.e. the electron charge).

ACKNOWLEDGMENTS

We want to acknowledge the Ministerio de Ciencia e Innovación through project TEC2012-31330 and the Grant agreement no: 604391 of the Flagship initiative “Graphene-Based Revolutions in ICT and Beyond”.

¹ D.V.Morgan and M.J.Howes, *Microwave Solid State Devices and Applications* (Peter Peregrinus Ltd. , New York, 1980).

² I. Ferain, C. A. Colinge and J.-P. Colinge, *Nature*, **479**, 310 (2011).

³ F.Schwierz, H.Wong, J.J.Liou, *Nanometerr CMOS* (Pan Stanford, 2010).

⁴ F. Schwierz, *Nature Nanotechnology*, **5**, 487 (2010).

⁵ B. Pellegrini *Physical Review B*, **34(8)**, 5921 (1986).

⁶ S. Ramo *Proceedings of the I. R. E.* , **27**, 584 (1939) .

⁷ W. Shockley *J. Appl. Phys.* **9**, 635 (1938).

⁸ A. Benali, F.L.Traversa, G. Albareda, M.Aghoutane and X.Oriols, *Fluctuation and Noise Letters* **11(3)**, 1241002 (2012).

⁹ A. Benali, F. L. Traversa, G. Albareda, M. Aghoutane, and X. Oriols *Appl. Phys. Lett.* **102**, 173506 (2013).

Random Telegraph Noise (RTN) analyzed by using Weighted Time Lag Method in Resistive Switching devices

M. Maestro^{1*}, J. Diaz¹, A. Crespo-Yepes¹, J. Martin-Martinez¹, R. Rodriguez¹, M.B. Gonzalez², F. Campabadal², M. Nafria¹ and X. Aymerich¹

¹Universitat Autònoma de Barcelona department of electronic engineering

*e-mail address: marcos.maestro@uab.es

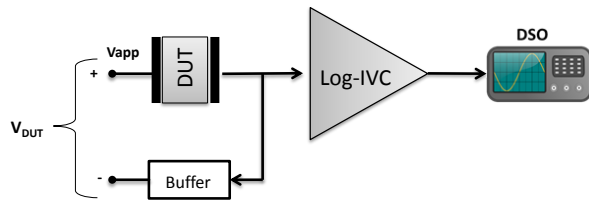
²Institut de Microelectrònica, IMB-CNM (CSIC)

I. INTRODUCTION

Resistive Random Access Memories (RRAMs) are one of the most promising candidates to replace the current flash memories due to their low power operation, fast switching and great scalability^{1,2}. Despite these excellent characteristics, RRAMs present some reliability problems such as the occurrence of current fluctuations on the different resistive states due to random telegraph noise (RTN)^{3,4}. The RTN spectra can be crucial to determine the memory window and the correct memory cell performance. Therefore, a precise characterization of the RTN fluctuations in emerging RRAM cells becomes necessary. Until now, standard characterization equipment has been used to characterize RTN, such as semiconductor parameter analyzers (SPAs), with a measuring time resolution of ~2ms. In this work, we propose an experimental method to measure RTN that allows a higher characterization time resolution than that available with standard characterization equipment. This new method provides additional and relevant information about the RTN phenomenon, which cannot be detected using standard characterization setups.

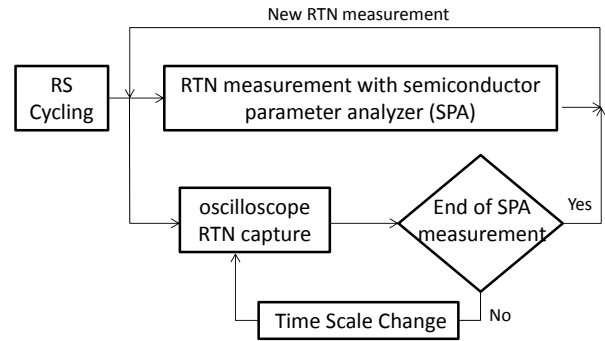
II. MEASUREMENT SETUP AND RESULTS

Devices under test (DUT) consist on a stack of Ni/HfO₂/Si with a 200nm thickness of Ni as the top electrode, an oxide (HfO₂) thickness of 20nm, and highly-doped n-type Si as bottom electrode. The devices area is 5x5µm². Firstly, the devices were subjected to 30 resistive switching cycles, changing successively the dielectric conductivity between a high and a low resistance state (HRS and LRS respectively) with a current limit of 10µA to reach the LRS. Secondly, with the device at HRS, a RTN signal was sought by applying different voltage bias. When current fluctuations were detected, a sequential RTN measurement (using both SPAs and oscilloscope captures) were carried out. Fig. (1) shows a schematic of the advanced experimental setup used to characterize RTN.



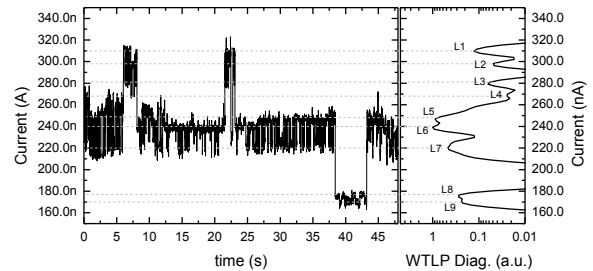
“FIG.1:Schematics of the experimental setup to measure RTN signals. V_{app} is the applied voltage from the semiconductor parameter analyzer and V_{DUT} is the voltage drop across the DUT”.

The voltage, at which RTN appeared (V_{app}), was applied to one of the terminals of the DUT by the SPA, which also allows measuring the current through this terminal. The other terminal of the DUT was connected to a high impedance buffer, which allows measuring the voltage drop across the DUT, and to a logarithmic current-to-voltage converter (Log-IVC), which converts the current into an equivalent voltage to be derived to the oscilloscope (digital storage oscilloscope, DSO).

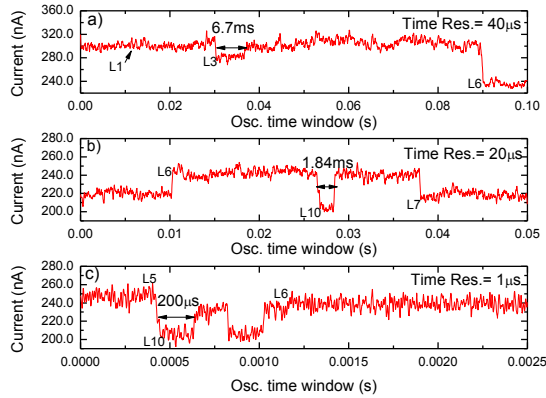


“FIG.2:Block diagram of the RTN measurement process once the RTN signal is detected”.

Fig. (2) shows the block diagram of the RTN measurement process. During the SPA measurement, several oscilloscope captures are registered at different time scales. When the SPA measurement finishes, the sequence defined in Fig. (2) starts again. In this work, about 325 SPA measurements were done and 21 oscilloscope captures were obtained in each measurement.



“FIG.3: (Left) Typical multilevel RTN signal measured by a semiconductor parameter analyzer at V_{app}=1.25V, step time ~6ms and number of measured points 8000. (Right) Trap levels obtained by using the WTLP method”.



“FIG.4: (a) Oscilloscope measurement captured between 7.26s and 9.68s of the SPA measurement with 40 μ s time resolution. (b) Capture between 9.68s and 12.15s with a time resolution of 20 μ s. (c) Capture between 19.5s and 21.93s with a time resolution of 1 μ s”.

Fig. (3 left) shows a typical multilevel RTN signal measured by the SPA with a time resolution of 6ms. On the other hand, Fig. (4) shows three oscilloscope captures at different time scales (40, 20 and 1 μ s), i.e. different time resolution, measured during the same SPA measurement. In all of them some charge trapping and detrapping processes responsible for the RTN signals appear with emission and capture times below 6ms. These fast current fluctuations would be impossible to detect with the SPA. Therefore, it is proved that with the oscilloscope captures it is

possible to determine both the current jumps of existent traps detected in the SPA measurement and new traps not detected with the SPA. In addition, by using the weight time lag plot (WTLP) method⁵ the different states (or levels) of the traps can be accurately calculated (Fig. 5), where the peaks of the diagonal of the WTLP correspond to trap levels.

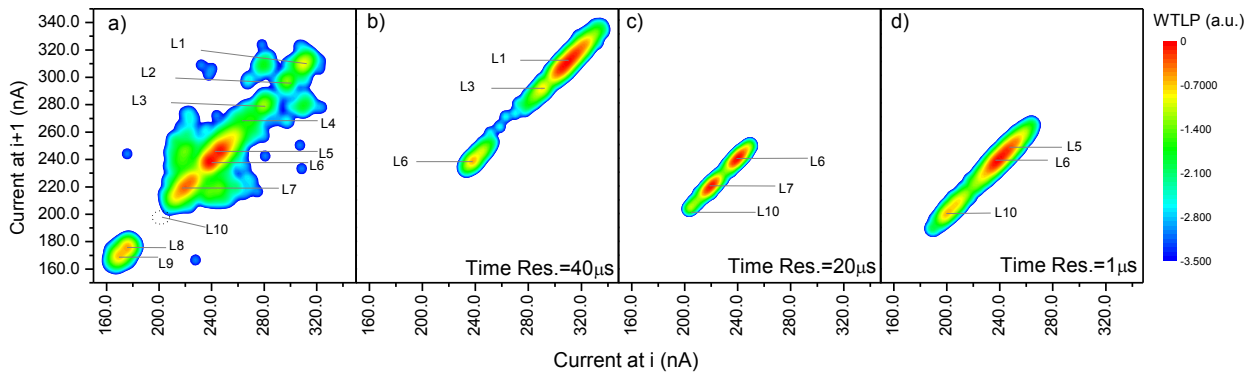
In Fig. 5a, 9 levels (From L1 to L9) are obtained from the RTN signal measured with the SPA shown in Fig. (3 left) using the WTLP method. These levels are also represented in Fig. (3 right). Besides that, the levels detected in the three oscilloscope captures of Fig. (4) are also shown using the WTLP (Fig. 5b, c and d). Comparing these figures with Fig. (5a), a new trap level (L10) in the SPA measurement, indicating that a new trap is detected but with a low probability of occurrence.

III. CONCLUSIONS

A new high time resolution method to characterize RTN signals is presented. The method is able to detect accurate time constants in the microsecond range and fast traps not detected by using standard RTN characterization methods.

ACKNOWLEDGEMENTS

UAB authors acknowledge funding from the Spanish MINECO and ERDF (TEC2013-45638-C3-1-R) and the Generalitat de Catalunya (2014SGR-384). IMB-CNM authors thank the support of the Spanish MINECO under Project No. TEC2011-27292-C02-02.



“FIG.5:WTLP method applied to a)the RTN measured by the SPA (Fig. 4a). 9 trap levels are detected; b) Oscilloscope capture with a time resolution of 40 μ s (Fig. 4b), where 3 trap levels appear; c) Oscilloscope capture with time resolution of 20 μ s with 3 trap levels (Fig. 4c); d) Oscilloscope capture at lower time resolution of 1 μ s with 2 trap levels (Fig. 4d)”.

¹ R. Waser and M. Aono, Nat Mater 6, 833–40 (2007).
² L. Baldi and G. Sandhu, ESSDERC, 30-36 (2013).
³ S. Ambrogio, et. al. IEEE TED 61, 2920–27 (2014)..
⁴ S. Balatti, et. al. IEEE IRPS (2014).
⁵ J. Martin-Martinez, et. al. IEEE EDL 35, 479–81 (2014).

On the Role of Current-Voltage Correlations on the Electric Power Consumption of Electronic Devices

Guillermo Albareda,¹ Fabio Lorenzo Traversa,² and Xavier Oriols³

¹*Institute of Theoretical and Computational Chemistry and Physical Chemistry Department, Universitat de Barcelona, 08028 Barcelona, Spain*
e-mail address: *albareda@ub.edu*

²*Department of Physics, University of California, San Diego, La Jolla, CA 92093-0319, USA*
e-mail address: *example2@physics.edu*

³*Departament d'Enginyeria Electrònica, Universitat Autònoma de Barcelona, 08193 Bellaterra, Spain*
e-mail address: *xavier.oriols@uab.cat*

I. INTRODUCTION

In Landauer's work "Irreversibility and Heat Generation in the Computing Process"¹ it was argued that computing machines inevitably involve devices which perform logical functions that do not have a single-valued inverse. This logical irreversibility is associated with physical irreversibility and requires a minimal heat generation typically of the order of kT for each irreversible function. This dissipation serves the purpose of standardizing signals and making them independent of their exact logical history. Commonly known as Landauer's principle, this seminal paper has led to considerable interest in the study of reversible computing. Recently, physical experiments have tested Landauer's principle^{2,3}.

Landauer's principle can be argued in terms of the first and second laws of thermodynamics for an overall closed system. However, much less is known about the role of the thermodynamic laws in open quantum systems far from equilibrium⁴⁻⁶, for example nanoelectronic devices. Typically, the concept of entropy production in nanoelectronic devices is discussed in terms of heat generation. In this conference, we will focus on the role played by the *local* electrical power (i.e. the rate at which kinetic energy is generated or subtracted from a particular region of the space) on the *local* generation of heat. The electric power is usually understood as a (mean field) observable defined as the product of the current by the (mean field) voltage drop,

$$P_{mf}(t) = \langle I(t) \rangle \langle V(t) \rangle. \quad (1)$$

with $\langle \dots \rangle$ denoting the quantum ensemble average. We will show that a proper treatment of the many body problem can actually induce the breaking down of this definition for open quantum systems. Even while overall electric power of the total system can be still defined as the standard product $P_{mf}(t)$, individual parts of a system may violate this definition.

II. OVERVIEW OF THE PROBLEM

The openness of quantum electron systems has been studied extensively in the literature, but few works are devoted to discuss its effect on the computation of electric

power. Here, we provide a novel expression for the accurate estimation of the electric power in nanoscale open systems deduced from a many-particle electron transport formalism that goes beyond the standard mean field approximation^{7,8}. Surprisingly, we show that the usual expression of the electric power in the device active region, i.e. $P_{mf}(t)$ is inappropriate when dealing with systems with strong (time-dependent) Coulomb correlations. Once such correlations are taken into account, a much more complex recipe is needed to compute the electric power in the active region.

In order to go beyond the mean field approximation, we formulate the problem in terms of the correlation between the (Bohmian) velocity of the i -th electron $\mathbf{v}_i(t)$ and the electrostatic force $q_i \mathbf{E}_i(t)$ made by the rest of electrons of the whole (closed) system on it. It can be shown that the exact mean electric power, P_{corr} , associated to the $N(t)$ electrons enclosed in an open system reads:

$$P_{corr} = \sum_{i=1}^{N(t)} q_i \langle \mathbf{v}_i(t) \mathbf{E}_i(t) \rangle_T, \quad (2)$$

Only when the electric field acting on the i th particle is roughly equal to its mean field value, i.e. $\mathbf{E}_i(t) \approx \mathbf{E}_{mf}(t)$, expression (2) for an open system becomes equal to (1). Let us notice that, although the electric power defined in (2) refers only to those $N(t)$ electrons in the open system, its value is clearly affected by all the M particles composing the whole closed circuit. Since energy is continuously entering and leaving an open system through the interaction among carriers inside and outside its spatial limits, it is of critical importance to properly model the boundary conditions through which the dynamics of electrons within and outside the open system become correlated⁹.

III. CHALLENGES

Given the above result, we will provide new insights into the use of electron Coulomb correlations to manipulate the *local* heat generation of a given device. More specifically, we will address the following question:

Can we design electron-electron Coulomb correlations to manipulate the way in which energy is dissipated along different regions of a circuit?

The answer to this question could be quite relevant considering the fact that power consumption is one of the main drawbacks that electronics must affront when scaling down any new technology¹⁰. Moreover, from a theoretical point of view, the results of this work shed new light into how many-body interactions could affect the thermodynamic limits of computing machines.

ACKNOWLEDGMENTS

This work has been partially supported by the “Ministerio de Ciencia e Innovación” through the Spanish Project TEC2012-31330 and by the Grant agreement no: 604391 of the Flagship initiative “Graphene-Based Revolutions in ICT and Beyond”. G. A. acknowledges the Beatriu de Pinós Program for financial support through Project No. 2010BP-A00069.

¹ R. Landauer, IBM J. Res. Dev. 5, 183 (1961).

² A. Bérut et al., Nature 483, 187 (2012).

³ Y. Jun, et al., Phys. Rev. Lett. 113, 190601 (2014).

⁴ M. Horodecki, and J. Oppenheim. Nat. Comm. 4 (2013).

⁵ P. Skrzypczyk, A. J. Short, and S. Popescu. Nat. Comm. 5 (2014).

⁶ F. Brandao, et al. PNAS doi:10.1073/pnas.1411728112, (2015).

⁷ X. Oriols, Physical Review Letters, 98 (2007) 066803.

⁸ G. Albareda, J. Suñ'e and X. Oriols, Physical Review B, 79 (2009) 075315.

⁹ G. Albareda, H. López, X. Cartoixà, J. Suñ'e, and X. Oriols, Phys. Rev. B, 82, 085301 (2010).

¹⁰ International Technology Roadmap for Semiconductors (2010 Update) <http://www.itrs.net>

$1/f^\beta$ fluctuations from sequences of rectangular pulses

Vaidas Juknevičius, Bronislovas Kaulakys, and Julius Ruseckas

Institute of Theoretical Physics and Astronomy,

Vilnius University, A. Goštauto 12,

LT-01108 Vilnius, Lithuania

e-mail address: bronislovas.kaulakys@tfai.vu.lt

I. INTRODUCTION

Many processes observed in nature, technology and some other areas can be viewed as consisting of many separate events. Such events are localized in time in the sense that their contribution to the whole process is significant only in time intervals that are much shorter than the observation time of the whole process. The processes are usually measured as a change of some quantity y in time t that can be called a signal $y(t)$. Each discrete event that contributes to the process in question can therefore be represented by a *pulse* in the signal $y(t)$ with definite *time of occurrence* and *duration*¹.

Even though the underlying discreteness of the process may not be obvious due to the fact that often only a collective effect of a large number of contributing sources can be observed, the understanding of many phenomena still requires the insight into the discrete nature of entities creating the signal. Most notable, much researched, but still not completely solved problem is the $1/f$ noise in electronic devices².

We investigate stochastic signals that consist of rectangular pulses. The stochasticity here appears as a consequence of random variation of pulse duration and timing of the pulse occurrence. The power-spectral densities (PSD's) of such sequences of pulses under appropriate conditions have a power-law shape¹. Since the power-law-shaped PSD's are ubiquitous in natural phenomena, technology and even quantitative social sciences, the investigation of the conditions under which pulse sequences exhibit such PSD's can be useful for the better understanding of a wide range of phenomena.

In this contribution we present the conditions under which the PSD $S(f)$ of the sequence of pulses obtains power-law shape for small frequencies $S(f) \sim 1/f^\beta$ and how the spectral power β depends on the statistical parameters of pulse timing. We also present a model of charge carrier trapping in disordered materials that satisfies the conditions for producing $1/f$ noise.

II. OVERLAPPING AND NON-OVERLAPPING PULSES

Let us consider a process that consists of discrete events and can be represented by a signal $y(t)$ – a sequence of pulses. $y(t)$ can be expressed as a sum of individual pulses $x_k(t)$ shifted in time:

$$y(t) = \sum_k x_k(t - t_k) \quad (1)$$

Here $x_k(t)$ is the shape of the k -th pulse and t_k – the time of its occurrence. The shape of each pulse $x_k(t)$ is described by a set of parameters (for example, the amplitude, duration etc.) which can obtain random values.

We investigate a simple case of stationary sequences of rectangular pulses of constant amplitude whose durations $\{\tau_k\}$ are independent identically distributed (i.i.d.) random variables.

The timing of pulses can be defined either by the time interval $\theta_k = t_{k+1} - t_k$ between the occurrence of successive k -th and $(k+1)$ -st pulses or by the time interval $\delta_k = t_{k+1} - t_k - \tau_k$ between the end of the k -th pulse (at time $t_k + \tau_k$) and the start of the $(k+1)$ -st pulse (at time $t_{k+1} > t_k + \tau_k$). We will call δ_k the *gap* between successive pulses. We assume that one of these two quantities – either θ_k or δ_k – together with the pulse duration τ_k are i.i.d., and thus there are two distinct possibilities for the construction of the pulse sequences in this case: (*possibly overlapping pulses* where the duration and timing of pulses are defined by two independent quantities τ_k and θ_k , and *non-overlapping pulses* where the $(k+1)$ -st pulse begins only after the k -th pulse ends, and therefore the two independent quantities describing the pulse duration and timing are τ_k and δ_k).

A schematic representation of a signal described above in the case of rectangular pulses with constant amplitude a is given in Fig. 1.

III. SPECTRAL PROPERTIES

The one-sided power-spectral density (PSD) of the signal $y(t)$ is defined as follows:

$$S(f) = \lim_{T \rightarrow \infty} \left\langle \frac{2}{T} \left| \int_{t_i}^{t_f} dt y(t) e^{-i2\pi ft} \right|^2 \right\rangle \quad (2)$$

Here T is the observation time, $T = t_f - t_i$.

Under the assumptions of stationarity and ergodicity of $y(t)$ (1) with pulses $x_k(t)$ sufficiently localized in time, one gets the following PSD's for rectangular pulses with *exponentially distributed durations* τ_k :

$$S(f) = \frac{4\bar{\nu} a^2 \bar{\tau}^2}{1 + (2\pi f \bar{\tau})^2} \left[\Re \left\{ \frac{\chi_\theta(f)}{1 - \chi_\theta(f)} \right\} + 1 \right] \quad (3)$$

for possibly overlapping pulses and

$$S(f) = \frac{4\bar{\nu} a^2 \bar{\tau}^2}{1 + (2\pi f \bar{\tau})^2} \Re \left\{ \frac{1 - i2\pi f \bar{\tau} (1 - \chi_\delta(f))}{(1 - \chi_\delta(f)) - i2\pi f \bar{\tau}} \right\} \quad (4)$$

for non-overlapping pulses (this case is often called *random telegraph noise*). Here \Re denotes the real part, $\chi_\theta(f)$ and $\chi_\delta(f)$ are the characteristic functions of θ_k and δ_k , respectively. $\bar{\nu}$ is the *average rate of pulse occurrence* which is $\bar{\nu} = \bar{\theta}^{-1}$ and $\bar{\nu} = (\bar{\theta} + \bar{\delta})^{-1}$ for the respective cases (3) and (4), and $\bar{\tau}$, $\bar{\theta}$ and $\bar{\delta}$ are the averages of the quantities τ_k , θ_k and δ_k , respectively.

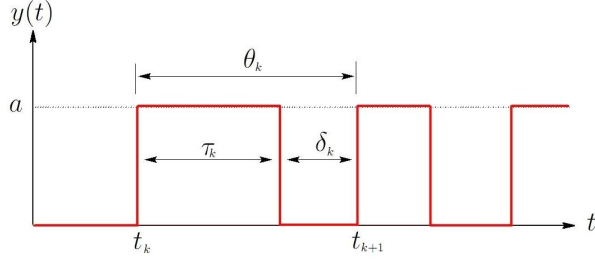


FIG. 1. A schematic representation of a signal, consisting of rectangular pulses with constant amplitude a . The three quantities that define pulse timing (only two of them independent): pulse duration τ_k , gap between successive pulses δ_k and inter-pulse time (time between the occurrence of successive pulses) θ_k .

IV. POWER-LAW SPECTRA

Analytical and numerical calculations suggest that, for sequences of rectangular pulses (1) with exponentially distributed pulse durations, the *power-law* PSD with power β for small frequencies

$$S(f) \sim \frac{1}{f^\beta} \quad (5)$$

can be obtained in both cases (3) and (4) when either the times between the occurrence of successive pulses θ_k or the gap durations δ_k between pulses are power-law distributed with the power $\gamma > 1$ or, alternatively, $\gamma = 1 + \alpha$ with $\alpha > 0$:

$$p(\vartheta) \sim \vartheta^{-(1+\alpha)}, \quad \vartheta_{\min} \leq \vartheta < \vartheta_{\max}, \quad (6)$$

Here $p(\vartheta)$ denotes the probability density of the quantity ϑ which can be one of the quantities θ_k or δ_k and the bounds of the power-law region $\vartheta_{\max} \gg \vartheta_{\min}$.

The additional condition for the occurrence of the power-law PSD (5) is that the average $\bar{\tau}$ of the exponentially distributed pulse duration τ_k must be greater than the average inter-pulse time $\bar{\vartheta}$, that is $\bar{\tau} \gg \bar{\vartheta}$.³ For

$\alpha > 1$ we can get the finite average value $\bar{\vartheta} = \frac{\alpha}{\alpha-1} \vartheta_{\min}$ for $\vartheta_{\max} \rightarrow \infty$. However, in order for $\bar{\vartheta}$ to be finite in the case $\alpha \leq 1$, ϑ_{\max} must be finite.

If the above conditions are fulfilled, then we get the power-law PSD (5) for the frequencies between $f_{\min} \approx \vartheta_{\max}^{-1}$ and $f_{\max} \approx \vartheta_{\min}^{-1}$ where the power β depends on α as follows:

$$\beta(\alpha) \approx \begin{cases} \alpha & \alpha < 1 \\ 2 - \alpha & 1 \leq \alpha < 2 \\ 0 & \alpha \geq 2 \end{cases} \quad (7)$$

We see that the $1/f$ noise ($\beta=1$ in (5)) is obtained when $\alpha = 1$, i.e., the distribution of the inter-pulse time ϑ (either θ_k or δ_k) has a power-law distribution $p(\vartheta) \sim \vartheta^{-2}$ for a wide range of ϑ . Such case is shown in Fig. 2.

V. CHARGE CARRIER TRAPPING

The results presented above have been applied to the model describing current fluctuations in defective materials due to the charge carrier trapping⁴.

The model states that a charge carrier moving through some disordered material is successively trapped in and released from trapping centers with widely distributed release rates. For the appropriately chosen distribution of the release rates, the resulting current corresponds to the signal of non-overlapping pulses with power-law distribution of gaps between pulses with the power -2 , resulting in the $1/f$ PSD in a wide range of frequencies.

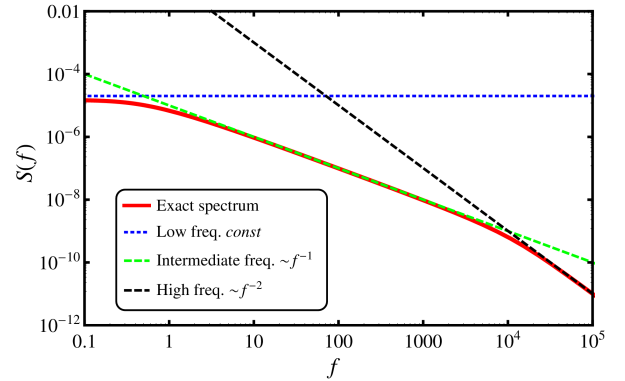


FIG. 2. The PSD $S(f)$ resulting from the model of charged particle trapping. The thick red line shows the exactly calculated spectrum, dashed and dotted lines are approximations for different frequency regions (see legend).

¹ B. Kaulakys, V. Gontis and M. Alaburda, Phys. Rev. E Review **71**, 051105 (2005).

² L. K. J. Vandamme and F. N. Hooge, IEEE Trans. Electron. Devices **55**, No. 11, 3070 (2008)

³ F. Grüneis, Fluct. Noise Lett. **9**, No. 2, 229-243 (2010).

⁴ T. Grasser, Microelectron. Reliability **52**, 39-70 (2012).

D'yakonov-Perel' spin decay in the weak scattering regime and the case of graphene

Xavier Cartoixa¹

¹*Departament d'Enginyeria Electrònica, Universitat Autònoma de Barcelona, 08193 Bellaterra, Barcelona, Spain
e-mail address: Xavier.Cartoixa@uab.cat*

I. INTRODUCTION

In the past two decades, there has been a strong interest in spin effects in semiconductors for applications in spintronics^{1,2}. The use of electron spin for information processing, storage and transmission naturally demands a detailed knowledge of the spin dynamics within the host material.

When a spin imbalance is created in a semiconductor, typically there are three mechanisms that will try to restore equilibrium, namely (a) the Elliot-Yafet (EY) mechanism^{3,4}, related to the fact that states with a general \mathbf{k} are not strict spin eigenstates, and thus there is a finite probability for a spin flip at an otherwise spin-independent scattering event; (b) the Bir-Aronov-Pikus mechanism⁵, related to a hyperfine-like interaction between electrons in the conduction band and holes in the valence band; and (c) the D'yakonov-Perel'⁶ (DP) mechanism, related to spin precession about a random magnetic effective field caused by the spin-orbit interaction in a non-centrosymmetric system.

As of lately, the interest in the dynamics of spins in 2DEGs has revived due to the special characteristics of graphene⁷. In the traditional analysis of the DP mechanism^{6,8}, expressions are obtained for the spin lifetime tensor in the strong scattering regime, meaning that $\omega_L \tau_p \ll 1$, where ω_L is a characteristic Larmor frequency for spin precession and τ_p is the momentum relaxation time. Under these conditions, it can be shown^{6,8-11} that the spin lifetime τ_s is proportional to τ_p^{-1} , a feature that is extensively used to discriminate the DP mechanism from other forms of spin decay. Experimental observations in graphene have found that at low temperatures $\tau_s \propto \tau_p$, as characteristic for the EY mechanism¹²; however, results at low carrier densities suggest that a combination of both mechanisms is at play¹³.

We will present in this conference theoretical evidence that the results in graphene can be understood from the DP mechanism operating in the *weak* scattering regime, e.g. $\omega_L \tau_p \gg 1$. There have been some passing comments^{14,15} that $\tau_s \propto \tau_p$ when $\omega_L \tau_p \gg 1$, and here we will present a series expression for the spin lifetime valid in the general $\omega_L \tau_p$ case confirming the weak scattering behavior $\omega_L \tau_p \gg 1$. Obtaining a closed (or few-term) form for the general case remains an open question.

II. RESULTS

The Hamiltonian describing the spin-orbit interaction for electrons in the conduction band of an n -dimensional semiconductor can usually be written as

$H(\mathbf{k}) = \hbar/2 \mathbf{\Omega}(\mathbf{k}) \cdot \boldsymbol{\sigma}$, where $\mathbf{\Omega}$ is a precession vector, which depends on the electron momentum \mathbf{k} , and $\boldsymbol{\sigma}$ is a vector composed of the three Pauli matrices. This Hamiltonian indicates that spins evolve deterministically until the electron scatters, when a new \mathbf{k} is obtained probabilistically. Thus, the overall evolution of a single spin is a stochastic problem.

The time evolution of a single spin can be cast quantitatively as

$$i\hbar \frac{\partial |\psi\rangle}{\partial t} = H[\mathbf{k}(t)]|\psi\rangle, \quad (1)$$

where $|\psi\rangle$ is the spinor describing the state of an individual state. The spinor univocally determines an expectation value; and the converse is also true except for an overall phase of the spinor. If we define $\mathbf{s} \equiv \langle \psi | \boldsymbol{\sigma} | \psi \rangle$, a standard derivation from Eq. (1) readily yields the classical expression

$$\dot{\mathbf{s}} = \mathbf{\Omega}[\mathbf{k}(t)] \times \mathbf{s} = \overline{\overline{\mathbf{\Omega}}}[\mathbf{k}(t)] \mathbf{s}, \quad (2)$$

where $\overline{\overline{\mathbf{\Omega}}}$ is an antisymmetric matrix providing the vector product of $\mathbf{\Omega}$ with whatever follows.

Since, in general, Hamiltonians at different times do not commute, the time evolution operator cannot be written as $U(t, t_0) = \exp\left\{-i/\hbar \int_{t_0}^t H(t') dt'\right\}$. Most commonly, the solution to Eq. (1) is written as a Dyson series¹⁶, though lately the Magnus expansion¹⁷ applied to Eq. (2) has gained favor¹⁸ because it preserves the unitarity of the evolution to all orders in the series.

The techniques from the preceding paragraph and others^{8,11} are well suited for the study of spin dynamics in the strong scattering regime. In the conference, we will present a highly intuitive approach naturally suited to the study of the weak scattering regime. Let us study the evolution of a *single* spin, initially at \mathbf{s}_i from an initial time t_0 to a final time t . Class n processes will be those where the electron momentum has scattered n times during the interval $(t - t_0)$, and the spin has evolved into a value $\mathbf{s}_n(t)$ given by

$$\mathbf{s}_n(t) = \prod_{j=0}^n \frac{1}{t_{j+2} - t_0} \int_{t_0}^{t_{j+2}} dt_{j+1} R[(t_{j+1} - t_j)\mathbf{\Omega}(\mathbf{k}_j)] \mathbf{s}_i, \quad (3)$$

where t_j is the time at which an individual scattering event takes place, $t_{j \geq n} = t$ and proper averaging of the times of the scattering events has been made¹⁹. The probability that evolution from t_0 to t has actually been of class n will be given by a Poisson distribution with mean τ_p , the momentum scattering time. From

Eq. (3) the following recurrence relationship immediately follows:

$$\mathbf{s}_n(t) = R[(t - t_n)\mathbf{\Omega}(\mathbf{k}_n)] \mathbf{s}_{n-1}(t_n), \quad p_n = \frac{(t/\tau_p)^n e^{-t/\tau_p}}{n!}, \quad (4)$$

where $R[t\mathbf{\Omega}]$ is a rotation of angle $t|\mathbf{\Omega}|$ about the vector $\mathbf{\Omega}$, and with the Poisson distribution explicitly stated. The time evolution of an ensemble will necessarily involve additional integrations over the distribution of momenta of the particles.

The results above are valid for any values of $\omega_L\tau_p$, but it is hard to extract any information valid for all regimes. However, under weak scattering conditions only the first terms in the series will need to be taken into account. In the case of a 2D material with spherical bands and isotropic elastic scattering, for a given energy one readily has

$$\langle \mathbf{s}(t) \rangle \simeq e^{-t/\tau_p} \left\{ \frac{1}{2\pi} \int_0^{2\pi} d\theta_0 R[(t - t_0)\mathbf{\Omega}(k, \theta_0)] + \frac{1}{(2\pi)^2\tau_p} \int_0^{2\pi} d\theta_0 \int_0^{2\pi} d\theta_1 \int_0^t dt_1 R[(t - t_1)\mathbf{\Omega}(k, \theta_1)] \times R[(t_1 - t_0)\mathbf{\Omega}(k, \theta_0)] \right\} \mathbf{s}_i, \quad (5)$$

where $\langle \rangle$ denotes an ensemble average.

Equation (5) clearly shows that in the weak scattering regime the spin lifetime will be exactly the momentum relaxation time, ie. $\tau_s = \tau_p$, even though we are in a situation where only the DP spin relaxation mechanism

is allowed. Such conditions are expected to take place in high quality graphene, with mean free paths of the order of $1 \mu\text{m}$ at room temperature and 100 's of μm 's at low T ²⁰, which translate into momentum relaxation times of the order of 1-100 ps, for a precession frequency of ~ 120 THz for graphene on Au(111)²¹.

Discussion – Among the many surprising properties of graphene, one of them might be that it is the first material where the DP spin relaxation mechanism manifests itself in the weak scattering regime, with the spin lifetime having the same temperature dependence as the momentum relaxation time. The treatment that will be presented at the conference allows obtaining results under a few specific conditions, but a more general formalism is still missing. The study of the information that can be provided by the characterization of the fluctuations in the spin signal is in its infancy^{22,23}. Finally, it should always be kept in mind that a problem very similar to DP spin relaxation is studied in Nuclear Magnetic Resonance, and any insight from one field would have an immediate impact on the other.

ACKNOWLEDGMENTS

The author acknowledges financial support by the Spanish Ministerio de Economía y Competitividad under Project No. TEC2012-31330. Also, the research leading to these results has received funding from the European Union Seventh Framework Programme under grant agreement No. 604391 Graphene Flagship.

-
- ¹ G. A. Prinz, Phys. Today **48**, 58 (1995).
² S. A. Wolf, D. D. Awschalom, R. A. Buhrman, J. M. Daughton, S. von Molnár, M. L. Roukes, A. Y. Chtchelkanova, and D. M. Treger, Science **294**, 1488 (2001).
³ R. J. Elliott, Phys. Rev. **96**, 266 (1954).
⁴ Y. Yafet, in *Solid State Physics*, edited by F. Seitz and D. Turnbull (Academic Press, New York, 1963), vol. 14, pp. 1–98.
⁵ G. L. Bir, A. G. Aronov, and G. E. Pikus, Zh. Eksp. Teor. Fiz. **69**, 1382 (1975), [Sov. Phys. JETP **42**, 705 (1976)].
⁶ M. I. D'yakonov and V. I. Perel', Fiz. Tverd. Tel. **13**, 3581 (1971), [Sov. Phys. Solid State **13**, 3023 (1972)].
⁷ D. V. Tuan, F. Ortmann, D. Soriano, S. O. Valenzuela, and S. Roche, Nature Physics **10**, 857 (2014).
⁸ G. E. Pikus and A. N. Titkov, in *Optical Orientation*, edited by F. Meier and B. P. Zakharchenya (North Holland, Amsterdam, Netherlands, 1984), vol. 8, pp. 73–131.
⁹ M. I. D'yakonov and V. Y. Kachorovskii, Fiz. Tekh. Poluprovodn. **20**, 178 (1986), [Sov. Phys. Semicond. **20**, 110 (1986)].
¹⁰ W. Knap, C. Skierbiszewski, A. Zduniak, E. Litwin-Staszewska, D. Bertho, F. Kobbi, J. L. Robert, G. E. Pikus, F. G. Pikus, S. V. Iordanskii, et al., Phys. Rev. B **53**, 3912 (1996).
¹¹ N. S. Averkiev and L. E. Golub, Phys. Rev. B **60**, 15582 (1999).
¹² W. Han and R. K. Kawakami, Phys. Rev. Lett. **107**, 047207 (2011).
¹³ P. J. Zomer, M. H. D. Guimarães, N. Tombros, and B. J. van Wees, Phys. Rev. B **86**, 161416 (2012).
¹⁴ D. Culcer and R. Winkler, Phys. Rev. B **76**, 195204 (2007).
¹⁵ M. Dyakonov, in *Spin Physics in Semiconductors*, edited by M. I. Dyakonov (Springer Berlin Heidelberg, 2008), vol. 157 of *Springer Series in Solid-State Sciences*, pp. 1–28, ISBN 978-3-540-78819-5.
¹⁶ F. J. Dyson, Phys. Rev. **75**, 1736 (1949).
¹⁷ W. Magnus, Comm. Pure and Appl. Math. **7**, 649 (1954), ISSN 1097-0312.
¹⁸ S. Blanes, F. Casas, J. Oteo, and J. Ros, Phys. Rep. **470**, 151 (2009), ISSN 0370-1573.
¹⁹ Of course, there is no integral over the final time t .
²⁰ L. Wang, I. Meric, P. Y. Huang, Q. Gao, Y. Gao, H. Tran, T. Taniguchi, K. Watanabe, L. M. Campos, D. A. Muller, et al., Science **342**, 614 (2013).
²¹ D. Marchenko, A. Varykhalov, M. Scholz, G. Bihlmayer, E. Rashba, A. Rybkin, A. Shikin, and O. Rader, Nature Comm. **3**, 1232 (2012).
²² G. M. Müller, M. Oestreich, M. Römer, and J. Hübner, Phys. E **43**, 569 (2010), ISSN 1386-9477.
²³ J. Hübner, F. Berski, R. Dahbashi, and M. Oestreich, phys. stat. sol. (b) **251**, 1824 (2014), ISSN 1521-3951.

Current Fluctuations Originating from Non-Metallic (Physical) Leads

Guillermo Albareda,¹ Liping Chen,² Xavier Oriols,³ and Ignacio Franco⁴

¹*Institute of Theoretical and Computational Chemistry and Physical Chemistry Department, Universitat de Barcelona, 08028 Barcelona, Spain*
e-mail address: *albareda@ub.edu*

²*Department of Chemistry, University of Rochester, Rochester NY 14627, United States*
e-mail address: *liping.chen@rochester.edu*

³*Departament d'Enginyeria Electrònica, Universitat Autònoma de Barcelona, 08193 Bellaterra, Spain*
e-mail address: *xavier.oriols@uab.cat*

⁴*Department of Chemistry, University of Rochester, Rochester NY 14627, United States*
e-mail address: *ignacio.franco@rochester.edu*

I. OVERVIEW OF THE PROBLEM

The modelization of the conductance in nanoscale systems requires the consideration of overall charge neutrality and current conservation^{1,2}. Imposing overall charge neutrality assures that unbalanced charges at the borders of the active region bring about the correct voltage drop along the leads and reservoirs through the Poisson equation. In addition, the total (particle and displacement) current in the active region must be equal to the total current measured on the surface of an ammeter located far away from the active region, in the reservoir, i.e. current conservation.

The conservation of the electrical current

The conservation of the electrical current, i.e. the total (conduction plus displacement) current computed on a surface in the simulation box is equal to the total current measured on a surface of an ammeter located far from the sample, is a necessary requirement for the prediction of ac conductances, specially at high frequencies. The explicit consideration of the displacement current assures that the total current density is a divergenceless vector. Important theoretical contributions were done by Büttiker and co-workers for predicting ac properties of mesoscopic systems within a frequency-dependent scattering matrix formalism, in weakly nonlinear regimes^{1,3}.

The overall charge neutrality

The importance of overall charge neutrality, i.e. that the total charge in the whole device is zero, was clarified by the work of Landauer, Büttiker, and co-workers⁴ on the “two-terminal” and the “four-terminal” conductance of ballistic devices. The well-known standard textbook expression of the dc (zero-temperature) conductance through a tunneling obstacle is known as the two-terminal equation because it is defined as the current divided by the voltage drop sufficiently far from the obstacle. However, the original formulation of the conductance proposed by Landauer⁵ in 1957 was known as the four-terminal conductance because its experimental val-

idation needs two additional voltage probes to measure the voltage drop close to the tunneling obstacle. The presence of resistances in the leads explains the difference between both expressions. The ultimate origin of such resistances is the requirement of overall charge neutrality that transforms unbalanced charges in the leads into a voltage drop via the Poisson (Gauss) equation. As a relevant example of their deep understanding of time-dependent mesoscopic scenarios, they predicted the value of the resistance in a quantum RC⁶ which has been recently experimentally confirmed⁷.

Quantum transport models

Electron-transport models do include reasonable approximations that guarantee the accomplishment of the overall charge neutrality requirement. In addition, those simulators that are developed within a time-dependent or frequency-dependent framework can also assure the current conservation requirement. However, the expensive treatment of quantum and atomistic effects can only be applied to a very limited number of degrees of freedom. In fact, a very small simulation box is a mandatory requirement in modern electron transport simulators. Small means here that the leads, the spatial region separating ideal metallic conditions from the active region of the electronic device, are excluded from the simulations. For most circuit designs it can be assumed that the leads do not contribute to the electrical effects of individual components. This assumption, however, begins to break down at high frequencies and very small scales. Capacitances between the ends of the leads where they connect to the device and inductances and resistances along them can become important at high frequencies and even crucial when trying to predict the noise performance of such devices.

II. CHALLENGES

In principle, the problem of excluding the leads from the simulation box could be solved by providing adequate boundary conditions (BCs) on each of the “open” borders of the simulation box⁸. Unfortunately, at far from equilibrium conditions, neither the charge density,

the electric field nor the scalar potential have easily predictable values at the borders of the active region, specially when an external time-dependent field is being applied⁹. Among several attempts to formulate accurate BCs that reach both overall charge neutrality and current conservation none is accurate enough to capture far from equilibrium conditions. Moreover, the performance of these algorithms for time-dependent scenarios is usually even worse.

Based on the recent development of a time-dependent BCs algorithm that is able to preserve both current conservation and overall charge neutrality^{10,11}, in this conference we will present new insights into the time-dependent fluctuations of electrical characteristics that arise from the assumption of a more realistic contact model. We will focus, in particular, on the current fluctu-

ations originating from finite screening lengths in molecular devices operating under the effect of an external electromagnetic field¹².

ACKNOWLEDGMENTS

This work has been partially supported by the “Ministerio de Ciencia e Innovación” through the Spanish Project TEC2012-31330 and by the Grant agreement no: 604391 of the Flagship initiative “Graphene-Based Revolutions in ICT and Beyond”. G. A. acknowledges the Beatriu de Pinós Program for financial support through Project No. 2010BP-A00069.

¹ Y. M. Blanter and M. Büttiker, Phys. Rep. 336, 2 (2000)

² R. Landauer, Phys. Scr. T42, 110 (1992).

³ M. Büttiker, H. Thomas, and A. Prêtre, Phys. Lett. A 180, 364 (1993); M. Büttiker, A. Prêtre, and H. Thomas, Phys. Rev. Lett. 70, 4114 (1993); M. Büttiker, H. Thomas and A. Prêtre, Z. Phys. B 94, 133 (1994); M. Büttiker, J. Phys.: Condens. Matter 5, 9361 (1993); M. Büttiker and S. E. Nigg, Nanotechnology 18, 044029 (2007).

⁴ M. Büttiker, Y. Imry, R. Landauer, and S. Pinhas, Phys. Rev. B 31, 6207 (1985).

⁵ R. Landauer, Philos. Mag. 21, 863 (1970); R. Landauer, IBM J. Res. Dev. 1, 223 (1957).

⁶ M. C. Goorden and M. Büttiker, Phys. Rev. Lett. 99, 146801 (2007).

⁷ J. Gabelli, et al., Science 313, 499 (2006).

⁸ M. Javid and P. M. Brown, *Field Analysis and Electromagnetics* McGraw-Hill, New York, USA, 1963.

⁹ P. Myöhänen, R. Tuovinen, T. Korhonen, G. Stefanucci, and R. van Leeuwen, Phys. Rev. B 85, 075105 (2012)

¹⁰ G. Albareda, H. López, X. Cartoixà, J. Suñé, and X. Oriols, Phys. Rev. B 82, 085301 (2010).

¹¹ G. Albareda, A. Benali and X. Oriols, J. Comp. Electr. 12, 730 (2013).

¹² L. Chen, T. Hansen, I. Franco, J. Phys. Chem. C 118, 20009 (2014)

Elastic response and secondary structure of single-stranded DNA

Xavier Viader-Godoy,¹ Joan Camunas-Soler,¹ Maria Marti-Prieto,¹ and Felix Ritort^{1,2}

¹*Departament de Física Fonamental, Universitat de Barcelona, Diagonal 647, 08028 Barcelona, Spain*

²*CIBER de Bioingeniería, Biomateriales y Nanomedicina, Instituto de Salud Carlos III, Madrid, Spain*
email: fritort@gmail.com

Single-stranded DNA (ssDNA) plays a major role in several biological processes, such as replication or transcription. Therefore, it is of fundamental interest to understand how the elastic response and the formation of secondary structures are modulated by non specific base pairing and the electrostatic interactions. In general, these are non-specific interactions that make the elastic properties of ssDNA more complex than for double-stranded DNA (dsDNA). Furthermore, its properties have been less well studied than for dsDNA. Single-stranded DNA is obtained by mechanically unzipping a DNA hairpin attached to two micron-sized beads using optical tweezers, and the thermal fluctuations play a major role since the energies involved in the formation of this secondary structure are of the order of $k_B T$. The mechanical response of ssDNA has been collected in four different-length DNA-hairpin molecules: 6770bp, 3665bp, 1758bp and 480bp, and it shows two different regimes.

I. ELASTIC RESPONSE OF SSDNA

Over 15pN (at room temperature) the elastic behaviour of the force-extension curves can be fitted using the Worm-Like Chain model:

$$f = \frac{k_B T}{L_p} \left[\frac{1}{4} \left(1 - \frac{x}{L_0} \right)^{-2} + \frac{x}{L_0} - \frac{1}{4} \right]. \quad (1)$$

Where L_p and L_0 are the persistence length and the contour length, the characteristic elastic parameters of the studied molecules. The force only depends on the relative x/L_0 since the original hamiltonian is obtained by only considering local deformation terms, which agrees with previous data¹, within the uncertainty.

II. SECONDARY STRUCTURE OF SSDNA

Under stretching forces of 10pN, the ssDNA molecules show a plateau that indicates the formation of a non-specific secondary structure.

Nucleic acids, specially RNA, have been found^{2,3} to be able to create long-range structures. In the force-relative extension curves shown in Fig. (1), they would appear in the form of differences between the force-plateau of different-length molecules: higher plateau-forces for longer molecules. Despite what has been previously

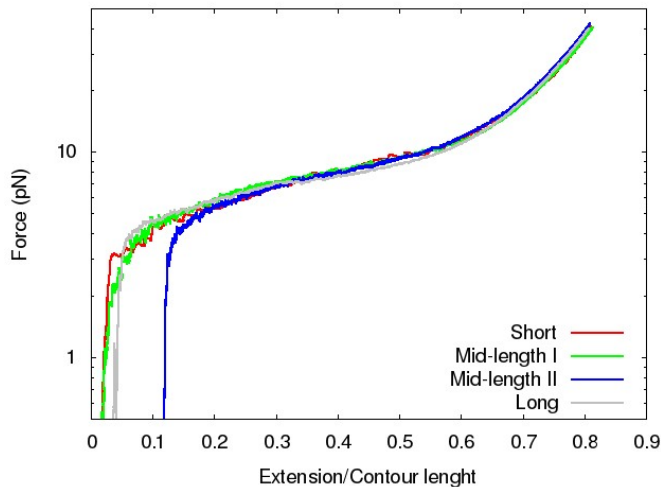


FIG. 1. Data of Short (480bp), Mid-length I (1758bp), Mid-Length II(3565bp) and Long (6770bp) are depicted in this semilogarithmic Force-Normalized Extension. It can be seen the elastic response over 15pN, and under 10pN the emergence of a secondary structure that does not depend on the length of the studied molecules. Data has been averaged in order to minimize the thermal fluctuations.

shown¹, this differences are not found in the random sequences we are working with. Furthermore, a cinematic model based on a previous one⁴ of structural disorder is being develop in order to describe the results shown in Fig. (1).

¹ A. Bosco, J.Camunas-Soler and F. Ritort, *Nucleic Acids Res.* **42**, 2064–2074 (2014).

² I. Tinoco Jr, C. Bustamante, *J Mol Biol.* **293**, 271–281 (1999)

³ D. Sen, W. Gilbert, *Nature* **334**, 364–366 (1988).

⁴ J. Camunas-Soler *et al.*, *ACS Nano.* **7**, 5102–5113 (2013).

Thermodynamic and kinetic analysis of a DNA hairpin using optical tweezers and a temperature controller

Marc Rico-Pasto,¹ Marco Ribezzi-Crivellari,¹ and Felix Ritort^{1,2}

¹*Departament de Física Fonamental, Facultat de Física,*

Universitat de Barcelona, Diagonal 645, 08028 Barcelona, Spain

²*Centro de Investigacion Biomedica en Red-Bioingenieria, Biomateriales y Nanomedicina (CIBERN-BBN)*
e-mail address: fritort@gmail.com

In the last decades a large number of astonishing molecular nano-structures and nano-machines operating inside the cell have been discovered. Examples range from the DNA double helix, the most dense memory support in nature, to molecular motors, which are far more efficient than macroscopic machines. In the study of these objects, one of the most important new technologies are optical tweezers (OT).

OTs can trap and manipulate microscopic objects in a non-invasive way using light¹. They consist of highly focused laser beams and can trap nano and microscopic dielectric objects, from neutral atoms to plastic microbeads. By trapping we mean the ability to exert forces on one object and thus to constrain its position in a certain region of space. For example we are able to exert force on a single cell, or to measure the force required to unfold the secondary structure of a double stranded deoxyribonucleic acid (dsDNA) molecule².

As temperature plays a key role in all biological processes, slight changes of temperature may lead to completely different behaviours of biological systems, or in our case the behaviour of a short DNA hairpin. In fact, living matter carry out its function in a small range of temperature. Therefore, it is interesting to study and understand what is the effect of temperature in biological systems. In this project we aim to understand and characterize the thermodynamic, kinetic and elastic response of a DNA hairpin at different temperature.

We have used the OT technique in order to measure and exert force in a DNA hairpin. Under the effect of a mechanical force at different temperatures we can perform two kinds of experiment: 1) Equilibrium (Hopping) experiment and 2) Non-equilibrium (Pulling) experiments.

A DNA hairpin is a single stranded deoxyribonucleic acid (ssDNA) that can fold into themselves to form a hairpin structure. This structure has two different part, the first one that is called stem is the region of the ssDNA that can form base-pairs (in our case 20 base-pairs), it means that when the DNA hairpin is folded the stem forms a dsDNA. The other part of the hairpin is called loop. The loop is the region of the ssDNA that can not form base-pairs, this part connects each strand of the dsDNA when the hairpin is unfold, in our case we have a tetraloop (4 bases). This molecule is attached between two polystyrene microscopic beads flanked by two dsDNA handles at each side of the molecule. The aim of the handles is to prevent non-specific interactions

(Fig 1-a).

To exert mechanical force to the molecule one bead is trapped in the optical trap, whereas the other bead is held fixed at the tip of a micro-pipette. With this setup we can exert force on the molecule maintaining one bead fixed on the tip of the micro-pipette, and manipulating the other using the optical trap. Controlling the distance between the centre of the OT and the tip of the micro-pipette, distance λ , we can increase or decrease the exerted force on the molecule. To perform hopping experiments we maintain constant λ , while to perform experiments out of equilibrium we increase/decrease λ to change the exerted force. Then we obtain the elastic response of the molecule in a Force-Distance curve (FDC) (Fig. 1-b).

By fitting the stretching response (FDC) of DNA hairpin to a semi-flexible polymer model, equation 1, we have obtained the temperature dependence of the persistence length, L_p ³.

$$L_p = \frac{k_B T}{f_U} \left(\frac{4}{\left(1 - \frac{x_{ssDNA}}{L_c}\right)^2} + \left(\frac{x_{ssDNA}}{L_c}\right) - 4 \right), \quad (1)$$

where f_U is the measured force when the molecule becomes unfolded. L_c is contour length, $k_B T$ is the product between the temperature and the Boltzmann constant and finally x_{ssDNA} is:

$$x_{ssDNA} = \frac{\Delta f}{k_{eff}^F} + d_0 \cdot \left(\coth \frac{f_U \cdot d_0}{k_B T} - \frac{k_B T}{f_U \cdot d_0} \right). \quad (2)$$

In equation 2 Δf is the difference of force at the moment when the stem breaks. k_{eff}^F is the slope of the FDC at moment of the molecule breaks in the branch when the molecule is folded. Finally d_0 is the diameter of the DNA hairpin when is folded.

Taking into account this elastic parameter we can characterize the free energy difference, ΔG_0 , between the folded and unfolded state of the molecule. To calculate ΔG_0 we calculate de energy difference between both states performing hopping experiment (Fig. 1-c). To measure this we use the Kramer's theory that relates differences in energy whit the kinetic involved in each transition, Fig. 1-d.

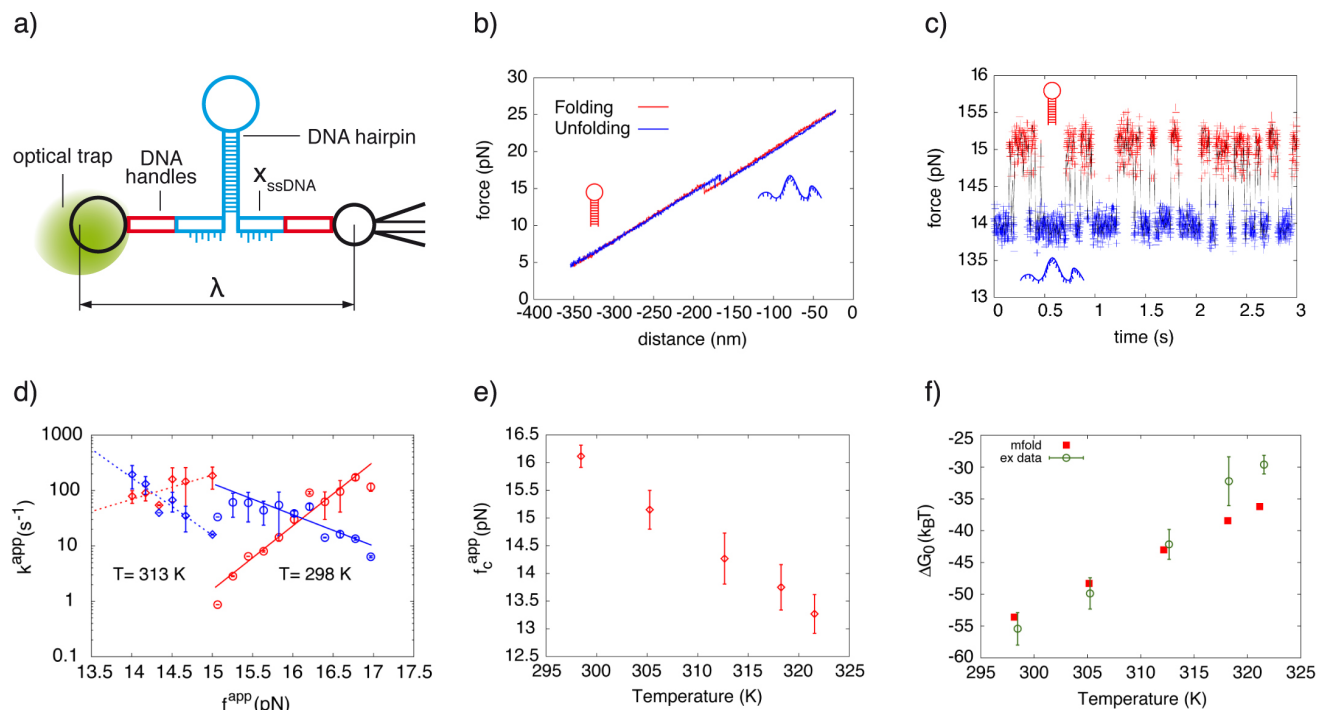


FIG. 1. a) The molecular construct is attached between two beads, one held by the suction of a micro-pipette and the other captured in the optical trap. b) Elastic response of a DNA hairpin presented in a Force-Distance curve (FDC). The rip in the FDC shows the moment when the molecule unfolds. c) Force-Time curve obtained during a hopping experiment. The blue points (high forces) are obtained when the molecules is folded while the red ones (low forces) are obtained when the molecule is unfolded. d) Kinetic rates at different force and temperature. The kinetics increase with temperature. The coexistence force is defined as the moment when both kinetics, unfolding and folding are equals. Lines (solid and dotted) are fits of equation 3 (blue) and 4 (red) e) Coexistence force as a function of temperature. The coexistence or the necessary force to open the hairpin decreases with temperature. f) ΔG_0 as a function of temperature.

$$k_{F \rightarrow U} = \frac{1}{\langle t_F \rangle} = k_0^* \exp[\beta(x_U \cdot f)] \quad (3)$$

$$k_{F \leftarrow U} = \frac{1}{\langle t_U \rangle} = k_0^* \exp[\beta(\Delta G - x_F \cdot f)] \quad (4)$$

In equations 3 and 4 k_0^* is the attempt rate, $\langle t_i \rangle$ is the average life time at each state, x_i is the distance between the minimum of potential for each state and the potential barrier. This barrier is the potential barrier that the molecule needs to overcome to change its state, ($i = F$ or U). Finally ΔG is the energy difference between the folded and unfolded state. As we can see at a certain value of the force, f_c , both kinetic are equals, at this mo-

ment we say that the molecule are in coexistence, k_c .

$$\Delta G_0 = \Delta G - W_{handles} - W_{trap} - W_{ssDNA} - W_d \quad (5)$$

To find the free energy difference we need extract the contribution of each element to the energy difference (equation 5)⁴. W_{trap} is the work done by the OT, $W_{handles}$ is the work done by the handles, W_d is the work performed to orient de DNA hairpin when is folded and finally W_{ssDNA} is the work to stretch the ssDNA when the stem is unfolded.

In this report we present data obtained in a temperature range between 10 and 50 degrees. In Fig.1 are presented some significant results and also some plots to understand the main ideas behind this experiments.

¹ A. Ashkin, et. al., Phys. Rev. Lett. **24**(4), 156-159 (1970)

² M.T. Woodside, et. al., PNAS **314**, 1001-1004 (2006)

³ A. Alemany and F.Ritort, Biopolymers **101**(12), 1193-1199

(2014)

⁴ N. Forns, et. al., Biophysical Journal **100**, 1765-1774 (2011)

Causality analysis of ANS activities by multidimensional directed coherence on body temperatures variations

Akio Nozawa¹ and Shizuka Bando¹

¹College of Science and Engineering, Aoyama Gakuin University,
5-10-1 Fuchinobe, Chuo-ku, Sagamihara, Kanagawa 252-5258, Japan
e-mail address: akio@ee.aoyama.ac.jp

I. INTRODUCTION

Several studies have indicated the significance of a tympanum temperature (TT) as a physiological index. The TT has been regarded as a substitute for the temperature of the brain, especially hypothalamus, which has been known as the control center of the autonomic nervous systems (ANS). Since a very little has reported that a forehead temperature (FHT) has had a strong correlation with the TT, which has been indicated that the FHT could be possible index as a substitute for the TT. Meanwhile, a nasal skin temperature (NST) has been known as a physiological index strongly related for ANS activity. A declining NST has been the sign of the activation of the sympathetic nervous system (SNS), which has been a part of ANS. And the FHT has been considered as a 'reference' for the core body temperature, which has been stable and has had less relation with ANS activity in NST studies. Thus, there has been a inconsistency in interpretation of the FHT in physiological aspect, and this has been considered as one of the unsolved problem on noise in biological systems. The relationship between the temperatures have to be clarified, however, those has never been analyzed from the view of the biological system. The objective of present study is to analyze the causal relationship between body temperatures as an ANS activity index. The multidimensional directed coherence (MDC) has been know as an quantitative index of causal relationship between periodical signals^{1,2}. In this paper, MDC has been calculated between body temperatures time series measured in psychophysiological experiment.

II. EXPERIMENTAL

Experiment was conducted for six 22- to 23-years-old healthy subjects (three males and three females). Subject sat on chair in front of desk while the experiment. Experiment was constructed with six 90-seconds experimental periods for a task and six 60-seconds experimental periods for a rest. Six experimental periods for a task were T1, T2, T3, T4, T5 and T6, and R1, R2, R3, R4, R5 and R6 those for a rest assigned in chronological order. Each experimental period for a rest was aligned after the period for a task, respectively. Thus, each task came in every 150 seconds. In the period for a task, the subject was instructed to perform a mental arithmetic task (MAT) as fast as possible in order evoking an acute stress. The MAT was an addition of two double-digit numbers without carrying, which presented every 5 sec-

onds by PC installed in front of the subject. The subject had to type the answer to the PC with numerical keyboard on the desk. In the period for a rest, the subject was instructed to sit with closing the eyes. Physiological data time series were measured through the experimental periods at a sampling frequency of 0.5 Hz, which were right FHT (FHT_R), left FHT (FHT_L), NST, right TT (TT_R), left TT (TT_L) and mean blood pressure (MBP). The data were subjected to MDC analysis after resampling process at a sampling frequency of 4 Hz with a linear interpolation.

III. MULTIDIMENSIONAL DIRECTED COHERENCE ANALYSIS

The causal interrelations between an arbitrary number of time series signal are calculated as follows. A model of linear system for generating multi-channel sequences is described as multidimensional autoregressive model (MAR model) such that

$$\mathbf{x}_n = \sum_{m=1}^M \alpha_m \mathbf{x}_{n-m} + \beta \mathbf{w}_n \quad (1)$$

The order M is optimized by Akaike's Information Criterion (AIC). a_{ij}^m is the autoregressive coefficients, the input sequence w_i is the signal source that is white noise satisfying (2) of the output time sequence $x_i(n)$, and β is a weighting factor.

$$\mu = \frac{1}{N} \sum_{n=1}^N w_i(n), \sigma = \sqrt{\frac{1}{N} \sum_{n=1}^N (w_i(n) - \mu)^2} \quad (2)$$

where μ is the average of $w_i(n)$ and σ is the standard deviation. Fourier transform of (1) is given as

$$\mathbf{X}(f) = \mathbf{A}(f)\beta\mathbf{W} \quad (3)$$

Here respectively $\mathbf{X}_i(f)$ and $\mathbf{W}_i(f)$ are Fourier transformation of $x_i(n)$ and $w_i(n)$, I is identity matrix, and Δt is a sampling interval.

The power spectrum $P_{x_i}(f)$ and the cross spectrum $P_{x_i x_j}(f)$ are defined using $\mathbf{X}(f)$ as follows:

$$\begin{bmatrix} P_{x_1}(f) & \cdots & P_{x_1 x_k}(f) \\ \vdots & & \vdots \\ P_{x_k x_1}(f) & \cdots & P_{x_k}(f) \end{bmatrix} = E[\mathbf{X}(f) \cdot \mathbf{X}^t(f)] \\ = \mathbf{A}(f) \cdot \beta \cdot \beta^* \cdot \overline{\mathbf{A}(f)}^* \quad (4)$$

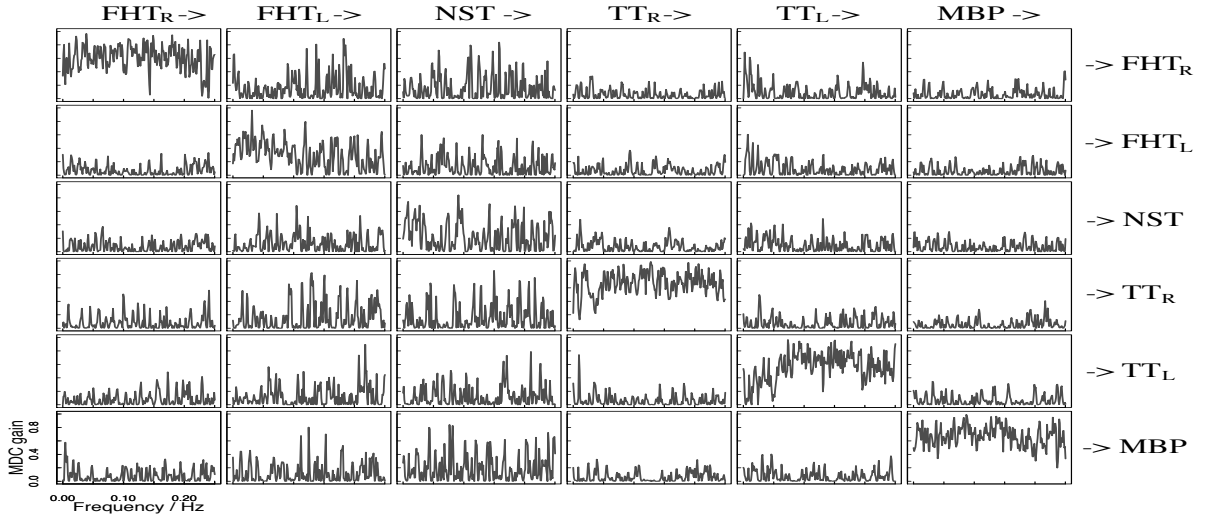


FIG. 1. The examples of the MDC gain of signals. (Subject F)

where E is an ensemble mean, $*$ is transposed matrix, and an overline is the complex conjugate. The power spectrum $P_{w_i}(f)$ of the signal source $w_i(n)$ satisfies $P_{w_i}(f) = 1$. MDC of an output sequence x_i from a signal source W_{x_i} is defined as

$$\begin{aligned} \gamma_{x_i x_j}(f) &= \frac{P_{x_i W_{x_j}}(f)}{\sqrt{P_{x_i}(f) \cdot P_{W_{x_j}}(f)}} \\ &= \frac{b_{x_i x_j} A_{x_i x_j}(f)}{\sqrt{P_{x_j}(f)}} \quad (j = 1, 2, \dots, k) \end{aligned} \quad (5)$$

These directed coherence also signify a composition ratio between P_{x_i} and $P_{W_{x_i}}$. A generation source of $x_i(n)$ is $w_i(n)$, therefore, the power spectrum $P_{x_i}(f)$ must be generated from any of $P_{W_{x_i}}(f)$. Considering the composition ratio, the gain transformed from $W_{x_i}(f)$ of P_{x_j} is represented

$$\begin{aligned} G_{x_i \rightarrow x_j}(f) &= \frac{|b_{x_i x_j} A_{x_i x_j}(f) P_{W_{x_i}}(f)|^2}{P_{x_j}(f)} \\ &= \frac{|b_{x_i x_j} A_{x_i x_j}(f)|^2}{P_{x_j}(f)} \end{aligned} \quad (6)$$

A correlation between the directed coherence and the power composition ratio is given as follows by (5) and (6)

$$G_{x_i x_j}(f) = \frac{|b_{x_i x_j} A_{x_i x_j}(f)|^2}{P_{x_i}(f)} = |\gamma_{x_i x_j}(f)|^2 \quad (7)$$

IV. RESULTS AND DISCUSSION

Fig.1 shows total combinations of the MDC gains of the physiological signals. Horizontal axis represents frequency of the signal, and MDC gain is on vertical axis. Hereinafter, MDC gain of A on B is referred to as $G_{A \rightarrow B}$. The MDC gains aligned on the diagonal lines from upper-left to lower-right in the figure indicate a 'signal source' referred to as G_A , which represents MDC gain of A on itself. Higher gain in the signal source indicate that the signal flows more to itself, lower gain indicates less, as well. Frequency bands around 0.01 Hz and 0.20 Hz are focused. It is assumed that 150-seconds task-rest period make the signals have 0.01 Hz frequent responses, and 5-seconds repeated MAT questionnaire periodically reflects on the signals as 0.20 Hz fluctuations as well. G_{TT_L} shows low gain in a frequency band of 0.01 Hz in the figure, which indicates TT_L is the source and has an impact on other signals in the band. Corresponding to the low gain in G_{TT_L} , $G_{TT_L \rightarrow FHT_R}$ and $G_{TT_L \rightarrow FHT_L}$ have high gains in the band around 0.01 Hz, while $G_{FHT_L \rightarrow FHT_R}$ has high. Those clarifies that thermal signal flows from left tympanum to forehead. Regarding G_{FHT_R} as a source, G_{FHT_R} has slight low gain in the band around 0.01 Hz, and $G_{FHT_R \rightarrow MBP}$ has high gain in the band, while G_{MBP} has high gain in the band. $G_{MBP \rightarrow NST}$ shows a small impact MBP on NST, while TT_L recurrently has the impact from MBP. It is assumed that the thermal signal generated in left tympanum flows to blood pressure and nasal region by way of forehead region from the view point of biological system.

¹ Bjorn Schelter et al., Journal of Neuroscience Methods, **152**(1), 210-219 (2005)

² Luiz A. Baccala et al., Biological Cybernetics, **84**(6), 463-474 (2001)

Fluctuations on cancer growth dynamics in Chronic Myeloid Leukemia

N. Pizzolato,¹ D. Persano Adorno,^{1,*} D. Valenti,¹ and B. Spagnolo^{1,2}

¹*Dipartimento di Fisica e Chimica, Università di Palermo,
Group of Interdisciplinary Theoretical Physics, Università di Palermo and CNISM,
Unità di Palermo, Viale delle Scienze, Edificio 18, 90128 Palermo, Italy*

²*Istituto Nazionale di Fisica Nucleare, Sezione di Catania, Via S. Sofia 64, I-90123 Catania, Italy*

I. INTRODUCTION

Chronic Myeloid Leukemia (CML) is a cancer of blood where too many myeloid cells (one of the main types of white blood cells) are produced and released into the blood when they are immature and unable to work properly. Despite the front line therapy for the treatment of CML, based on the administration of highly effective tyrosine kinase inhibitors (TKI), represents the first example of a successful molecular targeted therapy, the appearance of resistance is observed in a proportion of patients. The evolutionary dynamics of cancer initiation and progression can be theoretically approached by mathematical deterministic equations^{1,2} or stochastic models³⁻⁶, both using the basic idea that cancer arises when a single non-differentiated cell experiences multiple mutations.

In this work, we study the fluctuations on cancer growth dynamics in patients affected by CML and developing resistance to the standard therapy. The evolutionary dynamics of cancerous cell populations is modeled in numerically simulated patients treated by an intermittent targeted therapy (IT). In our model, initially healthy cells can experience genetic mutations and change their reproductive behavior, becoming leukemic clones. We simulate a TKIs-based treatment of CML by modifying the fitness and the death rate of cancerous cells. In CML context, a temporary interruption of the therapy was found to significantly reduce the presence of leukemic cells in a resistant patient^{7,8}. Here we explore the fluctuations occurring in patient leukemic cells treated by a therapy where the simulated drug administration follows a continuous or pulsed time scheduling. A permanent disappearance of leukemic non-resistant clones is achieved with a continuous therapy. However, our findings demonstrate that an intermittent therapy could represent a valid alternative in patients with high risk of toxicity, being a suitably tuned pulsed therapy more effective to reduce the probability of developing resistance.

II. THE MODEL

In our model cells are distributed over four populations: healthy cells (type-0), first-mutated cells (type-1), double-mutated leukemic cells (type-2) and resistant leukemic clones (type-3). Each population is assumed to be composed of the sum of stem cells, progenitors, differentiated and terminally differentiated cells. We study the dynamics of $N=10^4$ replicating cells. This value is sev-

eral orders of magnitude lower than the typical total contents of blood cells in humans, but it is great enough for the statistical study of the cancer development in a single blood compartment. In order to simulate the random process of cell selection for reproduction, mutation and death we adopt a Monte Carlo approach, as already done in several theoretical studies⁴⁻⁶. Each elementary step of the stochastic process consists of a birth and a death event, i. e. a Moran process⁹. For the birth, one of the N cells is randomly chosen proportionally to its capacity to reproduce. The fitness of type-0 and type-1 cells are set equal to 1 as already adopted in other theoretical studies^{4,6}. In the absence of therapy, the reproductive rate of a leukemic cell is assumed to be 10 times that of a normal cell. The treatment lowers this value only for those cells which are sensitive to the drug. The reproductive capability of resistant cells remains unchanged. Fitness values have been chosen in order to match the response of type-2 leukemic cells to that experimentally observed in patients treated by TKIs-based targeted therapy^{1,3}.

Healthy cells mutate to cells of type-1 (first allele mutation) at a rate M_{01} equal to 0.0005; type-1 cells mutate to type-2, which are leukemic cells sensitive to the therapy, at a rate M_{12} equal to 0.002. These values, comparable with the mutation rates adopted in the models of Refs.^{1,4}, guarantee a good agreement between our findings and clinical results. For the same reason, in our model we have assumed that type-2 cells become resistant type-3 by mutating at a rate M_{23} which has not a constant value, but increases with the number N_2 of leukemic double-mutated cells. The specific set of chromosomal mutations that causes the cancerous cell to become resistant can be considered an evolutionary reaction of the cell against the drug. On this basis we assume that, during the periods of absence of therapy, the mutation rate M_{23} is reduced to such very low values that we reasonably keep it equal to zero. In our simulations time is measured in units of cell divisions, and we assume 500 cell divisions per day. Using this time scaling from cell divisions to days we get a complete restore of healthy cells in almost 100 days, as experimentally observed in clinical cases of optimal therapy response^{1,3}.

III. NUMERICAL RESULTS AND DISCUSSION

Our simulated patients, subjected to a continuous therapy for the first 100 days, are then treated by three different therapeutic strategies characterized by: (i) continuous drug administration (namely, "CT"), (ii) long

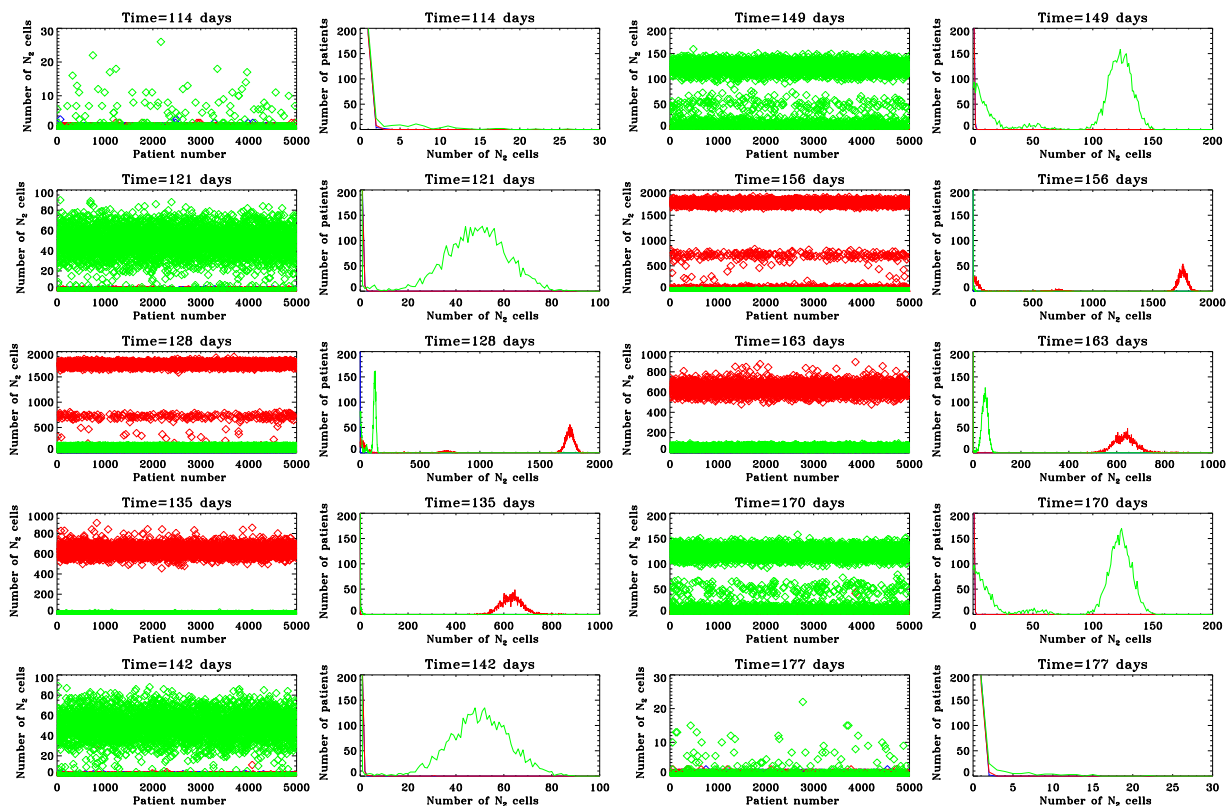


FIG. 1. Distributions of type-2 leukemic cells among patients. Blue symbols/curves refer to patients treated by a continuous therapy. Red and green diamonds/curves are used for intermittent therapies with breaks of 7 days and 1 day, respectively.

interruptions (7 days of stop after 21 of continuous therapy, namely "IT21-7") or (iii) short breaks (one day yes, one day no, namely "IT1"). In Fig. 1 we show how the number of type-2 leukemic cells is distributed among all the simulated patients after the first 100 days, at fixed time steps of 7 days for 10 weeks. In particular the blue colour is used for patients treated by CT, red for IT21-7 and green for IT1. Fig. 1 also shows the distribution of patients with a given number of type-2 leukemic cells. The crucial point for patient long-term survival to CML is avoiding those mutations causing a type-2 leukemic cell to become type-3 resistant to the therapy. In our model the occurrence probability for such harmful mutations depends on the presence of the drug, and increases with the number of type-2 leukemic cells. This is the reason why the study of fluctuations in the number of type-2 leukemic cells is so crucial for a clear estimate of the bal-

ance between the benefits of the therapy and the risk of developing cancer resistance. Of course the best results, in terms of lower levels of the type-2 leukemic cells, are achieved with a continuous therapy. However, the results shown in Fig. 1 demonstrate that an IT could also represent a valid choice in patients who cannot assume drug continuously due, for example, to a problem of toxicity. In fact, even if an increase of the average number of type-2 leukemic cells is observed during an intermittent therapy, this effect is partially counterbalanced by a reduction in the probability of developing resistance. Finally, our IT results clearly show the presence of multiple states of dynamical equilibrium in the number of type-2 leukemic cells. But, unfortunately, the most populated equilibrium state has always the highest number of leukemic cells. The possibility of achieving a population reverse in CML progression is still an unsolved problem.

* dominique.persanoadorno@unipa.it

¹ F. Michor, T.P. Hughes, Y. Iwasa, S. Branford, N.P. Shah, C.L. Sawyers, M.A. Nowak, *Nature* **435**, 1267 (2005).

² L.H. Abbott, F. Michor, *British Journal of Cancer* **95**, 1136 (2006).

³ I. Roeder, M. Horn, I. Glauche, A. Hochhaus, M.C. Mueller, M. Loeffler, *Nature Medicine* **12**, 1181 (2006).

⁴ Y. Iwasa, F. Michor, M. Nowak, *Genetics* **166**, 1571 (2004).

⁵ V.P. Zhdanov, *Eur. Biophys. J.* **37**, 1329 (2008).

⁶ N. Pizzolato, D. Valenti, D. Persano Adorno et al., *C. Eur. J. Phys.* **7**, 541 (2009).

⁷ M.C. Müller, T. Lahaye, A. Hochhaus, *Dtsch. Med. Wochenschr.* **127**, 2205 (2002).

⁸ A. Hochhaus, P. La Rosée, *Leukemia* **18**, 1321 (2004).

⁹ P.A.P. Moran, *The Statistical Processes of Evolutionary Theory* (Oxford: Clarendon Press, 1962).

Analysis of Fluctuation in Repeated Handwriting Based on Psychophysiological Factors

Amir Maleki¹, Yuki Oshima¹, Akio Nozawa², Tota Mizuno¹ and Masafumi Uchida¹

¹The University of Electro-Communications, Tokyo, Japan

e-mail addresses: amir@zidane.ee.uec.ac.jp, mizuno@uec.ac.jp, uchi@ee.uec.ac.jp

²Aoyama Gakuin University, Tokyo, Japan

e-mail address: akio@ee.aoyama.ac.jp

I. INTRODUCTION

During walking or running, we execute voluntary and repeated activities where repeated voluntary activities need a conscious mind^{1,2}. In this study, we introduce the term *repeated voluntary movement* which refers to repeated movements during daily activities. These movements need a certain mental workload. By clarifying the correlation between repeated voluntary movement and mental workload, it becomes possible to improve the workers' well-being and safety at work. In order to confirm the correlation between repeated voluntary movement and mental workload, we selected handwriting as an everyday repeated activity which imposes a mental workload³⁻⁷. In our study three terms of *cognitive control*, *physical control* and *cognitive load* are going to be used in order to extract the features of repeated activities.

II. EXPERIMENTAL METHOD

Dual-task method was selected for the experiment's procedure in which two tasks are to be performed simultaneously (for our experiment, writing at a specific timeframe). The experiment's system is consisted of two PCs. These PCs control a pen tablet, generate an auditory stimulus, and measure biometric signals (ECG, EEG and also body temperature). There are three tasks of writing as shown in Fig. (1), in which each task was performed by the subject at three different writing speeds which is considered as the task difficulty (low, medium and high speed). The experiment was performed during 6 non-consecutive days so that on the first three days a set of tasks *WZ*, and on the last three days a different set of tasks *WL* were performed. In this report we have applied obtained data of one male student at the age of 24 for the analysis.



FIG. 1. Writing Tasks

III. EXPERIMENTAL PROTOCOL

The experimental protocol is shown in Fig. (2). First the subject fills in two questionnaires to measure the psychological factors, *Profile of Mood States (POMS)* and *State-Trait Anxiety Inventory (STAI)*. Then, the subject rests with closed eyes for 150s and performs a task of writing with a specific speed by 250 times. Finally, the subject rests with closed eyes for 150s and answers to the *POMS/STAI* questionnaires again.



FIG. 2. Experiment's Protocol

IV. ANALYSIS METHOD

Synchronization error between writing and audio-stimulus and spatial error tend to occur during performing each task. It means, depending on the task difficulty, the subject will find it difficult to synchronize repeated-handwriting with the audio-stimulus. Furthermore in each set, each writing task has different start and stop point. In this study we applied the Synchronization error between writing and audio-stimulus as a factor of our analysis and for simplicity we refer to it as *WSE (Writing Synchronization Error)* which is shown in Fig. (3)^{8,9}.

For the procedure of the analysis, first measured data was normalized to $N(0, 1)$, then the autocorrelation coefficient was applied to the *WSE*:

$$c(i) = \sum_{k=1}^{L-i} \frac{N[k] \times N[k+1]}{L} \quad (for \ i = 1, 2, \dots, L-1) \quad (1)$$

Where L is the length of the normalized data, $N[k]$ and $N[k+1]$ are K^{th} and $(K+1)^{th}$ term of the normalized data. After that, Fast Fourier Transform was applied to the autocorrelation coefficient in order to calculate the Power Spectral Density (PSD). Finally *Self-Similarity Feature* and *Natural Period Feature* were derived from the PSD.

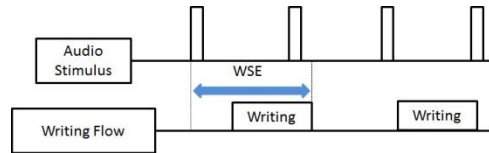


FIG.3. WSE (Writing Synchronization Error)

A. SELF-SIMILARITY FEATURE

The Power Spectrum Density of the *WSE* on a log-log plot is inversely proportional to the frequency. Generally this feature is referred to as *1/f noise*, Eq. (2) explain the general form of the *1/f noise* in which α has a range of -2 to 0.

$$S(f) \propto f^\alpha \quad -2 < \alpha < 0 \quad (2)$$

We applied the least squares method in order to find the best fit line (linear regression) to the PSD where the gradient of this line represents the value of α in Eq. (2). Our results show that the value of α for each writing task is statistically self-similar. Fig. (4) shows the result of the experiment for the *Self-Similarity Feature* of WSE. The horizontal axis represents the writing tasks where W_Z is related to the writing task, W of the WZ set, and W_L is related to the writing task, W of the WL set. The vertical axis represents the value for α of each writing tasks. The red, brown and yellow bars are related to the highest, medium and lowest writing speeds, respectively. Obviously, the value of α in each set is dramatically proportional to the writing speed. When α has a more negative value, the task needs less mental workload and the *physical control* is dominant, and when α has a value near to zero, the task needs more mental workload and the *cognitive control* is dominant. The reason of this matter is that at the highest writing speed, the subject only performed a physical activity and found it difficult to synchronize his writing flow with the audio-stimulus. On the other side, at the lowest writing speed the subject has concentrated better on the task and easily has synchronized his writing flow with the audio-stimulus. For the medium speed of the writing task, both of the *cognitive control* and the *physical control* took part in controlling the writing activity. In this study, when α tends to approach -1 the case is called "*tendency to 1/f noise (pink noise)*", this happened at the medium speed of the writing task in our experiment; and when α tends to approach to zero, the case is called "*tendency to the white noise*" which happened at the lowest speed of the writing task. But when we want to talk about the difficulty of writing letters not writing speed, we can't easily distinguish the difference between the writing tasks. For instance the writing task of W has more breaking points than the writing task of L and it would be more difficult to write, so the *cognitive control* should be dominant. Therefore we'd have expected that at the writing tasks of W the cognitive control would have more influence on the task but it wasn't satisfied. We conclude that one of the reasons of this problem is that the control of the writing task was influenced by other controls of different tasks on the mental workload during experiment.

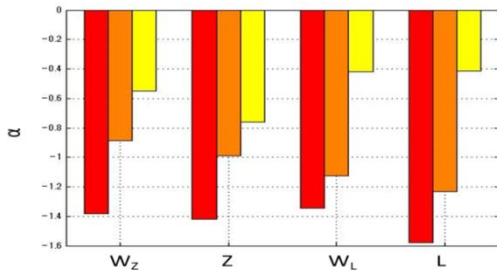


FIG.4. the Self-Similarity Feature of WSE

B. NATURAL PERIOD FEATURE

Difference between the PSD and the linear regression of the PSD ($DPower(f)$) is another factor that expresses the frequency characteristics. The mean value of the $DPower(f)$ was defined as μ and the standard deviation of the $DPower(f)$ was defined as σ . The number of points that the value of the $DPower(f)$ exceeds $\mu + \sigma$ was defined as $Power(f)$. By dividing the $Power(f)$ by the length of the $DPower(f)$ a new term can be derived which we call it $PeakT$. In Fig. (5) we can see the value of the $PeakT$ for each writing task. We can see that except for writing task of L , the other

writing tasks at the lowest speed (yellow bars) have greater values for $PeakT$ than of the highest speed (red bars). It means, the lowest speed of the writing task has a higher level of the *cognitive load* than the highest speed. At the highest writing speed (red bars), the values of $PeakT$ are on their lowest values which means the *cognitive load* is at its lowest level. And finally for the medium speed, depend on the writing task the *cognitive load* has variable value and it is difficult to recognize the level of the *cognitive load* at this stage of the study and more experiments must be performed to make it more clear. The parameter "difficulty of writing letters" in this section is the same as what we have discussed in the previous section and to discover the detailed reasons of the misclassification problem, more experiments must be performed.

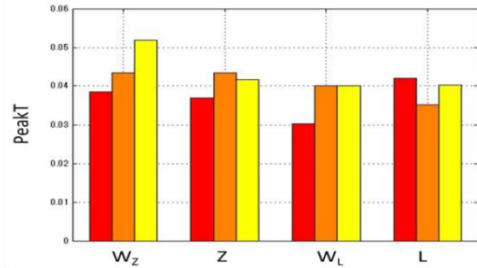


FIG.5. the Natural Period Feature of WSE

- 1 D. Kahneman and A. Treisman, *Varieties of attention* (Academic Press, Inc, 1984), pp. 29-61.
- 2 W. Schneider and R. Shiffrin, *Psychological Review*, 84, pp.1-66. (1977).
- 3 Y. Kimura, K. Odaka and M. Uchida, *SICE (Proceedings of ISBPE / 22nd BPES)*, pp.187-190, (2008).
- 4 M. Nishizawa, M. Uchida, K. Odaka and Y. Kimura, *SICE (Proceedings of ISBPE / 22nd BPES)*, pp.191-194, (2008).
- 5 K. Odaka, Y. Kimura and M. Uchida, *SICE (Proceedings of ISBPE / 22nd BPES)*, pp.195-198, (2008).
- 6 K. Saito, Y. Park and M. Uchida, *ICROS-SICE International Joint Conference 2009, 2C12-3*, (2009).
- 7 K. Saito, Y. Park and M. Uchida, *The Fifteenth International Symposium on Artificial Life and Robotics 2010 (AROB 15th `10)*, OS1-3, (2010).
- 8 T. Komatsu and Y. Miyake, *Trans. of SICE*, 39(10), pp.952-960, (2003).
- 9 Y. Miyake, Y. Onishi and E. Poppel, *Trans. of The Society of Instrument and Control Engineers*, 38(12), pp.1114-1122, (2002).

Probabilistic characteristics of noisy Van der Pol type oscillator with polynomial damping

A.A. Dubkov¹ and I.A. Litovsky¹

¹*Radiophysical Department, Lobachevsky State University,
Gagarin ave.23, 603950 Nizhni Novgorod, Russia
e-mail address: dubkov@rf.unn.ru
e-mail address: litovskii@list.ru*

The Van der Pol oscillator has a long history of being used in both the physical and biological sciences^{1,2}. For instance, in biology, FitzHugh and Nagumo extended the Van der Pol equation in a planar field as a model for action potentials of neurons^{3,4}. The equation has also been utilized in seismology to model the two plates in a geological fault⁵.

For noisy Van der Pol oscillator the unsolved problem can be formulated as: Is it possible to distinguish between soft and hard excitation of self-oscillations using the probabilistic characteristics of amplitude?

Trying to solve this problem, we consider a noisy Van der Pol type oscillator which is governed by the following equation

$$\ddot{y} + \lambda F(y)\dot{y} + [\omega^2 + \eta(t)]y = \xi(t), \quad (1)$$

where: λ is a small parameter ($\lambda \ll \omega$), $F(y) = \sum_{n=0}^k C_n y^n$ is the nonlinear polynomial damping, $\xi(t)$ and $\eta(t)$ are statistically independent white Gaussian noise sources with zero mean and the intensities $2D$ and $2D_1$ respectively. Introducing by the usual manner the phase variables

$$\begin{aligned} y &= A \cos \Psi, \\ \dot{y} &= -A\omega \sin \Psi, \end{aligned} \quad (2)$$

where $\Psi = \omega t + \Phi$, and applying a functional approach⁶ to derive the Fokker-Planck equation for the joint probability density function (PDF) of amplitude and phase, we arrive at

$$\begin{aligned} \frac{\partial P}{\partial t} = & - \left(\frac{\partial}{\partial A} \frac{\sin \Psi}{\omega} + \frac{\partial}{\partial \Phi} \frac{\cos \Psi}{A\omega} \right) \left[\lambda P F(A, \Psi) A \omega \sin \Psi \right. \\ & - \frac{D_1}{\omega} A \cos \Psi \left[\frac{\partial}{\partial A} \left(\frac{AP}{2} \sin 2\Psi \right) + \frac{\partial}{\partial \Phi} (P \cos^2 \Psi) \right] \\ & \left. - D \left(\frac{\partial}{\partial A} \frac{P \sin \Psi}{\omega} + \frac{\partial}{\partial \Phi} \frac{P \cos \Psi}{A\omega} \right) \right]. \end{aligned} \quad (3)$$

Using the standard procedure of averaging over the oscillation period and integrating over the phase, one can obtain from equation (3) the following truncated equation for the probability distribution of the amplitude

$$\begin{aligned} \frac{\partial P}{\partial t} = & \frac{\lambda}{4} \frac{\partial}{\partial A} \left[AP [a_0(A) - a_2(A)] \right] + \frac{D}{2\omega^2} \left(\frac{\partial^2 P}{\partial A^2} - \frac{\partial}{\partial A} \frac{P}{A} \right) \text{ and stationary PDF} \\ & + \frac{D_1}{4\omega^2} \left[\frac{1}{2} \left(\frac{\partial}{\partial A} A \right)^2 P - \frac{\partial}{\partial A} AP \right]. \end{aligned} \quad (4)$$

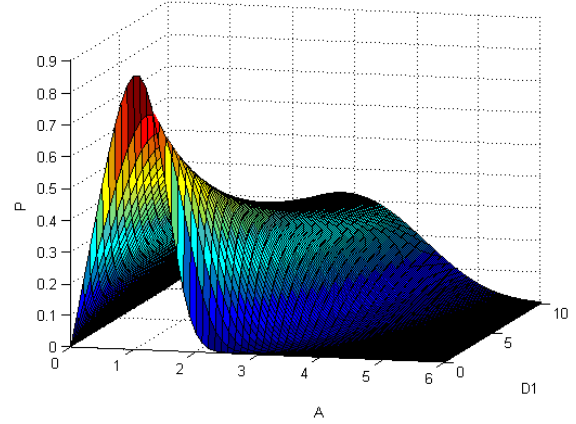


FIG. 1. The stationary probability distribution of the amplitude for different values of the intensity D_1 of frequency fluctuations. The parameters are: $\lambda = 0.01$, $\omega = 3$, $D = 1$, $\alpha = 1$, $\beta = 2$.

Here $a_0(A)$ and $a_2(A)$ are two coefficients of Fourier series expansion of the polynomial damping function $F(A \cos \Psi)$.

The stationary probability density function of the amplitude can be easily found from equation (4) and takes the form

$$P_{st}(A) = C_0 A \exp \left[-2\lambda\omega^2 \int \frac{a_0(A) - a_2(A)}{4D + D_1 A^2} A dA \right], \quad (5)$$

where C_0 is the normalization constant.

As an example, we explore the Van der Pol oscillator with the nonlinear damping $F(y) = -1 - \alpha y^2 + \beta y^4$ corresponding to the hard excitation of self-oscillations. As a result, we obtain the following Fourier coefficients

$$\begin{aligned} a_0 &= \frac{3}{4} \beta A^4 - \alpha A^2 - 2, \\ a_2 &= \frac{1}{2} \beta A^4 - \frac{1}{2} \alpha A^2. \end{aligned}$$

$$P_{st}(A) = C_0 A \left(D + \frac{D_1 A^2}{4} \right)^q \exp[-S(A)], \quad (6)$$

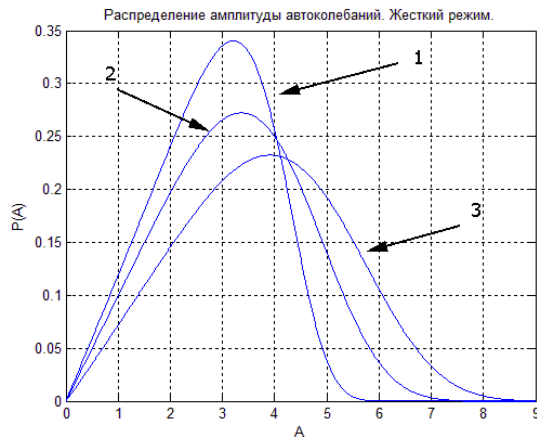


FIG. 2. The probability distribution of the amplitude: 1 - in the presence of only additive noise source; 2 - in the presence of both noise excitations; 3 - in the presence of only frequency fluctuations. The parameters are: $\lambda = 0.01$, $\omega = 1$, $D = D_1 = 1$, $\alpha = \beta = 1$.

where

$$q = -\frac{2\lambda\omega^2}{D_1} \left[2\beta \left(\frac{D}{D_1} \right)^2 + \alpha \frac{D}{D_1} - 1 \right],$$

$$S(A) = \frac{\lambda\omega^2}{D_1} \left[\frac{\beta A^4}{8} - \left(\frac{\alpha}{2} + \beta \frac{D}{D_1} \right) A^2 \right].$$

The 3D plot of PDF $P(A, D_1)$ as a function of the amplitude A and the intensity D_1 of multiplicative noise is

depicted in Fig. (1). It is clearly visible the characteristic peak corresponding to the limit cycle. The maximum of PDF decreases with increasing the intensity of frequency fluctuations.

In the absence of additive noise the PDF (6) takes the form

$$P_{st}(A) = C_0 A^{q_\eta} \exp[-S_\eta(A)], \quad (7)$$

where

$$q_\eta = 1 + \frac{2\lambda\omega^2}{D_1}, \quad S_\eta(A) = \frac{\lambda\omega^2}{D_1} \left(\frac{\beta A^4}{8} - \frac{\alpha}{2} A^2 \right).$$

In the absence of multiplicative noise from equation (6) we have

$$P_{st}(A) = C_0 A \exp[-S_\xi(A)], \quad (8)$$

where

$$S_\xi(A) = \frac{\lambda\omega^2}{48D} (\beta A^6 - 3\alpha A^4 - 24A^2).$$

The plots of PDF $P(A)$ for different noise excitations of the Van der Pol oscillator (1) are shown in Fig. (2). As seen from Fig. (2), the PDF of the amplitude in the case of only one multiplicative noise is wider than in the case of only one additive noise source of the same intensity.

Our results demonstrate that it is quite difficult to distinguish between soft ($\beta = 0$, $\alpha < 0$) and hard excitation of the Van der Pol oscillator using only the stationary PDF of the amplitude.

¹ R.L. Stratonovich, *Topics in the Theory of Random Noise. Vol. I* (Gordon & Breach, NY, 1963).

² V. Afraimovich et al, *Nonlinear Dynamics and Complexity* (Springer, Berlin, 2014).

³ R. FitzHugh, *Biophysics J.* **1**, 445 (1961).

⁴ J. Nagumo, S. Arimoto, and S. Yoshizawa, *Proc. IRE* **50**,

2061 (1962).

⁵ J. Cartwright et al, *Int. J. Bifur. Chaos* **9**, 2197 (1999).

⁶ A.A. Dubkov and B. Spagnolo, *Fluct. Noise Lett.* **5**, L267 (2005).

Noise activated switching of a levitated nanoparticle in a bistable potential.

F. Ricci¹, R.A. Rica¹, M. Spasenovic² and R. Quidant¹

¹ ICFO–Institut de Ciències Fotoniques, Mediterranean Technology Park, 08860 Castelldefels (Barcelona), Spain
e-mail address: francesco.ricci@icfo.es

² Institute of Physics, University of Belgrade, Pregrevica 118, 11080 Belgrade, Serbia

Bistable systems are encountered in many different situations. Classical examples in chemistry and biology include relaxation kinetics in chemical reaction [1] and stochastic resonance processes such as neuron firing [2,3]. Likewise, bistable systems play a key role in signal processing and information handling at the nanoscale, giving rise to intriguing applications such as optical switches [4], coherent signal amplification [5,6] and weak forces detection [5].

The interest and applicability of bistable systems are intimately connected with the complexity of their dynamics, typically due to the presence of a large number of parameters and nonlinearities. Moreover, the presence of non-negligible noise in the system makes appropriate modeling and analytical approaches quite challenging. In spite of increasing the complexity of a system, the presence of noise can play a crucial role in some situations, being for example responsible for the activation of switching between the stable states and for giving access to resonant conditions triggering stochastic resonances.

The possibility to experimentally recreate noisy bistable systems in a clean and controlled way, where the noise can be properly tuned, has recently become very appealing. With this aim, we combined optical tweezers with a novel active feedback-cooling scheme to develop a well-defined opto-mechanical platform reaching unprecedented performances in terms of Q-factor, frequency stability and force sensitivity [7,8]. Our experimental system consists of a single nanoparticle levitated in high vacuum with optical tweezers, which behaves as a non-linear (Duffing) oscillator under appropriate conditions. We introduce a controlled source of noise by modulating the power of the trapping laser with a white Gaussian noise signal of variable amplitude.

We demonstrate bistable dynamics of the nanoparticle by noise activated switching between two stable oscillation states, discussing our results in terms of a double-well potential model. We also show the flexibility of our system in shaping the potential at will, in order to meet the conditions prescribed by any noisy bistable system that could therefore then be simulated with our setup.

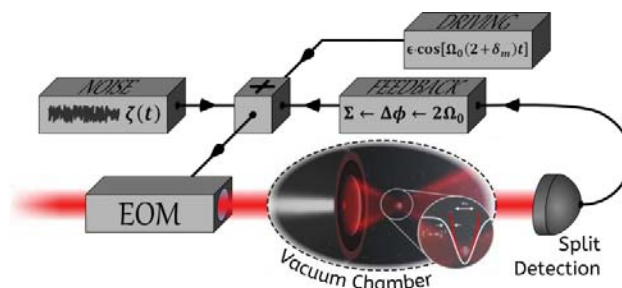


FIG.1 Experimental set-up. A silica nanoparticle is trapped inside a vacuum chamber by means of a tightly focused laser beam. The beam intensity is modulated via an electro-optical modulator (EOM) according to a signal which is a compound of three contributions: the feedback signal responsible for the parametric cooling of the particle, the driving signal that gives access to the nonlinear regime leading to bistability and the noise signal that activates stochastic switching within the two stable oscillation states.

¹ T. Amemiya, T. Ohmori, M. Nakaiwa, T. Yamamoto, and T. Yamaguchi, “Modeling of Nonlinear Chemical Reaction Systems and Two-Parameter Stochastic Resonance,” *J. Biol. Phys.* **25** (1999) 73

² F. Moss, L. M. Ward, and W. G. Sannita, “Stochastic resonance and sensory information processing: a tutorial and review of application” *Clinical neurophysiology* **115** (2004) 267

³ M. Platkov, and M. Gruebele, “Periodic and stochastic thermal modulation of protein folding kinetics” *J. Chem. Phys.* **141** (2014) 035103

⁴ T. Tanabe, M. Notomi, S. Mitsugi, A. Shinya and E. Kuramochi. “Fast bistable all-optical switch and memory on a silicon photonic crystal on-chip”. *Opt. Lett.*, **30** (2005) 2575

⁵ R. L. Badzey and P. Mohanty. “Coherent signal amplification in bistable nanomechanical oscillators by stochastic resonance” *Nature*, **437** (2005) 995

⁶ W. J. Venstra, H. J. R. Westra, and H. S. J. van der Zant. “Stochastic switching of cantilever motion,” *Nature Communications*, **4** (2013) 3624

⁷ J. Gieseler, B. Deutsch, R. Quidant, and L. Novotny “Subkelvin parametric feedback cooling of a Laser-Trapped nanoparticle” *Phys. Rev. Lett.* **109** (2012) 103603

⁸ J. Gieseler, M. Spasenović, L. Novotny, and R. Quidant, “Nonlinear Mode Coupling and Synchronization of a Vacuum-Trapped Nanoparticle,” *Phys. Rev. Lett.* **112** (2014) 103603

Modeling long-range dependent inverse cubic distributions by nonlinear stochastic differential equations

Bronislovas Kaulakys, Miglius Alaburda, and Julius Ruseckas
*Institute of Theoretical Physics and Astronomy,
 Vilnius University, A. Goštauto 12,
 LT-01108 Vilnius, Lithuania
 e-mail address: bronislovas.kaulakys@tfai.vu.lt*

I. INTRODUCTION

Many systems show large fluctuations of macroscopic quantities that follow non-Gaussian, heavy-tailed, power-law distributions with the power-law temporal correlations¹, scaling, and the fractal features^{2,3}. The power-law distributions are often related both with the nonextensive statistical mechanics⁴⁻⁶ and the power-law behavior of the power spectral density, i.e., $1/f^\beta$ noise “ambiguity” (see, e.g.,^{3,6-8} and references herein).

One common way for describing all the above-mentioned forms of evolution is by means of the stochastic differential equations^{7,9,10}. These nondeterministic equations of motion are used in many systems of interest, such as simulating the Brownian motion in statistical mechanics, field theory models, the financial systems, biology, and in many other areas.

One of the principal statistical features characterizing the activity in financial markets is the distribution of fluctuations of market indicators such as the indexes. Frequently heavy-tailed long-range distributions with characteristic power-law exponents are observable. Power laws appear for relevant financial fluctuations, such as fluctuations of number of trades, trading volume and price. The well-identified stylized fact is the so-called inverse cubic power-law of the cumulative distributions, which is relevant to the developed stock markets, to the commodity one, as well as to the most traded currency exchange rates. The exponents that characterize these power laws are similar for different types and sizes of markets, for different market trends and even for different countries—suggesting that a generic theoretical basis may inspire these phenomena¹¹⁻¹⁴.

Here we model the long-range dependent inverse cubic cumulative distributions by square multiplicative stochastic differential equations^{7,10} and taking into account a transition from Stratonovich to Ito convention in noisy systems¹⁵ according to Wong-Zakai theorem¹⁶, with decrease of the driving noise correlation time when the market proceeds from turbulent to calm behavior.

II. STOCHASTIC DIFFERENTIAL EQUATIONS

We start from the squared stochastic differential equation (SDE)

$$dx = x^2 \circ_\alpha dW_t \quad (1)$$

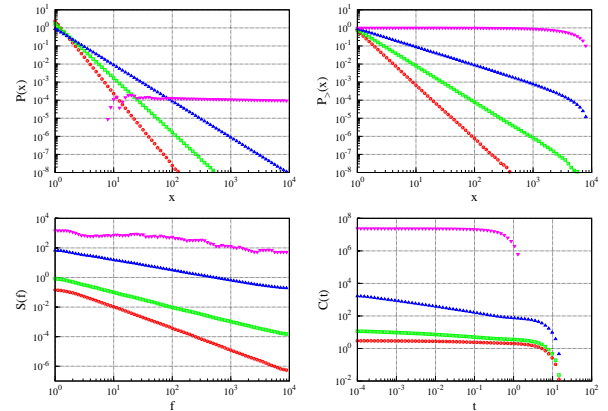


FIG. 1. The steady-state probability distribution function, cumulative distribution, power spectral density and autocorrelation function of the variable x generated by Eq. (3) for different parameters $\alpha = 0; 1/4; 1/2$ and 1 with restriction between $x_{\min} = 1$ and $x_{\max} = 10^4$.

where W_t is a Wiener process and α is the interpretation (convention) parameter, defining the α -dependent stochastic integral in Eq. (1),

$$\int_0^T f(x(t)) \circ_\alpha dW_t \equiv \lim_{N \rightarrow \infty} \sum_{n=0}^{N-1} f(x(t_n)) \Delta W_{t_n}. \quad (2)$$

Here $t_n = \frac{n+\alpha}{N}T$, $0 \leq \alpha \leq 1$. Common choices of the parameter α are: (i) $\alpha = 0$, pre-point (Itô convention), (ii) $\alpha = 1/2$, mid-point (Stratonovich convention) and (iii) $\alpha = 1$, post-point (Hänggi-Klimontovich, kinetic or isothermal convention). More generally, the value of α may be variable, even coordinate x and/or the system parameters dependent quantity. Eq. (1) with $\alpha \neq 0$ may be transformed to Itô equation

$$dx = 2\alpha x^3 dt + x^2 dW_t \quad (3)$$

Eq. (3) is a particular case of the general Itô equations

$$dx = \left(\eta - \frac{\lambda}{2} \right) x^{2\eta-1} dt + x^\eta dW_t, \quad \eta \neq 1, \quad (4)$$

yielding the power-law steady-state, $P_{ss}(x) \sim x^{-\lambda}$, distribution of the signal with the power-law spectrum, $S(f) \sim 1/f^\beta$, with the exponent

$$\beta = 1 + \frac{\lambda - 3}{2(\eta - 1)}. \quad (5)$$

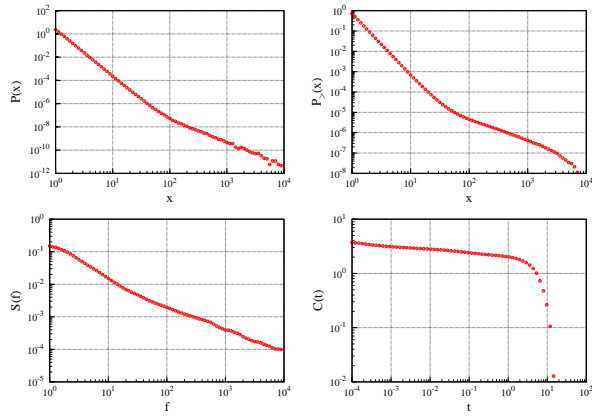


FIG. 2. The steady-state probability distribution function, cumulative distribution, power spectral density and autocorrelation function generated by Eqs. (6)–(9) with $x_c = 100$ and restriction between $x_{\min} = 1$ and $x_{\max} = 10^4$.

The relations between the parameters α and λ in Eqs. (3) and (4) for $\eta = 2$ are: $\lambda = 4(1-\alpha)$, $\alpha = 1-\lambda/4$. It should be noted that for the cumulative inverse cubic distribution $P_{>}(x) \sim x^{-3}$, i.e., $\lambda = 4$, according to Eq. (5) $\beta > 1$, for all $\eta > 1$ and, therefore, the modeled process is not long-range dependent. [Note that the definition of the long-range process corresponds the power-law autocorrelation function $C(t) \sim 1/t^\gamma$ with $0 < \gamma < 1$, which takes place for $0 < \beta < 1$ and $\gamma = 1 - \beta$.] Fig. 1 demonstrates statistics of solutions of Eq. (3) for different values of the parameter $\alpha = 0; 1/4; 1/2$ and 1 , i.e., for $\lambda = 4; 3; 2$ and 0 .

III. LONG-RANGE DEPENDENT INVERSE CUBIC DISTRIBUTION

For modelling of this phenomena we generalise Eqs. (1)–(4) with $\alpha(x)$ -dependent parameter, e.g.,

$$\alpha(x) = \frac{1}{2} \left[1 - \exp \left\{ - \left(\frac{x}{x_c} \right)^2 \right\} \right], \quad (6)$$

where x_c is the process crossover parameter,

$$dx = 2\alpha(x)x^3dt + x^2dW_t \quad (7)$$

Eqs. (6) and (7) represents transition from Stratonovich to Itô convention with decreasing variable x and the driving noise correlation time for small x , according to Wong-Zakai theorem. The calculations are performed with the variable step of integration

$$\Delta t_k = \kappa^2/x_k^2 \quad (8)$$

with $\kappa \ll 1$, yielding to the difference equation

$$x_{k+1} = x_k + 2\kappa^2\alpha(x_k)x_k + \kappa x_k \varepsilon_k. \quad (9)$$

Here ε_k is a set of uncorrelated normally distributed random variables with zero expectation and unit variance. Fig. 2 demonstrates results of the numerical calculations.

IV. CONCLUSION

Equations (6) and (7) with the variable dependent convention parameter $\alpha(x)$, according to Wong-Zakai theorem modeling decrease of the driving noise correlation time when the market proceeds from turbulent to calm behavior, may reproduce the long-range dependent inverse cubic phenomena.

¹ R. N. Mantegna and H. E. Stanley, *An Introduction to Econophysics: Correlations and Complexity* (Cambridge University Press, Cambridge, UK, 2001).
² B. B. Mandelbrot, *Multifractals and 1/f Noise: Wild Self-Affinity in Physics* (Springer-Verlag, New York, 1999).
³ S. B. Lowen and M. C. Teich, *Fractal-Based Point Processes* (Wiley-Interscience, New Jersey, 2005).
⁴ C. Tsallis, *J. Stat. Phys.* **52**, 479 (1988).
⁵ C. Tsallis, *Braz. J. Phys.* **39**, 337 (2009).
⁶ J. Ruseckas and B. Kaulakys, *Phys. Rev. E* **84**, 051125 (2011).
⁷ B. Kaulakys and M. Alaburda, *J. Stat. Mech.* **2009**, P02051 (2009).
⁸ A. A. Balandin, *Nature Nanotechnology* **8**, 549 (2013).
⁹ R. L. S. Farias, R. O. Ramos and L. A. da Silva, *Phys. Rev. E* **80**, 031143 (2009).

¹⁰ J. Ruseckas and B. Kaulakys, *Phys. Rev. E* **81**, 031105 (2010).
¹¹ P. Gopikrishnan, M. Meyer, L. A. N. Amaral and H. E. Stanley, *Eur. Phys. J. B* **3**, 139 (1998).
¹² X. Gabaix, P. Gopikrishnan, V. Plerou and E. Stanley, *Nature (London)* **423**, 267 (2003).
¹³ B. Podobnik, D. Horvatic, A. M. Petersen and H. E. Stanley, *PNAS* **106**, 22079 (2009).
¹⁴ G.-H. Mu and W.-X. Zhou, *Phys. Rev. E* **82**, 066103 (2010).
¹⁵ G. Pesce, A. McDaniel, S. Hottovy, J. Wehr and G. Volpe, *Nature Commun.* **4**, 2733 (2013).
¹⁶ E. Wong and M. Zakai, *Ann. Math. Stat.* **36**, 1560 (1965).

Passive and active vibrations allow self-organization in large-scale electromechanical systems

Arturo Buscarino¹, Carlo Famoso¹, Luigi Fortuna¹, Mattia Frasca¹

¹*DIEEI, University of Catania, Catania, Italy*

e-mail address: [arturo.buscarino, carlo.famoso, luigi.fortuna, mattia.frasca]@dieei.unict.it

I. EXTENDED ABSTRACT

In this contribution our attention is devoted to the fundamental role of mechanical noise¹ to favor the working of a complex electromechanical system. In the literature it has been studied how uncertainty allows self-organization of pendulums arrays². The idea of our contribution is to show that mechanical noise can play a fundamental role in the self-organization of complex electromechanical systems.

The considered system is essentially based on a low weight mechanical structure that supports very simple rotating coils. With this term we indicate coils realized with few turns of a copper wire. The i -th coil can be described with a nonlinear dynamical model:

$$\begin{cases} \dot{X}_i = Y_i \\ \dot{Y}_i = \frac{1}{J}(I_a S B \sin(X_i) - K_1 Y_i) \end{cases} \quad (1)$$

where X_i ($i = 1, \dots, N$ with N indicating the number of coils) represents the phase of the coil, Y_i the angular velocity, J the angular momentum, K_1 the damping factor, I_a is the current flowing into the coil and is given by $I_a = \frac{V_a - Y S B \sin(X_i)}{R_a}$ with V_a the voltage supplied to the coil, S the coil area, B the magnetic field and R_a the contact resistance, which, due to the coil construction constraint, is nonlinear: $R_a = \begin{cases} 0.4\Omega & \text{if } X < \pi \\ 10k\Omega & \text{if } X \geq \pi \end{cases}$.

The structures that are considered are of the type shown in Fig. 1, where the coils are hosted in the various slots and powered by a unique voltage source.

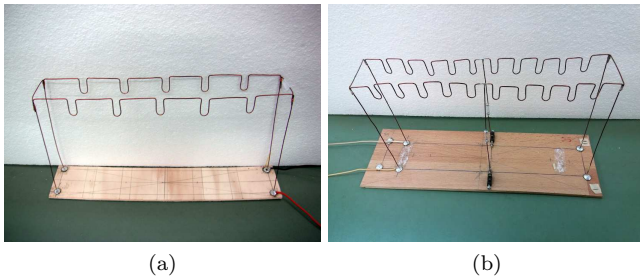


FIG. 1. Structures used to host the coils: (a) rectangular structure with 5 slots; (b) rectangular structure with 10 slots.

The investigated structures are classified in the family of large scale dynamical systems, in the sense that the low weight of the structure, including the coils, is negligible with respect to the volume. The task that we want to achieve is, at the first step, to have the complete start

up of the various coils and, then, to get a complete synchronization of the coils, both as regards their angular speed and phase.

The mechanical structure is a flexible structure³ where the natural modes have the main frequency between 10Hz and 30Hz. The coils, even if they are easily represented by the model in equation (1), globally should be considered nonlinear uncertain systems, due to the practical difficulties in building identical coils. Another source of uncertainty derives from the fact that the coils are located in the mechanical structure free of moving in the three directions. Moreover, the structure and the slots, where the coils are located, are different each other. Therefore, there are tremendous negative conditions to get a regular behavior of the system.

Depending on the initial conditions, when the power is switched on, typically it occurs that some coils start rotating, while others do not. The idea is to design flexible structures that, mechanically excited by their self-oscillations, allow the coils which are not working to receive solicitations in order to win the off condition and to start working. This should occur globally and due to the mechanical vibrations that couple each coil with the other. Therefore, the mechanical vibrations should allow the self-organization of the system in order to win the uncertainties.

In the structure of Fig. 2(a) the mechanical vibrations elicited by those coils, which do start when the power supply is switched on, are enough large to let the other coils to also start. So, in the structure of Fig. 2(a), over a relevant number of trials under the same power supply conditions, the various coils work. In Fig. 3 the trends of the angular velocities of the five coils are reported and in Fig. 2(b) the horizontal mechanical displacement that allows the self-organization of the coils is shown.

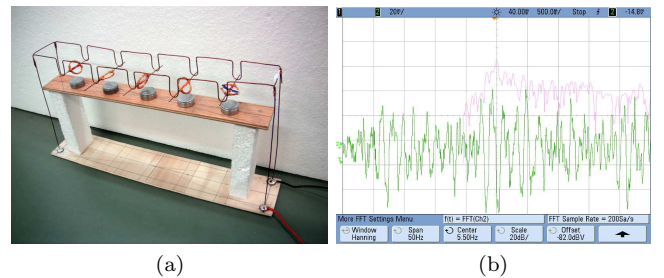


FIG. 2. (a) Structure of Fig. 1(a) with the coils. (b) Horizontal displacement of the structure.

Coupling more structures of this type, as shown in Fig. 4, by using mechanical springs a global start up of a

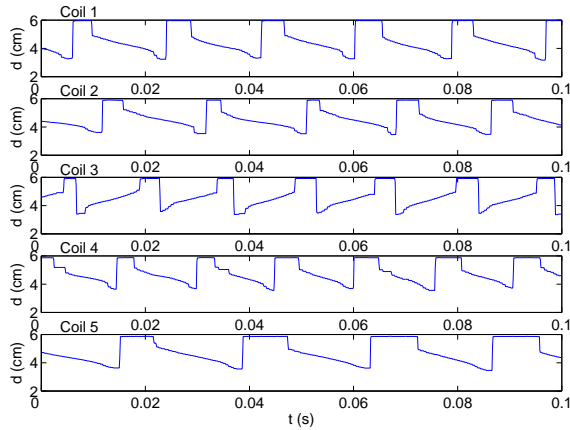


FIG. 3. Angular velocity for the 5 different coils.

system with 10 coils can be achieved, while for the structure of Fig. 1(b) an active solution has to be envisaged.

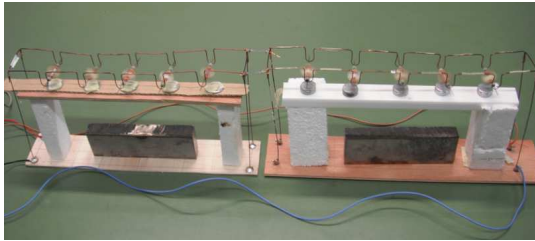


FIG. 4. Two structures with 5 coils coupled through two springs.

The resulting structure is more rigid, and, therefore, the self-generated vibrations of the coils cannot allow the complete start up of all the coils of the system. In order to overcome this drawback, a shock system actuated with low power electromechanical transducer has been conceived to excite the mechanical structure to favor active vibrations helping the start up of coils. The electromagnetic actuator is driven by a chaotic signal generated by a Chua's circuit⁴. This signal works in the range of the natural frequencies of the mechanical system, to give suitable electrical signal in order to stimulate in an active way the system to start. In Fig. 5(a) the proposed structure is reported. In Fig. 6 the trends of the angular velocities of the various coils are reported and in Fig. 5(b) the induced mechanical vibrations. After the start up of the system, the actuator is switched off.

The project will consist of coupling a great number of coils and study the possibility to favor the self-organization of the coils by using different ways such as: self-elicited oscillation of the structure, passive coupling and active generation of mechanical vibrations. The project is conceived in order to design and realize experimentally a system with hundreds of coils. The main idea is to establish the conditions under which a global behavior can be obtained in high order structures of coils by exploiting the self-organization principle and using pas-

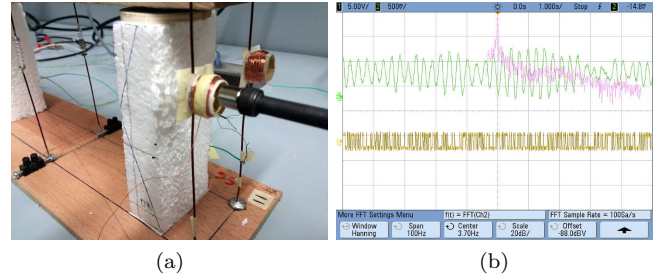


FIG. 5. (a) Structure of Fig. 1(b) including the coils and the active shock system. (b) Horizontal displacement of the structure.

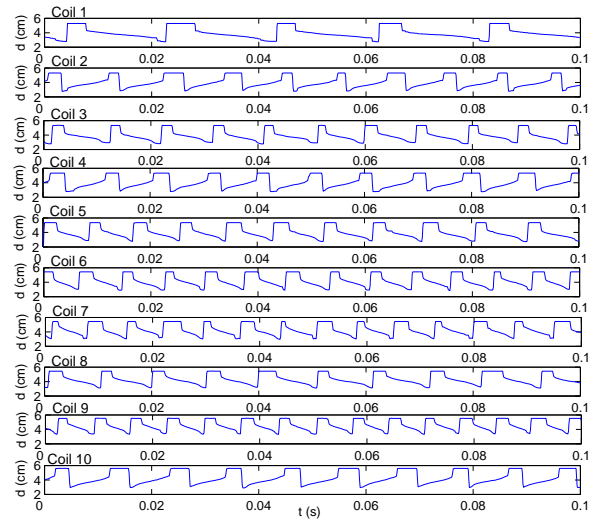


FIG. 6. Angular velocity for the 10 different coils.

sive low level power induced fluctuations or external powered devices; this latter solution is needed only during the complete start up of the system.

¹ J.J. Thomsen, *Vibrations and stability* (McGraw Hill, 1997).

² Y. Braiman, J. F. Lidner, and W. L. Ditto, *Nature*, **378**, 465467 (1995).

³ W. Gawronski, *Balanced control of flexible structures* (Springer, 1996).

⁴ L. Fortuna, M. Frasca, and M.G. Xibilia, *Chua's Circuit Implementations: Yesterday, Today and Tomorrow* (World Scientific Series on Nonlinear Science, Series A - Vol. 65, 2009).

Randomness and Earth's climate variability

Levinshtein M.E.¹, Dergachev V. A.², Dmitriev A. P.³, and Smakov P. M.⁴

¹Ioffe Institute, St. Petersburg, Russia

e-mail address: melev@nimis.ioffe.ru

²Ioffe Institute, St. Petersburg, Russia

e-mail address: v.dergachev@mail.ioffe.ru

³Ioffe Institute, St. Petersburg, Russia

e-mail address: apd1812@gmail.com

⁴Ioffe Institute, St. Petersburg, Russia

e-mail address: pshmakov@yandex.ru

I. INTRODUCTION

The problem of studying and predicting the natural phenomena evolution of our planet is vital for all of us and for the Humanity as a whole. At present, there are steadily increasing changes of the natural conditions in various geospheres on the Earth's surface. It is widely believed that the rise in the average temperature on the Earth's surface in the past few decades is caused by the increasing human activity. Based on this assumption, trillions of dollars are spent to fight the global warming.

At the same time, the opponents of this concept argue that the periods of relative cooling and warming repeatedly alternated in the Earth's history without any human intervention. Suffice it to mention that only 20 000 years ago the whole territory of North Europe was occupied by a glacier with a thickness reaching 2.5 - 3 km. It is known for sure that approximately 9 – 10 thousand years ago this monstrous ice armour melted without any impact of human activity.

The only scientific way to try to predict the future trends of these changes is by making a correct analysis of the climatic changes in the past. The Paleo-Sciences have accumulated over the years of studies tens of thousands of very different records related to climatic changes. Such important parameters as solar insolation, temperature, content of the oxygen isotope ($\delta^{18}\text{O}$), atmospheric radiocarbon, deuterium, etc., have been recorded and analyzed. The researchers have tried to identify periodic and quasi-periodic processes in these paleoenvironmental records. In this paper, we show that this analysis is incomplete, and that *random processes*, namely *single-time-constant random processes* (noise with a Lorentzian noise spectrum) play a very important and, perhaps, a decisive role in numerous natural phenomena.

II. METHOD OF CALCULATIONS

We consider a paleoenvironmental record of some quantity φ as a random function ("noise") $\varphi(t)$. The spectral density of fluctuations $S^\varphi(f)$ is calculated as follows. Another random function $\varphi'(t)$ is introduced defined as $\varphi'(t) = \varphi(t) - \bar{\varphi}$, where $\bar{\varphi}$ is the average value of $\varphi(t)$ over a long time interval T :

$$\bar{\varphi} = \frac{1}{T} \int_{-T/2}^{T/2} \varphi(t) dt \quad (1)$$

The average value of $\varphi'(t)$ is zero, so it describes the deviation of $\varphi(t)$ from the mean. The spectral noise density of fluctuations $S^\varphi(f)$ can be expressed through the Fourier transform $\varphi(f)$ of the $\varphi'(t)$ function:

$$S^\varphi(f) = \frac{1}{T} |\varphi(f)|^2, \quad (2)$$

$$\text{where } \varphi(f) = \int_{-T/2}^{T/2} \varphi'(t) \exp(i2\pi ft) dt, \quad T \rightarrow \infty \quad (3)$$

The function $S^\varphi(f)$ was calculated numerically.

III. RESULTS AND DISCUSSION

Paleoenvironmental records have, at first sight, the form of noise (so called "grass"). As an example, Fig 1 shows the time dependence of the virtual axial dipole moment (VADM) for last 800000 years (800 Ka)¹.

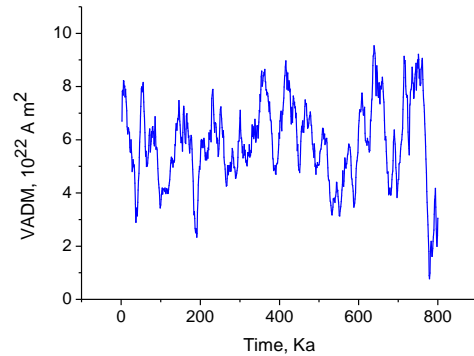


Fig. 1 The time dependence of the virtual axial dipole moment (VADM) for 800 Ka¹.

Of course, periodic and quasi-periodic processes can be (and should be) identified in the dependence shown in Fig. 1. At the same time, this dependence can be regarded as "noise". In this case, the frequency dependence of the spectral density $S(f)$ of this "noise" should be calculated.

Fig. 2 presents the frequency dependence of the spectral density fluctuations $S^{DM}(f)$ for the time dependence of virtual axial dipole moment (VADM) presented in Fig. 1.

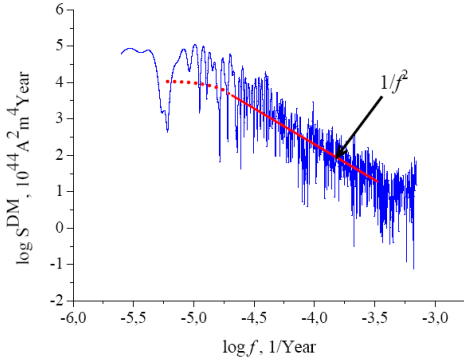


Fig. 2. The frequency dependence of spectral density fluctuations for the time dependence of VADM presented in Fig. 1. The lines are guidelines to the eye.

It can be seen in Fig. 2 that the overall run of S^{DM} curve in the frequency range $10^{-5} \leq f \leq 10^{-3.5}$ 1/year is quite well described by a single Lorentzian with a characteristic time constant $\tau_0 \sim 10^{4.7}/2\pi \approx 8000$ years. This means that, along with the possible periodic and quasi-periodic processes in the time dependence of VADM, an important (and possible dominant) influence is exerted by a random process with a characteristic time constant $\tau_0 \sim 8000$ years.

We calculated spectral densities of fluctuations for several very important paleoenvironmental records.

Fig. 3 presents the frequency dependence of spectral density fluctuations, S^{2H} for the deuterium content (Vostok Ice Core Deuterium Data for 420,000 years²).

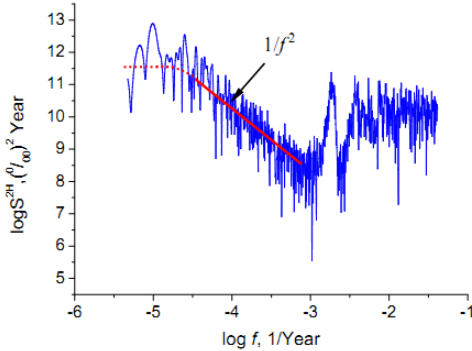


Fig. 3. The frequency dependence of spectral density fluctuations for the deuterium content².

It is seen from Figure 3 that the overall behavior of S^{2H} dependence in the frequency range $f \geq 10^{-5}$ 1/years is well described by a single Lorentzian with a characteristic time constant $\tau_0 \sim (10^{4.5} - 10^{4.7})/2\pi \approx (5 \div 8) \times 10^3$ years.

Very similar dependence was observed for the deuterium data for 740,000 years from EPICA Dome C Ice Cores³.

It is interesting to compare the data presented in Figs. 2 and 3 with $S^{\delta^{18O}}$ dependence for the content of oxygen ^{18}O isotope⁴ (Fig.4).

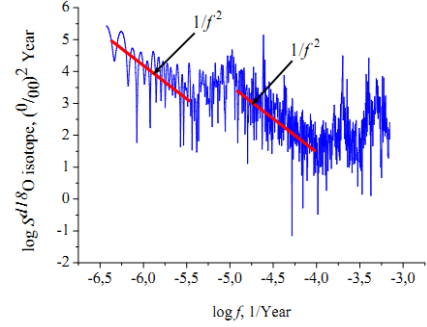


Fig. 4. The frequency dependence of spectral density fluctuations for globally distributed benthic $\delta^{18}O$ records⁴.

The data presented in ⁴ span 5.3 Myr and are an average of 57 globally distributed benthic $\delta^{18}O$ records, aligned by an automated graphic correlation algorithm. It can be seen from Fig. 4 that there are two characteristic parts in the frequency dependence of spectral density, in which the dependence follows the law $S \sim 1/f^2$. For the part in the frequency range $10^{-4.7} \leq f \leq 10^{-4.0}$ 1/year, the value of τ_0 is close to the values of τ_0 , found for the plots shown in Figs. 2 and 3. For the “low-frequency” part $10^{-6.3} \leq f \leq 10^{-5.3}$ 1/year, the value of τ_0 cannot be found from the data presented. It is obvious, however, that τ_0 for this random process, exceeds 10^5 years.

The above-mentioned random process with the same time constant $\tau_0 \sim (10^{4.5} - 10^{4.7})/2\pi$ years for several records is certainly not universal.

For example, the frequency dependence of the spectral density of the atmospheric radiocarbon content fluctuations⁵ is quite well described by a Lorentzian with a characteristic time constant $\tau_0 \sim 300$ years.

Obviously, the most intriguing problem is the physical interpretation of the data, i.e., the identification of the random processes with a single time constant which are responsible for the appearance of single Lorentzians in the $S(f)$ dependences analyzed in this paper.

IV. CONCLUSION

The time dependences of several important paleoclimatic parameters are considered for the first time as random processes (“noise”). It is shown that *single-time-constant random processes* (noise with a Lorentzian noise spectrum) play a very important and, perhaps, a decisive role in some such important dependences.

To the best of our knowledge, this is the first indication of the role played by random processes in climate variations. Identification of the random processes responsible for the appearance of single Lorentzians in the $S(f)$ dependences that were revealed in this work will allow a better understanding of the nature of climatic changes

¹ Y. Guyodo, and J.P. Valet, Nature **399**, 249–252 (1999).

² J.R. Petit et al., Nature **429**, 429–436 (1999).

³ Epica community members., Eight glacial cycles from an

Antarctic ice core. Nature **429**, 623–628, (2004).

⁴ L.E. Lisiecki and M.E. Raymo, Paleoceanography **20**, PA1003 (2005)

⁵ M. Stuiver et al., Radiocarbon **40**, 1041–1083 (1998).